Molecular requirements for TGF-β1 activation mediated by integrin αVβ8 or monoclonal antibodies

Mathieu Jamez

Juin 2026

Thèse présentée en vue de l'obtention du grade
de docteur en sciences biomédicales et pharmaceutiques
Secteur des sciences de la santé

Supervisor

Pr. Sophie Lucas
de Duve Institute, UCLouvain

Co-supervisor

Tiphanie Gomard, PhD.
de Duve Institute, UCLouvain

Jury

Internal members

Pr. Laure Dumoutier, President of the Jury
de Duve Institute, UCLouvain

Pr. Pierre Coulie
de Duve Institute, UCLouvain

Pr. Nathalie Vigneron, Secretary of the Jury
de Duve Institute, UCLouvain

External members

Pr. Savvas Savvides
Ghent University, Belgium

Pr. Dean Sheppard
UCSF, U.S.A

À mes grands parents,

Mes remerciements s'adressent en premier lieu à ma promotrice Sophie. Merci pour ces six belles années au sein de ton laboratoire et pour l'ensemble de tes enseignements. Le temps passé sous ta supervision aura fait de moi un meilleur chercheur. Je garderai en mémoire ces traits distinctifs qui font de toi une grande scientifique : à savoir ta perspicacité, ton souci du détail et ta persévérance, des qualités que j'espère pouvoir appliquer à mon tour dans ma carrière.

Je remercie également ma co-promotrice Tiphanie. Merci pour ton accompagnement dans ce projet. Merci pour la justesse de tes conseils, ton humanité et ton soutien dans les moments de doutes. Merci de m'avoir toujours encouragé à aller de l'avant et aidé à tenir le cap jusqu'à cette dernière étape.

Je remercie les autres membres de mon comité, ma présidente la professeure Laure Dumoutier, la professeure Nathalie Vigneron et le professeur Pierre Coulie pour leurs conseils avisés, leur encadrement toujours bienveillant, rigoureux et pertinent. Merci pour les discussions, les questionnements et les échanges qui ont jalonné mon parcours.

Merci à mes deux membres externes, Dean Sheppard de l'université UCSF et Savvas Savvides de l'université UGhent d'avoir pris le temps d'évaluer mon travail de participer à la défense privée et pour leurs précieux retours.

Une thèse est un long chemin, parfois difficile, mais profondément enrichissant, tant sur le plan professionnel qu'humain. Je mesure la chance d'avoir été entouré de personnes extraordinaires sans lesquelles ce parcours aurait été bien différent. Un immense merci à mes collègues pour leur amitié si précieuse à mes yeux. Merci à Camille et Ananyashree d'avoir formé avec moi ce trio incassable au sein duquel nous avons vécu tellement de beaux moments. Merci d'avoir toléré mes plantes de trois kilomètres et mon bureau en « léger » désordre. Merci au Jingle office dans son ensemble, avec Catherine, Laurence, Lysa et Margaux pour cette ambiance unique et ces éclats de rires à en percer les tympans (et les murs). Merci aux Fluo Rangers : Coralie, Douae, Eléonore, Grégoire et Séverine pour nos petites pauses café. Merci d'avoir supporté mes « On mange ! » quotidiens entre 12 :00 et 12 :05 et mes nombreuses pauses papotes quand je ne voulais pas travailler. Merci au Sweet Office : Aydine, Dechen, Emilie, Eurydice, Fatima, Séverine et Valentin de m'avoir nourri, tant physiquement, qu'à coups de ragots en tout genre et de sourires malicieux.

Merci également à la branche PCO : Gérald, Nathalie et Nicolas pour votre sympathie et votre aide au quotidien, même pour les questions les plus anodines. Un immense merci à Suzanne pour ta gentillesse et ta gestion administrative du laboratoire, et à Guillaume pour ton efficacité et ton aide dans les commandes. Merci aux anciens membres des équipes PCO et SLU: Charlotte, Clément, David, Fanny, Julien, Mélanie, Noora, Pierre, Sara, Walther et Xuhao pour le chemin parcouru ensemble, au labo comme en dehors.

Merci aux étudiants que j'ai eu le bonheur d'encadrer : Hugo, Louis, Mathis, ainsi qu'à mes mémorants, Imane et Justin, pour leur contribution à mon projet.

Merci à Julie pour tes conseils, tes paroles rassurantes et pour avoir été une inépuisable source d'information ainsi que de chocolats.

Merci aux équipes MEMI, NVI, ZHU et BVDE du 3ème étage dont la proximité géographique (et thématique) a mené à de nombreux échanges scientifiques ou non scientifiques. Merci également aux équipes du 4ème étage, en particulier l'équipe GEDI pour les nombreuses discussions et collaborations ainsi qu'aux filles du LDU pour me rappeler qu'il est toujours bon de chanter un petit Feliz Navidad même en dehors de la période de Noël.

Merci à la PhD Society de continuer à promouvoir les échanges entre doctorants de tout l'Institut, de nous rappeler que nous ne sommes pas seuls dans cette aventure et que de belles amitiés peuvent émerger à l'issue de ce parcours. Merci à tous les doctorants et doctorantes que je n'ai pas pu citer directement mais que j'ai eu l'occasion de côtoyer, à ceux qui sont déjà partis et courage à ceux qui poursuivent. J'ai hâte de célébrer vos futures défenses.

Merci à l'ensemble des membres de l'Institut de Duve - mémorants, stagiaires, techniciens, postdocs, PI's - pour ces interactions, ces coups de main et ces conseils. Je remercie notamment Donatienne Tyteca, Marie Verfaillie, Marine Ghodsi, Noémie Avalosse et Sophie Quiquempoix pour leur aide en microscopie confocale. Merci également au personnel administratif et technique, les vrais rouages de notre institut, sans qui notre travail serait impossible.

Merci à mes amis d'avoir été de véritables piliers pendant toutes ces années. Merci à ceux qui ont partagé l'expérience de la thèse pour leurs échanges, et aux autres pour leur présence et leurs encouragements. Je remercie donc les BBMCs, les Canards, la Colokriek, Eclipse, le Good Old Squad, le Mistral, le Vélogang ainsi que tous les autres.

Merci à famille, ma belle-famille et aux Couscous pour l'intérêt que vous avez toujours porté à mon travail et pour votre soutien.

Merci à mes parents, à qui je dois tant, pour m'avoir guidé, pour leur présence constante et leur soutien sans faille, tout en m'ayant toujours laissé la liberté de faire mes propres choix. Vous m'avez offert des bases solides sur lesquelles je pourrai m'appuyer tout au long de ma vie.

Enfin, merci à Grégory de partager ma vie depuis plus de six ans. Nous avons traversé ensemble les hauts et les bas de la thèse, mais aussi bien d'autres moments qui comptent encore plus. Ta présence, ton soutien et ta patience ont été essentiels tout au long de ce parcours. J'ai hâte de voir ce que l'avenir nous réserve et de continuer à avancer ensemble.

TABLE OF CONTENTS

Table of contents

LIST OF ABBREVIATIONS **12**

SUMMARY **16**

INTRODUCTION **20**

1 General background on TGF-β1 22

2 TGF-β1 production, processing and activation 24

2.1 Biosynthesis and reservoirs of latent TGF-β1 ..... *24*

2.2 TGF-β1 latency explained through structural data *28*

2.3 Activation *41*

3 TGF-β1 activation: by whom, how, when and where? 59

3.1 Epithelial cells *59*

3.2 Myeloid cells *59*

3.3 Regulatory T cells *60*

3.4 B cells *61*

3.5 Mesenchymal stromal cells *61*

3.6 Platelets *61*

3.7 Hepatic stellate cells *62*

3.8 Fibroblasts and contractile stromal cells *63*

3.9 Endothelial cells *63*

4 Cellular effects of TGF-β1 signaling 66

4.1 Effects on the innate immune system *66*

4.2 Effects on the adaptive immune system *68*

4.3 Effects on fibroblasts, epithelial and endothelial cells *71*

5 Modulation of TGF-β1 activity using monoclonal antibodies to block or activate the latent cytokine 74

5.1 Blocking antibodies *75*

5.2 Activating mAbs *79*

AIM OF THE STUDY **84**

RESULTS **88**

1 Identification of candidate proteins that contribute to activation of latent TGF-β1 presented by GARP in Tregs or other cell types 90

1.1 Construction of a human Treg cDNA library ... 90
1.2 The screening system ... 91
1.3 Screening in the absence of αVβ8 ... 92
1.4 Screening in the presence of αVβ8 ... 103
1.5 Discussion ... 104
1.6 Material and methods ... 113
2 Molecular requirements for TGF-β1 activation by αVβ8 or monoclonal antibodies ... 119
Article by Jamez et al., to be submitted: ... 120
Integrin αVβ8 passively activates TGF-β1 by transmitting cell-generated tensile forces without direct interaction with the cytoskeleton, allowing paracrine TGF-β1 activity ... 120

DISCUSSION ... 156

1 Starting point: the cDNA library and screening ... 158
1.1 Limitations of the cDNA library ... 158
1.2 Is there any potential bias induced by the screening strategy? ... 159
2 First candidate: the case of galectin-9 ... 161
2.1 Could forces be implicated in TGF-β1 activation by GAL-9? ... 161
3 Force-dependent activation mediated by αVβ8 ... 162
3.1 Reminder: αVβ8 versus other integrins ... 162
3.2 The entropy redistribution model is (in part) incompatible with our proposed model 163
3.3 Do integrins need their IC tail for the transmission of activating forces? ... 165
4 Force-dependent activation mediated by mAbs ... 166
4.1 Bivalent versus monovalent mAbs, soluble versus coated mAbs ... 166
4.2 Bispecific mAbs ... 167
4.3 Can mAbs activate any latent TGF-β1 pool? ... 168
5 *Cis*- or *trans*- activation? ... 171
5.1 How can structural data guide us? ... 172
5.2 Preliminary results in immunofluorescence on adherent cells ... 174
6 Conclusion and physiological relevance ... 176

REFERENCES ... 178

ANNEXES ... 194

Lambert et al. (2025): Antibody-mediated TGF-β1 activation for the treatment of diseases caused by deleterious T cell activity ... 195

LIST OF ABBREVIATIONS

LIST OF ABBREVIATIONS

aa	Amino Acid
ADMIDAS	Adjacent to Metal Ion-Dependent Adhesion Site
AML	Acute Myeloid Leukemia
ATCC	American Type Culture Collection
BCR	B Cell Receptor
CAF	Cancer-Associated Fibroblast
CAM	Cell-Adhesion Molecule
cDNA	Complementary DNA
CD	Cluster of Differentiation
CNS	Central Nervous System
Co-IP	Co-Immunoprecipitation
Co-SMAD	Co-mediator SMAD
CRD	Carbohydrate Recognition Domain
Cryo-EM	Cryo-electron Microscopy
C-ter	Carboxy-terminal
CTL	Cytotoxic T Lymphocyte
DC	Dendritic Cell
DNA	DeoxyriboNucleic Acid
ECL	Enhanced Chemiluminescence
ECM	Extracellular Matrix
EGF	Epidermal Growth Factor
EMT	Epithelial-Mesenchymal Transition
EndoMT	Endothelial-to-Mesenchymal Transition
FasL	Fas Ligand
FI	Fold Increase
FLuc	Firefly Luciferase
GAL-9	Galectin-9
GARP	Glycoprotein A Repetition Predominant (= LRRC32)
GvHD	Graft *versus* Host Disease
HC	Heavy Chain
HSCs	Hepatic Stellate Cells
HUVEC	Human Umbilical Vein Endothelial Cell
IFN-γ	Interferon-gamma
Ig	Immunoglobulin
IL-x	Interleukin-x
iTreg	Induced Treg
kDa	Kilodalton
KO	Knock-Out
LAP	Latency Associated Peptide
LC	Light Chain
LHG	Llama anti-Human GARP
LHT	Llama anti-Human TGF-β1
LMT	Llama anti-Mouse TGF-β1
LRR	Leucin Rich Repeats

LIST OF ABBREVIATIONS

LRRC32	Leucin Rich Repeats containing Protein 32 (= GARP)
LRRC33	Leucin Rich Repeats containing Protein 33
LTBP	Latent TGF-β1 Binding Protein
mAb	(activating) Monoclonal Antibody
MHG	Mouse anti-Human GARP
MIDAS	Metal Ion-Dependent Adhesion Site
MMP	Matrix Metalloproteinase
mRNA	Messenger RNA
MSCs	Mesenchymal Stromal Cells
NK cell	Natural Killer cell
NMR	Nuclear Magnetic Resonance
N-ter	Amino-terminal
ORF	Open Reading Frame
PBMC	Peripheral Blood Mononuclear Cell
PC	Proprotein Convertase
PCR	Polymerase Chain Reaction
PMF	Primary Myelofibrosis
PSI	Plexin-Semaphorin-Integrin
pTregs	Peripherally-induced Treg
qPCR	Quantitative PCR
RLuc	Renilla Luciferase
RNA	RiboNucleic Acid
ROS	Reactive Oxygen Species
R-SMADs	Receptor-Regulated SMADs
RT	Retro-Transcribed
SDL	Specificity Determining Loop
SP	Signal Peptide
SyMBS	Synergistic Metal Ion Binding Site
TβRI	TGF-β Receptor type I (also known as ALK-5)
TβRII	TGF-β Receptor type II
TβRIII	TGF-β Receptor type III (also known as betaglycan)
TCR	T Cell Receptor
TGF-β	Transforming Growth Factor beta
TGM	Transforming Growth factor-β Mimic
Th	T Helper cell
tTreg	Thymic-derived Treg
Treg	Regulatory T cell
TSP-1	Thrombospondin-1
xGvHD	xenogeneic Graft *versus* Host Disease

SUMMARY

SUMMARY

Transforming Growth Factor β1 (TGF-β1) is a highly pleiotropic cytokine and a key element in various biological processes such as cell proliferation, phenotypic plasticity, migration, cell metabolism and immunity functions. Despite these various roles, and to the contrary of many other cytokines, TGF-β1 expression is barely regulated nor is its detection by cells as its heterotetrameric receptor is virtually ubiquitously expressed. It is at the post-translational level that most of the regulation occurs, when the mature TGF-β1 is released from the embrace of the Latency Associated Peptide (LAP). Although this process, known as “TGF-β1 activation” has been broadly described and studied, many questions remain unanswered. TGF-β1 activation is a cell type-specific process which depends on presenting molecules that expose latent TGF-β1 to activating partners. Our laboratory and others have shown that TCR-stimulated regulatory T cells (Tregs) activate latent TGF-β1 through a mechanism that depends on transmembrane proteins GARP and integrin αVβ8.

This work originated from the observation that T cells stably expressing GARP and αVβ8 fail to activate latent TGF-β1 unless they are stimulated via the TCR. This indicates that expression of the two proteins is not sufficient for activation and that additional partners are required. To identify genes contributing to this mechanism, we screened a Treg cDNA library in a TGF-β-reporter system.

In a first screen, we used cells co-expressing GARP and TGF-β1 but not αVβ8 and identified galectin-9 (GAL-9) as a candidate activator of latent TGF-β1. However, neither genetic deletion nor overexpression of GAL-9 in GARP:TGF-β1 expressing T cells altered their capacity to activate TGF-β1. In a second screen, we used cells co-expressing GARP, TGF-β1, and αVβ8 and identified three intracellular proteins – RHOA, ADCK1, TUBA4A – the expression of which enhanced TGF-β1 activation. This suggested a role for cytoskeleton-associated processes.

We therefore started to focus on force-dependent mechanisms of latent TGF-β1 activation. To investigate the contribution of cytoskeleton-generated mechanical forces, we first assessed the role of the intracellular (IC) and transmembrane (TM) domains of GARP and the β8 chain of αVβ8. Partial or complete deletion of the IC domains of either partner did not impair latent TGF-β1 activation in the cellular systems tested. Similarly, deletion of the TM domain of β8 did not prevent latent TGF-β1 activation. In contrast, deletion of the TM domain of GARP, as well as pharmacological disruption of cytoskeletal dynamics inhibited activation. Together, these results indicate that GARP- and αVβ8-dependent activation of TGF-β1 does not require direct interaction with the cytoskeleton through their IC domains, but instead relies on cellular dynamics and membrane anchorage.

Finally, using activating monoclonal antibodies developed in our laboratory as mechanistic tools, we propose a model in which force-dependent TGF-β1 activation requires **two anchorage points** – either within the membrane or against a fixed extracellular support – and the **transmission of cell-generated tensile forces** to **LAP** via a **binding partner**, such as an integrin or an activating antibody.

INTRODUCTION

INTRODUCTION

This introduction aims to describe the known mechanisms governing TGF-β1 latency and activation. We first provide a brief overview of TGF-β1 biology, followed by a deeper examination of the structural features of the latent and active cytokine, and its interaction with its receptor.

Building on this, we will explore the activation mechanisms documented in the literature, with a particular focus on the molecular processes that destabilize the latent complex and facilitate the release of the mature cytokine. We will also consider the potential cellular sources of active TGF-β1 before analyzing the downstream cellular responses it triggers. Finally, we will conclude by discussing how TGF-β1 activation can be modulated using monoclonal antibodies – either inhibitory or activating – developed in our laboratory to shape immune responses in the context of cancer and autoimmune diseases.

1 General background on TGF-β1

The TGF-β superfamily is a large group of 33 ligands composed of growth factors, cytokines, and hormones that regulate cell growth, differentiation, development, and tissue homeostasis. It includes two main subgroups: Bone Morphogenetic Proteins (BMPs) and the TGF-β family, which signal through SMAD1/5 and SMAD2/3, respectively. Their heterotetrameric receptors function as serine/threonine kinases that activate these downstream pathways (*1*). Latency and activation are central to the regulation of this cytokine superfamily. All members are produced as dimeric pro-proteins that are cleaved into a mature C-terminal cytokine and an N-terminal pro-domain. Most remain inactive (latent) because the mature cytokine stays bound to the pro-domain, preventing receptor interaction. However, several BMPs exhibit constitutive activity due to weak interactions between the pro-domain and mature cytokine, allowing release of the active form (*2, 3*). Their activity is mainly regulated through binding to other molecules (*4*). In contrast, in cytokines such as TGF-βs, the pro-domain tightly binds the mature domain through non-covalent interactions, masking receptor-binding sites and maintaining latency.

The TGF-β family includes activins A and B, Nodal, Growth and Differentiation Factors (GDFs), and TGF-β1, TGF-β2, and TGF-β3. Antagonistic ligands such as inhibin, which blocks activin receptors, and Lefty1/2, which inhibit Nodal co-receptors, are also part of this family (*5*). The three TGF-β isoforms are encoded by distinct genes and share 71-79% identity in their C-terminal sequences. Although they bind the same receptors, they exert distinct biological functions due to different temporal and spatial expression patterns (*1, 6, 7*). TGF-β2 and TGF-β3 mainly function during embryonic development, with some roles in fibrosis (*6, 8*). TGF-β1 is the predominant isoform in adult tissues, especially in immune cells, and is highly represented in the tumor microenvironment (*6, 9*). It is essential for maintaining tissue homeostasis and regulating immune responses after birth. Consistent with this, *Tgfb1*$^{-/-}$ mice either die during embryogenesis due to severe vascular defects, or are born but develop fatal systemic inflammation and autoimmunity within 3-4 weeks after birth (*10, 11*). Because of its implication in a wide range of biological processes, TGF-β1 is the most studied and one of the most tightly regulated cytokines of the family.

Recognition of TGF-β1 by its receptors is a multi-step process requiring sequential assembly of a receptor complex before SMAD signaling occurs. Mature TGF-β1 first binds with high affinity to the TGF-β type II receptor (TβRII) homodimer (*12*), which then recruits the TGF-β type I receptor (TβRI, also known as ALK-5) homodimer to form a stable heterotetrameric complex. Upon ligand binding, TβRII phosphorylates itself and TβRI, which subsequently phosphorylates the receptor-regulated SMADs SMAD2 and SMAD3. Phosphorylated SMAD2/3 associate with SMAD4 and translocate to the nucleus, where they regulate transcription of TGF-β-responsive genes in a context-dependent manner (*13*).

2 TGF-β1 production, processing and activation

2.1 Biosynthesis and reservoirs of latent TGF-β1

TGF-β1 is initially synthesized as a large precursor protein known as pre-pro-TGF-β1. This precursor includes a signal peptide (SP), a long (25 kDa) N-terminal domain called the latency-associated peptide (LAP), and a shorter (12.5 kDa) C-terminal mature TGF-β1 peptide (**Figure 1**). Upon removal of the SP in the secretory pathway, the pro-TGF-β1 forms a homodimer through the formation of three interchain disulfide bonds: two disulfide bridges link the monomers in the LAP region, while a third bond stabilizes the homodimer in the mature TGF-β1 region. The pro-TGF-β1 homodimer is then processed by the convertase Furin, which cleaves the mature cytokine from the LAP (*14-16*). Despite this cleavage, the LAP and mature TGF-β1 dimers remain non-covalently associated, forming a complex known as latent TGF-β1. This latent complex is inactive, as the LAP surrounds the mature TGF-β1, preventing it from binding to TGF-β receptors (*17-19*).

Latent TGF-β1 is produced by nearly all cell types, which secrete it into the extracellular space either as "free latent TGF-β1" (a soluble form) or bound to other proteins through disulfide linkage to cysteine residues (Cys33) in the two LAP monomers. TGF-β1-binding proteins include Latent TGF-β1 Binding Proteins (LTBPs), Leucine Rich Repeat Containing protein 32 (LRRC32, also called GARP), and LRRC33 (or NRROS). They help to stabilize and promote the proper folding and secretion or presentation at the cell surface of latent TGF-β1 (*20, 21*).

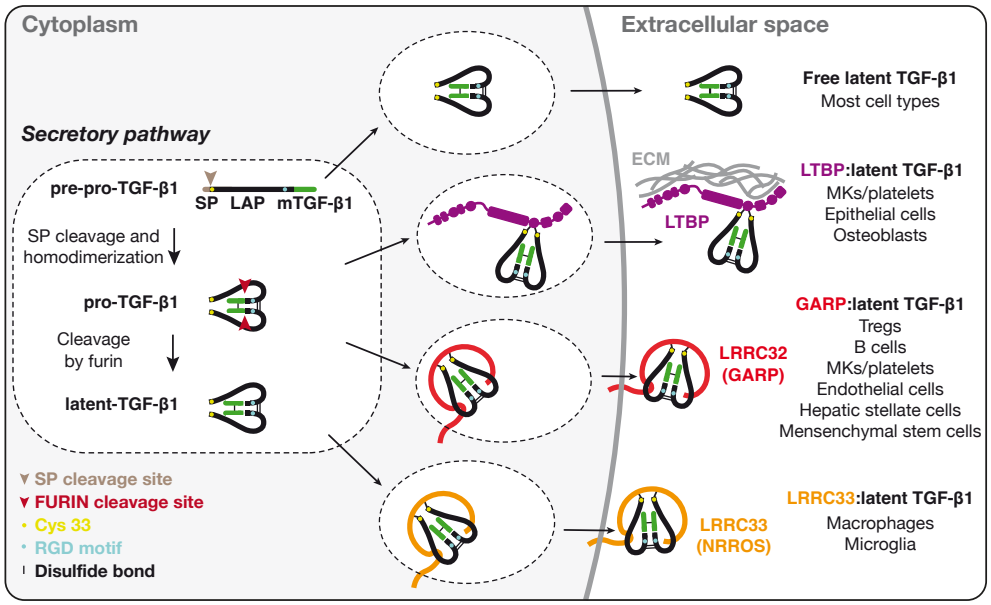

Figure 1: Schematic representation of the secretory pathway of TGF-β1.
Figure adapted from Stockis et al., 2013 (Review) (*22*). TGF-β1 is first synthesized as a precursor known as "pre-pro-TGF-β1". Following removal of the signal peptide, the protein undergoes homodimerization through disulfide bonds formation. The resulting pro-TGF-β1 is then cleaved by the protease Furin to generate the latent TGF-β1. In this complex, the N-terminal Latency Associated Peptide (LAP) remains non-covalently bound to the C-terminal mature (m)TGF-β1 dimer, thereby maintaining the cytokine in an inactive state. Latent TGF-β1 can be secreted freely by most cell types or covalently linked to anchoring proteins such as LTBP, GARP or LRRC33 in a cell-specific manner. SP, signal peptide; LAP, latency associated peptide; mTGF-β1, mature TGF-β1.

2.1.1 LTBP:TGF-β1 complexes (matrix-deposited)

In many cell types, including mesenchymal cells and platelets, latent TGF-β1 is secreted in complex with LTBPs. LTBP 1 to 4 are large (120-140 kDa) extracellular glycoproteins that facilitate both efficient secretion of latent TGF-β1 and its subsequent sequestration within the extracellular matrix (ECM). Only LTBP-1, LTBP-3, and LTBP-4 can covalently associate with latent TGF-β1 through disulfide bonds involving a conserved cysteine residue in each LAP monomer and two cysteins within the same LTBP molecule (*23*). Following secretion, LTBPs form covalent and non-covalent interactions with ECM components such as fibrillin and fibronectin, promoting stable deposition of latent TGF-β1 within the matrix. This ECM-anchored pool constitutes a major reservoir of latent TGF-β1 that can be locally mobilized upon tissue remodeling, inflammation, or injury, thereby enabling rapid and spatially controlled activation when required (*17*).

2.1.2 GARP:TGF-β1 complex (anchored to the cell membrane)

In addition to sequestration in the ECM, latent TGF-β1 can be retained at the surface of TGF-β1 producing cells through association with dedicated presenting proteins. GARP (LRRC32) is a type I transmembrane protein expressed by a restricted set of cell types and capable of forming a covalent complex with latent TGF-β1, thereby enabling stable membrane anchoring and surface presentation of the latent cytokine (*24*). Similar to LTBPs, GARP associates covalently with the LAP, allowing cells to maintain a readily available pericellular reservoir of TGF-β1 (*25*). Soluble GARP:TGF-β1 complexes have also been detected in the supernatant of cultured Tregs, suggesting that shedding of surface GARP: TGF-β1 may occur through proteolytic cleavage of GARP by an unidentified protease (*20*).

The cellular sources of GARP:TGF-β1 are relatively limited but span both hematopoietic and non-hematopoietic compartments. These include Tregs (*26-28*), stimulated B cells (*29*), megakaryocytes and activated platelets (*30, 31*), endothelial cells (*31, 32*), subsets of fibroblasts and mesenchymal cells (*33, 34*), hepatic stellate cells (*22, 35*), and NK cells (*36*).

2.1.3 LRRC33:TGF-β1 complex (anchored to the cell membrane)

LRRC33/NRROS is a closely related protein to GARP and also enables cell-surface docking of latent TGF-β1. It is primarily expressed in myeloid cells, such as macrophages and microglial cells. Although LRRC33 shares limited sequence identity with GARP, both proteins display conserved features that enable covalent association with the LAP (*37-39*). In contrast to GARP, LRRC33 appears selective for latent TGF-β1 and does not interact with TGF-β2 or TGF-β3, suggesting that distinct presenting proteins may contribute to isoform-specific regulation of TGF-β bioavailability and activation *in vivo* (*40, 41*).

2.1.4 GRP78:TGF-β1 complex (presented at the cell membrane)

Although not well established, it has been reported that GRP78 (also known as HSPA5/BiP) could act as another presenting protein for latent TGF-β1. GRP78 is a ubiquitous cytoplasmic chaperone that plays a key role in ensuring proper protein folding within the lumen of the endoplasmic reticulum. It is particularly expressed in immune, neuronal, and thyroid follicular cells. Several groups identified the presence of GRP78:TGF-β1 complexes on the cell surface, in the absence of other known TGF-β1 presenting proteins (*42, 43*). Whether GRP78 covalently associates with latent TGF-β1 or not has not been described yet.

2.2 TGF-β1 latency explained through structural data

Once secreted, these pools of latent TGF-β1 are maintained in an inactive state. Biological activity requires that mature TGF-β1 is liberated from the LAP, a process referred to as "TGF-β1 activation". Activation mechanisms are cell type-specific and context-dependent, and can occur through proteolysis (e.g., enzymatic cleavage), physicochemical alteration (e.g., reactive oxygen species (ROS), pH changes), or force-mediated processes, notably via integrins. These distinct modes of activation will be discussed in **Section 2.3**. Before addressing them, we will first examine the concept of TGF-β latency and its structural basis.

2.2.1 Mature TGF-β1 and its receptor

A clear understanding of TGF-β1 latency requires first to understand how the mature cytokine engages its receptor (**Figure 2**). As described in the introduction (**Section 1**), the TGF-β receptor is a heterotetrameric structure composed of two homodimers of type I receptor (TβRI) and two homodimers of type II receptor (TβRII).

The mature TGF-β1 homodimer (**AB**) adopts a characteristic butterfly-like conformation composed of two slightly curved "left hands", each consisting of 3 fingers: finger 1, finger 2, and a thumb, connected to a rigid palm and wrist (**Figure 2A**). Each hand is formed by elements originating from both monomers: for example, finger 1 and finger 2 are formed by anti-parallel β strands (β6 and β7) and a flexible loop from **mTGF-β1 A**, while the thumb is formed by the α3 helix of the opposite **mTGF-β1 B**. This way, the two monomers adopt opposite orientations in a symmetric arrangement (**Figure 2A**). The wrist region of each hand is formed by the α1 helix of the same monomer that provides the thumb (e.g., **mTGF-β1 B**). The palm of the structure is rigid and stabilized by a cystine knot formed by three intrachain disulfide bonds (*19, 44-46*).

The first contact between the ligand and the receptor occurs between the tips of the fingers of mature TGF-β1 and the TβRII homodimer (*zone 1*) (**Figure 2B-C**). This interaction is mediated by salt bridges and hydrogen bonds, forming a high-affinity interaction. Once the TGF-β1:TβRII complex is formed, it recruits two monomers of TβRI, which then interact with the palm face of the other two fingers (*zone 2*) and the thumb (*zone 3*) (**Figure 2B-C**). In contrast

to the TGF-β1:TβRII interaction, these interactions represent a lower-affinity interface, primarily mediated by hydrophobic patches (*47*).

In the latent complex, the LAP surrounds the key residues that mediate interaction with receptor chains and encapsulates the mature cytokine, preventing both receptor binding and free diffusion.

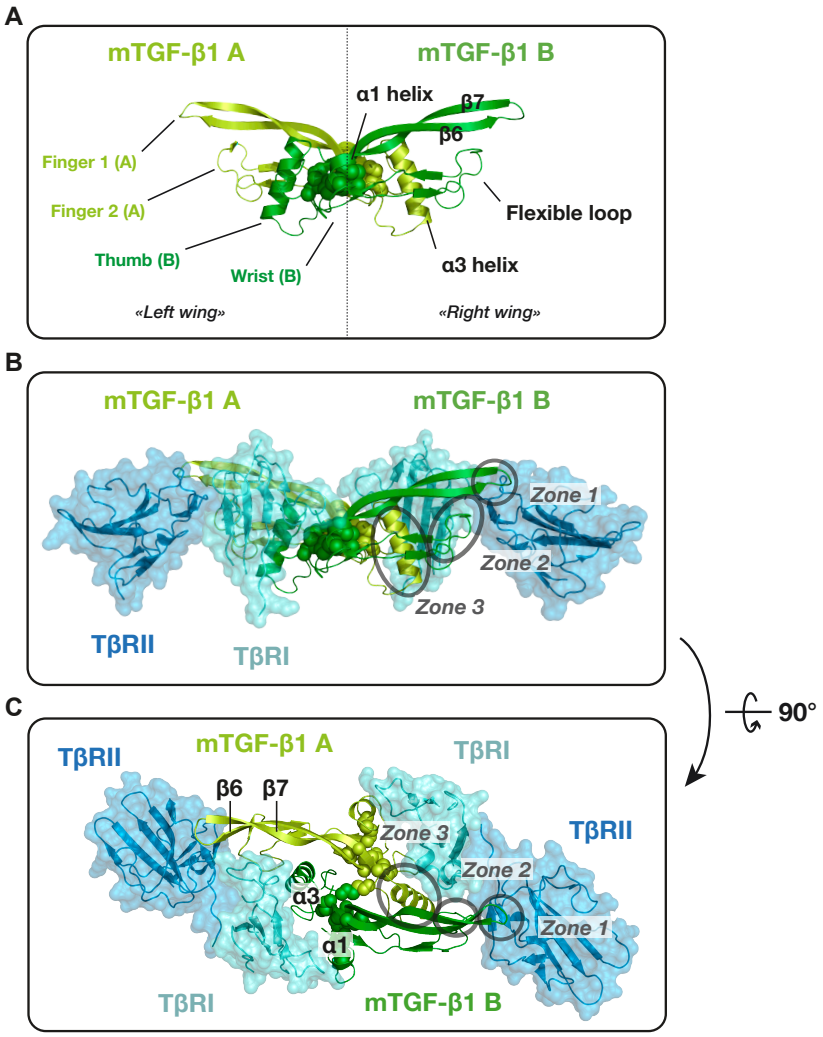

Figure 2: Mature human TGF-β1 interacting with its receptor.
Figure adapted from Fanny Lambert's thesis (*48*). (**A**) Cartoon representation, front view, highlighting the characteristic butterfly-like conformation of active TGF-β1. The two mature TGF-β1 chains are depicted in green (monomer A in light green and monomer B in dark green). Spheres represent cysteines engaged in disulfide bonds. A vertical symmetry axis separating the left and right wings is represented by a dotted line. Regions from the left wing are annotated as; fingers 1 and 2 (from monomer A) and the thumb and wrist (from monomer B), and corresponding structural elements from the right wing are annotated as; α1, α3 helices and β6 and β7 fingers. (**B**) Same as A, but with surface transparency applied to TβRI and TβRII that are shown in light blue and dark blue, respectively. Interaction interfaces are indicated by grey circles. (**C**) Top view showing the full interactions interfaces. Crystal structure derived from: Radaev et al 2010 (*47*) (PDB 3KFD).

2.2.2 Latent TGF-β1

In 2011, Timothy Springer's team solved the crystal structure of porcine latent TGF-β1, providing key insights into the concept of latency and offering a basis for further investigations into the structural changes that likely occur during activation (*19*). Since then, extensive structural studies expanded this framework through additional structures of latent TGF-β1, both alone and in complex with various partners (*40, 49-52*). Structural elements were described as follow; each LAP monomer consists of a rigid "arm" domain and a so-called straitjacket domain (which corresponds to the secured forearm), together keeping the two hands of mature TGF-β1 confined within the LAP. The two arms are linked by disulfide bonds at Cys194 and Cys196 (*19*) at the neck, creating a robust dimerization interface known as the “bowtie” (**Figure 3A-B**).

2.2.2.1 The arms

The arm domain’s rigidity is attributed to its structure, which consists of two anti-parallel, four-stranded β-sheets. The α2 and α5 helices of the arm domain help to fully encircle the mature TGF-β1. A robust interaction between the N-terminal segment of the arm and the C-terminal portion of the α1 helix from the straitjacket, referred to as the "fastener," stabilizes the straitjacket and completes the coverage of the palm face of the first two fingers. In the shoulder region of the arm domain, a flexible loop connecting two β-strands (β7 and β10) contains an RGDLXX(L/I) motif, which is known to interact with a subset of integrins (**Figure 3A-B**).

2.2.2.2 The dimerization interface

At the neck of the latent TGF-β1 structure, the two monomers are joined by two interchain disulfide bonds between the arm domains, creating a bowtie-like shape. This dimerization interface is further stabilized by two salt bridges and a cation-π interaction (**Figure 3A-B**). The significance of this interface in maintaining latency is highlighted by Camurati-Engelmann disease, where patients harbor mutations in the LAP amino acids responsible for stabilizing this interface. These mutations lead to abnormal TGF-β1 activity, resulting in malformations of long bones and the skull (*53*).

2.2.2.3 The forearms (or straitjacket)

The straitjacket domain of LAP is composed of the α1 helix and the latency lasso, a flexible loop that connects the α1 helix to the arm domain. This structural arrangement enforces latency by concealing the key interaction sites between the mature TGF-β1 cytokine and its receptor. The latency lasso surrounds the tips of the TGF-β1 fingers, blocking the first interaction site with TβRII. It also partially shields the palm face of the fingers (zone 2) through both the lasso and the α1 helix (**Figure 2B-C, Figure 3A**). Additionally, the α1 helix is positioned deeply between the first two fingers and the thumb (zone 3), which shifts the thumb away from the fingers compared to its position in active TGF-β1 bound to the receptor (**Figure 3A, C**). Therefore, the LAP not only prevents receptor binding by masking critical residues but also stabilizes the mature TGF-β1 in a distinctly different conformation.

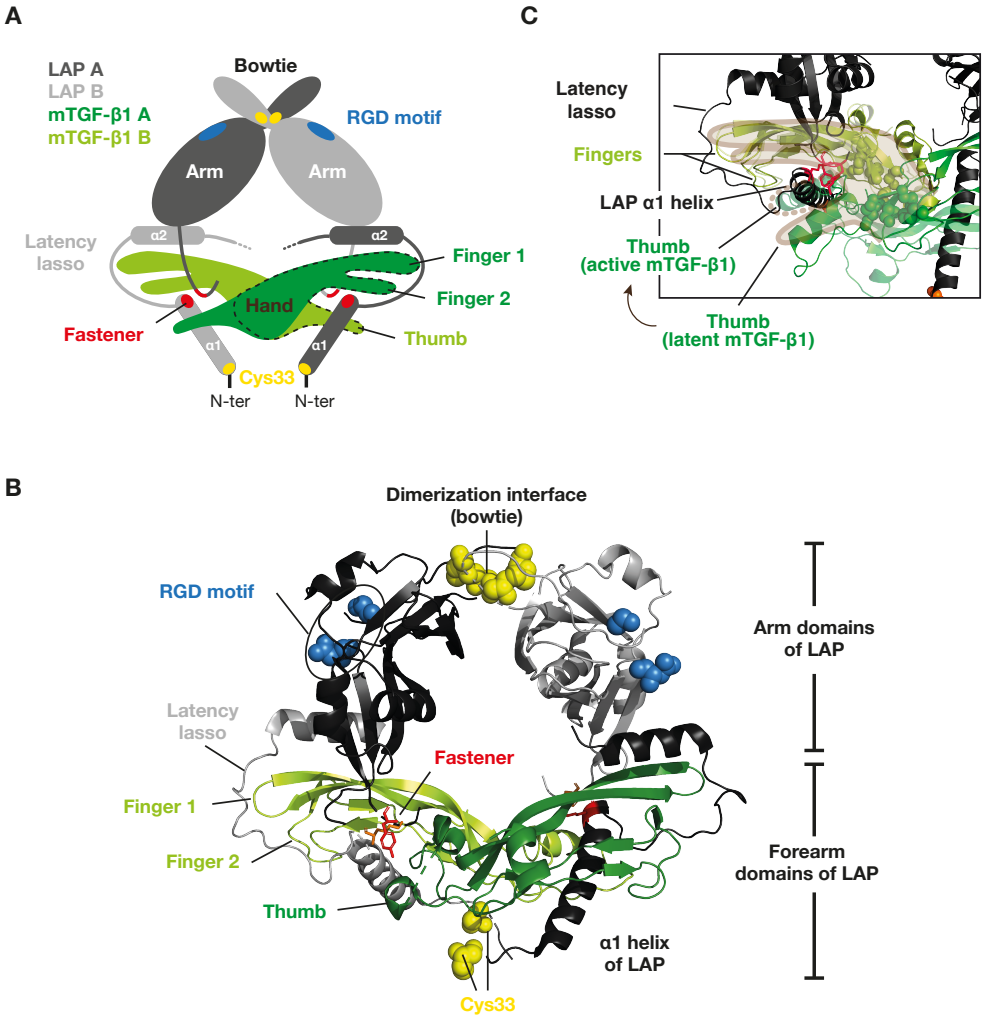

Figure 3: Structure of human latent TGF-β1.
(**A**) Schematic representation of the latent TGF-β1, adapted from Stephanie Liénart's and Fanny Lambert's thesis (*48, 54*). (**B**) Cartoon diagram of the human latent TGF-β1 crystal structure reporter by Lambert et al. (*51*) (PDB ID: 8REW). (**C**) Illustration of the conformational rearrangement of mature TGF-β1 during activation, highlighting the transition from the "open-hand" conformation in the latent form to the "closed-hand" conformation in the active form. Superposition of latent TGF-β1 (PDB 5VQF, cartoon representation without transparency) with the position of helix a3 (thumb) in active TGF-β1 (PDB 3KFD; cartoon representation with transparency). Residues closing the fastener are shown as red sticks.

2.2.2.4 The *contralateral* model

Although both the arm domain and the mature TGF-β1 dimer are relatively rigid, latent TGF-β1 as a whole remains a flexible complex, particularly in the linker regions and the loops connecting the more structural elements. This extrinsic flexibility has long complicated accurate structural modeling of the connection loops. As a result, the relative arrangement of the two prodomain monomers with respect to each other was unclear and for many years assumed to follow an "*ipsilateral*" model, in which each prodomain monomer embraced the mature cytokine on the same side (**Figure 4A**). Recent work from Nishimura's laboratory has demonstrated, using chimeric constructs, that the latent complex follows a "*contralateral*" organization of the arm-forearm domains (*55*). In this configuration, the arm domain of monomer A connects to the α2 helix of the forearm on the opposite side of the complex, thereby shielding the *contralateral* fingers of the mature TGF-β1 dimer (**Figure 4C**). This architecture implies that when mechanical forces are applied to LAP by RGD-binding integrins (cfr. **section 2.3.3**), tension is transmitted in a *contralateral* manner, rather than *ipsilateral* (**Figure 4 B, D**). The authors of this study claim that such configuration supports an entropy redistribution model for TGF-β1 activation by the αVβ8 (cfr. **section 2.3.3**). However, no clear justification from the authors regarding the functional implications of this orientation was provided, particularly with respect to maintenance of latency and force-dependent activation.

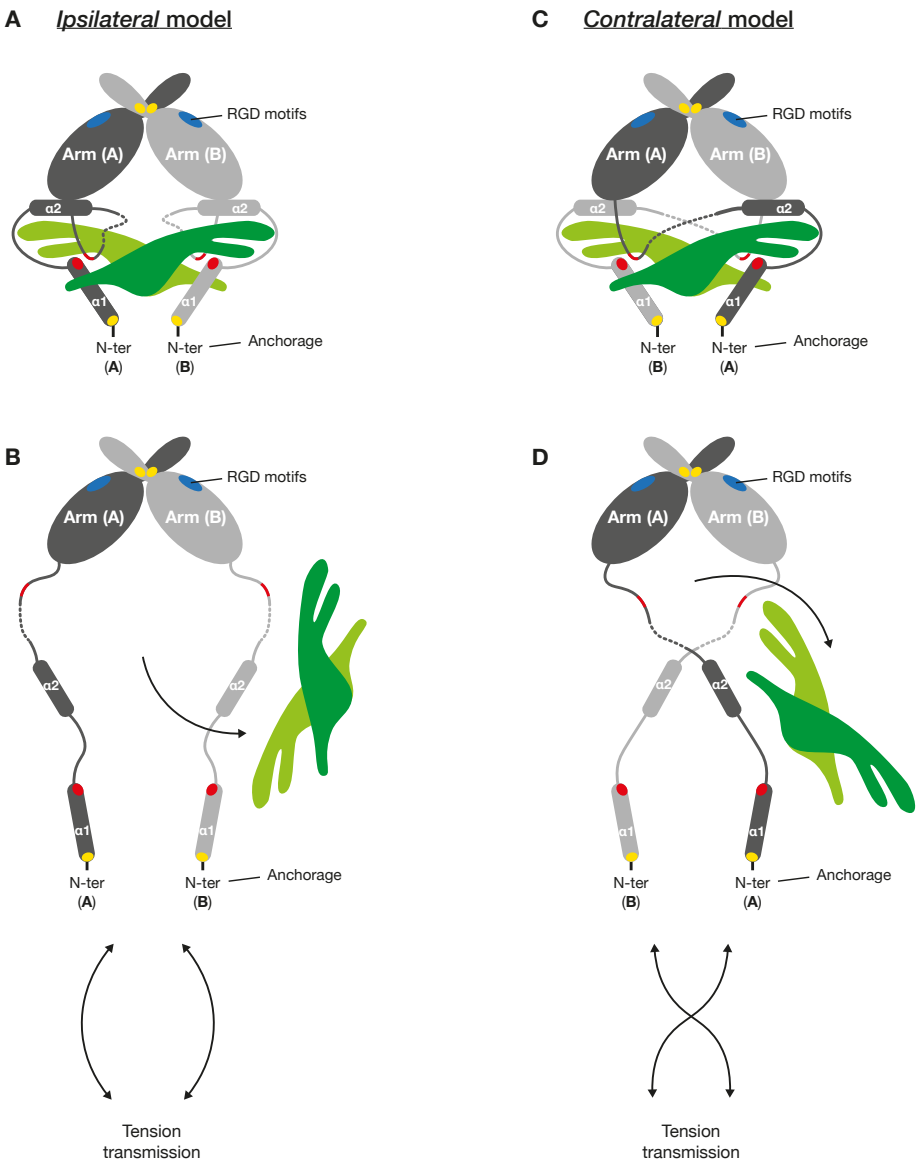

Figure 4: *Ipsi-* and *contralateral* models.
(**A**) Schematic representation of the formerly accepted *ipsilateral* model where the latency lasso of each monomer embraces mature TGF-β1 digits on the same side as its arm domain. (**B**) When RGD-binding integrins activate latent TGF-β1, forces are applied on top of the arm domain and resistance is met if the complex is anchored at the N-ter. In this model, tension is distributed following the *ipsilateral* distribution of the arm-forearm domains. (**C**) In the now newly demonstrated *contralateral* model, the latency lasso of each monomer crosses the complex and embraces mature TGF-β1 on the opposite side of its arm domain. (**D**) Accordingly, if forces are applied by RGD-binding integrins, tension is distributed across the complex to the opposite anchorage site.

2.2.3 Tethering of latent TGF-β1 and presenting proteins

The connection of the straitjacket N-termini to TGF-β1-presenting proteins further confines the mature TGF-β1, thereby stabilizing its latent form (*19*). Presenting proteins also anchor latent TGF-β1 on potentially tension resistant supports, such as ECM or cellular surfaces.

2.2.3.1 LTBPs

LTBPs are large extracellular glycoproteins composed of multiple domains (**Figure 5**). Their sequence includes tandem arrays of calcium-binding (**cb**) epidermal growth factor (**EGF**) repeats interspaced with **8-Cys** domains, which can be subdivided into; (i) TGFβ-binding (**TB**) domains (although most do not directly bind TGF-β), and (ii) **hybrid domains** that closely resemble TB domains, but also contain EGF-like features at their C-termini. In addition, LTBP1 and 2 also contain an N-terminal **4-Cys** domain that shares sequence similarity with the **fibrillin unique N-terminal region** (*56*). Despite their size and multidomain organization, the full 3D structure of a complete LTBP, or its complex with TGF-β1, has not yet been resolved. Nonetheless, the structure of the third 8-Cys domain – identified as the only 8-Cys domain capable of interacting with latent TGF-β1 – was solved by nuclear magnetic resonance (NMR) in 2003 (*57*). This globular domain, composed of six β-strands and two α-helices, is stabilized by four disulfide bonds. Notably, the "2-6" disulfide bond can be disrupted to associate with the LAP homodimer without unfolding the domain. The formation of interchain disulfide bonds is further facilitated by electrostatic interactions involving residues proximal to the reactive cysteines in each protein (*58, 59*). Following secretion, LTBPs are incorporated into the ECM, where they are proposed to associate with fibronectin through heparan sulfate proteoglycans via the hinge region (*60, 61*), and to interact with fibrillin through their C-terminal region (*56*).

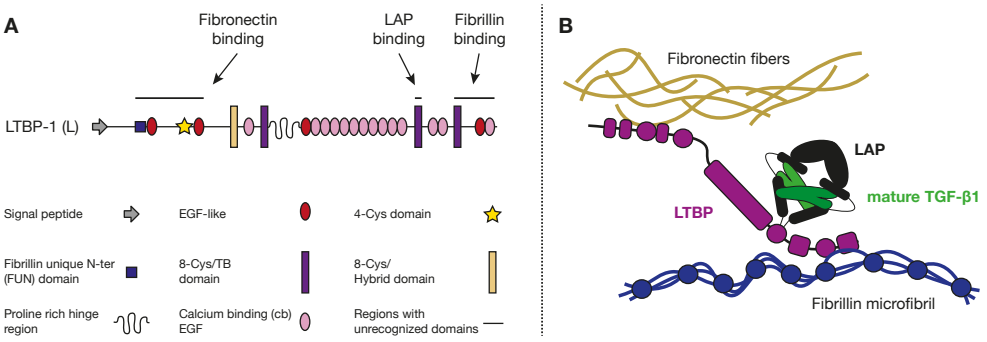

Figure 5: LTBPs structure and insertion into the ECM.
(**A**) Schematic representation of the multidomain structure of the long isoform (L) of LTBP-1. The fibronectin binding region, LAP binding region and fibrillin binding region are shown with a horizontal line and arrows. (**B**) Simplified schematic representation of latent TGF-β1-presenting LTBP anchored in the extracellular matrix (ECM). LTBP associates through its N-ter region to fibronectin and through its C-ter region to fibrillin. Adapted from Robertson et al., 2016 and Rifkin et al., 2022 (*21, 58*).

2.2.3.2 GARP and LRRC33

Both GARP:TGF-β1 and LRRC33:TGF-β1 complex structures have been solved, by X-ray crystallography for GARP (*52*) and by cryo-EM for LRRC33 (*40*). Although GARP and LRRC33 share only ~34% amino acid sequence identity, they display a similar structural organization, characterized by a short intracellular domain and a large extracellular leucine-rich repeat (LRR) domain containing the same number of repeats (*37-39*). The extracellular domain adopts a characteristic horseshoe-like tridimensional structure described as particularly well suited for protein-protein interactions (*62*).

More specifically, both proteins comprise 20 LRR motifs. Each motif typically consists of 20–30 residues enriched in hydrophobic amino acids such as leucine and asparagine. These repeats follow a conserved consensus sequence (LxxLxLxxNxL), where “L” refers to Leu/Ile/Val and “N” refers to Asn/Thr/Ser/Cys. This pattern drives each repeat to form a loop with a short β-strand around a hydrophobic core, and the sequential arrangement of repeats generates a solenoid-like fold forming the typical horseshoe-shaped scaffold. β-strands form hydrogen-bonded sheets along the concave surface, while the convex surface displays protruding secondary structures (loops and short α-helices) reflecting variations in LRR length. While GARP adopts a near-perfect circular arrangement, LRRC33 shows a more pronounced inward curvature in its central region (*40*) (**Figure 6**).

Both GARP and LRRC33 contain conserved cysteine residues (Cys211-Cys350 and Cys201-Cys341, respectively), enabling disulfide bonding with LAP Cys33 (*37-40*). In GARP:TGF-β1 and LRRC33:TGF-β1 complexes, latent TGF-β1 adopts a similar binding orientation on the lateral surface of the LRR proteins. The N-terminal region of the first LAP monomer (LAP_A) is sheltered within a hydrophobic pocket, while the N-terminal of the second monomer (LAP_B) remains exposed on the lateral surface of the LRR and is stabilized by van der Waals interactions. In addition, the α3 helix (thumb) and a loop (residues 323 to 337) of the mature TGF-$β1_B$ monomer form non-covalent interactions with the LRR proteins. A notable difference between the GARP:TGF-β1 and LRRC33:TGF-β1 complexes consists in a 35° rotational difference between the LRR proteins (**Figure 7**). However, it is important to note that the LRRC33:TGF-β1 complex was modeled without any additional binding partners, whereas the GARP:TGF-β1 structure was determined by X-ray crystallography in the presence of an anti-GARP:TGF-β1 antibody (not shown in Figure 7), which may account for a slight rotation in the complex (*40, 52*).

Although the overall structure of latent TGF-β1 remains conserved when binding to GARP or LRRC33, conformational changes are observed at the interface. These changes indicate that latent TGF-β1 is structurally flexible, facilitating its interaction with a variety of structurally diverse proteins, such as LRRs and LTBPs. Notably, cryo-EM analysis of the LRRC33:TGF-β1 complex shows this flexibility, especially in the loop containing the RGD motif, which may promote recognition by the integrins (*40*).

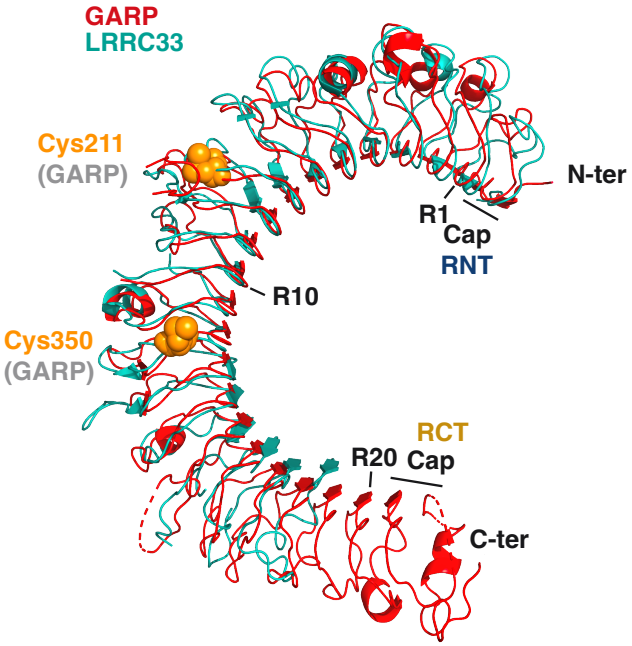

Figure 6: Overlay of GARP and LRRC33.
Figure reproduced from Fanny Lambert's thesis (48). Three-dimensional cartoon representation of GARP (red) and LRRC33 (blue), based on the GARP:TGF-β1 (PDB 6GFF) and LRRC33:TGF-β1 (PDB 7Y1R) complex structures determined by X-ray crystallography and cryo-electron microscopy, respectively. Leucine-rich repeat (LRR) motifs are labelled sequentially from R1 to R20. Cysteine residues involved in disulfide bond formation with LAP are indicated as orange spheres. Abbreviations: N-ter, N-terminus; C-ter, C-terminus; R, leucin-rich repeat; RNT, N-terminal leucine-rich repeat domain; RCT, C-terminal leucine-rich repeat domain.

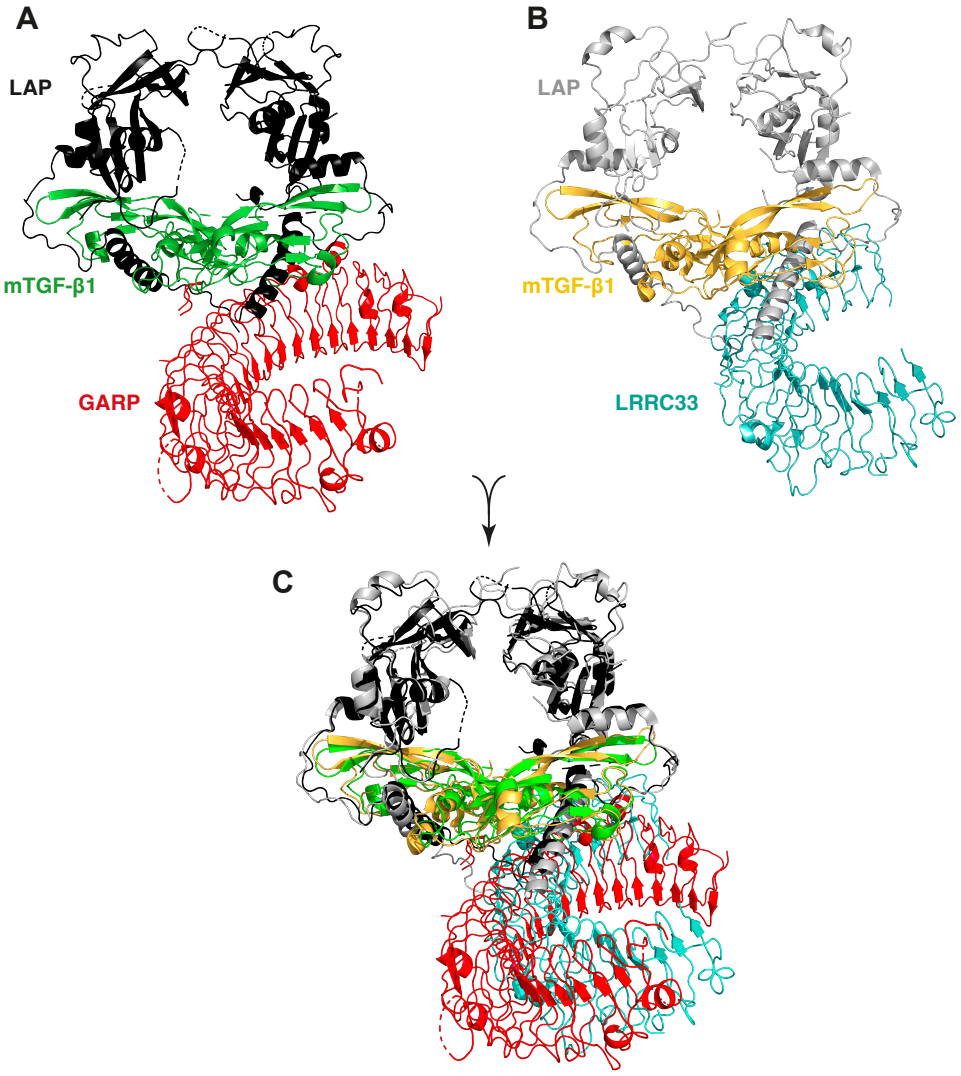

Figure 7: Individual or overlaid structures of GARP:TGF-β1 and LRRC33:TGF-β1 complexes. Figure reproduced from Fanny Lambert's thesis (*48*). Structural overlay of the L-TGF-β1:GARP and the L-TGF-β1:LRRC33 complexes (PDB 6GFF and 7Y1R, respectively), aligned on the L-TGF-β1 component. In comparison to GARP, LRRC33 exhibits an approximate 35° rotational shift around the L-TGF-β1 axis.

2.3 Activation

To bind its receptor, mature TGF-β1 must be released from the LAP or undergo a significant restructuring of the latent complex, a process referred to as “TGF-β1 activation”. Given the pleiotropic effects of TGF-β1 and the widespread production of its latent form, this process must be tightly controlled in space and time. Accordingly, TGF-β1 activation is limited to a restricted set of cell types, each relying on distinct molecular mechanisms to trigger bioavailability of the cytokine. First, proteolysis-dependent activation (involving plasmin, MMP-2, MMP-9, MMP-14 metalloproteases) has been frequently observed *in vitro*, though their relevance *in vivo* remains uncertain as they are poorly regulated and lack specificity. Another mechanism implicates Thrombospondin-1 (TSP-1), where this matrix-secreted protein competes with a portion of the LAP to release key amino acids from mature TGF-β1. Finally, the most described and probably the most relevant mechanism *in vivo* depends on the interaction of TGF-β1 presented by a tethering protein with an RGD-binding integrin, which facilitates the mechanical deformation of the latent complex (*17, 21*). While the *in vivo* relevance of some of those mechanisms remains unclear, studying them has revealed key principles of TGF-β1 activation. Importantly, understanding how latency is overcome also helps refine the molecular basis of the latent state described in **Section 2.2**. We therefore decided to systematically investigate these mechanisms to highlight key molecular requirements for both TGF-β1 latency and activation.

2.3.1 Proteolysis-dependent activation

2.3.1.1 Plasminogen/plasmin proteolysis

Proteolytic activation of latent TGF-β1 by plasmin was initially demonstrated *in vitro*, where plasmin efficiently cleaves the LAP and releases mature TGF-β1 (*63*). Plasmin is a trypsin-like serine protease that preferentially cleaves C-terminal to basic residues such as Lys or Arg with low motif constraints compared to other proteases (*64*). Its activity is further influenced by substrate accessibility, with flexible loops and solvent-exposed regions being favored cleavage sites (*65*). Since LAP contains many basic residues and solvent-exposed regions, plasmin may cleave at more than one location, and the precise cleavage site(s) have not been

clearly defined. Genetic evidence has consistently failed to support a dominant physiological role for plasmin-dependent activation, as plasminogen-deficient mice do not exhibit phenotypes characteristic of TGF-β1 deficiency (*66*). Accordingly, protease-mediated activation is now considered to occur primarily in pathological or highly proteolytic environments, rather than serving as a general mechanism of TGF-β1 activation *in vivo* (*21, 67*).

2.3.1.2 MMPs

Matrix Metalloproteinases (MMPs) also referred as matrix metallopeptidases are zinc-dependent proteases best known for their ability to degrade a wide range of extracellular matrix components to regulate tissue remodeling (*68*). Several MMPs have been reported to activate TGF-β1 through proteolytic cleavage of the LAP, including MMP-2, MMP-3, MMP-9 and MMP-14 (or MT1-MMP).

MMP-2 and MMP-9

MMP-2 and 9 activate TGF-β1 when localized at the surface of tumor cells where they can be recruited by CD44 (*69*) but their precise cleavage site(s) has not been clearly identified. Mice lacking both MMP-2 and MMP-9 display a normal phenotype under physiological conditions that do not recapitulate the severe defects associated with TGF-β1 deficiency which suggest a minor role in TGF-β1 regulation (*70*).

MMP-3

MMP-3 is reported to cleave LAP between **Ala79** and **Leu80** (**Figure 8**), a site located immediately upstream of the latency lasso within the α2 helix (patent: WO2005/023870) (*71*). Similar to MMP-2 and MMP-9, *Mmp3*$^{-/-}$ mice are viable and show no major abnormalities under normal conditions.

MMP-14

MMP-14 has been studied more extensively, in part because it can be recruited by the integrin αVβ8, another TGF-β1 activator (**cfr. 2.3.3.1**). Although definite MMP-14 cleavage motifs within LAP have not been established, MMP-14 preferentially recognizes PXXL motifs (**Figure 8**). LAP contains several solvent-accessible **PXXL** sites, including one within the latency lasso (Pro70), right next to a **PXXV** motif conserved in the α2 helix of all three TGFβ isoforms

(Pro74), that may therefore constitute another plausible target (*72*). Among MMP KO models, MMP-14-deficient mice display the most severe phenotype, characterized by osteopenia, dwarfism, and fibrosis. These abnormalities are generally attributed to defective collagen turnover, a key function of MMP-14, rather than to impaired TGF-β1 activation (*73*). Consistent with this, although Mmp2/Mmp14 double-KO mice die shortly after birth, their developmental defects do not closely match those of TGF-β-deficient animals (*74*).

2.3.1.3 Glycosidases

Finally, *in vitro* studies have shown that latent TGF-β1 can be activated by various glycosidases, including N-glycanase, sialidase and influenza virus neuraminidase (*75, 76*). Notably, sialidase NEU3 has been shown to desialylate LAP, promoting the release of mature TGF-β1, potentially through disruption of LAP conformation and/or weakening of electrostatic interactions that stabilize the latent complex (*77*). There are two identified N-glycosylation sites on LAP that could be targeted by NEU3, one of which is located within the α2 helix (**Asn82**) right after the MMP-3 cleavage site (**Figure 8**). But again, the physiological relevance of TGF-β1 activation through deglycosylation remains uncertain.
Together the *in vivo* data do not support a widespread or dominant role for plasmin, MMPs or other enzyme-mediated proteolysis in physiological TGF-β1 activation. However, all identified cleavage sites cluster within either the latency lasso or the α2 helix, highlighting these regions as key structural determinants of latency and implying that their disruption can trigger TGF-β1 activation through release of mature TGF-β1.

2.3.2 Interaction/conformation-dependent activation

2.3.2.1 ROS

Several studies have reported that reactive oxygen species (ROS) can promote TGF-β1 activation with *in vitro* (*78*), or suggest *in vivo* relevance in the context of radiation-induced injury (*79*). Mechanistic insight was subsequently provided by *in vitro* work demonstrating that **Met253** (**Figure 8**) within the LAP arm domain (just above the α2 helix) functions as a ROS-sensitive switch, enabling activation of TGF-β1 under oxidative conditions (*80*). In

experimental models of lung injury and fibrosis, ROS have further been implicated as critical amplifiers of TGF-β1 signaling, notably through NADPH oxidase-dependent pathways. Specifically, NOX4 activity is required for TGF-β1-driven myofibroblast activation, ECM deposition and fibrosis. NOX4 inhibition suppressed fibrosis (*81*). More recently, DUOX1 has been shown to sustain TGF-β1 signaling and to promote lung fibrosis (*82*). Nevertheless, while these studies strongly support a functional link between ROS and TGF-β1 activation/signaling *in vivo*, they only provide indirect evidence for ROS-mediated activation of latent TGF-β1.

2.3.2.2 Thrombospondin-1 (TSP-1)

Thrombospondin-1 (TSP-1) is a secreted ECM protein produced by various cell types, including platelets, endothelial cells, fibroblasts, smooth muscle cells, and immune cells. Although TSP-1 has multiple functions independent of TGF-β1, it has been proposed to act as an important activator of latent TGF-β1 (*83*). TSP-1-mediated activation involves its direct interaction with the LAP (*84*). A short sequence located within TSP-1 – commonly described as KRFK – has been proposed to interact with the **LSKL** motif (this lysine being implicated in the fastener) in LAP (**Figure 8**), thereby destabilizing the non-covalent association that maintains latency and enabling release of active TGF-β1 (*19, 83, 85-88*). Consistent with this model, KRFK peptide can mimic TSP-1-dependent activation of latent TGF-β1, whereas LSKL peptide inhibits activation, both in cell-based systems and *in vivo* (*85, 89*). *In vivo*, TSP-1 knockout (*Tsp1*$^{-/-}$) mice show a partial phenotypic overlap with *Tgfb1*$^{-/-}$ mice, including epithelial and vascular abnormalities in multiple tissues, supporting the hypothesis that TSP-1 contributes to physiological TGF-β1 activation during development. However, the comparatively mild inflammatory phenotype of *Tsp1*$^{-/-}$ animals relative to the severe autoimmune syndrome of *Tgfb1*$^{-/-}$ mice suggest that additional, non-redundant mechanisms of TGF-β1 activation are required for immune homeostasis (*89*). Finally, TSP-1 is implicated in wound healing by its modulation of cell adhesion, angiogenesis and matrix remodeling (*90*). The increase in TSP-1 expression following tissue injury supports the idea that TSP-1 may contribute to activation of the latent TGF-β complex during repair, consistent with the established role of TGF-β1 in wound healing (*91*). TSP-1 is also broadly expressed during development, where it may similarly contribute to TGF-β1 activation in multiple tissues (*92, 93*).

In conclusion, the review of these mechanisms highlights the **α2 helix**, the **latency lasso** and the **fastener** as a key structural determinants of TGF-β1 latency (**Figure 8**). A residue in the arm domain located in close proximity to the α2 helix, Met253, functions as a ROS-sensitive switch. Oxidation of Met253 may weaken the stabilizing association between the arm domain and the α2 helix, thereby promoting LAP destabilization and unfolding. Similarly, putative MMP cleavage sites appear to be enriched in the α2 helix or in the latency lasso, further emphasizing their role as critical structural elements in maintaining latency. Finally, TSP-1 may facilitate activation by disrupting the fastener, thereby preventing key residues from interacting and maintaining the latent clamp.

This short review of force-independent activation mechanisms indicates that, although the latent TGF-β1 complex is intrinsically stable, perturbation of core structural element supporting latency (here: α2 helix, fastener, latency lasso…) may be sufficient to destabilize the complex and trigger activation.

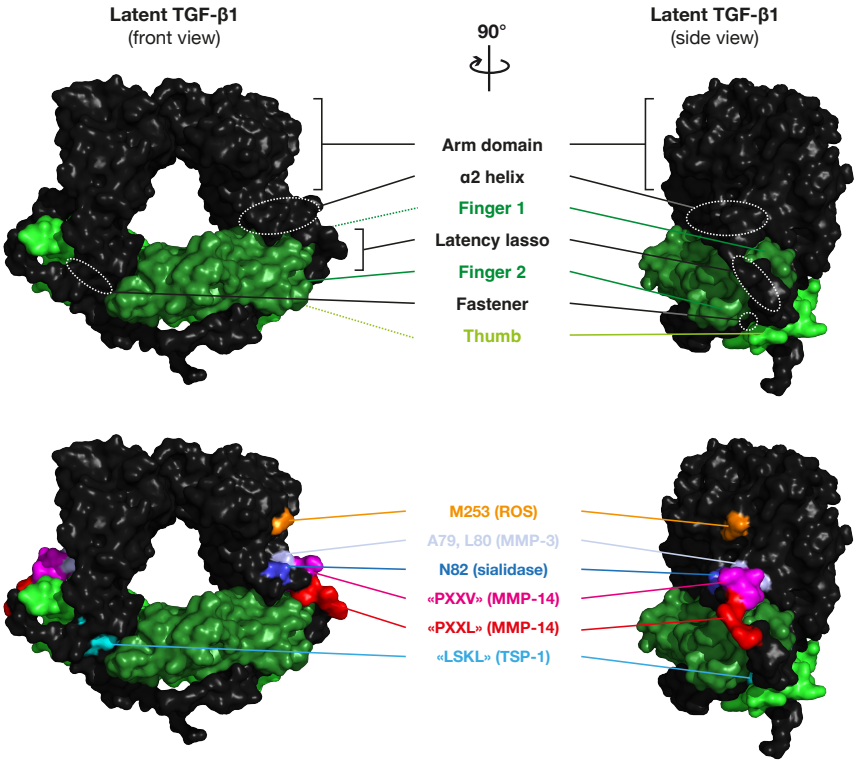

Figure 8: Key interaction and putative cleavage sites involved in TGF-β1 activation.
Surface diagram of the human latent TGF-β1 crystal structure reported by Lambert et al. (*51*) (PDB ID: 8REW). The top panel shows relevant structures presented in Figure 3, displayed in front or side view. LAP regions are shown in black, and the homodimer of mature TGF-β1 in two shades of green. Hidden structures in the front view are pointed with a dashed line. Particular attention should be paid to the **fastener** and the **latency lasso**, which wrap around the three fingers of mature TGF-β1. The bottom panel highlights sites relevant to TGF-β1 activation. These include reactive or interaction sites – **Met253** (a ROS-sensitive switch) in the arm domain and the **LSKL** motif recognized by TSP-1 at the fastener – as well as cleavage or enzymatic activity sites involved in activation such as: **Ala79** and **Leu80** (MMP-3), **Asn82** (sialidase), and **PXXV** and **PXXL** motifs (MMP-14). Interestingly, these sites cluster within or close to the **α2 helix**, the **fastener** or **latency lasso**, highlighting them as hubs for TGF-β1 activation. For clarity, the RGD motif and other sites considered less relevant (poorly accessible or distant from the mentioned structures) are not shown.

2.3.3 Force-dependent activation (integrins)

In vivo, force-dependent TGF-β1 activation is mediated by integrin binding to the RGD motif located in the arm domain of LAP. Upon binding, cytoskeleton-generated forces transmitted through the integrin induce unfolding of the LAP, ultimately leading to the release of mature TGF-β1. Integrins are a large family of proteins, but only a restricted subset of RGD-binding integrins – namely αVβ1, αVβ6, and αVβ8 – have been identified as ligands for latent TGF-β1 *in vivo*. Integrins αVβ3 and αVβ5 can also bind LAP, but with markedly lower efficiency (*94, 95*). Importantly, integrin structure, activation and signaling mechanisms are complex and not necessarily conserved across all family members.

Many mechanistic studies and structural models have relied on αIIbβ3 (and a limited number of other integrins) as a prototype. Although these models have provided fundamental insights, there is no universal consensus that all integrins strictly follow the same activation mechanism. The general concepts of integrin structure and activation have been extensively reviewed (*96-98*) and briefly summarized here to provide the necessary framework for understanding integrin-TGF-β1 binding and activation (**Figure 9**).

To date, no additional force-dependent mechanisms of TGF-β1 activation has been clearly demonstrated *in vivo*. Our lab recently developed monoclonal antibodies capable of activating TGF-β1 (*51*). Although structurally very distinct from integrins, their activity also appears to rely on force transmission, possibly through a partially overlapping mechanism. These mechanisms are discussed in more detail in **Section 5.2** and of the **Introduction**, as well as in the **Results** section and **Annexes** (Lambert et al., 2025) at the end of this manuscript.

2.3.3.1 αβ integrins

Integrins are heterodimeric transmembrane proteins composed of non-covalently associated α- and β-subunits. Together, these subunits form a globular **headpiece** supported by **two legs**. Each leg can be subdivided into **upper** and **lower** segments, while the headpiece comprises the ligand-binding head domain together with the upper legs. Eighteen α and eight β subunits assemble into 24 distinct integrin heterodimers with diverse biological functions (*99, 100*).

Integrins function as bidirectional signaling receptors, transmitting information from inside the cell to the extracellular space ("inside-out" signaling) and from ligand engagement back into the cell ("outside-in" signaling). Through these mechanisms, integrins regulate cell-cell and cell-ECM interactions. In the context of force-dependent TGF-β1 activation, we focus primarily on the inside-out signaling, which implies integrin intracellular activation, extracellular extension and ligand engagement. This process requires precise coordination among multiple structural domains, making a detailed understanding of integrin architecture essential.

The α chain ectodomain

The α chain ectodomain is composed of four or five extracellular domains, including a **β-propeller**, a **thigh**, and two **calf** domains. Nine of the eighteen α chains additionally contain an inserted **αI** domain within the β-propeller; these integrins do not belong to the RGD-binding subfamily and will not be discussed here. Two major points of interdomain flexibility are present within the α chain ectodomain: the linker between the β-propeller and thigh domains, and the **genu** (or "knee") between the thigh and calf I domains (**Figure 9A**). This knee is located near the corresponding bending region in the β chain (see hereafter), allowing coordinated extension of both subunits upon integrin activation (*96*).

The β chain ectodomain

The β chain ectodomain consists of seven domains connected by flexible linkers. A **βI** domain, which contains the ligand-binding site, is inserted within a **hybrid** domain, itself inserted in a plexin-semaphorin-integrin (**PSI**) domain. These are followed by four **I-EGF** segments and a **β-tail** domain (**Figure 9A**). Overall, the β leg is considered more flexible than the α chain, particularly at the junctions between the hybrid, PSI (knee), and I-EGF domains, facilitating large-scale conformational rearrangement during activation (*96*).

The core ectodomain interaction is formed between the αV β-propeller and the βI domain. Immediately below the headpiece, αV and β continue to interact through contacts between the αV thigh domain (upper leg) and β-subunit regions directly connected to the headpiece. These interfaces provide mechanical continuity between head and legs. In the lower ectodomain, αV's calf-1/calf-2 domains run alongside the β-subunit I-EGF repeats (and β tail domain), forming additional stabilizing α-β contacts that differ between bent and extended conformations (*101-104*).

Cation binding sites within the β chain

Ligand binding occurs at the interface between the α-chain β-propeller and the β-chain βI domain and is, in part, regulated by three adjacent metal-ion-binding sites within the βI domain: the metal-ion-dependent adhesion site (**MIDAS**), flanked by the adjacent to MIDAS (**ADMIDAS**) site and the synergistic metal-ion binding site (**SyMBS**) (**Figure 9A**). Binding of Mg^{2+} at MIDAS promotes headpiece opening and ligand binding, whereas Mn^{2+} can further stabilize the active conformation. Ca^{2+} binding at the SyMBS stabilizes the ligand-binding pocket and facilitates coordination with the MIDAS, while Ca^{2+} binding at the ADMIDAS stabilizes the low-affinity, inactive state. Consequently, loss or replacement of Ca^{2+} (e.g. by Mn^{2+}) at the ADMIDAS favors integrin activation (*96*).

The transmembrane helices

Both α and β subunits possess single-pass transmembrane (TM) helices whose close association via "paired" residues within the cellular membrane maintains integrins in an inactive state. This association is stabilized by electrostatic interactions between charged residues (the **GFFKR** motif in the α chain and the **LLITIHD** motif in the β chain) (**Figure 9A-C**) as well as by constraints imposed by the resting ectodomain (*98*).

The cytoplasmic tails and their ligands

The α and β subunits possess a short intracellular (IC) domain of approximately 15 and 45 amino acids (aa), respectively, although lengths vary among integrins. These IC tails are intrinsically flexible and generally lack stable secondary structure in the absence of binding partners. Direct interactions between α and β IC tails remains debated, but most studies agree that such interactions, if present, contribute minimally to signal transduction (*96, 105*).

Functionally, the α-chain IC tail has received relatively little attention, as few robust partner interactions have been identified. The best-characterized examples involve α4 and α9, which bind paxillin (*106, 107*). Beyond these cases, the principal contribution of the α tail lies in the conserved GFFKR motif, which stabilizes the inactive αβ complex through electrostatic interactions at the TM-IC interface as mentioned above.

In contrast, the β-chain IC domain contains two conserved NPxY-type motifs that serve as docking sites for cytoskeleton adaptor proteins. The membrane **proximal NPxY** motif is recognized by talin, while a **distal NPxY** motif recruits kindlin. Talin binding disrupts α-β tails

interactions by breaking the **salt bridges**, which promotes tail dissociation and extension of the ectodomain into the extended-closed conformation. Because talin also binds actin, it enables transmission of cytoskeletal forces that drive leg separation and headpiece opening (**Figure 9A-C**), yielding the fully active extended-open state (*98*).

Ligand binding (headpiece) and integrin activation

Ligand binding occurs upon integrin activation, which involves coordinated conformational changes across its multiple domains. Inactive integrins adopt a **bent-closed conformation**, positioning the headpiece near the plasma membrane and limiting ligand accessibility. As mentioned above, separation of the IC tails triggers ectodomain extension into an **extended-closed** conformation, increasing ligand accessibility. Ligand affinity is subsequently enhanced through two non-mutually exclusive mechanisms:

1) First, cytoskeleton-generated forces applied through the β IC chain can reshape the ligand-binding site, increasing its accessibility. Indeed, during extension and legs opening, the hybrid domain moves away from the β-propeller, increasing the angle between the hybrid domain and βI domain. This switch triggers reshaping inside the βI domain and a coordinated movement of two α helices (**α7** and **α1**) that shift the βI domain from low-affinity to high affinity by bringing in loops containing the cation-coordinating residues, following a classical “inside-out” signaling (**Figure 9A**).
2) Second, ligand engagement itself and interaction with ADMIDAS can induce structural rearrangement of the βI and hybrid domains, leading to the opening of the headpiece extracellularly and the separation of the α- and β-legs, positioning them in the **extended-open** conformation to efficiently transmit contractile forces from the cytoskeleton to the ligand. The headpiece opening also stabilizes the ligand-bound state and tightens the ligand-integrin interface, which increases affinity (*108*), following an “outside-in” signaling.

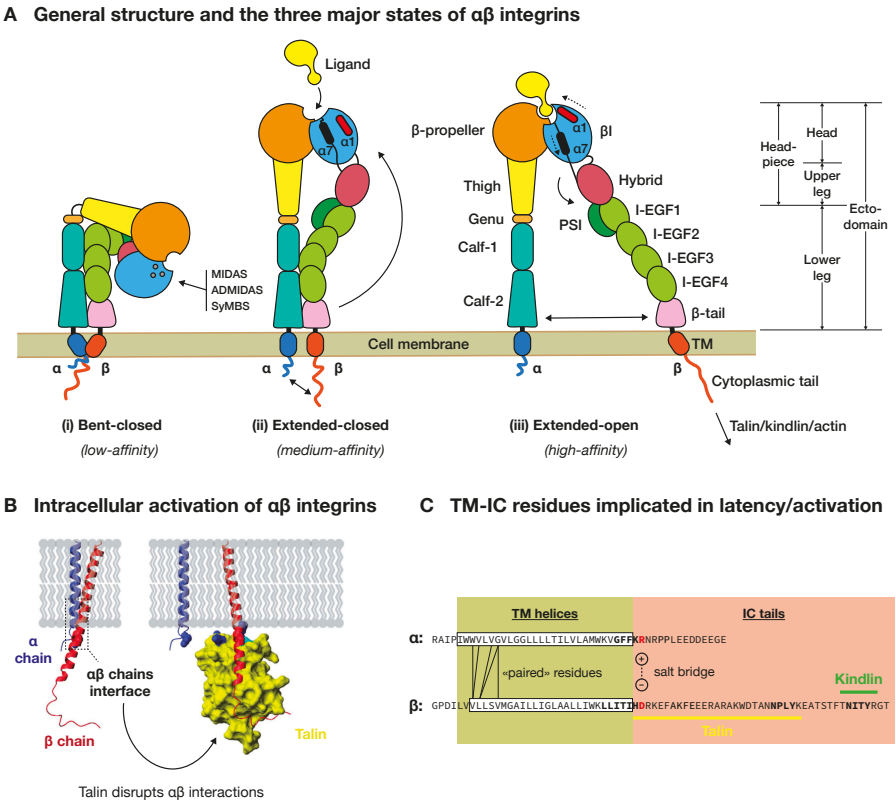

Figure 9: Structural organization and activation states of αβ integrins.
(**A**) Schematic representation of αβ integrin structure and activation. Major regions of the ectodomain are indicated, including the headpiece (head and upper leg) and the lower legs. The α chain comprises the β-propeller, thigh, genu, calf-1/2, transmembrane (TM) domain, and cytoplasmic tail, whereas the β chain comprises the βI, hybrid, and PSI domains, the I-EGF1–4 repeats, the β-tail, TM domain, and cytoplasmic tail. Metal-ion binding sites (MIDAS, ADMIDAS, SyMBS) are shown as grey circles in the βI domain, together with the α1 (red) and α7 (black) helices. Three conformational states are illustrated: (i) bent-closed (resting, low affinity), with the headpiece oriented toward the plasma membrane and association of the α and β TM domains; (ii) extended-closed (intermediate affinity), characterized by ectodomain extension and dissociation of the TM domains; and (iii) extended-open (high affinity, mechanosensitive), characterized by headpiece opening, hybrid-domain swing-out, separation of the legs, rearrangement of the α1 and α7 helices in the βI domain, and cytoskeletal engagement through the β cytoplasmic tail (e.g., talin/kindlin/actin). (**B**) Cartoon representation of the α and β TM and intracellular (IC) domains (adapted from Anthis et al., 2009) (*109*). In the resting state (left), the α and β TM helices interact through paired residues and a stabilizing salt bridge. Binding of adaptor proteins (e.g., talin) disrupts these interactions (right), promoting TM separation and integrin activation. (**C**) Amino-acid sequences of the α and β TM and IC domains (shown here for αIIb and β3; adapted from Wegener et al., 2008) (*98*). Residues mediating TM helix pairing are connected by black lines. The conserved α–β salt-bridge residues are highlighted in red (with annotated charges) and linked by a dashed line. Functional motifs are indicated in bold (GFFKR in the α chain; LLITIHD and NPLY/NITY in the β chain). The talin-binding region is underlined in yellow and the kindlin-binding region in green.

In summary, integrin activation follows the indicated sequence of events: Inactive (**bent-closed**) → IC tails separation → extracellular extension (**extended-closed**) → initial ligand binding → actin cytoskeleton engagement, leg extension and headpiece opening, increased affinity (**extended open**) (**Figure 9A**). These three conformations are in dynamic equilibrium. While each state can coexist under physiological conditions, the equilibrium can shift toward either low-affinity or high-affinity states depending on the regulatory context.

RGD-binding integrins and TGF-β1 activation

Integrins can be broadly classified into three functional groups based on ligand specificity; fibronectin and cell adhesion molecules (CAMs)-binding integrins, laminin/collagen-binding integrins, and RGD-binding integrins, which are the focus of this section.

RGD motifs are abundant within the ECM and can be recognized by RGD-binding integrins. However, a subset is specialized in the recognition of the RGDLXX(L/I) motif (RGD-LATI) in the LAP (latent TGF-β1). This motif in the shoulder region of the arm domain lies opposite to the cysteine residues responsible for covalent linkage of LAP to tethering proteins such as LTBPs or GARP (*94, 110*). This organization strongly supports a mechanical activation model in which pulling and retention forces applied in opposite directions – through integrin binding on one side and anchoring to presenting proteins on the other – induce unwrapping of the LAP and release of mature TGF-β1 (**Figure 10**).

The relevance of RGD-binding integrins in TGF-β1 activation has been demonstrated *in vivo*, notably using *Tgfb1*$^{RGE/RGE}$ mice in which the aspartate residue is replaced by a glutamate residue, thereby preventing recognition by integrins. Similar to *Tgfb1*$^{-/-}$ mice, *Tgfb1*$^{RGE/RGE}$ mice die from vascular problems during embryonic development or from inflammation affecting multiple organs around 3 weeks of age, despite having normal levels of latent TGF-β1 (*111*).

To date, only three RGD-binding integrins – αVβ1, αVβ6, and αVβ8 – have been demonstrated to activate latent TGF-β1 *in vivo*. Although RGD motifs are present in many proteins, notably within the ECM, αVβ6, and αVβ8 appear to bind preferentially to TGF-β. This specificity can be explained by distinct structural features (*40, 94*).

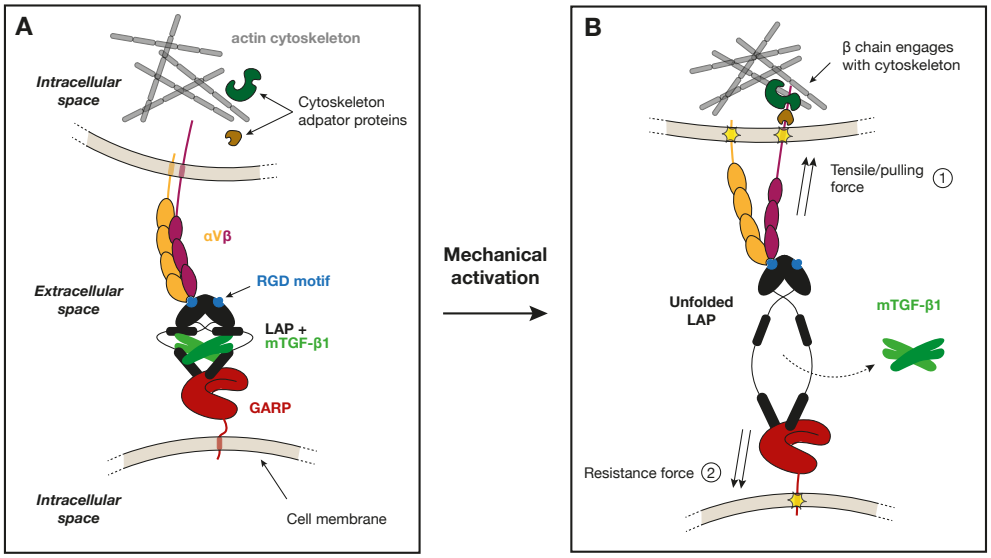

Figure 10: Mechanical activation model of TGF-β1 by RGD-binding integrins.
Simplified schematic representation of the integrin-mediated mechanical model (**A**) αVβ integrins bind the RGD motif located in the arm domain of LAP. (**B**) Following integrin intracellular activation, cytoskeleton-generated tensile/pulling forces (1) are transmitted through the integrin to the covalently linked latent complex, where they encounter opposing resistance forces (2). The combination of these forces leads to conformational changes and unwrapping of LAP. Anchorage points are highlighted by yellow stars.

* *αVβ1*

Individually, the αV and β1 subunits are implicated in numerous integrin heterodimers and are broadly expressed across tissues. In contrast, expression of the αVβ1 heterodimer is restricted to a limited subset of cells, complicating functional analyses based on genetic deletion. Indeed, global or conditional inactivation of αV or β1 disrupts multiple integrin complexes, making it difficult to attribute phenotypes specifically to αVβ1.

To overcome these limitations, Dean Sheppard and colleagues developed αVβ1-specific inhibitory molecules and combined their use with selective inactivation of other αV-containing integrins. Using activated fibroblasts – which express integrins αVβ1, αVβ3, αVβ5, and αVβ8 – and by blocking the three other β subunits individually or collectively in combination of their newly developed inhibitor, they demonstrated that αVβ1 plays a non-redundant role in TGF-β1 activation in these cells (*112*).

Mechanistically, αVβ1 expressed by myofibroblasts activates TGF-β1 through interaction with the latent complex presented by LTBPs within the ECM. This activation is strongly enhanced by myofibroblast contractility and is highly sensitive to the mechanical properties of the ECM, being promoted by increased matrix stiffness and markedly reduced in more compliant environments (*113*). These findings support a classical force-dependent activation model.

* *αVβ6*

The integrin αVβ6 is exclusively expressed in epithelial cells. Its expression is upregulated following tissue injury or inflammation, consistent with a role in barrier repair and immune regulation. Mice lacking the β6 subunit (*Itgb6*$^{-/-}$) develop a mild but chronic inflammatory phenotype, characterized by hair loss, hyperreactive airways, and accumulation of activated lymphocytes in the lung (*114*). Notably, these mice are also protected from fibrosis, a pathological process in which excessive TGF-β1 signaling plays a central role (*18*).

In vitro studies have established that binding of αVβ6 to latent TGF-β1 is necessary but not sufficient for activation. Two additional requirements must be met: (i) anchoring of the latent complex to a presenting protein such as LTBP-1 or GARP, and (ii) coupling of the β6 cytoplasmic tail to the actin cytoskeleton (*18, 25, 60*). Together, these observations support a mechanical activation model in which cytoskeleton-generated forces are transmitted through αVβ6 to induce LAP deformation and TGF-β1 release.

Structural studies have provided a detailed molecular basis to explain the high affinity of αVβ6 to LAP. The RGD motif of LAP is located within a flexible, solvent-accessible loop directly connected to the rigid arm domain and oriented opposite to the tethering site. Upon binding to αVβ6, the RGD inserts into a deep pocket formed at the interface between the αV β-propeller and the β6 βI domain. The RGD is followed by the LXXL/I motif (“LATI”), which adopts an amphipathic α-helix that engages a hydrophobic pocket within the βI domain. In addition, three specificity-determining loops (SDLs) from the β6 βI domain establish extensive contacts with LAP, creating a highly interdigitated interface that enforces a precise orientation between integrin and ligand (*94*) (**Figure 11**).

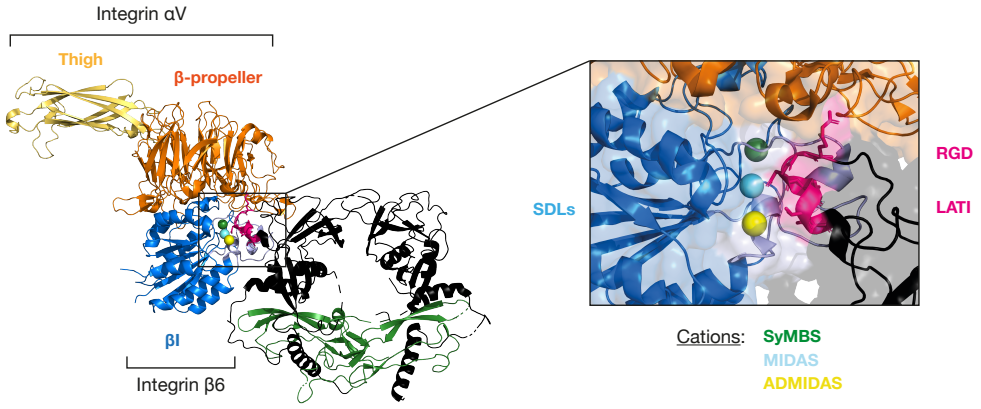

Figure 11: Integrin αVβ6 ligand binding site (illustrated with TGF-β1).
Cartoon representation of the crystal structure of the αVβ6 headpiece in complex with latent TGF-β1 (PDB: 5FFO; Dong et al., 2017) (*50*). The same color code as in Figure 9A is used: the αV β-propeller is shown in dark orange, the thigh domain in light yellow, and the βI domain in dark blue. A magnified view of the interaction interface highlights the specificity-determining loops (SDLs) of the βI domain (sky blue), the LAP RGDLATI motif (magenta, shown as sticks), and coordinated metal ions (green: SyMBS; cyan: MIDAS; yellow: ADMIDAS).

As a consequence, αVβ6 binds latent TGF-β1 with an affinity up to 1,000-fold higher than that observed for other RGD-containing ligands. This extraordinary affinity (with a K_d down to 0.18 nM) likely reflects a functional specialization of αVβ6 toward TGF-β activation rather than classical adhesive or migratory roles.

Building on this structural framework, computational simulations performed by Timothy Springer's group demonstrated that traction forces applied through the β6 subunit are efficiently transmitted via the rigid integrin arms to the LAP fastener region. Disruption of these stabilizing interactions induces elongation of the latency lasso, ultimately releasing mature TGF-β1 (*50*). In contrast, force application through the αV subunit fails to induce comparable structural rearrangements, highlighting the asymmetric role of the β6 chain in force transmission. Note that only the head (integrin αV β-propeller and thigh, integrin β6 βI domain) was used in this simulation.

* *αVβ8*

Expression pattern and in vivo relevance

Integrin αVβ8 is expressed by a broad range of cell types, including epithelial cells (*115, 116*), fibroblasts (*117*), dendritic cells (DCs) (*118, 119*), monocytes (*120*), and regulatory T cells (Tregs) (*121, 122*). Consistent with this wide expression pattern, genetic ablation of β8 results in a severe phenotype: *Itgb8*$^{-/-}$ mice die either in utero or shortly after birth due to vascular defects (*123*). Similar phenotypes are observed upon conditional deletion of β8 in neuroepithelial or glial cells, highlighting a critical role for αVβ8-mediated TGF-β signaling in vascular development and stability within the central nervous system (*124*).

Tissue-specific deletion studies further support a context-dependent role for αVβ8 in immune and inflammatory regulation. Conditional inactivation of *Itgb8* in fibroblasts leads to pulmonary fibrosis and asthma (*117, 125*), whereas deletion in DCs results in autoimmune colitis and encephalomyelitis (*118, 126, 127*). In contrast, conditional deletion in Tregs does not cause overt spontaneous pathology, although these cells exhibit a reduced capacity to restrain inflammatory responses under challenge conditions (*122*). Collectively, these findings indicate that αVβ8-dependent activation of TGF-β1 is a key contributor to immune homeostasis, with cell type-specific requirements.

Proposed mechanisms of TGF-β1 activation by αVβ8

In contrast to αVβ6, the mechanism by which αVβ8 activates latent TGF-β1 remains incompletely resolved and may vary depending on the cellular context. In epithelial cells and monocytes, αVβ8-mediated activation requires recruitment of the transmembrane metalloprotease MMP14 (MT1-MMP), which cleaves LAP and thereby releases active TGF-β1 (*116, 120*). In this protease-dependent model, the IC domain of β8 is dispensable, suggesting that classical force transmission through the cytoskeleton is not required.

However, this mechanism does not appear to be universal. In Tregs, inhibition of metalloproteases, including MMP14, does not prevent αVβ8-dependent production of active TGF-β1 (*121, 128*). Instead, activation in this context requires retention of latent TGF-β1 at the cell surface by GARP, pointing towards a non-proteolytic, potentially force-dependent mechanism analogous to that described for αVβ6 (*25, 27, 40*).

Structural and signaling particularities of αVβ8

Several structural and signaling features distinguish αVβ8 from other αVβ integrins known to activate TGF-β1. Notably, the β8 cytoplasmic tail lacks canonical NPXY motifs, precluding binding of talin and kindlin, which are essential for integrin activation and force transmission in αVβ1 and αVβ6 (**Figure 12**). Alternative interaction motifs have been identified within the β8 IC domain and proposed to bind members of the Band 4.1 family (*129-131*) and spinophilin, potentially linking αVβ8 to the cytoskeleton through non-classical adaptors (*132*). However, the functional relevance of these interactions for TGF-β1 activation remains unexplored.

Another defining feature of αVβ8 is its constitutively extended-closed conformation, which contrasts with the bent resting state adopted by most integrins. Notably, αVβ8 resides in the extended-closed conformation, even in the presence of ligand, with limited examples of the extended-open state. This property is likely due to two structural aspects: (i) the absence of conserved residues (LLITIHD) required for stabilizing interchain electrostatic interactions between the α and β subunits (*133*), (ii) the absence of two conserved cysteines within the I-EGF3 domain that would otherwise stabilize the bent conformation (*134*). Consequently, αVβ8 may bypass the need for an inside-out activation step to reach the extended-closed state. Furthermore, the β8 subunit lacks the ADMIDAS cation-binding site within the βI domain, a feature that is critical for headpiece opening in other αVβ integrins. In principle, this should preclude adoption of the canonical extended-open conformation (*49, 133, 135*). Nevertheless, even in the extended-closed state, αVβ8 displays incredibly high affinity (K_d = 0.013 nM) for latent TGF-β1 – thanks to distinct α loop/α helix coupling in the βI domain – which may be sufficient to support force-dependent activation (*135*).

To note, in the extended-closed conformation, αVβ8 remains a stable heterodimer with the α and β legs largely apposed (**Figure 12**), while headpiece opening is prevented by the absence of hybrid-domain swing-out (*134*).

Competing structural models for αVβ8-mediated TGF-β1 activation

Recent cryo-EM studies by Stephen Nishimura and colleagues have provided new structural insights into the αVβ8:latent TGF-β1 complex. These analyses revealed substantial flexibility within both the integrin ectodomain – particularly at the lower leg – and regions of TGF-β1 distal to the binding interface, resulting in rotational freedom around the integrin headpiece (*49, 55, 136*). Based on these observations, the authors proposed that αVβ8-mediated

activation may not rely on the generation of mechanical forces to fully release mature TGF-β1 from LAP like proposed for αVβ6. Instead, they suggest that conformational flexibility may permit exposure of the mature cytokine to a TβRI:TβRII heterodimer – rather than the canonical receptor heterotetramer – at the surface of the TGF-β1 expressing cell, thereby initiating a minimal signaling cascade without complete liberation of the mature cytokine, in an autocrine manner.

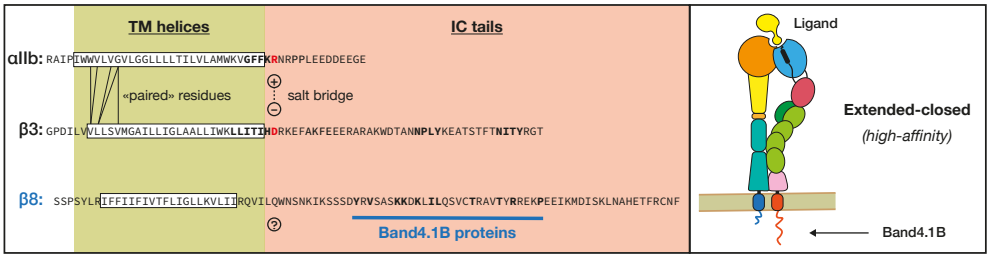

Figure 12: Atypical integrin αVβ8 properties.
(**Left**) Based on Figure 9C, comparison of the β8 cytoplasmic tail with other β integrin family members (here, β3) reveals that the typically conserved LLITIHD and NPxY motifs are absent in β8. Instead, the β8 IC tail contains Band 4.1-binding motifs highlighted in bold and underlined by a blue line. (**Right**) This structural divergence is associated with a constitutive preference for the extended-closed conformation, characterized by high ligand affinity. This state may be stabilized, at least in part, by the reduced association between the α and β TM-IC domains.

Taken together, studies on αVβ1, αVβ6, and αVβ8 establish RGD-binding integrins as key mediators of spatially and mechanically controlled TGF-β1 activation *in vivo*. While all three integrins recognize the conserved RGD motif within LAP, they differ substantially in cell-type expression, structural organization, and modes of force transmission, resulting in distinct and context-dependent activation mechanisms. Whereas activation by αVβ1 and αVβ6 can be explained by relatively well-defined traction-based models, the mechanism by which αVβ8 activates latent TGF-β1 remains only partially understood, with evidence supporting both protease-dependent and non-proteolytic pathways, and several structural aspects still poorly defined. Notably, the roles of the β8 IC domain and the cytoskeleton in αVβ8-dependent TGF-β1 activation remain unclear in most cell types. Finally, it is still unresolved whether integrin-mediated TGF-β1 activation can occur in cis (i.e., within the same cell co-expressing latent TGF-β1 and an RGD-binding integrin). Examples of *trans*-activation were highlighted in the literature but *cis*-activation remains challenging to demonstrate.

3 TGF-β1 activation: by whom, how, when and where?

As mentioned previously, TGF-β1 activation is cell-type- and context-dependent. As a result, the literature contains complex information that makes broad generalization difficult. In the following section, we therefore highlight selected examples of what is currently known (or not known) about TGF-β1 activation across different cell types. This overview represents only a fraction of the available work and is not intended to capture the full complexity of TGF-β1 bioavailability in tissues.

3.1 Epithelial cells

Epithelial cells form protective tissue barriers and actively shape local inflammation and tissue remodeling by sensing environmental signals and secreting cytokines. They are among the best-established activators of latent TGF-β1 *in vivo*, notably via integrin αVβ6, in settings such as tissue repair and fibrosis, particularly in the lung (*18, 96, 137*). In these contexts, activation is generally thought to occur from ECM-sequestered latent TGF-β1 pools, where the latent complex is tethered to the matrix through LTBPs. Accordingly, epithelial αVβ6-driven activation is linked to LTBP-dependent matrix presentation, rather than to GARP- or LRRC33-mediated surface display, although contributions from latent TGF-β1 presented by neighboring cells was proposed to control the epithelial residence of DCs and memory $CD8^+$ T cells (*19, 67, 115*). It was also suggested that epithelial cells could activate TGF-β1 through an αVβ8 and MMP-14-dependent mechanism (*116*).

3.2 Myeloid cells

Myeloid cells are innate immune cells – such as monocytes, macrophages, and DCs – that provide early defense and tissue surveillance by sensing danger signals, producing cytokines, and orchestrating adaptive immune responses. They represent a major immune source of TGF-β1 activation, largely mediated by integrin αVβ8, notably in DCs (*110, 119*). In human

monocytes, this process is MMP-14-dependent (*120*) although the mechanism in other lineages remains unclear. In these cells, LRRC33 emerged as the key presenter that anchors latent TGF-β1 for integrin-mediated activation. Early work in acute myeloid leukemia (AML) models showed that LRRC33 co-localizes and forms complexes with latent TGF-β1 at the cell surface, and that TGF-β1 activation in these myeloid leukemia cells requires integrins – supporting LRRC33 as a functional regulator of myeloid TGF-β1 bioactivity (*37*). This observation was then extended *in vivo* to the central nervous system (CNS), where LRRC33 on microglia – immune cells of the myeloid lineage – was shown to enable highly localized integrin αVβ8-dependent activation of latent TGF-β1 by astrocytes, with *Lrrc33*$^{-/-}$ mice developing reactive microglia and lethal neurodegeneration (*38*). More recently, LRRC33-dependent TGF-β1 activation was directly linked to tumor immune evasion, as loss of LRRC33 on tumor-infiltrating myeloid cells impaired surface display and latent TGF-β1 activation, slowed tumor growth and metastasis, and enhanced innate and adaptive anti-tumor immunity across syngeneic models (*41*).

3.3 Regulatory T cells

Regulatory T cells (Tregs) are a specialized subset of CD4^{+} T lymphocytes that maintain immune tolerance and prevent excessive immune responses. Tregs represent the most clearly defined example of GARP-dependent latent TGF-β1 activation (*138*). Upon antigen-dependent stimulation, Tregs upregulate GARP and integrin αVβ8 and generate active TGF-β1, establishing a membrane-tethered latent pool that can be activated in a TCR-stimulation-dependent manner (*27, 30, 52, 110, 122, 139*). Consistent with this model, TGF-β1 activation by Tregs can be blocked by antibodies targeting GARP, αV or β8 subunits *in vitro* and *in vivo* (*121*). Functionally, this pathway enables highly localized TGF-β1 activation within suppressive niches such as tumors and is strongly associated with immune evasion (*140, 141*). To note, stable expression of GARP and αVβ8 appears insufficient to enable TGF-β1 activation in the absence of TCR stimulation, suggesting that additional activating partner(s) are required (*121*).

3.4 B cells

B cells are adaptive immune lymphocytes involved in humoral immunity through antibody production and can also regulate immune responses through antigen presentation and cytokine secretion. Similarly to Tregs, our group has demonstrated that B cell receptor (BCR)-stimulated B cells express GARP:TGF-β1 complexes on their surface and can activate TGF-β1 *in vitro* (*29*). BCR-stimulated B cells have not been found to express any RGD-binding integrins so far. Therefore, activation is more likely to occur in *trans* by interaction with integrin-expressing cells, such as subepithelial dendritic cells in Peyer's patches, which express integrin αVβ8, or through an alternative mechanism (*29, 142, 143*).

3.5 Mesenchymal stromal cells

Mesenchymal stromal cells (MSCs) are multipotent stromal cells capable of differentiating into connective tissue lineages such as osteoblasts, chondrocytes, and adipocytes, and they contribute to tissue repair and immunomodulation. MSCs are suggested to possess immunomodulatory functions through GARP-mediated TGF-β1 activity, as silencing of GARP reduces the ability of mouse MSCs to inhibit T cell proliferation *in vitro* (*34, 144*).

3.6 Platelets

Platelets are anuclear fragments originating from megakaryocytes that contribute to hemostasis and to other processes such as wound healing, angiogenesis, inflammation, and immunity by releasing α-granule contents upon activation, including large stores of latent TGF-β1. In this context, TGF-β1 can be secreted and deposited with LTBPs in the ECM (*145, 146*) or, presented at their surface via GARP (*30, 147, 148*). Originally, platelets were thought to activate TGF-β1 in a TSP-1-dependent mechanism (*85, 87, 149*). However, this model was challenged by experiments showing that platelets from *Tsp1*$^{-/-}$ mice stimulated *in vitro* still generate active TGF-β1 and that TSP-1 inhibitors do not prevent TGF-β1 activation. These platelets, when exposed to thrombin (a protease produced during blood clotting and known to induce platelet activation), produced as much active TGF-β1 as WT platelets (*150, 151*).

Indeed, it was more recently proposed that thrombin promotes GARP-dependent TGF-β1 activation by cleaving GARP at two sites, thereby destabilizing the GARP-latent TGF-β1 complex and enabling the release of active TGF-β1 (*152*). Finally, in addition to the involvement of tethering proteins, potential other « physical » mechanisms have been suggested to mediate TGF-β1 activation. Since platelet-derived latent TGF-β1 is present in the circulation, intravascular shear force was proposed as a traction force contributing to TGF-β1 activation in the circulation (*153*).

3.7 Hepatic stellate cells

Hepatic stellate cells (HSCs) are resident perisinusoidal cells located in the subendothelial cell spaces between hepatocytes and sinusoidal endothelial cells. HSCs contribute to liver development, regeneration, metabolic processes and immune regulation. They are also implicated in liver fibrosis in the case of liver injury by producing excess ECM. HSCs express GARP and produce latent TGF-β1. In a study using HSCs from TGF-$\beta1^{+/-}$ mice (since *Tgfb1*$^{-/-}$ mice are not viable), these cells showed a reduced ability to suppress T-cell activity compared with WT HSCs, and TGF-β signaling inhibition increased T-cell proliferation and IFN-γ production. Moreover, silencing GARP on HSCs impaired their capacity to suppress activated T cells, supporting a key role for GARP in this process. Together, these findings suggest that HSCs may activate TGF-β1 through a GARP-dependent mechanism (*35*). Florian Winau's group further showed that GARP expression on HSCs is required to induce liver fibrosis *in vivo*. In a NASH fibrosis model induced by diet, mice lacking GARP specifically in HSCs were protected from disease, and GARP-deficient HSCs failed to activate TGF-β. Moreover, inhibition of integrin αV also blocked TGF-β activation, indicating that both GARP and αV integrins are required for HSC-mediated TGF-β activation (*154*).

3.8 Fibroblasts and contractile stromal cells

Fibroblasts and contractile stromal cells are key mediators of tissue remodeling, generating extracellular matrix and mechanical forces that shape repair and fibrotic responses. They drive local latent TGF-β1 activation during wound healing, fibrosis, and tumor-associated remodeling, in contexts where ECM architecture and mechanical forces favor activation (*113, 155*). Stress and inflammatory signals enhance fibroblast production of latent TGF-β1 (*156*), which is frequently stored in the ECM as LTBP1-bound complexes (*157*) and is thought to be activated predominantly from these LTBP-tethered reservoirs rather than from GARP- or LRRC33-bound pools (*67, 96*), although GARP has been reported in lymph node fibroblasts and associated ECM (*158*). Mechanistically, both integrin- and protease-dependent pathways contribute, as αVβ1 inhibition reduces fibroblast-mediated activation in fibrosis models (*112*) and MMP-9 recruitment to the cell surface promotes activation, likely via LAP cleavage (*69, 159*).

3.9 Endothelial cells

Endothelial cells form the inner lining of blood and lymphatic vessels and regulate vascular homeostasis, inflammation, and tissue remodeling by controlling barrier function. They have been suggested to contribute to TGF-β1 activation during vascular remodeling, inflammation, and angiogenesis, although the dominant activation routes appear more context-dependent than in epithelial or dendritic lineages (*67, 160*). In many vascular environments, latent TGF-β1 is abundant within the basal membrane and perivascular ECM, supporting an important contribution of LTBP/ECM-associated reservoirs as a major source of activatable cytokine (*67*). GARP has also been reported on endothelial cells *in vivo* (*31*) and on blood endothelial cells in lymph node environments (*158*). Additionally, GARP-expressing mouse liver sinusoid endothelial cells have been shown to induce the differentiation of naïve T cells into Treg cells in co-culture assays, suggesting that GARP may contribute to TGF-β1 activation by endothelial cells (*161*). To this day however, the exact role of GARP in endothelial cells-mediated TGF-β1 activation remains incompletely resolved.

It has been proposed that endothelial TGF-β1 activation relies more on cooperation with other cells, such as mural cells, than on endothelial cells alone (*162*). Mural cells are either smooth muscles cells in veins and arteries or pericytes in capillaries, they are highly complex and essential in angiogenesis and vasculature maturation (*162*). Early co-culture studies showed that mural cells enable TGF-β-dependent growth arrest of blood endothelial cells, an effect abrogated by TGF-β1 neutralization (*163*), and more recent 3D models support a role for stromal partners in shaping vessel growth through TGF-β signaling (*164*). While the precise molecular mechanism of activation in these multicellular settings remains unresolved, these observations suggest that vascular niches combine pericellular interactions, ECM anchoring, and mechanical remodeling to promote local TGF-β1 activation (*162, 165*).

Mechanistically, integrins could contribute to endothelial-associated TGF-β1 activation, as αVβ6 and αVβ8 have been detected on unstimulated HUVECs (*142, 158*), while angiogenic endothelium also expresses αVβ3 and αVβ5, which primarily support migration on RGD-containing ECM ligands (*166*). However, because αVβ3 and αVβ5 do not efficiently bind or activate latent TGF-β1 in reconstituted systems (*94*), any contribution to activation is likely indirect and context-dependent (*167*). Protease-mediated remodeling may further contribute, as MMP-14 can cleave ECM components including LTBP-1 (*168, 169*), although active TGF-β signaling was not clearly detected in endothelial monocultures following MMP-14-dependent ECM degradation (*169*).

Together, these data support a model in which endothelial-associated TGF-β1 activation is largely shaped by ECM-tethered latent pools and vascular cell-cell interactions, with integrin-, protease-, and potentially GARP-dependent contributions that likely vary across tissues and conditions.

CELL TYPE	LATENT TGF-β1 PRESENTATION	INTEGRINS EXPRESSED	ACTIVATION MECHANISM
Epithelial cells	**LTBP:TGF-β1** (ECM)	integrin αVβ6, αVβ8	**αVβ6-** or **αVβ8/MMP-14** dependent activation
Myeloid cells (DCs, monocytes, macrophages, microglia)	**LRRC33:TGF-β1**	integrin αVβ8	**αVβ8**-dependent activation (**MMP-14** or…); supposed *trans*-activation mediated by αvβ8-expressing astrocytes on LRRC33:TGF-β1-expressing microglia
Regulatory T cells (Tregs)	**GARP:TGF-β1**	integrin αVβ8	**αVβ8**-dependent activation; exact mechanism unresolved
B cells	**GARP:TGF-β1**	UN	Likely ***trans*-activation by αVβ8-**expressing cells (e.g., dendritic cells) or other unresolved mechanism
Mesenchymal stromal cells (MSCs)	**GARP:TGF-β1**	UN	UN
Platelets	**GARP:TGF-β1** / **LTBP:TGF-β1** (ECM)	UN	Protease-dependent activation (**thrombin cleavage of GARP**); possible **shear-force**-mediated activation
Hepatic stellate cells (HSCs)	**GARP:TGF-β1**	UN	Likely **αV**-dependent activation (exact αVβ integrin subtype is unknown)
Fibroblasts / contractile stromal cells	**LTBP:TGF-β1** (ECM)	integrin αVβ1	**αVβ1**-dependent activation and protease-dependent activation (**MMP-9** cleavage of LAP)
Endothelial cells	**GARP:TGF-β1** / **LTBP:TGF-β1** (ECM)	integrins αVβ6, αVβ8, (αVβ3, αVβ5)	Mechanism unresolved; probable integrin-dependent (**αVβ6** / **αVβ8**) and protease-dependent (**MMP-14**) mechanisms implicating different cell types

Table 1: Summary of known cellular sources of TGF-β1 and their activation mechanisms (non-exhaustive).
Latent TGF-β1–presenting partners expressed by the different cell types are highlighted in bold and color (LTBP in purple, LRRC33 in orange, and GARP in red). UN, unknown.

4 Cellular effects of TGF-β1 signaling

Once activated and bound to its receptor, TGF-β1 mainly signals through the SMAD-dependent pathway. SMAD-independent, or non-canonical, pathways also exist and include the MAPK, JNK, Rho-like GTPase, PI3K–AKT, and ERK1/2 pathways, all of which contribute to the wide range of cellular responses induced by TGF-β1 signaling. Notably, the canonical TGF-β receptor is expressed almost ubiquitously, meaning that TGF-β1 can act on nearly any cell type, with effects that may vary – and even be opposite – depending on the biological context. For example, it can exert pro-inflammatory or anti-inflammatory actions and promote either cell proliferation or cytostasis. TGF-β signaling plays a critical role in T cell development and function (*1*). This is clearly illustrated by mice with a T cell-specific deletion of the *Tgfbr2* gene (*Cd4*^{cre} × *Tgfbr2*$^{fl/fl}$), which develop severe multi-organ inflammation similar to that observed in *Tgfb1*$^{-/-}$ mice and die within 3-4 weeks after birth (*10, 11, 170*). Below is a summary of the diverse effects of TGF-β1 on several relevant cellular subsets (**Figure 13**). Again, this represents only a selected fraction of the available literature and is not intended to be exhaustive.

4.1 Effects on the innate immune system

The innate immune system constitutes a readily available defense mechanism that is functional at birth and is rapidly activated upon infection. It initiates and regulates inflammation through the release of cytokines and chemokines, recruits immune cells to sites of infection, and activates the adaptive immune system via antigen presentations. It also contributes to pathogen clearance at sites of invasion. The cellular components of the innate immune system include dendritic cells (DCs), monocytes and macrophages, and natural killer (NK) cells, among others.

4.1.1 Dendritic cells

Dendritic cells (DCs) are specialized antigen-presenting cells and play a key role in the priming and activation of adaptive immune responses against tumors and pathogens. TGF-β1 is required for the development of Langerhans cells, a subset of specialized DCs in the skin (*171*). On the contrary, it has been shown to reduce the ability of DCs to prime cytotoxic T lymphocytes (CTLs) (*172*), notably by impairing antigen presentation by DCs in lymphoid organs and within tumors. This occurs through decreased surface expression of MHC class II complexes, as well as inhibition of DCs endocytosis and phagocytosis (*173*), and by promoting DC apoptosis (*174*). In addition, TGF-β1 decreases DCs maturation, promotes a tolerogenic phenotype (*175, 176*). Finally TGF-β1 can either promote or reduce DC migration by modulating the expression levels of chemokine receptors (*177*).

4.1.2 Monocytes & macrophages

Monocytes are produced in the bone marrow and circulate in the bloodstream before differentiating into DCs and tissue macrophages. In an overly simplified framework, macrophages are often divided into two main subsets: M1 and M2. M1 macrophages exhibit pro-inflammatory functions and are activated by TLR ligands (a major pathway involved in microbial recognition) as well as by pro-inflammatory cytokines. In contrast, M2 macrophages have anti-inflammatory properties and are typically induced by IL-4 or IL-13. While M1 macrophages contribute to the elimination of pathogens and cellular debris, M2 macrophages help resolve inflammation by promoting tissue repair and dampening immune responses. TGF-β1 acts as a chemoattractant for monocytes. In the intestine, it promotes monocyte trafficking to inflammatory sites and supports their differentiation into M2 macrophages, as well as their persistence within tissues (*178*). Conversely, TGF-β1 inhibits pro-inflammatory M1 macrophages by suppressing TLR signaling. In mice with monocyte- and macrophages-specific deletion of the *Tgfbr2* gene (insensitive to TGF-β1 signaling), susceptibility to inflammation is increased (*179*).

4.1.3 NK cells

Natural killer (NK) cells are innate lymphoid cells specialized in immune surveillance against tumor cells and virus-infected cells. NK-cell recognition of target cells is not antigen-specific, but instead depends on the integration of signals delivered by activating and inhibitory receptors. Once activated, NK cells can induce target-cell lysis through degranulation, leading to the release of perforin and granzymes. They also produce pro-inflammatory cytokines, including interferon-γ (IFN-γ). TGF-β1 signaling inhibits NK-cell maturation, activation, and effector functions. For instance, in a murine model in which NK-cells are insensitive to TGF-β signaling, newborn mice exhibit reduced susceptibility to postnatal infections (*180*). Conversely, TGF-β signaling downregulates the expression of NK-cell surface receptors such as NKG2D and NKp30, decreases IFN-γ production, and impairs NK-cell cytolytic activity (*176, 181*).

Overall, TGF-β1 modulates innate immune cell function at multiple levels. In DCs, it reduces antigen presentation and general functional activity, while being essential for Langerhans cell development. TGF-β1 acts as a chemoattractant for macrophages, inhibits pro-inflammatory M1 polarization, and promotes differentiation toward immunoregulatory M2 phenotype. In NK cells, TGF-β1 impairs maturation and effector functions.

4.2 Effects on the adaptive immune system

The adaptive immune system constitutes a second line of defense following the innate immune response. It comprises T and B lymphocytes, which are responsible for generating antigen-specific responses and establishing immunological memory. T cells can be divided into two major subsets: $CD4^+$ and $CD8^+$ T cells. Upon initial antigen encounter, both subsets differentiate into various effector populations. These include $CD8^+$ cytotoxic T lymphocytes (CTLs) and several $CD4^+$ T cell subsets, such as helper T cells (Th1, Th2, Th9, and Th17) and regulatory T cells.

4.2.1 CD8+ T cells

$CD8^+$ cytotoxic T lymphocytes (CTLs) eliminate cancer cells and virus-infected cells through the production and release of cytolytic factors. To the contrary of NK cells, for example, T cells activation is antigen-specific, in addition to co-stimulatory interactions and cytokines stimulation. TGF-β1 represses the differentiation and proliferation of pre-activated CTLs, notably through SMAD-mediated interactions with the transcription factor FOXP1 (*182, 183*). TGF-β signaling also inhibits the production of key CTL effector molecules, including IFN-γ, Fas ligand (FasL), perforin, and granzymes (*184*). In addition, TGF-β1 has been shown to upregulate PD-1 expression in CTLs (*185*). PD-1 is an immune checkpoint receptor whose signaling reduces T-cell survival, proliferation, activation, and effector functions.

4.2.2 CD4+ T cells

$CD4^+$ T lymphocytes play a major role in coordinating immune responses, notably through their cytokine production that activate B cells and macrophages and facilitates DC-mediated activation of $CD8^+$ T cells. TGF-β1 inhibits T-cell differentiation into Th1 and Th2 lineages by downregulating the expression of the transcription factors T-bet and GATA-3 (*186, 187*). Conversely, mice in which TGF-β signaling is specifically abrogated in T cells display an enhanced Th response (*188*). TGF-β1 also suppresses $CD4^+$ T-cell proliferation by inhibiting IL-2 production, a cytokine that normally supports Th-cell expansion (*189*). In addition, the SMAD signaling pathway cooperates with RORγt to promote the differentiation of Th17 cells. Th17 cells contribute to antibacterial and antifungal immunity but are also implicated in the development of autoimmune diseases. Similarly, TGF-β1 and IL-4 promote the differentiation of Th9 cells, another subset of proinflammatory $CD4^+$ T cells (*1*).

4.2.3 Tregs

Regulatory T cells (Tregs) are a subset of $CD4^+$ T lymphocytes that play a central role in immune tolerance by suppressing excessive immune responses. Although Tregs are among the major producers of active TGF-β1, which contributes to their immunosuppressive activity, they also respond to and require TGF-β1 signaling for their development and function. Tregs can be classified into two categories based on their origin: thymus-derived Tregs (tTregs),

which arise from T-cell progenitors in the thymus, and peripherally induced Tregs (pTregs), which differentiate from naïve $CD4^+$ T cells stimulated in peripheral secondary lymphoid organs. The generation of tTregs appears not to require TGF-β signaling (*190*), whereas pTregs differentiation is promoted by SMAD signaling, which enhances FOXP3 expression in the presence of IL-2 (*191*). Moreover, TGF-β1-induced FOXP3 expression is essential for maintaining Tregs function.

4.2.4 B cells

B cells are adaptive immune lymphocytes that classically mediate humoral immunity through antibody production, but also contribute to immune homeostasis via antigen presentation and cytokine-dependent regulatory functions. TGF-β1 regulates multiple aspects of B-cell biology. TGF-β1 exerts a cytostatic effect on B cells by reducing the expression of cyclin A, a key cell-cycle regulator, and by inactivating the cell cycle-dependent kinase CDK2 (*176*). Mice selectively insensitive to TGF-β signaling in B cells do not display excessive autoimmunity, but nevertheless exhibit a more activated and hyperresponsive phenotype, associated with the production of anti-double-stranded DNA (anti-dsDNA) antibodies (*192*). More broadly, TGF-β1 decreases immunoglobulin synthesis. Interestingly, our lab showed that it also promotes class-switch recombination toward IgA, which plays a critical role in mucosal barrier defense mechanisms (*29*). However, when examining mice with a specific deletion of *Garp* in B cells (*Mb1*^{Cre} x *Garp*$^{fl/fl}$), we did not observe reduced antigen-specific IgA production in response to intestinal bacterial infection by *Citrobacter rodentium,* or after immunization with proteins in adjuvant (*193*). This suggests that the active TGF-β1 required for IgA switching does not originate from B cells themselves under these conditions.

In summary, TGF-β1 inhibits the differentiation, proliferation, and effector functions of CTLs. It suppresses Th1 and Th2 differentiation and responses, while promoting the differentiation of Th17 and Th9 cells. In addition, it enhances the generation of Tregs. In B cells, TGF-β1 exerts cytostatic effects, reduces antibody production, and promotes class switching to IgA.

4.3 Effects on fibroblasts, epithelial and endothelial cells

Fibroblasts, epithelial cells, and endothelial cells are major non-immune cellular components of tissues that actively contribute to tissue organization, intercellular signaling, and responses to injury. Through these functions, they play essential roles in tissue homeostasis, repair, angiogenesis, and fibrosis – processes in which TGF-β1 is critically involved. These cell types were introduced in **Section 3**.

4.3.1 Fibroblasts

TGF-β1 is a well-established pro-fibrotic cytokine involved both in physiological tissue repair and in pathology-associated fibrosis. Notably, TGF
-β1 promotes ECM biosynthesis and inhibits its degradation (*194*) by increasing the expression of protease inhibitors (*194-196*). It acts as a chemoattractant for fibroblasts, promotes their activation, conversion to myofibroblasts as well as their dedifferentiation into cancer-associated fibroblasts (CAFs) (*197-200*). Activated fibroblasts further engage in paracrine signaling with epithelial cells, support angiogenesis, and recruit local innate and adaptive immune cells through the secretion of chemokines (*1, 201, 202*).

4.3.2 Epithelial cells

TGF-β1 strongly influences the phenotypic plasticity of epithelial progenitor cells, notably by regulating their differentiation and phenotypic transitions during development and tissue repair. It is considered one of the most potent and broadly acting signaling molecules driving the epithelial-mesenchymal transition (EMT). During EMT, epithelial cells lose their apico-basal polarity and intercellular adhesive contacts, while acquiring increased motility. Although EMT is essential for development and tissue repair, it also promotes tumor invasiveness and metastasis in breast, lung, renal, and hepatic carcinomas (*1*). Finally, TGF-β1 contributes to the expression of pro-fibrogenic factors in normal cells, but also in malignant epithelial cells in a model of lung metastasis (*203*).

4.3.3 Endothelial cells

TGF-β1 is crucial for blood vessel formation during embryogenesis. Mice deficient in TGF-β1 (*Tgfb1*$^{-/-}$) (*11*) or in key components of the pathway (*Alk1*$^{-/-}$, *Alk5*$^{-/-}$, *Tgfbr2*$^{-/-}$) die during embryonic development due to vascular defects, typically characterized by excessive vessel dilatation and increased vascular permeability (*204-207*). Endothelial cells can also undergo an endothelial-to-mesenchymal transition (EndoMT), a process often associated with pathological conditions such as pulmonary fibrosis. Recent evidence has linked TGF-β1 signaling to the regulation of this process (*208*). In cancer, the effects of TGF-β1 on endothelial cells are highly context-dependent and can either promote angiogenesis, for instance by stimulating the production of pro-angiogenic factors such as VEGF, or conversely exert cytostatic effects (*209*). The balance between these opposing outcomes is thought to be regulated by the relative contribution of ALK1 versus ALK5 (TβRI)-dependent signaling (*210*). In an MC38 tumor model, the combination of anti-PD-1 and anti-GARP:TGF-β increased the density and improved the intratumoral organization of blood vessels by raising pericyte coverage (*211*), likely by relieving the cytostatic effects of TGF-β1 on endothelial cells.

In conclusion, TGF-β1-activated fibroblasts exhibit increased ECM production and modulate regulatory signals affecting epithelial, immune, and endothelial cells. In epithelial cells, TGF-β1 regulates phenotypic plasticity, EMT, and the expression of profibrotic factors. Finally, TGF-β1 plays a central role in angiogenesis across various contexts, including in embryonic development, in normal or pathological conditions such as cancer, and also promotes EndoMT.

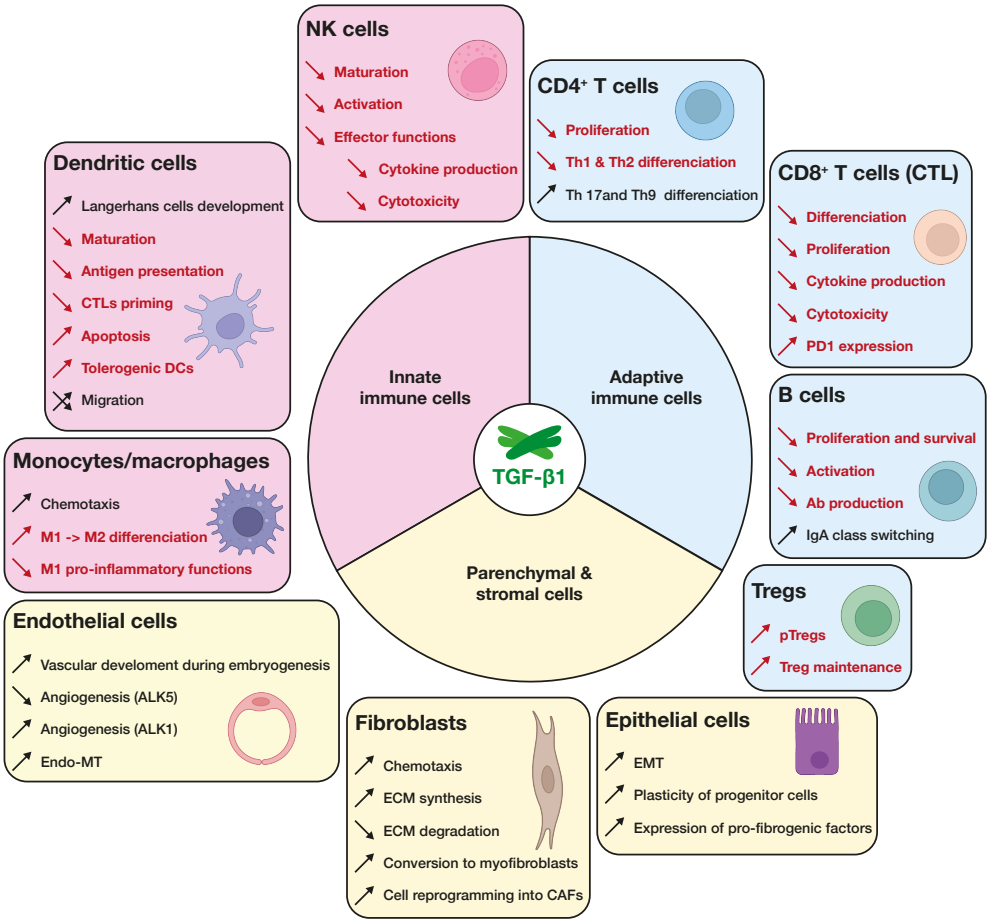

Figure 13: Overview of the effects of TGF-β1 signaling on selected cellular subsets (non-exhaustive).
Three major cell populations are summarized: innate immune cells, adaptive immune cells, and parenchymal/stromal cells. Effects directly associated with reduced immune response or reduce inflammation are highlighted in red.

5 Modulation of TGF-β1 activity using monoclonal antibodies to block or activate the latent cytokine

By reviewing the cellular outputs mediated by TGF-β1 signaling, it becomes clear that this cytokine is a central regulator of both tissue homeostasis and disease (*1, 176*).

In cancer, excessive or dysregulated TGF-β1 activity is commonly associated to impaired anti-tumor immunity, largely through its ability to establish and maintain an immunosuppressive tumor microenvironment (*212-214*). At the immune level, TGF-β1 dampens effector T-cell differentiation and function, including Th1 and cytotoxic responses, while promoting the generation of pTregs and strengthening Treg stability and suppressive capacity (*176*). Beyond immune regulation, TGF-β1 also supports tumor progression by shaping the stromal compartment, promoting ECM deposition and fibrosis-like context that can limit immune infiltration and facilitate metastatic spread (*213-215*).

In autoimmune and inflammatory diseases, the importance of TGF-β1 as an immunosuppressive mediator is particularly evident, since basal TGF-β1 signaling is required to preserve peripheral tolerance and to prevent excessive immune activation (*1, 176*). Accordingly, decreased TGF-β1 availability or disruptions in downstream signaling can result in uncontrolled inflammation, enhanced effector T-cell responses, and loss of immune equilibrium, ultimately driving tissue injury (*1, 216, 217*). In this sense, TGF-β1 acts as a central inhibitory checkpoint that limits pathogenic immune activity while sustaining the stability and function of regulatory T-cell populations (*176*).

Because of its central role, the TGF-β1 axis has long been considered a promising target for immunotherapy (*1, 140, 218-220*) that could apply both in diseases characterized by excessive TGF-β1 signaling (such as cancer and fibrosis) and in conditions driven by exaggerated immune responses (such as autoimmune disorders). However, non-selective strategies targeting TGF-β1 often lead to adverse effects due to a lack of specificity. A deeper understanding of the mechanisms regulating TGF-β1 bioavailability is therefore essential to

enable more refined and targeted therapeutic approaches. Based on current knowledge, our laboratory has developed monoclonal antibodies that either block or activate TGF-β1. These antibodies have contributed to elucidating the mechanisms governing TGF-β1 latency and activation and may represent promising therapeutic tools.

5.1 Blocking antibodies

5.1.1 Anti-human GARP: TGF-β1 antibodies

Our laboratory and others have shown that, upon TCR stimulation, human Tregs display latent TGF-β1 at their surface through disulfide-mediated coupling of the LAP to GARP (*26, 27, 30, 221, 222*). To determine whether GARP is required for TGF-β1 activation and for the suppressive activity of human Tregs, we generated a panel of monoclonal antibodies (mAbs) targeting human GARP using two strategies:

- First, hybridoma clones were produced from mice immunized with murine cells expressing human GARP; antibodies obtained using this approach were named **MHG** (Mouse anti-Human GARP).
- Second, in collaboration with argenx, llamas were immunized with murine cells co-expressing hGARP and hTGF-β1, or with plasmids encoding these proteins. Immunoglobulin variable-region cDNA libraries were then constructed, enriched by phage display based on binding to recombinant hGARP:hTGF-β1 complexes, and selected Fab sequences were reinserted into a human IgG1 backbone. Antibodies generated through this strategy were named **LHG** (Llama anti-Human GARP).

Among the 31 antibodies obtained, two efficiently inhibited the production of active TGF-β1 by human Tregs *in vitro*: MHG-8 and LHG-10 (*139*). Structural analysis of the human GARP:TGF-β1 complex bound to a Fab derived from MHG-8 revealed that this antibody recognizes a composite conformational epitope formed by residues from LAP, mature TGF-β1, and GARP (*52*). These observations led us to propose that blocking anti-GARP:TGF-β1 mAbs function as a molecular “glue,” stabilizing the latent complex and preventing the

conformational changes required for activation (**Figure 14**). Notably, these antibodies did not bind murine GARP, nor did they recognize human GARP unbound to TGF-β1.

We next assessed whether blocking GARP-dependent activation of TGF-β1 blocks Treg-mediated immunosuppression *in vivo*. In a xenogeneic graft-versus-host disease (xGvHD) model induced by transfer of human PBMCs into immunodeficient NSG mice, co-transfer of autologous human Tregs reduces disease severity by suppressing donor T-cell reactivity. Strikingly, this protective effect was lost upon administration of a blocking anti-GARP:TGF-β1 antibody, demonstrating that GARP-dependent generation of active TGF-β1 by human Tregs is required for their suppressive function in this setting (*139*).

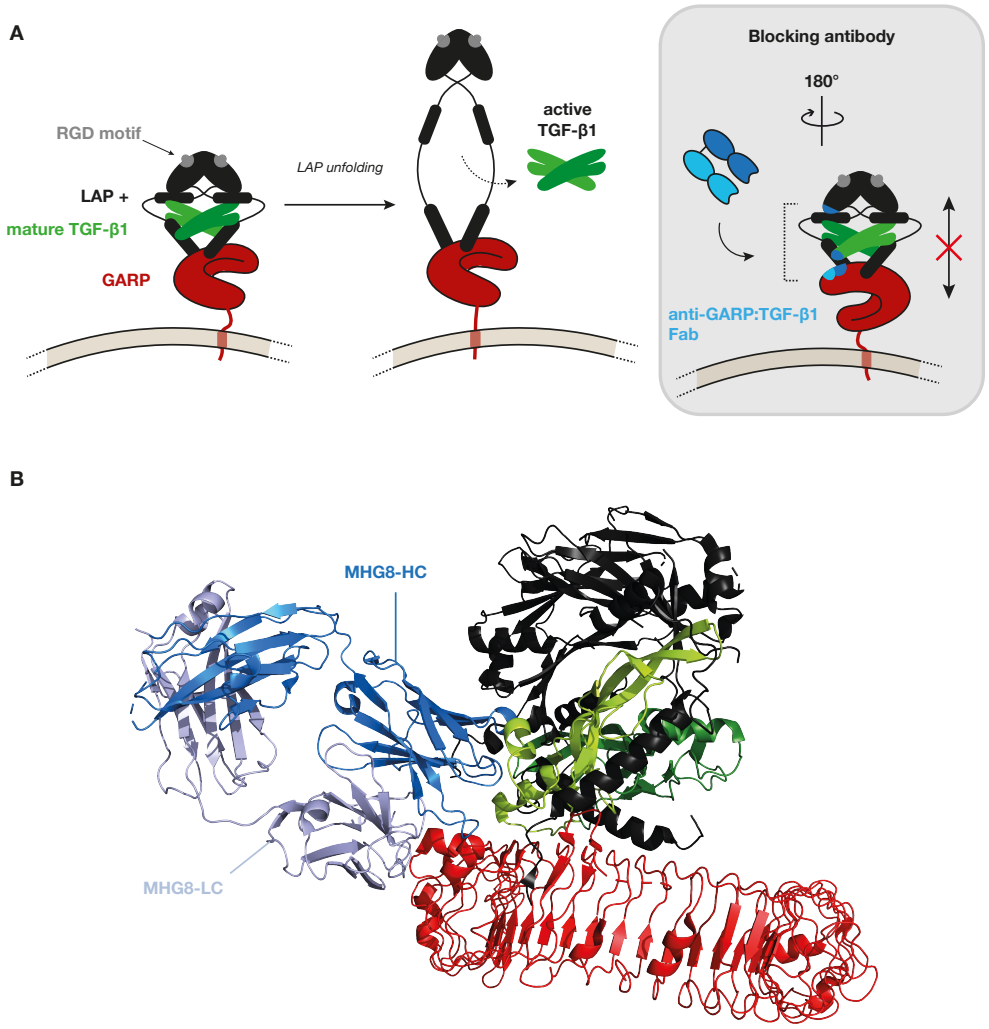

Figure 14: Blocking TGF-β1 activation with anti-GARP:TGF-β1 antibody.
(**A**) Schematic representation: binding of a Fab fragment from a blocking anti-GARP:TGF-β1 antibody crosslinks (dotted bracket) residues from the arm domain, the mature TGF-β1 thumb, and GARP, thereby preventing LAP unfolding. Footprints (recognized epitopes) from the anti-GARP:TGF-β1 Fab are highlighted in dark blue and light blue. (**B**) Cartoon representation of the MHG8 Fab fragment bound to GARP and latent TGF-β1 (PDB: 6GFF) (*52*). Heavy chain (HC) is in dark blue, and light chain (LC) is in light blue.

5.1.2 Anti-mouse GARP: TGF-β1 antibodies

In parallel, monoclonal antibodies were generated to selectively inhibit the production of active TGF-β1 from mouse GARP:TGF-β1 complexes *in vitro* :

- The antibodies were generated using a strategy similar to that employed for the LHG antibodies. In collaboration with argenx, llamas were immunized with plasmids encoding mGARP and mTGF-β1. Immunoglobulin variable-region cDNA libraries were subsequently constructed and enriched by phage display based on binding to recombinant mGARP:mTGF-β1 complexes. Selected Fab sequences were then reinserted into a murine IgG2a backbone. Clone **58A2** was selected among all the tested clones (*32*).

This antibody was again shown to suppress Treg-mediated immunoregulation *in vivo* and to enhance anti-tumor immunity across several murine cancer models. In the context of solid tumors, we reported that concomitant blockade of GARP:TGF-β1 and PD-1 induced regression of transplanted tumors that were refractory to anti-PD-1 monotherapy (*32, 211*). Anti-GARP:TGF-β1 (58A2) treatment also reduced tumor burden in a hematological malignancy model, where antibody administration alone was sufficient to elicit therapeutic benefit (*147*). In this study, the disease model was primary myelofibrosis (PMF), a myeloproliferative neoplasm associated with abnormal cytokine production and progressive bone marrow fibrosis.

Importantly, the anti-tumor effects observed in both solid and liquid cancer models were attributed primarily to the targeting of GARP-expressing Tregs, rather than GARP expressed by other cell types such as B cells, platelets, or megakaryocytes. Antibody-mediated interference with the GARP:TGF-β1 axis enhanced $CD8^+$ T-cell-driven anti-tumor responses, supporting the conclusion that Treg-derived activation of TGF-β1 is a key contributor to immunosuppression in tumor-bearing hosts.

Blocking anti-human GARP:TGF-β1 monoclonal antibodies (mAbs) are currently being evaluated in phase I and II clinical trials for their therapeutic efficacy in combination with anti-PD-1 therapy in patients with advanced or metastatic solid tumors (Clinicaltrials.gov: NCT03821935, NCT05822752, and NCT06109272).

5.2 Activating mAbs

Building on the mechanistic insights accumulated on GARP-mediated TGF-β1 activation by Tregs, as well as on the highly specific inhibition achieved by blocking anti-GARP:TGF-β1 antibodies, our group sought to develop antibodies designed this time to enhance, rather than inhibit, TGF-β1 activation. The underlying objective would be to reinforce Treg-mediated immunosuppression in diseases characterized by excessive T-cell activity.

Attempts to treat such conditions through administration of recombinant active TGF-β1 have so far proven unsuccessful, largely because the mature cytokine displays an extremely short plasma half-life (on the order of only a few minutes in preclinical models) resulting in rapid clearance and minimal therapeutic benefit (*223*). Nevertheless, a controlled strategy to increase TGF-β1 bioactivity could represent a valuable therapeutic approach in autoimmune and alloimmune diseases, which are generally characterized by a loss of self-tolerance and exaggerated B- and T-cell responses, ultimately driving chronic inflammation.

New monoclonal antibodies directed against latent TGF-β1 were generated in collaboration with Argenx by immunizing llamas with plasmids encoding human or mouse TGF-β1, similarly to what was described for the synthesis of LHGs mAbs. Here, the antibodies were named **LHT** or **LMT** (Llama anti-Human TGF-β1 or Llama anti-Mouse TGF-β1, respectively).

In total, 134 mAbs recognizing human or mouse GARP, GARP:TGF-β1 (*32, 139*), latent TGF-β1 (LHTs and LMTs), or related complexes were tested by Fanny Lambert (a former PhD student in our lab) for their ability to trigger TGF-β1 signaling in a reporter assay (*51*). Fourteen antibodies were validated as activators, including six anti-human latent TGF-β1 mAbs (LHT-4, -15, -18, -20, -22, -25) and eight anti-mouse latent TGF-β1 mAbs (LMT-2, -5, -6, -7, -9, -10, -11, -12). None of these antibodies were directed against GARP or GARP:TGF-β1 complexes, and none were cross-reactive between human and mouse latent TGF-β1. The activating mAbs bind epitopes near the LAP dimerization interface, close to but not overlapping with the RGD motifs. However, activation required more than binding: it depended on bivalent engagement (full IgG or $F(ab')_2$, but not Fab fragments). Structural analyses indicate that a single IgG cannot engage both LAP monomers within a single latent complex. Therefore, activation requires inter-complex crosslinking, consistent with a force-dependent

conformational unwrapping of LAP (**Figure 15**). Furthermore, activation occurred only when latent TGF-β1 was tethered to the cell surface via a transmembrane presenting protein such as GARP or LRRC33. In contrast, soluble or non-membrane-anchored pools (e.g., TGF-β1 expressed alone, GARP-ΔTM, or LTBP-1-associated complexes) were not activated despite antibody binding. Finally, mAb-mediated activation required an intact actin cytoskeleton, as it was abrogated by actin polymerization inhibitors (latrunculin A or cytochalasin D). Together, these findings support a model in which antibody-driven crosslinking of membrane-tethered latent complexes enables a force-dependent conformational change that relieves latency and permits receptor engagement (*51*).

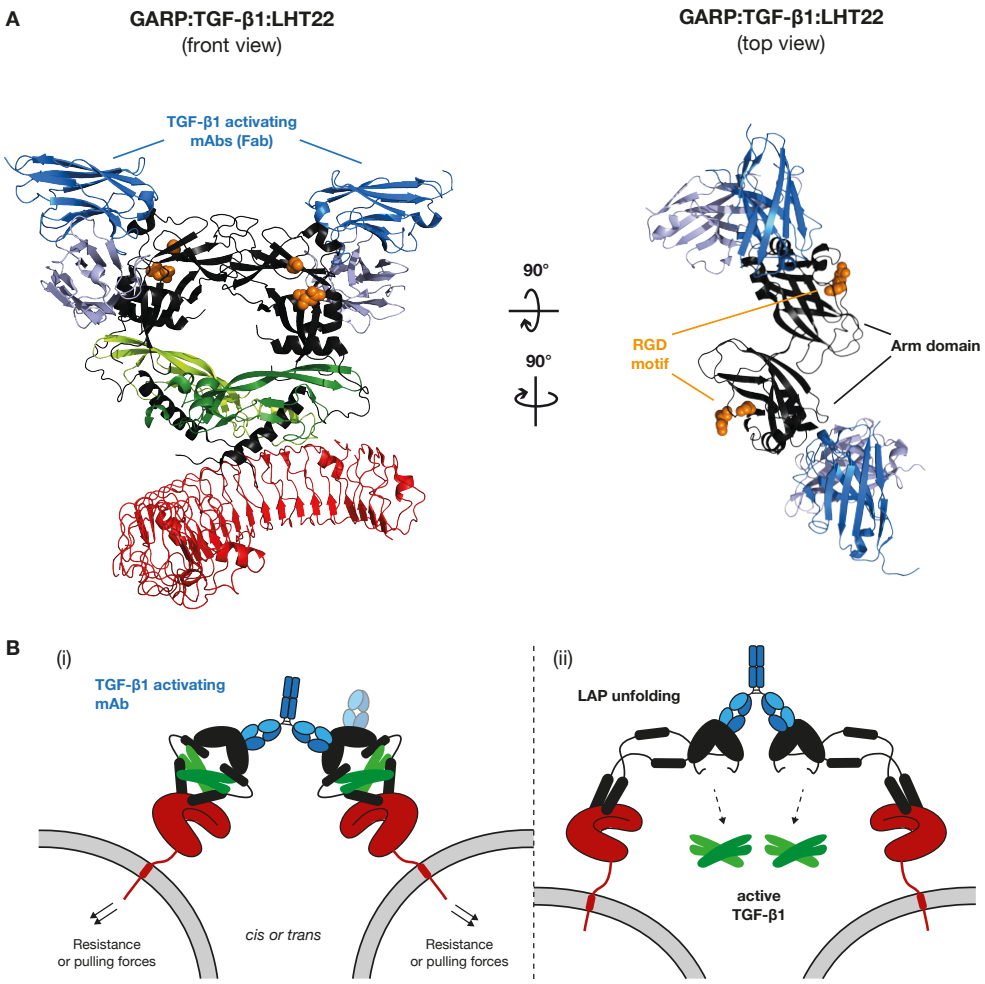

Figure 15: TGF-β1 activation with anti-LAP antibody.
(**A**) Cartoon representations of LHT22 Fab fragments bound to TGF-β1 presented by GARP. The heavy chain (HC) is shown in dark blue and the light chain (LC) in light blue. The front view depicts the entire complex, whereas the top view focuses on the upper arm domain bound by the two Fab fragments. Residues immediately surrounding the RGD motif are shown as orange spheres. The Fabs bind in close proximity to, but do not overlap with, the RGD motifs. Cryo-EM structure from Lambert et al. (2025) (PDB: 8REW) (*51*). (**B**) Schematic representation of the activation model proposed by Lambert et al. for mAb-mediated TGF-β1 activation. (i) A single mAb can only bind two distinct GARP:TGF-β1 complexes, either on the same cell membrane or on two closely apposed cells. Activation is proposed to depend on resistance or pulling forces that trigger LAP unfolding (ii), leading to the release of mature TGF-β1.

Therapeutically, administration of activating mAbs significantly reduced disease severity and improved survival in a murine model of GvHD. This benefit was associated with increased local TGF-β signaling in the spleen (elevated pSMAD2 and TGF-β target genes expression) and a trend toward increased Treg numbers. Importantly, efficacy required the presence of pre-existing Tregs, consistent with their role as a major reservoir of membrane-bound latent TGF-β1. In contrast, these antibodies showed no measurable benefit in several autoimmune models tested (including transfer colitis, lupus-prone mice, and EAE), although notably they did not exacerbate inflammation in these settings (*51*).

I had the opportunity to contribute to this research. In particular, my work – performed in collaboration with Séverine Wautier, another PhD student in our laboratory – helped define key mechanistic requirements for mAb-mediated TGF-β1 activation *in vitro*. This collaborative effort established the necessity of membrane anchorage, actin cytoskeleton activity and further showed *ex-vivo* that activating mAbs can directly trigger TGF-β1 activation on GARP-expressing murine Tregs (Figure 2B-D; **Lambert et al., 2025** (*51*)). For this reason, and since it provides direct context for the results presented in this manuscript, the study by Lambert et al. has been included as supplementary material in the **Annexes**.

Here, we employed these antibodies as molecular tools to probe the requirements for TGF-β1 activation, particularly in the context of force-dependent mechanisms, and to challenge the ability of molecules lacking cytoskeletal interactions to mediate this activation.

AIM OF THE STUDY

AIM OF THE STUDY

Our laboratory has long been interested in the mechanisms by which Tregs mediate immunosuppression, with a particular focus on the production of the immunosuppressive cytokine TGF-β1. We and others have shown that, upon activation, Tregs present latent TGF-β1 on their surface via binding to transmembrane protein GARP, and activate the cytokine in an integrin αVβ8-dependent manner (*121*). However, the mere expression of GARP and αVβ8 is not sufficient to trigger TGF-β1 activation, and this observation formed the starting point of this project. Indeed, we previously reported that Jurkat T cells transduced to express GARP:TGF-β1 complexes together with αVβ8 were unable to activate TGF-β1 unless the cells were additionally stimulated via their TCR (*22*). This finding indicated that at least one additional signal or partner protein is required for TGF-β1 activation by T cells such as Tregs.

In addition, how precisely αVβ8 mediates latent TGF-β1 activation remains incompletely understood. In particular, it is not known what is the exact role of the β8 IC domain (if any), and whether cytoskeleton-generated forces are required (*116, 120, 121, 128, 224*). Recently, a model for αVβ8-mediated TGF-β1 activation based on entropy redistribution suggested that it could be independent of cell-generated forces, and that such activation by entropy redistribution would allow autocrine, but not paracrine signals (*49, 55, 136*). However, previous studies by us and others report paracrine TGF-β1 activity following activation by αVβ8 (*27, 32, 52, 121, 128, 139, 147, 211, 225, 226*).

In light of these outstanding questions and discrepant observations, the **objectives of my work** were the following:

- Identify **candidate proteins** that contribute to activation of latent TGF-β1 presented by GARP in Tregs or other cell types

- Clarify the **molecular requirements governing TGF-β1 activation by αVβ8**. More specifically:

    - we sought to undisputably establish whether TGF-β1 activated by αVβ8 can exert paracrine activity;

    - we investigated the contribution of the IC domains of GARP and β8, as well as that of cytoskeleton-generated forces in TGF-β1 activation by αVβ8.

RESULTS

RESULTS

To identify missing partners that could cooperate with GARP and αVβ8 to activate latent TGF-β1 in Tregs, we resorted to constructing an activated human Treg cDNA library and screened this library in a reporter system able to detect TGF-β1 signals. Results of these efforts are presented in a first part of the Results (**Section 1**). Notwithstanding the fact that we screened the library in different conditions, we failed to identify an extracellular protein that appears to play a role in TGF-β1 activation in Tregs. However, we did identify intracellular candidates, leading us to consider that cytoskeleton or cytoskeleton-generated forces are important for TGF-β1 activation by αVβ8. We thus explored the roles of the IC domain of β8 and GARP, and that of cytoskeleton-generated forces using various biochemical and cell-based assays. These analyses are described in a second part of the Results (**Section 2**) and presented as a scientific article ready to be submitted for publication in a peer-review journal.

1 Identification of candidate proteins that contribute to activation of latent TGF-β1 presented by GARP in Tregs or other cell types

1.1 Construction of a human Treg cDNA library

The cDNA library was generated in the laboratory by a former Master's student, Nicolas Huyghe, under the supervision of Sara Lecomte (*227*). It does not constitute an integral part of my work. For this reason, only a brief overview of its construction is provided below.

The library was constructed from three distinct Treg cell lines: two polyclonal human $CD4^+$ Treg cell populations and one human Treg clone. The polyclonal Treg populations were derived from peripheral blood mononuclear cells (PBMCs) of patients with hemochromatosis. $CD4^+$ $CD25^{high}$ $CD127^{low}$ cells were sorted by flow cytometry and expanded *in vitro* with anti-CD3/CD28 in the presence of IL-2. The Treg clone (OTTO 13.2) was previously established in our laboratory, as described (*228*).

Total messenger RNA (mRNA) was extracted from these cells after a short restimulation on CD3/CD28, reverse-transcribed into complementary DNA (cDNA), and cloned into a pCMV_SPORT6 expression vector. The quality of the library was assessed based on the number of independent clones (>100,000), the size distribution of the inserted cDNAs (>0.5 kb and <4 kb), and the proportion of plasmids containing a cDNA insert. Following validation, the recombinant plasmids were electroporated into bacteria and plated on selective agar. After incubation, bacterial colonies were collected and pooled in groups of 100 to generate liquid cultures, each containing 100 individual cDNA clones. A total of 962 pools were generated, corresponding to a library complexity of approximately 100,000 independent clones.

1.2 The screening system

The screening system relied on a co-culture of two HEK 293T cell populations, both stably expressing surface GARP:TGF-β1 complexes. The first population ("**test cells**") was transfected with the cDNA pools from the library. The second population ("**reporter cells**") was co-transfected with a Firefly luciferase (FLuc) reporter driven by a SMAD-responsive promoter (CAGA promoter) and a Renilla luciferase (RLuc) construct under the control of a constitutive CMV promoter, used as a control for reporter cells number (**Figure 16**).

This co-culture format was designed to minimize the identification of candidates that would modulate intracellular SMAD signaling, without contributing to extracellular activation of latent TGF-β1. Finally, expressing GARP:TGF-β1 complexes on both test and reporter cells enables detection of activation occurring either in *cis* or in *trans*.

To note, the screening of the activated Tregs cDNA library was initially performed in the absence of αVβ8, in $293T^{GARP:TGF\text{-}\beta1+}$ cells only. Although TGF-β1 activation by Tregs is known to depend on both GARP and αVβ8, we hypothesized that the stimulated Tregs-derived cDNA library might also contain genes capable of promoting αVβ8-independent TGF-β1 activation. Such genes could therefore reveal alternative activation mechanisms operating in other cell types.

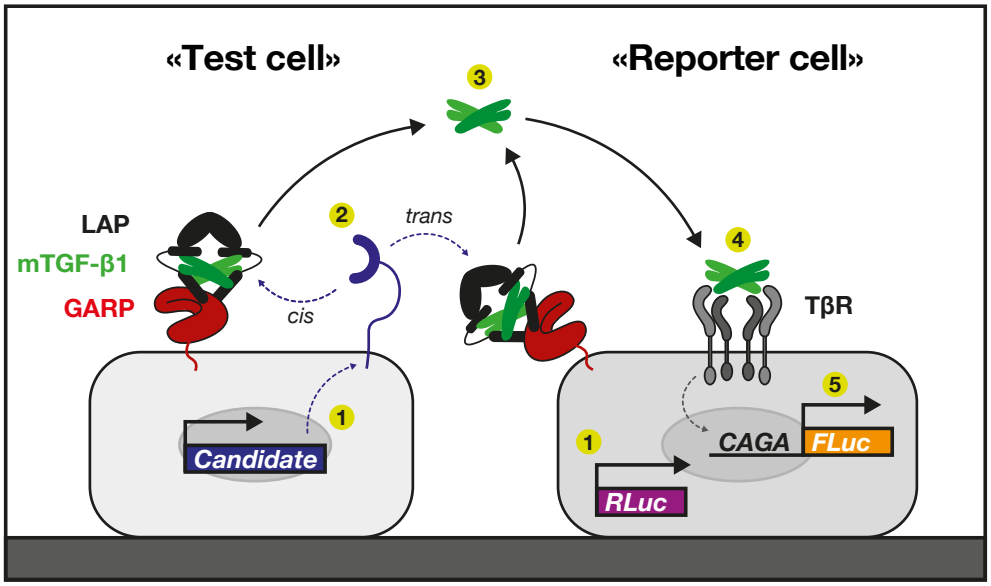

Figure 16: Co-culture assay (screening) in 293T cells expressing GARP:TGF-β1
Schematic representation of the co-culture reporter assay. (**1**) "**Test cells**" and "**Reporter cells**" are HEK 293T$^{GARP:TGF-β1+}$ cells transfected with candidate cDNAs from the library or the CAGA_Fluc/RLuc reporter system, respectively. (**2**) The candidate, represented here as a blue transmembrane protein, is expressed and (possibly) activates GARP-presented TGF-β1 in *cis* or *trans*. (**3**) If mature TGF-β1 is released, (**4**) it can bind to its receptor on the "**Reporter cells**". (**5**) Upon TβR engagement, the SMAD signaling triggers the production of FLuc under the CAGA promoter.

1.3 Screening in the absence of αVβ8

Each of the 962 pools of 100 cDNA clones was screened in the reporter assay described above, first in the absence of stably expressed αVβ8. Three internal controls were included in every experiment: (i) a negative control, consisting of an irrelevant cDNA pool transfected into the test cells; (ii) a positive control consisting of recombinant human TGF-β1 added directly to the co-culture at a final concentration of 1 ng/mL; (iii) a second positive control consisting of a plasmid encoding β8 transfected into test cells and spiked into the irrelevant pool at 1:1, 1:10, and 1:100 ratios.

A brief clarification is needed regarding the β8 control. In 293T cells expressing surface GARP:TGF-β1 complexes, transfection of β8 alone is sufficient to induce spontaneous TGF-β1 activation, without additional stimulation. We therefore used β8 as an internal assay control

and spiked it into an irrelevant pool. Detecting αVβ8-mediated activation when diluted served as a sensitivity benchmark, indicating that the screening conditions remained sufficiently robust. Accordingly, any pool inducing a comparable or stronger signal than the 1:10/1:100 dilutions could be interpreted as positive. However, we used an arbitrary cutoff of fold increase (FI) = 1.2 compared with the irrelevant pool and prioritized all pools exceeding this threshold (FI > 1.2) for downstream analysis (data not shown).

Once selected, positive pools were subjected to iterative deconvolution. Each initial pool was subdivided into subpools of 10 clones, which were re-screened under the same conditions. Positive subpools were subsequently separated into individual clones and tested in a final validation round. Once a single clone was confirmed, its cDNA insert was sequenced and analyzed using BLAST to identify the corresponding gene (**Figure 17**).

1.3.1 Candidates identified in the first screening

Out of the 962 pools, 8 were selected for further analysis and through the iterative deconvolution, 6 candidate genes were selected and identified; 4 genes coding for intracellular proteins: TRA2B, *ZC3H18*, *RHOA*, and *JUN*, 1 gene coding for a receptor: *TNFRSF1A*, and 1 gene coding for a secreted protein: *LGALS9* (**Figure 17**).

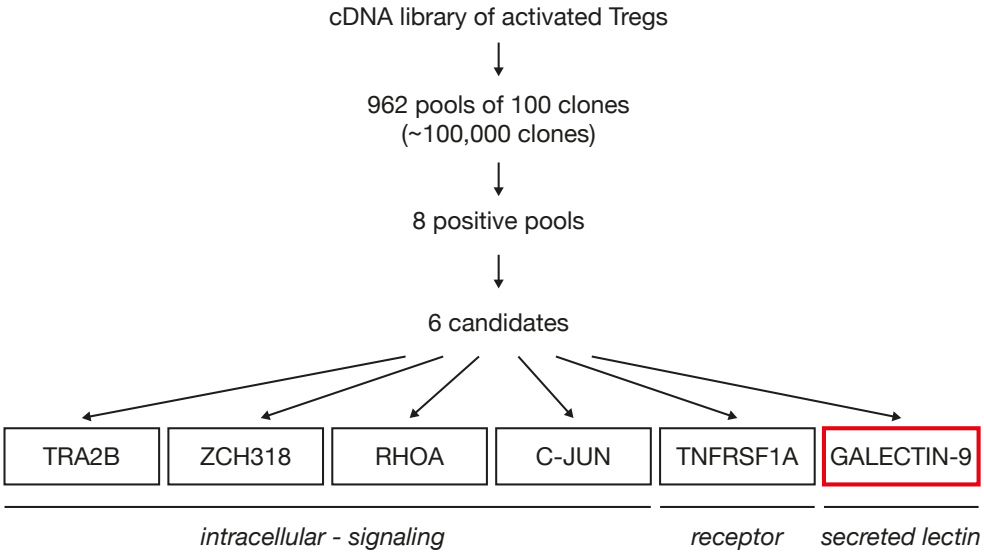

Figure 17: Candidate proteins identified from the screening
The cDNA library of activated Tregs is composed of 962 pools of 100 clones each. 8 of these pools were selected for further analysis, out of which 6 candidates were confirmed. After sequencing, the following candidate proteins were identified: TRA2B, ZC3H18, RHOA, C-JUN, TNFRSF1A and GALECTIN-9.

The intracellular candidates were not prioritized for downstream validation. As mentioned in **Section 1.2**, in our co-culture screening strategy, the SMAD reporter system was transfected in a "reporter cell" population, whereas the cDNA library was transfected into a separate "test cell" population. This design was chosen to primarily detect extracellular TGF-β1 activation and to minimize detection of purely intracellular modulators within the "test cells". Therefore, candidates encoding intracellular proteins or receptors were considered more likely to reflect indirect effects, such as changes in transcriptional profile, altered secretion of intermediate factors, or broader remodeling of cellular states, rather than direct participation in TGF-β1 activation at the cell surface. Since such mechanisms are difficult to validate functionally and may be context-dependent, we chose not to pursue these candidates further at this stage.

By contrast, ***LGALS9*** encodes a secreted lectin – GALECTIN-9 (or GAL-9) – that can act extracellularly and is therefore more consistent with the intended scope of our screening of identifying extracellular partners. In addition, extracellular proteins represent easier targets for potential therapeutic intervention (e.g., antibody-based blocking approaches), which aligns with what was done in our lab with the anti-GARP:TGF-β1 blocking antibodies (*140, 211*). For

these reasons, we focused our work on GALECTIN-9 and did not further investigate the other candidates. We acknowledge that this selection strategy may bias the analysis toward extracellular, targetable proteins and could exclude intracellular regulators that indirectly modulate TGF-β1 activation; these possibilities will be discussed in the final "**Discussion**" section.

1.3.2 Characterization of GAL-9 as the most promising candidate

GAL-9 isoform identified in the library is unknown and is more active than L isoform

GAL-9 is a β-galactoside-binding lectin of the galectin family, defined by conserved carbohydrate recognition domains (CRDs). It is a tandem-repeat galectin composed of two distinct CRDs – N-terminal and C-terminal – linked by a flexible linker. It typically exists as three classical isoforms: the long (L), medium (M), and short (S) forms. These isoforms differ in linker length due to alternative splicing. Several non-classical isoforms have also been described (*229*). Here, sequencing analysis of the cDNA identified during the screening revealed a previously uncharacterized variant resulting from atypical splicing between exons 3 and 5, leading to a partial deletion of the N-terminal domain. We named this variant GAL-9 delta (Δ) (**Figure 18A**).

To compare its functional activity with that of a canonical isoform, we cloned the GAL-9 (L) cDNA into the same expression vector and transfected them both in the 293T$^{GARP:TGFB1+}$ cells co-culture assay. Notably, the Δ variant induced a stronger signal than the L isoform, with a FI of 2 relative to the irrelevant clone, compared with an FI of 1.3 for the L isoform (**Figure 18B**).

Because this Δ variant has not been previously reported, we hypothesized that it might originate from a technical artifact, such as sequence recombination during library construction. To address this possibility, we designed two sets of GAL-9-specific primers for quantitative PCR (qPCR): one set specific for the Δ variant, recognizing the cDNA identified in the library but not the classical isoforms, and a second set designed to detect all known GAL-9 isoforms without discrimination. These primer sets were tested on several retro-transcribed (RT) mRNA samples into cDNA from our collection, including unstimulated or stimulated Tregs, Th cells and B cells isolated from hemochromatosis patients (referred to as: WIBE, CCSS, DING,

LAMD), and endothelial cells (**Figure 18C**). Using the all-GAL-9 primer set, GAL-9 expression was detected in all cell types except one of the two endothelial cell lines tested. The highest expression levels were observed in Tregs, with substantial expression also detected in Th cells and stimulated B cells, and lower levels in unstimulated B cells and one endothelial cell line (HUVEC PCS-100-010) (**Figure 18C, left panel**). In contrast, no signal was detected in any cell type when using the Δ variant-specific primer set (**Figure 18C, right panel**). We also re-tested by RT-qPCR the RNA pools at the origin of the library with the same sets, showing similar results (data not shown). These results strongly suggest that the Δ variant likely arose from uncontrolled sequence rearrangements during library generation.

Although the Δ variant appeared more potent than the L isoform in reporter assays, its lack of detectable endogenous expression indicates limited physiological relevance. Consequently, we prioritized the classical GAL-9 (L) isoform for the majority of subsequent experiments.

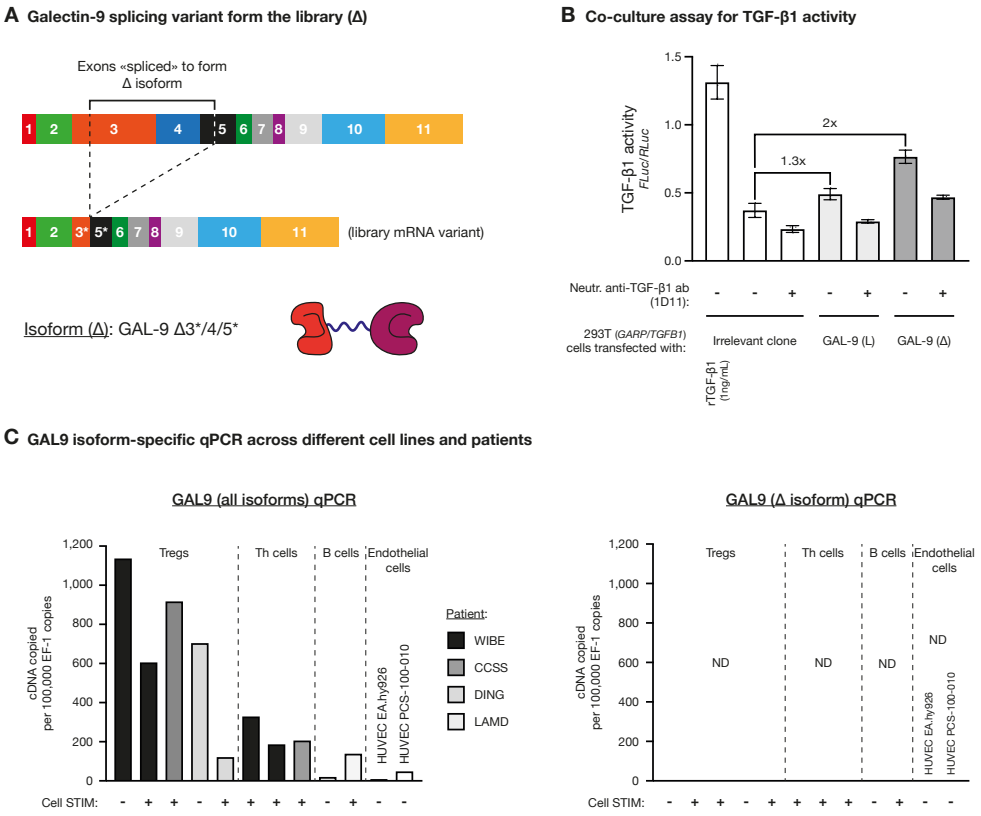

Figure 18: Comparison of GAL-9 (L) and GAL-9 (Δ) isoforms structure, function and expression profile.

(**A**) The GAL-9 (L) isoform comprises all 11 exons. The GAL-9 (Δ) isoform lacks part of exon 3, all of exon 4, and part of exon 5, resulting in an incomplete N-terminal CRD domain. (**B**) A co-culture assay measuring TGF-β1 activity shows an increased signal following transfection with GAL-9 (Δ) compared with GAL-9 (L). Data are presented as normalized luminescence values (FLuc/RLuc). (**C**) qPCR analysis targeting all GAL-9 isoforms shows that *LGALS9* is expressed across multiple cell types, particularly within the Tregs. Cellular stimulation only slightly affects expression levels, with a tendency toward downregulation. In contrast, qPCR specific for the GAL-9 (Δ) isoform shows no detectable expression in any cell type tested. Data are presented as number of cDNA copies per 100,000 EF-1 copies. ND: not detected.

GAL-9 is expressed in Jurkat cells at baseline and protein secretion is increased upon stimulation

We then investigated the function of GAL-9 in T cells, specifically using a Jurkat cell line engineered to stably express GARP and αVβ8 heterodimer. Similar to regulatory T cells, these cells activate TGF-β1 exclusively upon TCR stimulation (*121*). Previous work by Chabot et al. (2002) (*230*) reported that Jurkat cells express both the GAL-9 L and M isoforms, and that PMA stimulation enhances GAL-9 expression and surface display. However, because PMA stimulation is less physiological than TCR-mediated activation, we sought to re-evaluate these findings using anti-CD3-mediated TCR stimulation.

Quantitative PCR analysis confirmed that GAL-9 mRNA is expressed in Jurkat cells but revealed no increase following TCR stimulation (**Figure 19A**). Western blot analysis showed two bands corresponding to the expected molecular weights of the L and M isoforms; however, no difference was observed between unstimulated and stimulated conditions (**Figure 19B**). Flow cytometry analysis revealed no increase in surface GAL-9 expression upon TCR stimulation (**Figure 19C**). In contrast, ELISA analysis of Jurkat cells supernatant demonstrated a marked increase in GAL-9 secretion, with levels rising by at least fourfold following TCR stimulation (**Figure 19D**).

Together, these results indicate that physiological TCR stimulation of T cells does not enhance GAL-9 transcription or total protein abundance, with no impact on cell surface expression, but greatly increases its secretion into the extracellular milieu. This process may facilitate interactions between GAL-9 and the latent TGF-β1 complex, thereby contributing to subsequent TGF-β1 activation.

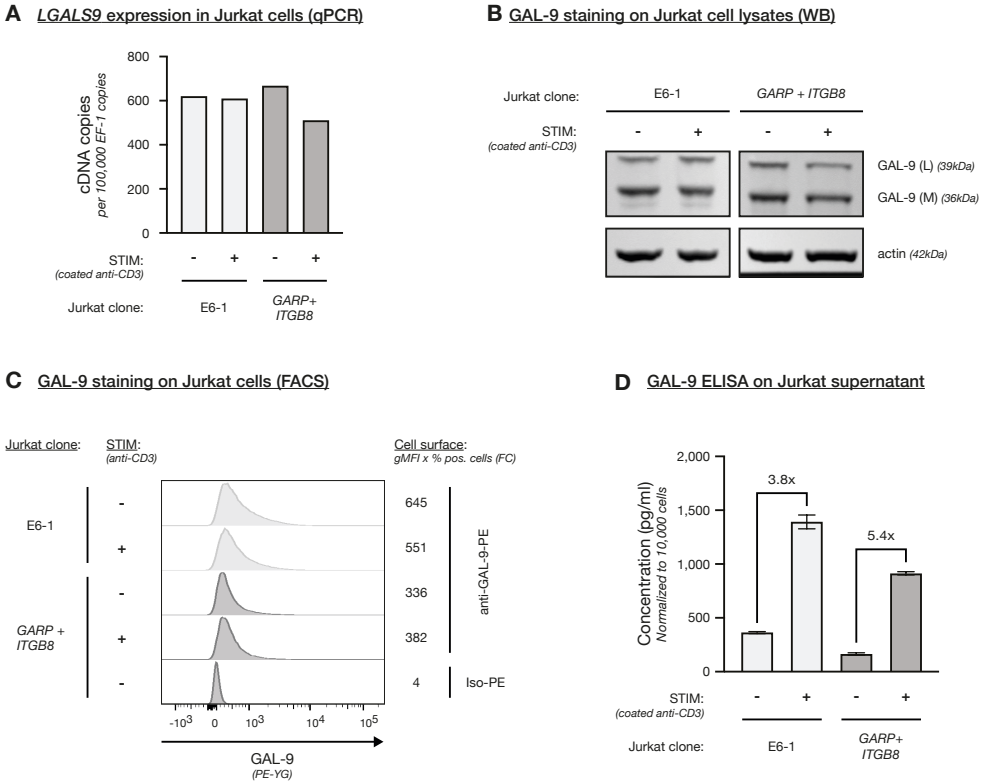

Figure 19: GAL-9 in Jurkat cells.
Each experiment includes both E6-1 and *GARP*/*ITGB8* stably expressing Jurkat cells, either unstimulated or stimulated with coated anti-CD3. Cells were harvested between 20 and 24 hours post-STIM. (**A**) qPCR analysis of *LGALS9* expression (all isoforms) shows robust expression in both clones, with no significant change upon TCR stimulation. Data are presented as cDNA copy number per 100,000 EF-1 copies. (**B**) Western blot analysis showing comparable expression levels of the L and M isoforms. (**C**) Flow cytometry (FACS) analysis showing surface GAL-9 expression in unstimulated versus STIM cells. The y-axis represents counts normalized to mode. (**D**) ELISA performed on cell culture supernatants shows a marked increase in GAL-9 levels following TCR stimulation. Values are expressed in pg/mL and normalized to 10,000 cells.

Jurkat *LGALS9*$^{-/-}$ retain the ability to activate TGF-β1

TGF-β1 activation in Jurkat cells depends on both GARP and αVβ8 and requires TCR stimulation. Given that TCR engagement induces the secretion of GAL-9, we hypothesized that GAL-9 may represent the additional partner required for TGF-β1 activation under these conditions. To test this hypothesis, we generated GAL-9 knockout (*LGALS9*$^{-/-}$) clones derived from parental Jurkat$^{GARP/ITGB8}$ using the CRISPR-Cas9 technology. Clonal knockout was validated for 11 clones using the same technical approaches described above: qPCR, Western blotting, flow cytometry, and ELISA, confirmed complete loss of GAL-9 expression in KO clones, except one. For clarity, we show the results for one representative clone (1.5) (**Figure 20A-D**).

Following validation, we assessed the capacity of each clone to support TCR-dependent TGF-β1 activation (**Figure 20E**). Unexpectedly, while some GAL-9-deficient clones completely lost the ability to activate TGF-β1, others retained this function. Further analysis revealed that all clones that failed to activate TGF-β1 also exhibited a marked loss of αVβ8 surface expression, as determined by flow cytometry. Because αVβ8 is indispensable for TGF-β1 activation in this model, these findings preclude any direct conclusion regarding the role of GAL-9 in TGF-β1 activation at this stage.

One possible explanation is that GAL-9 may contribute to the stabilization of αVβ8 at the cell surface in a clone-dependent manner. To test this hypothesis, we selected one GAL-9 knockout clone in which GAL-9 (L) was re-expressed via lentiviral transduction to assess whether αVβ8 surface expression could be restored. Analysis was performed on the reinfected bulk population (no single cell cloning). Efficient re-expression of GAL-9 was achieved; however, this did not lead to recovery of αVβ8 surface expression, nor did it restore TGF-β1 activation by these cells.

Taken together, these data indicate that GAL-9 is not required for TGF-β1 activation in T cells and suggest that the loss of αVβ8 expression observed in certain knockout clones likely reflects a GAL-9-independent clonal effect.

A *LGALS9* expression in Jurkat cells

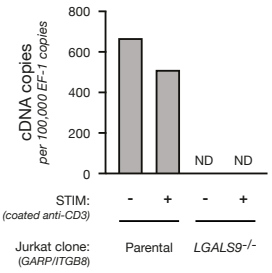

B GAL-9 staining on Jurkat cell lysates (WB)

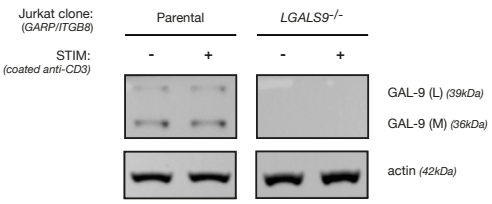

C GAL-9 staining on Jurkat cells (FACS)

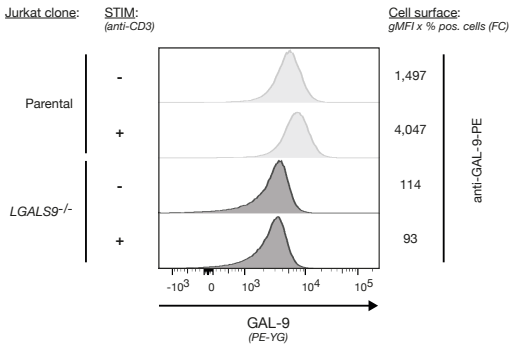

D GAL-9 ELISA on Jurkat supernatant

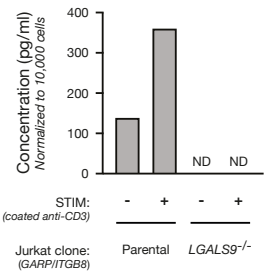

E Summary of *LGASL9* KO clones

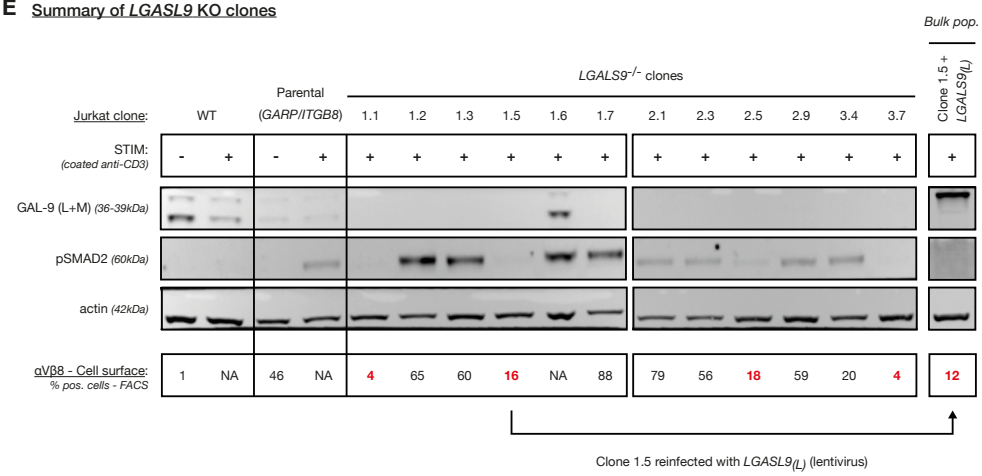

Figure 20: Generation of *LGALS9*$^{-/-}$ Jurkat clones to investigate GAL-9 implication in T cell-mediated TGF-β1 activation.
Each experiment includes *GARP*/*ITGB8* (parental) and *LGALS9*$^{-/-}$ clone 1.5 Jurkat cells. (**A**) qPCR analysis of LGALS9 expression confirms complete loss of *LGALS9* transcripts in the KO clone. Data are presented as cDNA copy number per 100,000 EF-1 copies. ND: not detected. (**B**) Western blot analysis confirms the absence of GAL-9 protein expression in the KO clone. (**C**) FACS analysis shows markedly reduced surface staining in the KO clone. The y-axis represents counts normalized to mode. (**D**) ELISA performed on cell culture supernatants shows complete loss of detectable GAL-9 in the KO clone. Values are expressed in pg/mL and normalized to 10,000 cells. (**E**) Summary panel showing GAL-9 detection (Western blot), SMAD2 phosphorylation (Western blot), and αVβ8 surface staining in WT, parental, *LGALS9*$^{-/-}$ clones, and clone 1.5 reinfected with the *LGALS9* (L) isoform. Although GAL-9 expression is abolished in the KO clones, some retain the ability to activate TGF-β1, as evidenced by pSMAD2 detection following TCR stimulation. Notably, clones that lose the ability to activate TGF-β1 consistently exhibit a marked reduction in surface αVβ8 expression. GAL-9 (L) re-expression did not restore their ability to activate TGF-β1. NA: not applicable.

1.4 Screening in the presence of αVβ8

In parallel with the work described in **Section 1.3**, we conducted a second screening using a similar reporter system. As in the initial screen, both the test cells and responder cells co-expressed GARP and latent TGF-β1. In addition, these cells were engineered to stably express αVβ8 heterodimers through lentiviral transduction. Under these conditions, the cells already exhibited spontaneous TGF-β1 activation, as evidenced by the reduction of background reporter signal upon treatment with 1D11 (data not shown). Nevertheless, we proceeded with the screening and were still able to detect additional increase in reporter activity.

All 962 pools of 100 cDNA clones were screened again under these conditions. In this second screen, only three candidates were validated: ADCK1, RHOA, and TUBA4A, all of which are intracellular proteins and are at least partly associated with cytoskeletal functions. At this stage, we decided not to pursue these candidates further and instead shifted our focus to the potential role of the cytoskeleton and the involvement of the cytoplasmic tails of GARP and β8. These results will be presented in the second part (**Section 2**) of the Results.

1.5 Discussion

T cells expressing the TGF-β1 partner proteins GARP and integrin αVβ8 do not spontaneously activate TGF-β1. Instead, additional TCR stimulation and downstream signaling are required, suggesting that one or more additional partners, beyond GARP and αVβ8, may be necessary for effective TGF-β1 activation. To identify such partners, we performed a screening (first, in the absence of αVβ8) of a cDNA library derived from TCR-stimulated Tregs, which led to the identification of GAL-9. In a second screening (in the presence of αVβ8), we only identified intracellular candidates. In this discussion, we examine our experimental findings in the context of the literature to highlight the multiple connections between GAL-9 and TGF-β1, the complexity of GAL-9 biology, the limitations of this study, and to propose hypotheses regarding a potential role of GAL-9 in TGF-β1 activation. Finally, we discuss how the second screening prompted us to focus on a potential role for the cytoplasmic tails of GARP and β8 and/or the cytoskeleton in TGF-β1 activation.

1.5.1 Galectin-9 biology

GAL-9 is a tandem-repeat galectin composed of two distinct CRDs linked by a flexible linker (**Figure 21A**). The two CRDs display differential glycan-binding specificities, enabling interactions with a broad range of cell-surface glycoproteins (*231-235*). GAL-9 exists in several isoforms (*229*), the three main ones being the long (L), the medium (M) and the short (S) isoforms. These isoforms differ in linker length due to alternative splicing of exons 5 and 6 (**Figure 21B-C**), a feature that may influence its cellular localization, secretion, and functional activity. In addition to the diversity of its isoforms, additional variability arises from post-translational modifications, including linker cleavage and oligomerization (*236*). In T cells, the L and M GAL-9 isoforms are constitutively expressed. GAL-9 expression is regulated by cell activation and inflammatory signals and can be detected intracellularly, at the cell surface, or released into the extracellular milieu through regulated, though still poorly understood, secretion mechanisms (*230*).

GAL-9 has emerged as a potent immunoregulatory molecule, particularly in the context of T-cell responses. It suppresses effector T-cell activity and promotes immune tolerance through interactions with inhibitory receptors such as TIM-3, a pathway implicated in chronic viral

infection and immune exhaustion (*237*). Beyond direct inhibition of effector T cells, GAL-9 plays a critical role in the induction and maintenance of Tregs. Recombinant GAL-9 promotes the conversion of naïve $CD4^+$ T cells into $Foxp3^+$ induced Tregs (iTregs), an effect that is strictly dependent on intact TGF-β signaling (*238*).

Consistent with its ability to potentiate TGF-β signaling, GAL-9 has been implicated in pathological immunosuppression in fibrosis and cancer. GAL-9-deficiency protects mice from bleomycin-induced fibrosis by attenuating TGF-β/Smad signaling and fibroblast activation (*239*). In cancer, GAL-9 is frequently overexpressed and contributes to immune evasion by suppressing cytotoxic lymphocyte function and reinforcing regulatory pathways. In malignant cells, GAL-9 expression is driven by a TGF-β1/Smad3-dependent transcriptional program activated downstream of hypoxia-responsive pathways, highlighting a self-sustaining immunosuppressive circuit in the tumor microenvironment (*240*).

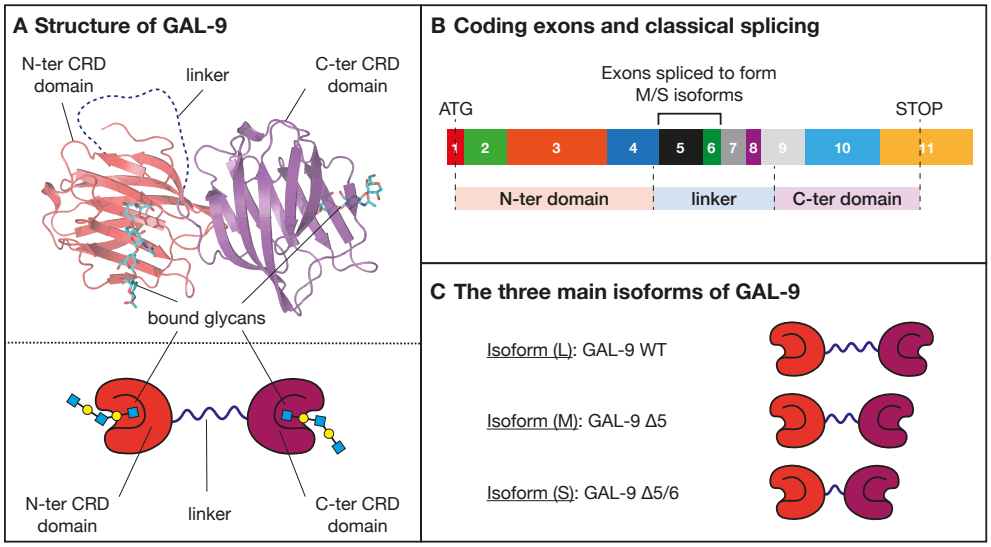

Figure 21: Structure and main isoforms of GAL-9
(**A**) Top panel: three-dimensional cartoon representation of the two CRDs of GAL-9 (N-terminal in red and C-terminal in purple). The flexible linker is shown as a dashed blue line. Two glycans are depicted at the recognition site of each CRD. Structural data from (*233*) (PDB 2ZHK). Bottom panel: schematic representation of GAL-9 using the same color code, with the linker shown as a blue connector. Putative bound glycan structures are shown as curved lines, with individual monosaccharide residues represented by blue squares and yellow circles. (**B-C**) GAL-9 is encoded by 11 exons. The N-terminal CRD is encoded by exons 1-4, the linker by exons 4-9, and the C-terminal CRD by exons 9-11. Alternative splicing of exons 5 and/or 6 generates the M and S isoforms, which are shorter than the L isoform.

1.5.2 Galectin-9 enhances TGF-β signaling

The precise mechanism by which GAL-9 amplifies TGF-β1 signaling remains incompletely understood. Wu et al. (2014) showed that, in iTregs, GAL-9 directly binds CD44, which in turn associates with TβRI. This interaction is thought to promote receptor crosslinking, thereby potentiating TGF-β signaling and enhancing both Treg stability and suppressive function (**Figure 22**) (*241*). In this context, GAL-9 expression is itself induced by the phosphorylated SMADS in iTregs, establishing a feed-forward loop that reinforces Treg identity.

In light of our observations, one possible interpretation of the screening results is that the increased TGF-β1 signaling reflects GAL-9-mediated clustering of TGF-β receptors, potentially resulting in ligand-independent activation or elevated basal signaling. However, HEK 293T cells are not known to express CD44, the surface protein implicated by Wu et al. (2014) in this mechanism. This discrepancy suggests that the signaling enhancement observed in our system may rely on an alternative process. Further experiments, such as the analysis of TβRI and/or TβRII surface clustering in the presence or absence of GAL-9 in 293T cells, would be required to address this possibility.

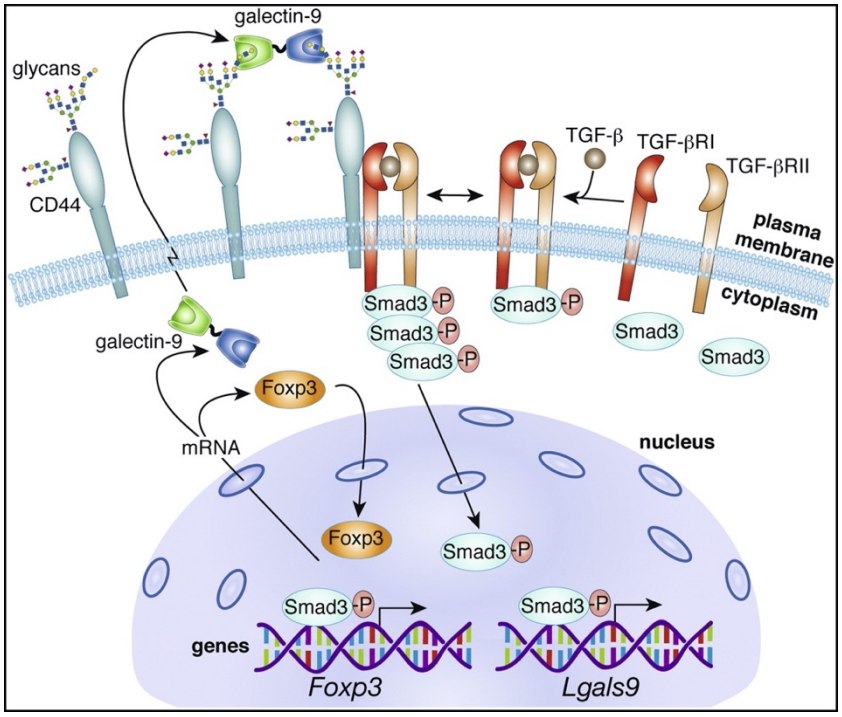

Figure 22: Wu et al. (2014) model: Galectin-9 signals iTregs through interactions with CD44
Figure reproduced from Cummings, 2014 (*242*). Through cooperation between GAL-9, CD44 and ligand-engaged TGF-β receptors, SMAD3 phosphorylation is increased, leading to nuclear translocation of SMAD3 and transcriptional upregulation of Foxp3 and GAL-9. This establishes a positive feedback loop in which GAL-9 reinforces Treg identity and function. Based on the results of Wu et al (*241*).

1.5.3 The bizarre TGM proteins in helminths and Galectin-9

Intestinal parasites, and helminths in particular, have evolved sophisticated strategies to modulate host immune responses in order to establish long-term infections. In many parasitic infections, TGF-β signaling has been associated with the expansion of Tregs, thereby suppressing host anti-parasitic immunity. Rick M. Maizels and colleagues investigated a family of helminth-secreted proteins known as transforming growth factor-β mimics (TGMs), whose function is to trigger host TGF-β1 signaling and thereby modulate immune responses (*243, 244*).

TGMs are classically composed of five globular domains. Domains 1, 2, and 3 interact with TβRI and TβRII, whereas domains 4 and 5 have been described as co-receptor-binding domains (*243*). Notably, domains 4-5 of TGM1 from *Heligmosomoides polygyrus* engage CD44 as a co-receptor, thereby enhancing TGF-β signaling and promoting Treg induction. In their discussion, the authors compared this mechanism to the model of Wu et al. (2014) – cfr. **Section 1.5.2** – which demonstrates that CD44 and TβRI cluster in a GAL-9-dependent manner in induced Tregs (*241*). Based on these observations, they propose that GAL-9 may be required for the function of the co-receptor–binding domains of TGM1 (*245*).

Supporting this hypothesis, a subsequent study from Maizels and colleagues identified GAL-9 by mass spectrometry in pull-down assays as one (among others) potential co-receptor for TGM1 and TGM4 (*246*). Together, these findings further strengthen the proposed link between GAL-9 and TGF-β1, even in the context of an evolutionarily distant system that intend to mimic and trigger TGF-β signaling in mammals.

1.5.4 Galectin-9 (Δ) isoform

Our data revealed that the GAL-9 sequence identified in the cDNA library corresponds to a previously uncharacterized “isoform”. This form lacked part of the N-terminal CRD as well as a portion of the linker region, while retaining an intact C-terminal CRD; we designated it the Δ variant. We ultimately concluded that this isoform is most likely an artifact without intrinsic physiological relevance. This conclusion was based on its absence from public databases and the inability to detect it in the original mRNA samples by qPCR. Nevertheless, its identification raises points worth considering.

Post-translational modifications are known to influence galectins functions. In particular, proteolytic cleavage leading to individual CRDs, as well as oligomerization, have been reported to alter galectins activity and signaling properties (*229, 236*). In this context, the artificial truncation of the N-terminal region in the Δ variant could plausibly affect GAL-9 multivalency, protein crosslinking capacity, and more broadly its tertiary and/or quaternary structure. Such a truncation could therefore mimic, at least partially, the functional consequences of specific post-translational modifications.

As mentioned in **Section 1.5.1**, the two CRDs of GAL-9 exhibit distinct glycan-binding specificities. While both recognize β-galactosides, the N-terminal CRD shows a pronounced preference for LacNAc motifs within poly-N-acetyllactosamine chains, whereas the C-terminal CRD preferentially engages complex N-glycans, including biantennary structures and sialylated ligands (*231-235*). This functional asymmetry, combined with potential cleavage or altered multivalency, could theoretically orient GAL-9 (Δ) activity toward C-terminal CRD-driven interactions.

We explored this possibility using a construct encoding only the C-terminal CRD of GAL-9; however, these experiments yielded inconclusive results with no TGF-β1 activation detected. Further investigation would be required to determine whether selective engagement of the C-terminal CRD can recapitulate any of the effects observed in the screening assay.

1.5.5 Are GARP and latent TGF-β1 ligands for GAL-9?

Although both GARP and latent TGF-β1 are known to be glycosylated (*52, 75, 247, 248*), the precise nature and composition of their glycans remain poorly characterized. As a result, while it cannot be excluded that glycan structures on GARP and/or latent TGF-β1 could, in principle, be recognized by GAL-9 through its N- or C-ter CRDs, there is currently no experimental evidence supporting such interactions. We therefore sought to assess whether GAL-9 is capable of directly binding GARP and/or latent TGF-β1; an interaction that – we hypothesized – could be a prerequisite for GAL-9-mediated TGF-β1 activation.

To address this question, we performed co-immunoprecipitation (Co-IPs) assays. However, these experiments did not yield conclusive results, as GAL-9 expression was associated with nonspecific signals, including when isotype control antibodies were used for immunoprecipitation (data not shown). This likely reflects nonspecific crosslinking or aggregation effects resulting from GAL-9 overexpression, which complicate the interpretation of such assays.

At this stage, we are therefore unable to confirm or exclude a direct interaction between GAL-9 and either GARP or latent TGF-β1.

1.5.6 Is GAL-9 involved in TGF-β1 activation in other cell types?

As described in **Section 1.2**, although the primary objective of the screening was to identify candidates involved in TGF-β1 activation in Tregs, it was first performed in the absence of αVβ8. This approach was chosen to allow the identification of potential αVβ8-independent mechanisms, including mechanisms that might operate in non-Treg cell types. Indeed, TGF-β1 has been widely reported to be expressed by a variety of cell types, either as a soluble cytokine or in a latent form presented at the cell surface through GARP or LRRC33. However, TGF-β1 expression and surface presentation do not necessarily imply efficient activation of the cytokine. For example, endothelial cells have been shown to present TGF-β1 via GARP (*142, 158*), and monocytes can present it via LRRC33 (*38, 142*). In both cases, spontaneous activation in monoculture under basal conditions has not been clearly demonstrated. We therefore investigated whether GAL-9 could trigger TGF-β1 activation in these cell types. To this end, the long (L) isoform of GAL-9 was overexpressed by lentiviral transduction in endothelial cells and monocytes. In parallel, GAL-9 was also overexpressed in 293T cells stably expressing both GARP and TGF-β1, which were included as a positive control, as this cellular system was used during the screening phase in which GAL-9 was initially identified.

We had only observed endogenous GAL-9 expression in THP-1 cells, where the medium (M) isoform was observed. We therefore used a THP-1$^{LGALS9-/-}$, kindly provided by Pierre Maus from Nisha Limaye's team (DDUV, UCLouvain). Efficient re-expression of GAL-9 (L) following lentiviral transduction was confirmed by qPCR, Western blotting, and flow cytometry (data not shown).

TGF-β1 activity was subsequently assessed by Western blot analysis of SMAD2 phosphorylation. No increase in pSMAD2 signaling was observed in any of the reinfected cell lines (HUVEC, THP-1, or 293T$^{GARP/TGFB1+}$). Reinfected 293T$^{GARP/TGFB1+}$ cells were also further tested using a TGF-β1 reporter co-culture assay identical to that used during the screening phase (**Figure 16**), with infected cells replacing the "test cells". Consistently, no increase in TGF-β1 activity was detected.

Together, these results suggest that GAL-9 re-expression alone is unlikely to contribute to TGF-β1 bioavailability in these cellular contexts. Notably, the absence of an effect in the 293T

model is unexpected, as this system was used in the initial screening in which GAL-9 was identified. While a definitive explanation is lacking, several hypotheses can be proposed.

- First, the screening identified an atypical GAL-9 (Δ) variant that consistently induced a stronger TGF-β1 signal than the canonical GAL-9 (L) isoform. It is therefore possible that the phenotype observed during screening was driven primarily by this Δ variant and cannot be efficiently recapitulated by re-expression of the L isoform alone.

- Second, transient transfection used in the screening may result in high and heterogeneous level of GAL-9 expression, potentially exceeding a threshold required to induce protein crosslinking, or indirect modulation of SMAD signaling. In contrast, lentiviral re-expression of GAL-9 (L) is more uniform and may not reach comparable functional levels, particularly at the cell surface or in the extracellular milieu.

- Additional factors may include differences in GAL-9 secretion, surface display, or post-translational processing. Together, these considerations suggest that the failure to reproduce the screening phenotype might also reflect differences between the Δ and L isoforms and between transient and stable expression contexts.

To conclude, GAL-9 has been described as a multifunctional and context-dependent molecule, implicated in a wide range of biological processes that may complicate data interpretation (*236*). Based on our observations and on the literature, it is likely that any effect associated with GAL-9 in our assays does not reflect direct activation of TGF-β1, but rather indirect consequences of GAL-9 overexpression, such as nonspecific protein crosslinking or modulation of TGF-β1 signaling. In conclusion, GAL-9 does not appear to participate in TGF-β1 activation in T cells.

1.5.7 The intracellular candidates

In the second screen performed in the presence of αVβ8, three candidates were validated: ADCK1, RHOA, and TUBA4A. All three are intracellular proteins, at least partially associated with cytoskeletal functions. Rather than directly characterizing these proteins, these results prompted us to investigate potential intracellular interactions involving the actin cytoskeleton and/or the cytoplasmic domains of GARP and β8. Both proteins contain intracellular (IC) domains but differ substantially in size: GARP has a short 14-amino acid IC tail, whereas β8 contains a longer 65-amino acid cytoplasmic tail.

The IC domain of GARP has been investigated previously. While loss of membrane anchorage was shown to impair TGF-β1 activation, deletion of the IC domain did not alter GARP-mediated immunosuppressive function. However, no clear mechanistic connection to TGF-β1 activation was established at that time (*25*). Similarly, the role of the β8 IC domain remains debated. In the present work, we therefore sought to determine whether the IC domain of both GARP and β8 are required for their function, specifically in the context of TGF-β1 activation. We also used previously described activating monoclonal antibodies (mAbs) to probe the molecular requirements for TGF-β1 activation.

The results of these investigations constitute a second chapter to this work and are compiled in the manuscript presented in the following section (**Section 2**). Our objective is to submit this work to a peer-reviewed research journal, and to deposit it on bioRxiv for open peer review.

1.6 Material and methods

1.6.1 Cell culture

All cell lines were maintained at 37°C in a humidified atmosphere with 5% CO_2 for Jurkat E6-1 cells or 8% CO_2 for HEK 293T, in media supplemented with 100 IU/mL penicillin and 0.1 mg/mL streptomycin (Sigma-Aldrich), unless otherwise specified.

- 293T cells

HEK 293T cells were cultured in DMEM (Gibco) supplemented with 10% fetal bovine serum (FBS, Cytiva), 1% GlutaMAX (Gibco), and antibiotics. At 70–90% confluency, cells were detached using 0.05% trypsin-EDTA (Gibco), neutralized with complete medium, centrifuged at 300 × g for 5 minutes, and resuspended in fresh medium for passaging at a 1:20 dilution. A HEK 293T clone stably co-expressing GARP and TGF-β1 was previously established in the lab via transfection of GARP-ORF and TGFB1 cDNA vectors, followed by limiting dilution under puromycin selection, with clonal validation performed by flow cytometry (FACS). A HEK 293T clone stably co-expressing GARP, TGF-β1 and ITGB8 was obtained via retroviral infection of 293T$^{GARP/TGFB1+}$, followed by single cell FACS cloning.

- Jurkat cells

Jurkat E6-1 cells were cultured in RPMI (Gibco) supplemented with 10% FBS, 1% GlutaMAX, and antibiotics. Cells were passaged every 2-3 days by dilution to 1×10^5 viable cells/mL when reaching 1-3 × 10^6 cells/mL. Jurkat cells expressing GARP and αVβ8 were generated by electroporation of HA-*ITGB8* in pDisplay, followed by selection under neomycin using limiting dilution conditions as previously described (*121*). The Jurkat + HA-*ITGB8* clone was subsequently transduced with a lentivirus encoding GARP as described in Stockis et al. (2009) (*27*) to generate Jurkat + *GARP* or Jurkat + *GARP* + *ITGB8*-HA cells. Jurkat *LGALS9*$^{-/-}$ cells were generated using CRISPR/Cas9 technology and later reinfected with a lentivirus encoding the long (L) isoform of GAL-9.

- Short-term stimulation (Jurkat) and treatments

Jurkat cells (2.5×10^6 cells/mL) were plated in X-VIVO 10 serum-free medium (Lonza) with plate-bound anti-CD3 (orthoclone OKT3; 1 µg/mL; Janssen-Cilag). Cells were treated with

rhTGF-β1 (R&D Systems), 1D11 (20 μg/mL), and incubated for 24 h under standard conditions.

- Co-culture assays

293T$^{GARP/TGFB1+}$ or 293T$^{GARP/TGFB1/ITGB8+}$ cells were seeded in 6w plates (±1.106/w) and co-transfected using TransIT-LT1 (Mirus Bio) on the same day. **Test cells** were transfected with a plasmid encoding human GAL-9 (L) or (Δ) isoforms, or empty vector controls, for a total of 2.5 μg DNA/well. **Reporter cells** were co-transfected with 99% pCAGA-12-Fluc (Firefly luciferase under TGF-β-responsive promoter, Promega), 1% pRL-TK (Renilla luciferase under constitutive promoter, Promega), for a total of 2.5 μg DNA/well.

24 h post-transfection, cells were harvested, counted, and mixed in 96-well plates at a 1:1 ratio (2×10^4 source cells + 2×10^4 reporter cells/well).

Co-cultures were treated directly with recombinant human TGF-β1 (rhTGF-β1, R&D Systems), anti-TGF-β1/2/3 (1D11, 20 μg/mL), and incubated for 16-24 h under standard conditions. Luciferase activity was measured using the Dual-Glo® Luciferase Assay System (Promega) and GloMax luminescence program (Promega). Firefly luciferase values were normalized to Renilla luciferase to control for transfection efficiency.

1.6.2 Cell genetic engineering

- CRISPR-Cas9

Jurkat LGALS9$^{-/-}$ clones were generated by nucleofecting Jurkat cells with recombinant Cas9, tracrRNA and tested three different guide RNAs targeting early regions in exons 1 and 2 of LGALS9 (sequences provided in **Table S1**), following the Amaxa nucleofection protocol for Jurkat cells. Nucleofection efficiency was assessed by flow cytometry via GAL-9 staining on the bulk population, followed by single-cell sorting. Clones were expanded and validated by FACS, Western blotting, and genetic analysis.

- Cloning and lentiviruses

For cloning of GAL-9 (L), the human LGALS9 mRNA sequence (NM_009587.3) was synthesized by IDT with KpnI and MluI restriction sites (see **Table S2**) and cloned into the pCMV-SPORT6 vector. To enable cloning into the lentiviral vector pTM945 (a lentiviral vector expressing mCherry under a CMV promoter, kindly provided by Thomas Michiels' group), the KpnI-MluI restriction sites were modified to SalI-XbaI via directed PCR. Lentiviral particles

were produced by transient co-transfection of 293T cells with the lentiviral vector and the packaging constructs pCMV_VSVg and psPAX2. Lentivirus-containing supernatants were clarified through a 0.45 μm filter and concentrated using Centricon Plus-70 filters (Millipore). Jurkat cells were infected with 3× concentrated lentivirus in the presence of 8 μg/mL polybrene, and selection was performed 3 days post-infection by FACS sorting of mCherry-positive cells.

1.6.3 Molecular biology

All recombinant DNA constructs were verified by sequencing and restriction analysis on agarose gels. Relevant primers are listed in **Table S3**.

- RT-qPCR

For RT-qPCR, total RNA was extracted using NucleoSpin Mini Columns (Macherey-Nagel), and RNA concentration was determined using a NanoDrop spectrophotometer (Thermo Scientific). Reverse transcription was carried out with the Maxima First Strand cDNA Synthesis Kit (Thermo Fisher). Real-time qPCR was performed using a master mix containing Takyon Master Mix (0.025 U/μL, Eurogentec), primers (300 nM each), Takyon probe (100 nM), and 1.25 μL of cDNA. Reactions were run on a QuantStudio3 device (Thermo Fisher) under fast conditions: 95°C for 3 minutes, followed by 45 cycles of 95°C for 3 seconds and 60°C for 30 seconds. Data analysis was conducted using the Thermo Fisher Cloud Portal. Expression levels of genes of interest were calculated as a ratio of mRNA copy numbers (mRNA/10^5 EF-1), evaluated using standard curves generated with recombinant DNA.

- Western blotting

For Western blotting, cells were counted, dry-pelleted, and stored at -80°C. Lysates were prepared in Laemmli buffer (Bio-Rad) supplemented with 5% 2-mercaptoethanol, homogenized by passage through a 23G (293T) or 25G (Jurkat) needle, boiled at 100°C for 5 minutes, and clarified by centrifugation at 12,000 × g for 5 minutes at 4°C. Equivalents of 5 × 10^4 HEK 293T cells or 1 × 10^5 Jurkat cells were loaded onto 4–12% Bis-Tris gels (Thermo Fisher Scientific) for protein separation. Proteins were transferred to nitrocellulose membranes using the iBlot2 system (Thermo Fisher Scientific). Membranes were blocked for 1 hour in 5% non-fat milk in PBS-Tween 0.1% and incubated with primary antibodies: GAL-9 (polyclonal rabbit IgG, Abcam #ab228686, or clone 1G3, Merck Millipore), pSMAD2 (clone

138D4, Cell Signaling Technology), and β-actin (clone AC-15, Merck Millipore) as a loading control. Secondary antibodies included anti-rabbit IgG-HRP (Cell Signaling Technology #7074) and anti-mouse IgG light chain-HRP (Jackson ImmunoResearch #115-035-174). Signals were detected using SuperSignal West Pico or Femto substrates (Thermo Fisher Scientific) and imaged on a Fusion Solo 4S system (Vilber-Lourmat).

- Flow cytometry

For flow cytometry, single-cell suspensions were counted using a Luna® cell counter with Acridine Orange/Propidium Iodide staining (Logos Biosystems). Cells were resuspended in FACS buffer (2 mM EDTA, 1% FBS in PBS) and incubated with the following antibodies for 20 minutes at 4°C: anti-αVβ8 integrin (clone ADWA-16, kind gift from Dean Sheppard (*249*)), anti-mouse IgG-PE (clone Poly4053, BioLegend), or anti-GAL-9-PE (clone 9M1-3, BD Biosciences). Labeled cells were analyzed on an LSR Fortessa cytometer (BD Biosciences), and data were processed using FlowJo software (Tree Star).

- Enzyme-linked immunosorbent assay (ELISA)

Secreted GAL-9 was quantified using the Human Galectin-9 DuoSet ELISA kit (R&D Systems #DY2045), following the manufacturer's instructions. Absorbance was measured at 450 nm (with a reference at 600 nm) using a GloMax reader (Promega).

1.6.4 Supplementary material

Supplementary Table 1: guide RNAs for *LGASL9*-KO

# collection	Target sequence	Specificity
CR129	GGGAGCCTGGGAACCGCTGA	*LGALS9* exon 1
CR130	GGACTTCAGATCACTGTCAA	*LGALS9* exon 2
CR131	CTTGAATAGTCCCAGAAAAG	*LGALS9* exon 2

Supplementary Table 2: GAL-9 mRNA sequence insert

Name	Sequence
KpnI-MluI-NM_009587.3	TAAGCAGGTACCCTTTGTTAAGTCGTTCCCTCTACAAAGGACTTCCTAGTG GGTGTGAAAGGCAGCGGTGGCCACAGAGGCGGCGGAGAGATGGCCTTCA GCGGTTCCCAGGCTCCCTACCTGAGTCCAGCTGTCCCCTTTTCTGGGACTA TTCAAGGAGGTCTCCAGGACGGACTTCAGATCACTGTCAATGGGACCGTTC TCAGCTCCAGTGGAACCAGGTTTGCTGTGAACTTTCAGACTGGCTTCAGTG GAAATGACATTGCCTTCCACTTCAACCCTCGGTTTGAAGATGGAGGGTACG TGGTGTGCAACACGAGGCAGAACGGAAGCTGGGGGCCCGAGGAGAGGAA GACACACATGCCTTTCCAGAAGGGGATGCCCTTTGACCTCTGCTTCCTGGT GCAGAGCTCAGATTTCAAGGTGATGGTGAACGGGATCCTCTTCGTGCAGTA CTTCCACCGCGTGCCCTTCCACCGTGTGGACACCATCTCCGTCAATGGCT CTGTGCAGCTGTCCTACATCAGCTTCCAGAACCCCCGCACAGTCCCTGTTC AGCCTGCCTTCTCCACGGTGCCGTTCTCCCAGCCTGTCTGTTTCCCACCCA GGCCCAGGGGGCGCAGACAAAAACCTCCCGGCGTGTGGCCTGCCAACCC GGCTCCCATTACCCAGACAGTCATCCACACAGTGCAGAGCGCCCCTGGAC AGATGTTCTCTACTCCCGCCATCCCACCTATGATGTACCCCCACCCCGCCT ATCCGATGCCTTTCATCACCACCATTCTGGGAGGGCTGTACCCATCCAAGT CCATCCTCCTGTCAGGCACTGTCCTGCCCAGTGCTCAGAGGTTCCACATCA ACCTGTGCTCTGGGAACCACATCGCCTTCCACCTGAACCCCCGTTTTGATG AGAATGCTGTGGTCCGCAACACCCAGATCGACAACTCCTGGGGGTCTGAG GAGCGAAGTCTGCCCCGAAAAATGCCCTTCGTCCGTGGCCAGAGCTTCTC AGTGTGGATCTTGTGTGAAGCTCACTGCCTCAAGGTGGCCGTGGATGGTC AGCACCTGTTTGAATACTACCATCGCCTGAGGAACCTGCCCACCATCAACA

	GACTGGAAGTGGGGGGCGACATCCAGCTGACCCATGTGCAGACATAGGC GGCTTCCTGGCCCTGGGGCCGGGGGCTGGGGTGTGGGGCAGTCTGGGT CCTCTCATCATCCCCACTTCCCAGGCCCAGCCTTTCCAACCCTGCCTGGGA TCTGGGCTTTAATGCAGAGGCCATGTCCTTGTCTGGTCCTGCTTCTGGCTA CAGCCACCCTGGAACGGAGAAGGCAGCTGACGGGGATTGCCTTCCTCAG CCGCAGCAGCACCTGGGGCTCCAGCTGCTGGAATCCTACCATCCCAGGAG GCAGGCACAGCCAGGGAGAGGGGAGGAGTGGGCAGTGAAGATGAAGCCC CATGCTCAGTCCCCTCCCATCCCCCACGCAGCTCCACCCCAGTCCCAAGC CACCAGCTGTCTGCTCCTGGTGGGAGGTGGCCTCCTCAGCCCCTCCTCTC TGACCTTTAACCTCACTCTCACCTTGCACCGTGCACCAACCCTTCACCCCT CCTGGAAAGCAGGCCTGATGGCTTCCCACTGGCCTCCACCACCTGACCAG AGTGTTCTCTTCAGAGGACTGGCTCCTTTCCCAGTGTCCTTAAAATAAAGAA ATGAAAATGCTTGTTGGCACATTCAACGCGTATCGAC

Supplementary Table 3: Primers sequences

Primer #	Primer sequence	Specificity
OPC4745	acgaagtcgaCCTTTGTTAAGTCGTTCCCTC	KpnI to SalI START LGALS9
OPC4746	agctctctagaTGAATGTGCCAACAAGCATTTTC	MluI to XbaI STOP LGALS9
OPC4528	CCAGACAGTCATCCACACAG	LGASL9 « all » FW (qPCR)
OPC4529	TGATGAAAGGCATCGGATAGG	LGALS9 « all » RV (qPCR)
OPC4530	TCTACTCCCGCCATCCCACCTAT	LGALS9 « all » probe FAM-TAMRA (qPCR)
OPC4531	TCTGGGACTATTCAAGGAGGT	LGASL9 « Δ » FW (qPCR)
OPC4532	GAGAAGGCAGGCTGAAAGTT	LGALS9 « Δ » RV (qPCR)
OPC4533	ACTGTCAATGGGACCGTTCTCAGC	LGALS9 « Δ » probe FAM-TAMRA (qPCR)
OPC1691	GCTTCACTGCTCAGGTGAT	EF-1 FW (qPCR)
OPC1692	GCCGTGTGGCAATCCAAT	EF-1 RV (qPCR)
OPC1693	AAATAAGCGCCGGCTATGCCCCTG	EF-1 probe (qPCR)

2 Molecular requirements for TGF-β1 activation by αVβ8 or monoclonal antibodies

Article by Jamez et al., to be submitted:

Integrin αVβ8 passively activates TGF-β1 by transmitting cell-generated tensile forces without direct interaction with the cytoskeleton, allowing paracrine TGF-β1 activity

Integrin αVβ8 passively activates TGF-β1 by transmitting cell-generated tensile forces without direct interaction with the cytoskeleton, allowing paracrine TGF-β1 activity

Mathieu Jamez,[1] Séverine Wautier,[1] Camille Michiels,[1] Ananyashree Kathotia,[1] Fatima Benhaddi,[1] Nicolas Dauguet,[1] Lore Mariën,[3] Manon Lesage,[3] Bas van der Woning,[3] Tiphanie Gomard,[1,4,*] and Sophie Lucas[1,2,4,*]

[1] de Duve Institute, UCLouvain, 1200 Brussels, Belgium

[2] WELBIO Department, WEL Research Institute, 1300 Wavre, Belgium

[3] argenx BV, Industriepark Zwijnaarde 7, 9052 Ghent, Belgium

[4] Senior authors

[*] Correspondence: sophie.lucas@uclouvain.be (S.L.) and tiphanie.gomard@uclouvain.be

ABSTRACT

Transforming Growth Factor β1 (TGF-β1) is produced by all cell types as a proTGF-β1 homodimer that is cleaved in the secretory pathway into latent TGF-β1, composed of the m(ature)TGF-β1 and Latency Associated Peptide (LAP). Depending on the cell type, LAP covalently associates with secreted LTBPs or transmembrane (TM) proteins GARP or LRRC33, resulting in latent TGF-β1 deposition in the extracellular matrix or presentation on the cell surface, respectively. Latent TGF-β1 is inactive because LAP masks sites required for mTGF-β1 interaction with the TGF-β receptor (TβR). The cytokine can be activated by integrins αVβ6 or αVβ8, which induce a conformational change in LAP allowing access of mTGF-β1 to the TβR. Activation by αVβ6 occurs via transmission of cell-generated tensile forces to LAP, thanks to interaction of the β6 intracellular (IC) domain with the cytoskeleton. Because the β8 IC domain lacks canonical motifs for interaction with the cytoskeleton, the tensile force model was suggested not to apply to TGF-β1 activation by αVβ8. An alternative model based on entropy-redistribution was proposed, in which activation by αVβ8 occurs without mTGF-β1 release from LAP, allowing autocrine, but not paracrine signaling. Here, we unequivocally show that TGF-β1 activated by αVβ8 can exert paracrine activity. We also show that an αVβ8 variant lacking the β8 IC and TM domains still activates latent TGF-β1, indicating that activation does not require direct interaction of β8 with the cytoskeleton or the cell membrane. This mode of activation is similar to that previously described for TGF-β1-activating monoclonal antibodies (mAbs). Activation by αVβ8 or mAbs requires that LAP is covalently linked to a protein anchored in a cell membrane on one side, and interacts with a protein that is itself anchored in a cell membrane or on a solid surface on the other. Inhibitors of actin polymerization abrogate TGF-β1 activation by mAbs and αVβ8, including when the β8 IC and TM domains are lacking. This suggests that cell-generated tensile forces are required and can be transmitted by αVβ8 or mAbs to LAP in the absence of direct contacts with the cytoskeleton. Altogether, our work shows that αVβ8, similar to TGF-β1 activating mAbs, passively activates TGF-β1 by transmitting cell-generated tensile forces to exert autocrine and paracrine activity.

KEYWORDS

transforming growth factor 1, integrin αVβ8, monoclonal antibodies, cytoskeleton

INTRODUCTION

Transforming Growth Factor-β1 (TGF-β1) is a pleiotropic cytokine that regulates key biological processes including morphogenesis, angiogenesis, and immune homeostasis (*1*). It is synthesized as a pre-pro-peptide that dimerizes after signal peptide removal in the ER. The resulting proTGF-β1 precursor is then cleaved by furin at a conserved RHRR motif to generate a C-ter homodimer corresponding to the mature cytokine (mTGF-β1), and a N-ter homodimer called Latency Associated Peptide or LAP (*2-4*). LAP remains non-covalently associated with mTGF-β1, forming a latent TGF-β1 complex that is inactive because LAP masks receptor-binding sites on mTGF-β1 (*5, 6*). In the vesicular pathway of TGF-β1 producing cells, LAP associates via disulfide bond formation with secreted Latent TGF-β Binding Proteins (LTBPs), or with transmembrane (TM) proteins GARP or LRRC33. This results either in deposition of latent TGF-β1 in the extracellular matrix when latent TGF-β1 is produced in association with LTBPs, or presentation on the cell surface when it is produced in association with GARP or LRRC33 (*5, 7-11*).

Latent TGF-β1 requires activation to exert biological activity. TGF-β1 activation involves conformational changes in LAP that permit engagement of the heterotetrameric TGF-β receptor (TβR) by the mature cytokine. Three heterodimeric RGD-binding integrins, namely αVβ1, αVβ6, and αVβ8, have been shown to activate latent TGF-β1 presented by LTBPs, GARP, or LRRC33. Activation by αVβ6 and αVβ8 appears to play predominant roles *in vivo*, as their combined deletion fully recapitulates the phenotype associated with TGF-β1 deficiency (*12-15*). TGF-β1 activation by αVβ6 is well characterized at a molecular level. It requires activation of αVβ6 itself, interaction of the β6 intracellular (IC) domain with cytoskeletal adaptor proteins such as talin and kindlin, and transmission of cytoskeleton-generated tensile forces by β6 to LAP, leading to the release of mTGF-β1 (*16-18*). This model of TGF-β1 activation is thought to apply to αVβ1 as well, but not to αVβ8 because β8 lacks canonical cytoskeletal adaptor motifs. Instead, β8 was shown to interact with Band 4.1B and RhoGDI1 proteins, which do not appear to contribute to TGF-β1 activation but rather to intracellular signaling and cell migration (*19, 20*). Thus, the mechanism of TGF-β1 activation by αVβ8 has remained debated. In epithelial cells and monocytes, the β8 IC domain is dispensable for activation, which rather implies proteolysis of LAP by extracellular MMP14 (*13, 21*). In astrocytes and regulatory T cells (Tregs) in contrast, αVβ8-mediated activation is independent of MMPs, suggesting a distinct mechanism (*22-24*). Cheng, Nishimura and colleagues proposed an entropy-redistribution model for TGF-β1 activation by αVβ8. In this model, binding of αVβ8 to latent

TGF-β1 presented by GARP or LRRC33 on the surface of cells induces limited conformational rearrangements in LAP that are sufficient to expose mTGF-β1 for receptor binding, without release of the cytokine. These authors proposed that activation by αVβ8 allows for autocrine, but not paracrine TGF-β1 activity, based on the argument that TGF-β1$_{R278A}$, a mutant form of TGF-β1 that is expected to resist cleavage by furin into LAP and mTGF-β1 homodimers, exerts an activity similar to that of wild type (WT) TGF-β1 (*25-27*). These authors suggested that the activity of the non-cleavable TGF-β1$_{R278A}$ mutant, which cannot be released from LAP in the extracellular space, demonstrates that WT TGF-β1 activated by αVβ8 can only act in an autocrine fashion on the TGF-β1 expressing cells.

We and others have extensively studied the suppressive functions exerted by human and mouse regulatory T cells (Tregs) on other immune cells. We have shown that immunosuppression by Tregs depends, at least in part, on the ability of Tregs to produce active TGF-β1 upon engagement of their T cell receptor (TCR). TCR stimulation induces expression of αVβ8 and GARP:TGF-β1 on the Treg surface, leading to TGF-β1 activation, and autocrine and paracrine activity on neighboring immune cells (*23, 24, 28, 29*). *In vitro*, the paracrine activity of Treg-derived TGF-β1 suppresses the proliferation, function and differentiation of effector T cells (Teff). This paracrine immunosuppressive activity requires Treg-Teff contacts and does not lead to the release of active mTGF-β1 (i.e. free from LAP) in solution in the extracellular space (*30*). Moreover, antibodies against αVβ8 or GARP:TGF-β1 that block TGF-β1 activation by human or mouse Tregs *in vitro* enhanced allogeneic and anti-tumor T cell responses *in vivo* (*24, 31-34*). Altogether, these observations suggest that TGF-β1 presented by GARP and activated by αVβ8 on the surface of Tregs induces paracrine immunosuppressive signaling through binding of TβR on neighboring cells, without release of LAP-free mTGF-β1 in the extracellular space.

We recently developed monoclonal antibodies that activate, rather than block, latent TGF-β1 presented by GARP or LRRC33 on the cell surface. TGF-β1 activating antibodies reduced alloreactive T cell responses in a Treg-dependent manner in murine graft-versus-host disease (*35*). Here, we used TGF-β1 activating antibodies, together with cells expressing various TGF-β1, GARP or αVβ8 variants to probe the mechanisms of TGF-β1 activation by αVβ8. Unless otherwise specified, experiments reported below were performed with human GARP, TGF-β1 and αVβ8 molecules. Some were repeated with murine molecules, with similar results. Our experiments unambiguously demonstrate that TGF-β1 activated by αVβ8 exerts paracrine activity on neighboring cells. TGF-β1 activation by αVβ8 requires actin cytoskeleton-generated forces but does not require that β8 directly interacts with IC proteins.

RESULTS

TGF-β1 activated by integrin αVβ8 exerts paracrine signaling

According to the entropy redistribution model proposed by the Cheng and Nishimura groups, αVβ8-mediated activation induces autocrine, but not paracrine TGF-β1 activity (*25-27*). Our previous *in vitro* and *in vivo* observations suggest however that TGF-β1 activated by αVβ8 on the surface of human and murine Tregs exerts paracrine activity on neighboring T cells (*24, 29, 32, 33*).

We used a co-culture reporter assay to resolve these discrepant interpretations. Cells expressing membrane-bound GARP:TGF-β1 complexes (i.e. adherent *TGFB1*$^{-/-}$ 293T cells transfected with *GARP* and *TGFB1*) were co-cultured with reporter cells expressing αVβ8 and a TGF-β1-responsive Firefly luciferase reporter (i.e. adherent *TGFB1*$^{-/-}$ 293T transfected with *ITGAV, ITGB8* and *CAGA-FLuc*). This system allows for the detection of paracrine, but not autocrine TGF-β1 activity, as the TGF-β1 activity is detected in reporter cells that do not express their own latent TGF-β1 (**Figure 1A**). Active recombinant TGF-β1 (rTGF-β1, 1 ng/ml), used as a control, induced a 5-fold increase in *Fluc* reporter activity. Co-culture with cells expressing surface GARP:TGF-β1 induced a similar 4-fold increase in reporter activity, which was abrogated by a neutralizing anti-TGF-β1 antibody (**Figure 1B**). These observations unambiguously demonstrate that membrane-bound latent TGF-β1 activated by αVβ8 in the extracellular space can exert paracrine activity on neighboring cells. We compared the paracrine activity emanating from serial dilutions of GARP:TGF-β1 expressing cells to that of rTGF-β1. Cells expressing TGF-β1 in complex with GARP produced the equivalent of ~2 pg active TGF-β1 per 10^3 cells (**Figure 1C**).

Interestingly, we also detected paracrine activity with cells expressing the TGF-$\beta1_{R278A}$ mutant, expected to resist cleavage by furin. This activity corresponded to ≤ 0.2 pg active TGF-β1 per 10^3 cells, corresponding to ≤ 10% the activity of WT TGF-β1. Levels of total and surface GARP:TGF-β1 complexes in cells transfected with WT or mutant TGF-β1 were similar, as determined by Western blot and flow cytometry (**Figure S1A-B**). Whereas ~16% of the total WT TGF-β1 was cleaved into mTGF-β1 (~27.5 pg mTGF-β1 / 10^3 cells), we observed that ~1.1% of TGF-$\beta1_{R278A}$ (~1.6 pg mTGF-β1 / 10^3 cells) was also cleaved in transfected cells, in spite mutation of the furin motif (**Figure S1A**). Low-level cleavage and release of the TGF-$\beta1_{R278A}$ mutant was previously reported by others (*36*). Such residual cleavage may account for the paracrine activity of the TGF-$\beta1_{R278A}$ mutant in co-culture assays, corresponding to ≤ 10% the activity of WT TGF-β1.

Overall, our data unequivocally demonstrate that TGF-β1 exerts paracrine activity when mTGF-β1 is cleaved from LAP prior to activation by αVβ8.

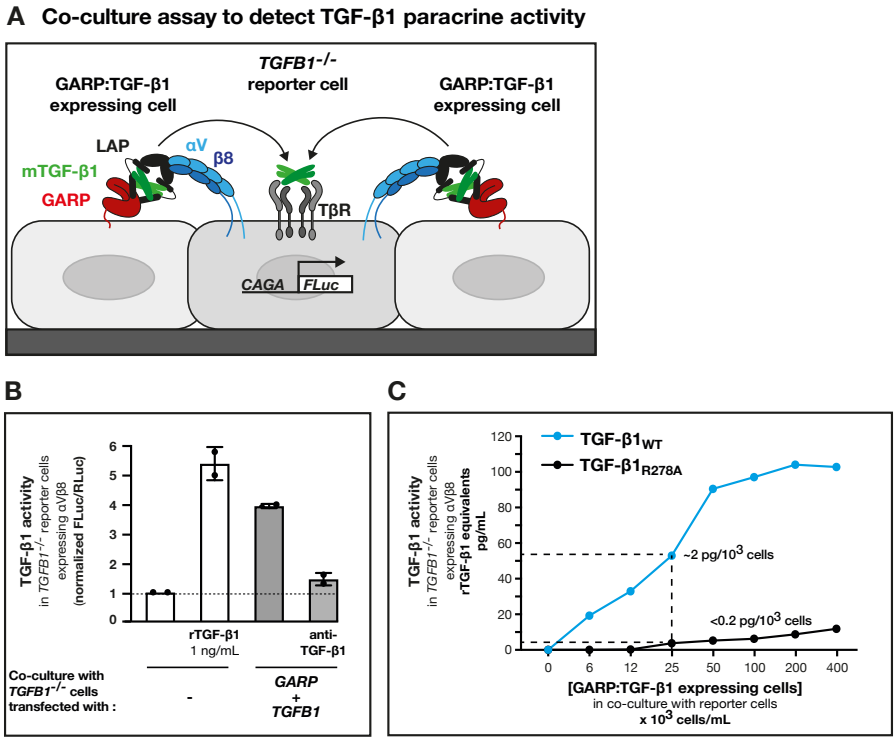

Figure 1: Activation of TGF-β1 by αVβ8 allows paracrine signaling
(**A**) Schematic representation of the co-culture assay used to measure paracrine TGF-β1 activity. 293T cells in which the *TGFB1* gene was deleted by CRISPR-Cas9 (*TGFB1*$^{-/-}$ 293T) were co-transfected with *GARP* and *TGFB1* (GARP:TGF-β1 expressing cells), or *ITGAV*, *ITGB8*, *CAGA-FLuc* and *RLuc* (*TGFB1*$^{-/-}$ reporter cells), respectively. (**B**) GARP:TGF-β1 expressing cells and *TGFB1*$^{-/-}$ reporter cells were co-cultured in 96W plates at a 1:1 ratio for a total of 2x10^5 cells/mL during 16-24 hours, before measuring FLuc and RLuc activites. rTGF-β1 (1 ng/ml) was used as a positive control, and a neutralizing anti-TGF-β1 mAb (clone 1D11, 10 µg/mL) as a control for specificity. Bar graphs indicate the mean TGF-β1 activity of two independent experiments, expressed as the FLuc/RLuc ratio normalized to the ratio in the control co-culture of reporter cells with untransfected cells. Each data point is the mean of technical duplicates within one experiment, and error bars indicate SD. A dotted line represents the value of the normalized negative control. (**C**) Assay performed as above with serial dilutions of GARP:TGF-β1 expressing cells in co-culture with fixed concentrations of reporter cells (10^5/mL). GARP:TGF-β1 expressing cells were transfected with plasmids encoding wild type (WT) or R278A mutant TGF-β1, as indicated. Data points indicate TGF-β1 activity expressed as rTGF-β1equivalents (pg/mL) calculated by comparison to FLuc/RLuc ratios measured with a rTGF-β1 standard curve. Western blot and flow cytometry analysis associated to Figure 1C can be found in Supplementary Figure 1.

Activation of TGF-β1 by αVβ8 does not require direct interactions with the cytoskeleton but requires anchorage of GARP and αVβ8 in the cell membrane

The β8 IC domain lacks the motifs that allow β6 to interact with and transmit tensile forces from the cytoskeleton to LAP during TGF-β1 activation. Whether the β8 IC domain is required in all cell types to activate latent TGF-β1 presented by GARP to αVβ8 is still debated (*13, 21-24*). On the other hand, it cannot be excluded that the short (14 aa) IC domain of GARP could interact with and transmit forces from the cytoskeleton to LAP during TGF-β1 activation by αVβ8. We thus generated a series of truncation mutants to investigate the roles of the β8 and GARP IC domains (**Figure 2A**): the $\beta8_{\Delta IC1}$ variant lacks the Band 4.1B–binding motifs, $\beta8_{\Delta IC2}$ lacks the entire IC domain, and $\beta8_{\Delta TM}$ lacks both IC and TM domains; the $GARP_{\Delta IC}$ variant lacks the entire IC domain, and the previously described secreted $GARP_{\Delta TM}$ variant lacks both IC and TM domains (*35, 37*). All full-length ($_{FL}$) and truncated β8 and GARP variants were expressed at high levels in lysates and on the surface of transfected 293T cells, with the exception of $GARP_{\Delta TM}$ which was not retained on the surface, as expected (**Figure S2A-B**). Less expected was the finding that $\beta8_{\Delta TM}$ was present on the cell surface at a level close to that of the other β8 truncation variants. This suggests that interaction with the extracellular part of αV is sufficient to anchor $\beta8_{\Delta TM}$ on the cell membrane.

We measured paracrine TGF-β1 reporter activity using the co-culture assay described above. By comparison to cells that do not express αVβ8, co-culture of cells expressing $\alpha V\beta8_{FL}$ with cells expressing $GARP_{FL}$:TGF-β1 induced a ~4-fold increase in TGF-β1 reporter activity (**Figure 2B**). Reporter activity also increased ~4-fold with $GARP_{\Delta IC}$:TGF-β1, but not with $GARP_{\Delta TM}$:TGF-β1. This indicates that whereas anchorage of the GARP TM domain in the membrane is required, as previously reported (*18, 35*), the GARP IC domain is dispensable for TGF-β1 activation by αVβ8. Both $\alpha V\beta8_{\Delta IC1}$ and $\alpha V\beta8_{\Delta IC2}$ variants also induced ~4-fold increases in reporter activity, whether TGF-β1 was presented by $GARP_{FL}$ or $GARP_{\Delta IC}$ (**Figure 2B**). Interestingly, even the $\alpha V\beta8_{\Delta TM}$ variant retained some ability to activate TGF-β1 presented by $GARP_{FL}$ or $GARP_{\Delta IC}$, in line with the observed expression of $\alpha V\beta8_{\Delta TM}$ on the cell surface (**Figure S2B**). Altogether, our data demonstrate that neither the IC domain of GARP nor that of β8 are required for TGF-β1 activation in 293T cells. Whereas GARP needs to be anchored in the cell membrane via its TM domain, retention of β8 on the cell surface via interaction with αV may be sufficient for activation. Because αV does not bind to the cytoskeleton (*38*), the observation that TGF-β1 presented by $GARP_{\Delta IC}$ is activated by all truncated αVβ8 variants

suggests that direct interactions between GARP or the integrin with cytoskeletal proteins are not necessary for activation by αVβ8.

We confirmed our observations in another cell type, namely suspension Jurkat T cell clones transduced to co-express GARP with $\alpha V\beta 8_{FL,}$ $\alpha V\beta 8_{\Delta IC1}$ or $\alpha V\beta 8_{\Delta IC2}$ (**Figure 2C and S2C**). TGF-β1 activity was assessed by monitoring SMAD2 phosphorylation (pSMAD2) after stimulation of the T cell receptor (TCR), as TCR stimulation was previously shown to induce MMP-independent TGF-β1 activation by αVβ8 in these cells (*24*). Here again, the $\alpha V\beta 8_{\Delta IC1}$ and $\alpha V\beta 8_{\Delta IC2}$ variants very efficiently activated TGF-β1 presented by $GARP_{FL}$ (**Figure 2B, Figure S2D**).

Together, these data demonstrate that neither GARP nor β8 IC domains are required for αVβ8-mediated activation of TGF-β1, provided that both β8 and GARP are anchored in the cell membrane, either directly via the TM domain for GARP, or at least indirectly via interaction with αV for β8.

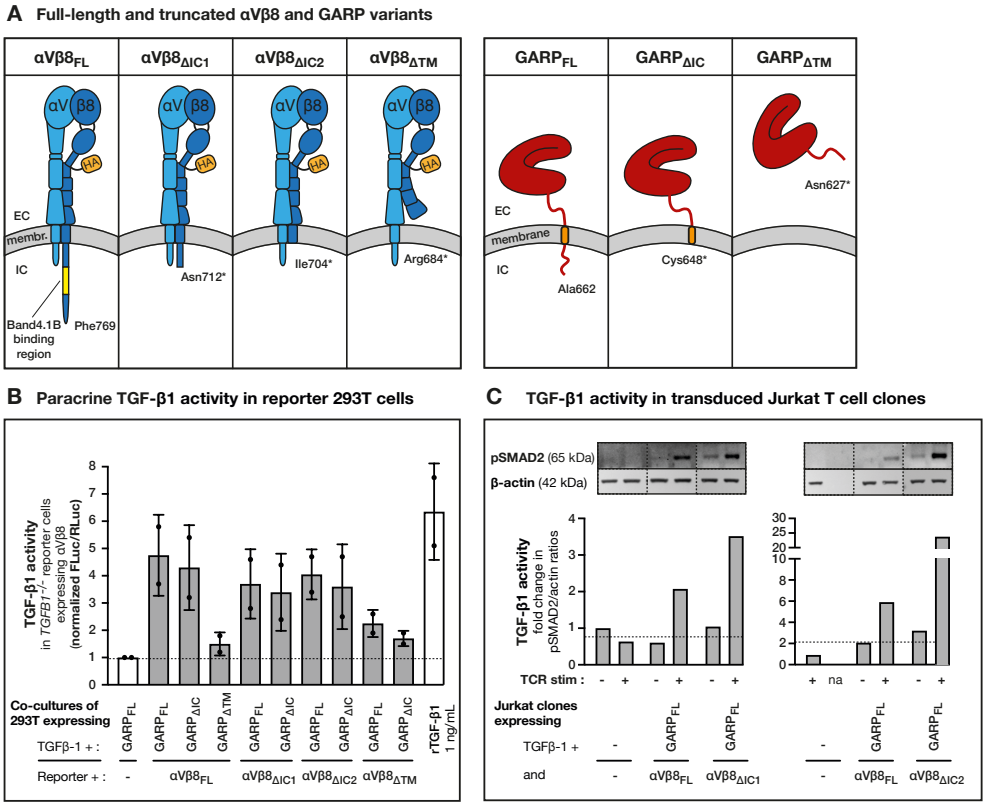

Figure 2: Activation of TGF-β1 by αVβ8 does not require the IC domains of GARP or β8, but requires anchorage of GARP and αVβ8 in the cell membrane

(**A**) Schematic representation of full-length (FL) and truncation variants of αVβ8 and GARP used to probe the requirements for TGF-β1 activation by αVβ8. Plasmids encoding the HA-tagged variants were constructed by inserting STOP codons downstream of the codons encoding residues indicated by an asterix (*). (**B**) Paracrine TGF-β1 activity was measured in a co-culture reporter assay performed as described in Figure 1, with *TGFB1*$^{-/-}$ 293T cells transfected with the full-length or truncation variants and WT TGF-β1, as indicated. Bar graphs indicate the mean TGF-β1 activity of two independent experiments, expressed as the FLuc/RLuc ratio normalized to the ratio in the control reporter co-cultured with non-transfected cells. Each data point is the mean of technical duplicates within one experiment, and error bars indicate SD. (**C**) Parental Jurkat T cells (clone E6-1) or clones of Jurkat T cells transduced with lentiviruses to express $GARP_{FL}$:TGF-β1 and $αVβ8_{FL}$, $αVβ8_{ΔIC1}$ or $αVβ8_{ΔIC2}$ were incubated during 24 hours on coated anti-CD3 (stim) or left resting in serum-free medium alone (unstim). Cell lysates were analyzed by Western blot with antibodies against phosphorylated SMAD2 (pSMAD2) and β-actin. ECL signals were quantified to establish pSMAD2/β-actin ratios and normalized to the signal in non-transduced cells. Values are indicated as bar graphs in the bottom panel. A dotted horizontal line shows the average pSMAD2/β-actin level (background) in non-stimulated conditions. Results are representative of 3 independent experiments. Full Western blot images are shown in Figure S2D.

TGF-β1 activation by antibodies also requires two anchorage points for efficient TGF-β1 activation

We next used chimeric antibodies and adherent or suspension cells to further define the molecular and cellular requirements for TGF-β1 activation. LMT-7 is a monospecific mAb that activates murine latent TGF-β1 through bivalent binding to LAP and crosslinking of two membrane-bound GARP:TGF-β1 complexes on the same cell or across different cells (*35*). CryoEM analyses showed that one bivalent activating mAb cannot bind the two epitopes on a single LAP dimer (*35*). Using Fab-arm exchange, we generated a bispecific chimera named LMT-7/28H6*, that binds mouse LAP with one arm and mouse GARP with the other. We tested LMT-7/28H6* and all relevant control chimeras (LMT-7/LMT-7*, LMT-7/IgG1*, IgG1/28H6*, IgG1/IgG1*) for their ability to activate TGF-β1 in reporter assays.

First, adherent *TGFB1*$^{-/-}$ 293T cells transfected to co-express murine GARP:TGF-β1 and the TGF-β1 reporter were incubated with antibodies in solution (**Figure 3A**). Monospecific bivalent LMT-7/LMT-7* induced a ~4 fold increase in TGF-β1 reporter activity by comparison to controls (no antibody or IgG1/IgG1*), whereas monovalent LMT-7/IgG1* did not, as expected (*35*). Interestingly, the bispecific LMT-7/28H6* chimera failed to activate TGF-β1. LMT-7/28H6* is capable to bivalently interact with a single GARP:TGF-β1 complex by binding LAP with one arm and GARP with the other. The IgG1/28H6* monovalent control, which also binds a single GARP:TGF-β1 complex, did not activate TGF-β1 either. This confirms that bivalent antibodies in solution on adherent cells activate TGF-β1 only if they bind two distinct latent TGF-β1 molecules.

Second, adherent *TGFB1*$^{-/-}$ 293T cells transfected to express the TGF-β1 reporter and mouse GARP (without TGF-β1) were co-cultured with *TGFB1*$^{-/-}$ 293T cells transfected to express mouse latent TGF-β1 in complex with mouse LRRC33 and incubated with antibodies in solution (**Figure 3B**). As above, monospecific bivalent LMT-7/LMT-7* activated TGF-β1, whereas monovalent LMT-7/IgG1* did not. In contrast however, bispecific LMT-7/28H6* now induced TGF-β1 activation in this assay. Here, bivalent binding by LMT-7/28H6* can only occur through binding to two distinct molecules on two adherent cells, one expressing LRRC33:TGF-β1, the other GARP without TGF-β1. The monovalent IgG1/28H6* control did not activate TGF-β1. This shows that one single bispecific antibody molecule such as LMT-7/28H6* can activate TGF-β1 by binding one latent TGF-β1 dimer with one arm, and a second distinct molecule (e.g. GARP without TGF-β1) with the other.

Third and finally, suspension Expi293 cells were transfected to co-express GARP:TGF-β1 and the TGF-β1 reporter, then incubated with antibodies in solution or immobilized on the tissue-

culture plastic (**Figure 3C**). In contrast with adherent cells, monospecific bivalent LMT-7/LMT-7* in solution failed to activate TGF-β1 on suspension Expi293 cells. Thus, bivalent binding to two distinct GARP:TGF-β1 complexes is not sufficient to activate TGF-β1 if cells that present latent TGF-β1 do not adhere on the tissue-culture plastic. Antibody immobilization on plastic restored activation by LMT-7/LMT-7*, and induced activation by all antibodies able to bind GARP:TGF-β1 with at least one arm (i.e. LMT-7/IgG1*, LMT-7/28H6* and IgG1/28H6*). The negative IgG1/IgG1* control did not activate TGF-β1, whether in solution or immobilized on plastic.

Together, these results suggest that antibody mediated TGF-β1 activation requires either *i)* that one antibody molecule bridges at least one latent TGF-β1 covalently linked to transmembrane GARP or LRRC33 and a second molecule anchored in the membrane of adherent cells; or *ii)* that one antibody molecule bridges one latent TGF-β1 linked to GARP on suspension cells and a solid surface such as tissue-culture plastic. Thus, it appears that mechanical resistance provided by adherence to plastic and covalent linkage of TGF-β1 to a transmembrane protein is required for TGF-β1 to be activated by cell-generated tensile forces.

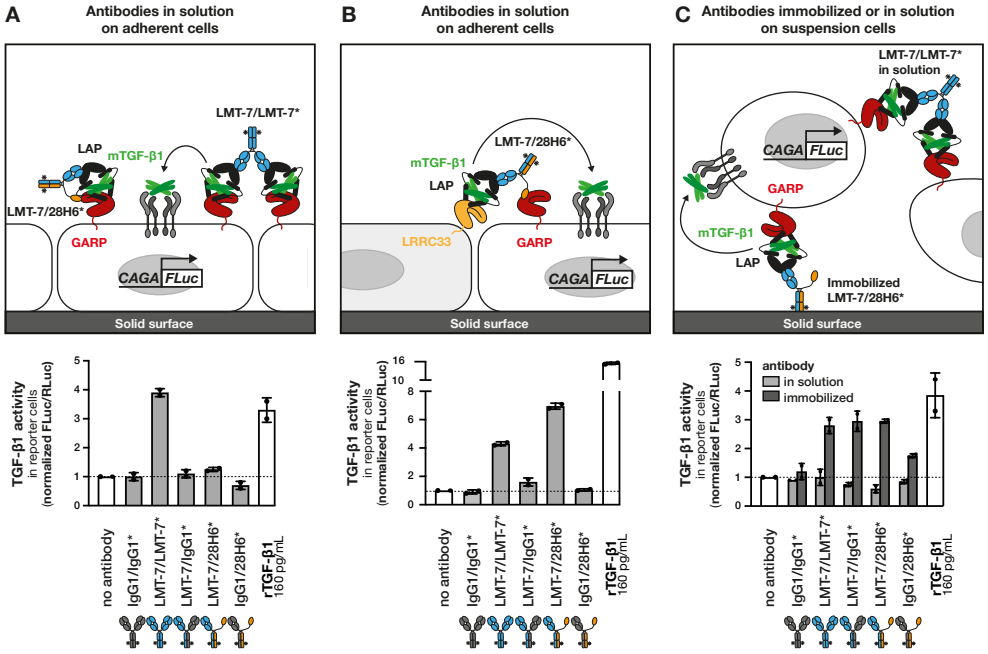

Figure 3: Two anchoring points are required to mediate TGF-β1 activation
(**A-B-C**) Schematic representations of the reporter assays in transfected *TGFB1*$^{-/-}$ 293T cells (A-B) or Expi293F cells (C) to measure activation of latent TGF-β1 presented by GARP or LRRC33 to the various antibody chimeras described in Figure S3. LMT-7 arms bind to murine LAP, 28H6 to murine GARP, and IgG1 (derived from motavizumab) to an irrelevant RSV epitope. (**A**) Reporter *TGFB1*$^{-/-}$ 293T cells are co-transfected to express murine GARP and murine TGF-β1. Bar graphs represent the mean TGF-β1 activity of technical duplicates, expressed as ratios of Fluc to Rluc activity normalized to the ratio in the control condition (no antibody). Error bars indicate SD. A dotted horizontal line shows FLuc/Rluc of the normalized negative control. (**B**) Same as (A) but a co-culture between reporter cells expressing murine GARP only with cells expressing murine LRRC33:TGF-β1 complexes. (**C**) Same as (A) but using non-adherent Expi-293F cells and testing antibodies in solution (light grey) or immobilized on plastic (dark grey). Data are representative of at least two independent experiments.

Biomechanical forces required for TGF-β1 activation by mAbs and αVβ8 originate from actin polymerization in cells expressing membrane-bound latent TGF-β1

Considering that neither antibodies nor GARP and αVβ8 variants need to directly interact with the cytoskeleton to activate TGF-β1, the origin of the tensile forces involved in TGF-β1 activation remain unclear. We examined whether actin polymerization was required.

Adherent *TGFB1*$^{-/-}$ 293T cells co-expressing GARP:TGF-β1 and the TGF-β1 reporter (assay as in Figure 3A) were incubated with antibodies in the presence of latrunculin-A, a well-established inhibitor of actin polymerization (**Figure 4**). Here, we transfected cells to express human GARP:TGF-β1 and used LHT-22, an activating mAb that binds human TGF-β1 (*35*). Similar to LMT-7 and as expected, LHT-22 whether in solution or immobilized on plastic activated TGF-β1 on the surface of adherent cells (4- to 5-fold induction by comparison to the IgG1 control). Latrunculin-A completely abrogated the ability of LHT-22 to activate TGF-β1, including when the mAb was immobilized on plastic (**Figure 4A**). GARP:TGF-β1 expressing cells treated with latrunculin-A remained adherent, but adopted a rounded morphology and exhibited markedly reduced motility, as previously reported (*14, 39*).

We also tested the effects of latrunculin-A on TGF-β1 activation by full-length and truncated αVβ8 variants expressed on adherent 293T cells in the paracrine co-culture assay used in Figure 1. Latrunculin-A abolished TGF-β1 activation by all αVβ8 variants, including αVβ8$_{\Delta TM}$ which lacks the IC and TM β8 domains (**Figure 4B**). This shows that TGF-β1 activation by αVβ8 requires cell-generated forces induced by actin polymerization, even though αVβ8, similar to activating mAbs, does not transmit tensile forces to LAP via direct interaction of β8 with the cytoskeleton or the cell membrane. Our observations suggest that cell movement and/or membrane dynamics contribute to the activation of TGF-β1 by antibodies or αVβ8 on the surface of adherent cells.

Finally, we examined whether actin polymerisation was also necessary to activate TGF-β1 on suspension cells, using the Jurkat T cell clone expressing GARP$_{FL}$:TGF-β1 and αVβ8$_{FL}$. Similar to previous results on suspension Jurkat or Expi293 cells (Figures 2 and 3), TCR stimulation or immobilization of antibody was required to activate TGF-β1 (**Figure 4C, Figure S4**). Latrunculin-A abrogated TGF-β1 activation induced by TCR stimulation, probably because actin polymerization is necessary to transduce TCR signals. In contrast, it did not abrogate activation by the immobilized mAb. Persistence of antibody-mediated TGF-β1 activation in the presence of latrunculin-A contrasts with observations in adherent 293T cells. This discrepancy may stem from cell type-specific differences in mobility: Jurkat cells remain in suspension and

retain passive movement when treated with latrunculin-A, whereas 293T cells continue to adhere on plastic but show markedly reduced motility.

Altogether, our results support a model in which αVβ8 and activating mAbs act as passive mechanotransducers of cell-generated tensile forces that do not need direct interaction with the cytoskeleton, but rather rely on cell movement or global mechanical activity to transmit tension across LAP and to activate TGF-β1.

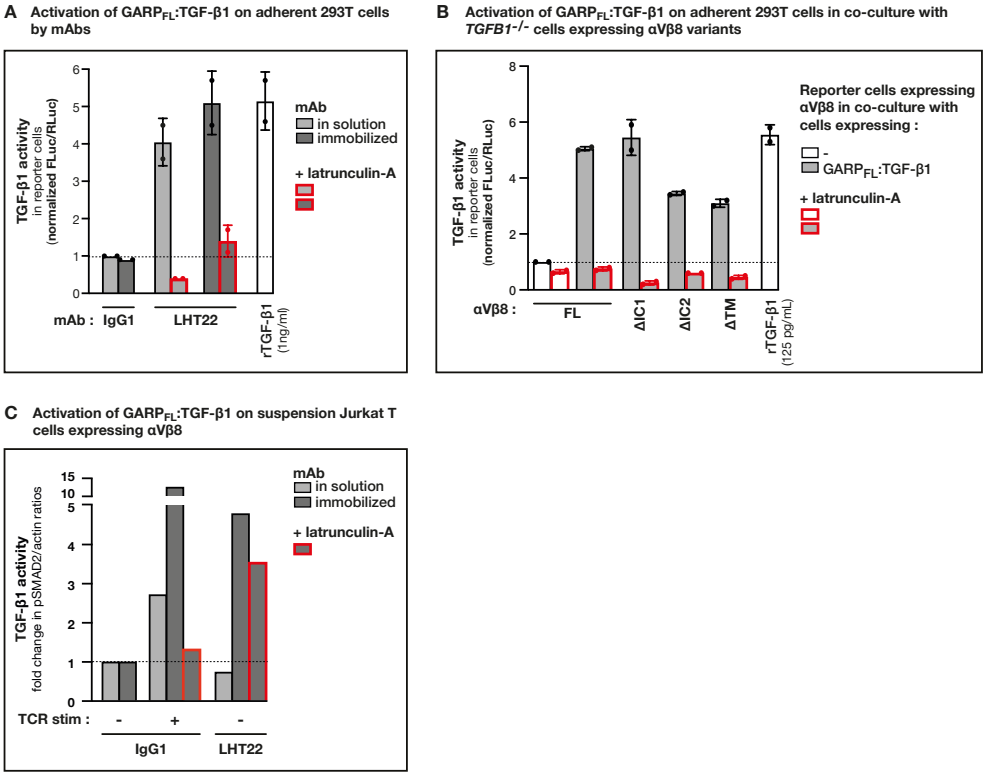

Figure 4: Cytoskeleton or cell dynamics are required for mAbs and ITGB8-dependent TGF-β1 activation

(**A**) Reporter assay as in Figure 3A. LHT22-activating mAb (anti-human LAP) and IgG1 isotype were either used in solution or immobilized on plastic. Latrunculin-a was added in the indicated conditions at a final concentration of 0.5 µg/mL. Bar graphs indicate the mean TGF-β1 activity of two independent experiments, expressed as the FLuc/RLuc ratio normalized to the ratio of the negative control condition (soluble IgG1). Each data point is the mean of technical duplicates within one experiment. Error bars indicate SD. A dotted horizontal line shows FLuc/Rluc of the normalized negative control. (**B**) Reporter assay as in Figures 1 and 2B. Bar graphs represent the mean TGF-β1 activity of technical duplicates, expressed as ratios of Fluc to Rluc activity normalized to the ratio in the non-transfected/untreated control condition (mean of technical duplicates). Data are representative of at least three independent experiments. (**C**) Jurkat T cells transduced with lentiviruses to express GARP$_{FL}$:TGF-β1 and αVβ8$_{FL}$ were treated as indicated in Figure 2C. LHT22-activating mAb and IgG1 isotype were either used as soluble molecules or coated. Cell lysates were processed by Western blot as indicated in Figure 2C. ECL signals were quantified on each membrane separately and normalized to the internal negative control (*) of each gel. Complete Western blots are available in Figure S4.

DISCUSSION

The mechanical model for αVβ1 and αVβ6 mediated TGF-β1 activation has been well established, but how αVβ8 activates TGF-β1 and whether this can result in paracrine activity has remained controversial (*19, 20*). Our results indicate that αVβ8, similar to TGF-β1 activating antibodies, passively activates TGF-β1 by transmitting cell-generated tensile forces without direct interaction with the cytoskeleton. Because we used assays that do not detect autocrine signals, our results also demonstrate that TGF-β1 activated by αVβ8 exerts paracrine activity (**Figure 5A**).

TGF-β1 activated by αVβ8 also most likely exerts autocrine activity, because the high affinity TβR is expressed on all mammalian cell types. Assays to detect autocrine activity at the single cell level would be required to prove that TGF-β1 can act on the same cell that produces it. Such assays, which still need to be developed, could furthermore resolve another pending question: can one αVβ8 molecule activate latent TGF-β1 present on the surface of the same cell (activation in *cis*), or does it need to be located on another cell (activation in *trans*)? Our schematic summary in Figure 5A suggest that both *cis* and *trans* activation can occur, but assays that are not performed with isolated single cells, including our own assays reported herein, can only demonstrate activation in *trans*.

Our results also suggest that only the mTGF-β1 that is cleaved and released from LAP by furin-like enzymes can exert paracrine activity upon activation by αVβ8 (**Figure 5A**). The residual activity detected with the TGF-$\beta1_{R278A}$ mutant (≤ 10% of WT) is in the same range as the residual cleavage (≤ 10% of WT) that we and others observed despite the furin motif mutation (*36*). Residual cleavage of TGF-$\beta1_{R278A}$ could be mediated by furin itself or by other proprotein convertases that compensate for furin activity, as reported by Dubois et al (*3*), and appears to account for all the TGF-β1 activity detected in our assays.

In the family of heterodimeric integrins, the IC tail of the β chain is generally required to allow both inside-out activation of the integrin and force transmission to an extracellular ligand via direct coupling with the cytoskeleton. Integrin αVβ8 is an exception: it does not require classical inside-out activation and constitutively binds LAP with high affinity, and it is not known to directly interact with the actin cytoskeleton (*13, 19, 20, 40, 41*). Nevertheless, it had remained debated whether the β8 IC domain was required for TGF-β1 activation in all cell types, and the role of the GARP IC domain in TGF-β1 activation had not been fully investigated (*18, 37*). Our results with β8 and GARP mutants lacking part or all of their IC tail or TM domain, clearly show that activation is preserved when both GARP and β8 IC domains are deleted. Even the β8

TM domain is dispensable, probably because the αVβ8$_{\Delta TM}$ heterodimer can still assemble and remains associated to the membrane thanks to the TM domain of the αV subunit (**Figure 5B, top row**). In contrast, activation does not occur when the TM domain of GARP and its association with the membrane is lost (**Figure 5B, top row**). Thus, rather than interaction with the cytoskeleton, it appears that TGF-β1 activation by αVβ8 requires two anchorage points in a cell membrane, one occurring via the integrin heterodimer, the other via GARP (or LRRC33).

Experiments reported here and previously (*35*) indicate that TGF-β1 activation by antibodies, which do not interact with the cytoskeleton, also requires two anchorage points (**Figure 5B, bottom row**). To activate TGF-β1, bivalent monospecific antibodies in solution need to cross-link two latent TGF-β1 molecules, each anchored in the cell membrane by disulfide linkage to a protein such as GARP (*35*). We show here that one of the two anchor points in a cell membrane can be replaced by immobilization on plastic, using monovalent chimeric antibodies that can bind one latent TGF-β1 molecule only. In solution, monovalent antibodies do not activate latent TGF-β1 anchored in a cell membrane (**Figure 5B, bottom row**). Similarly, previous studies also showed that recombinant αVβ8 in solution does not activate latent TGF-β1 anchored in a cell membrane, whereas it does when it is immobilized on plastic or inserted in lipid nanodiscs (*25-27*). Finally, using a bispecific antibody that binds only one latent TGF-β1 molecule, we show that one of the two anchorage points can be provided by a transmembrane protein located on a cell distinct from that expressing latent TGF-β1. Collectively, previous findings and those reported here show that high-affinity binding to LAP by αVβ8 or antibodies is not sufficient for activation, which also requires mechanical resistance provided by two anchorage points in a cell membrane. One anchorage point can be replaced by immobilization on an inert solid surface (**Figure 5B**), but cell activity or membrane dynamics from the other anchorage point appears indispensable.

Although direct contacts with the actin cytoskeleton are not involved, as indicated above, our experiments with inhibitors of actin polymerization on adherent cells confirm that an active cytoskeleton is required for activation by αVβ8 or antibodies (**Figure 5C**). This suggests that cell-generated mechanical forces are required to induce the conformational change in LAP that allows release and access of mTGF-β1 to the TβR. It also argues against an entropy redistribution model of activation by αVβ8, in which binding alone would be sufficient to trigger TGF-β1 activation.

Thus, it appears that tensile forces arise from cell-generated mechanical activity. Adherent 293T cells used in our assays are highly dynamic, continuously forming membrane protrusions and establishing transient cell–cell contacts (*42*). Our results with suspension Jurkat T cells are less

easy to interpret: the actin polymerization inhibitor did not abrogate activation by immobilized antibodies in these cells. It is plausible that in suspension cells, inhibition of actin cytoskeleton activity is compensated by passive cell movement.

In conclusion, our data shows that TGF-β1 activated by αVβ8 can exert paracrine signaling. This does not exclude that it can also exert autocrine activity, although this remains to be demonstrated at a single cell level. We propose an updated biomechanical model for activation by αVβ8 and by activating antibodies, similar to that proposed by Springer and colleagues for αVβ6 (*17*). In contrast to αVβ6 however, αVβ8 and antibodies can activate TGF-β1 without direct coupling to the cytoskeleton. Interaction of the β8 ectodomain with the membrane-anchored αV chain is sufficient to support transmission of cell-generated forces to LAP and trigger mTGF-β1 release. Activation by αVβ8 or by antibodies requires two anchorage points, high affinity interactions, and actin cytoskeleton dynamics. Altogether, we propose that αVβ8 and antibodies activate latent TGF-β1 through passive transmission of cell-generated tensile forces.

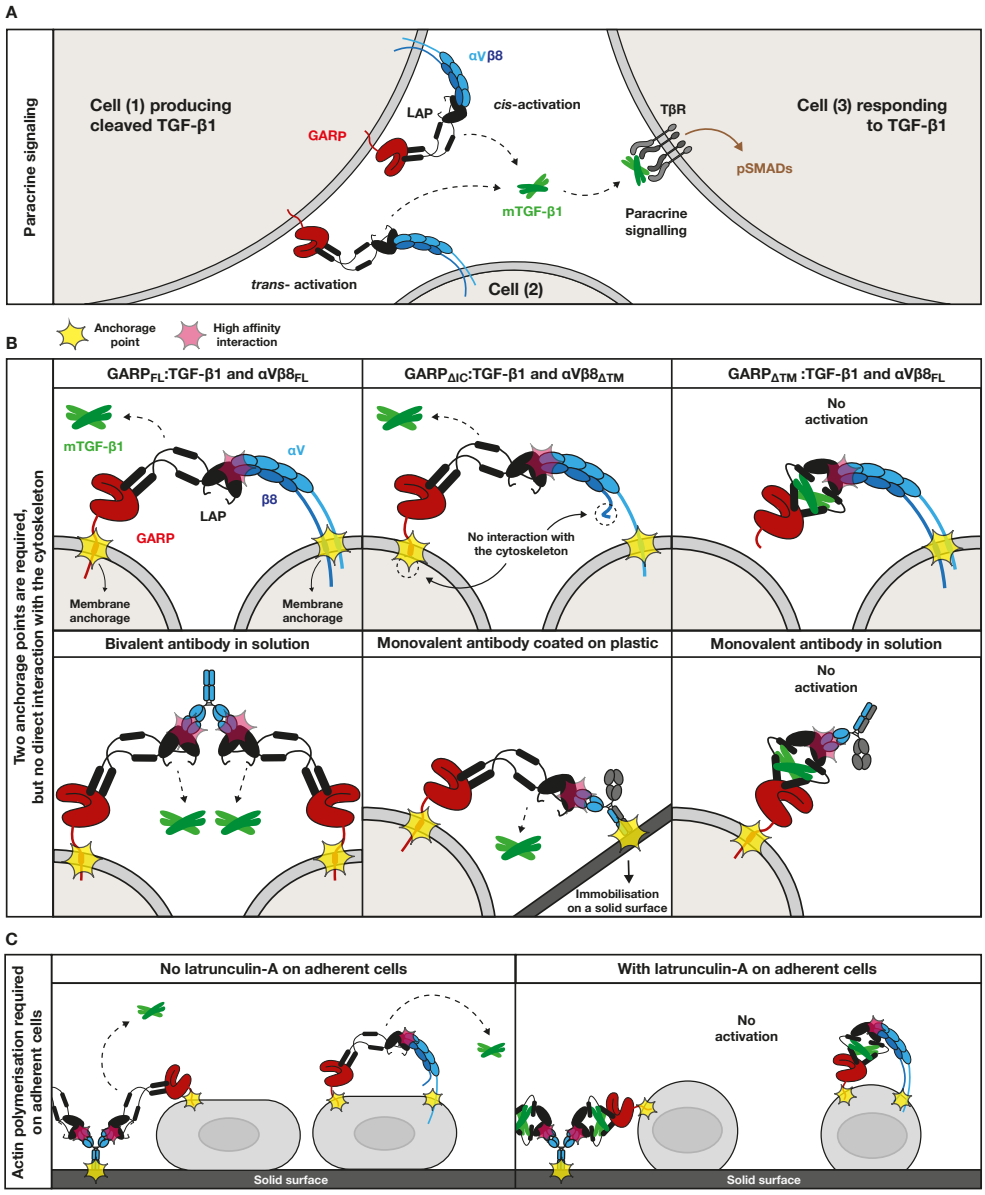

Figure 5: Model of TGF-β1 activation by integrin αVβ8 or mAbs, allowing paracrine activity

Schematic representations of TGF-β1 activation by the integrin αVβ8 or activating mAbs. (**A**) Model for paracrine TGF-β1 signaling. When activated by integrin αVβ8 either in *cis* (1) or *trans* (2), cleaved mature TGF-β1 can bind on TβR to signal on a neighboring responding cell (3). (**B**) Model for the requirement of two anchorage points during TGF-β1 activation by the integrin αVβ8 or activating mAbs. (**C**) Model for the requirement of an active actin-cytoskeleton during TGF-β1 activation by the integrin αVβ8 or activating mAbs. Yellow stars (☆) represent anchorage points (either in a cell membrane or on a solid surface), light red stars (☆) represent high affinity interactions.

MATERIAL AND METHODS

Primary cells and cell lines

All cell lines were maintained at 37°C in a humidified atmosphere with 5% CO_2 (Jurkat) or 8% CO_2 (293T, Expi293F). Culture media were supplemented with 100 U/mL penicillin and 0.1 mg/mL streptomycin (Sigma-Aldrich), unless otherwise specified.

293T *TGFB1*$^{-/-}$ cells

HEK 293T cells were cultured in DMEM (Gibco) supplemented with 10% fetal bovine serum (FBS, Cytiva), 1% GlutaMAX (Gibco), and antibiotics. At 70–90% confluency, cells were detached using 0.05% trypsin-EDTA (Gibco), neutralized with complete medium, centrifuged (300 × g, 5 min), and resuspended in fresh medium for passaging at a 1:20 dilution. A cell clone deleted for the *TGFB1* gene (293T *TGFB1*$^{-/-}$) was generated by CRISPR-Cas9, as previously described (*35*).

Expi293F cells

Expi293F cells were cultured in Expi293™ Expression Medium (Gibco) supplemented with antibiotics, under shaking. Cells were passaged every 3-4 days by diluting to 1 × 10^5 viable cells/mL when reaching 1-3 × 10^6 viable cells/mL, as determined by Acridine Orange/Propidium staining (LUNA™ cell counter, Logos Biosystems).

Jurkat E6-1 and Jurkat clones

Jurkat E6-1 cells were cultured in RPMI (Gibco) supplemented with 10% FBS, 1% GlutaMAX, and antibiotics. Cells were passaged by diluting to 1 × 10^5 viable cells/mL when reaching 1-3 × 10^6 viable cells/mL.

Jurkat cells stably expressing GARP were generated by lentiviral transduction as previously described (*29*). These cells were further transduced with lentiviruses encoding ITGB8-WT or mutants (see Lentivirus production) to generate GARP-ITGB8-WT or mutant Jurkat clones.

DNA and cloning

Relevant primers are mentioned in supplementary Table 1

ITGB8 cloning and mutagenesis

The human ITGB8 open reading frame (ORF) was amplified by PCR from a cDNA template using primers containing SfiI/SacII restriction sites, digested with the corresponding enzymes, and ligated into the pDisplay vector for N-terminal HA-tagging. Mutagenesis was performed using the Q5 Site-Directed Mutagenesis Kit (NEB, E0554S) to introduce two premature STOP codons after the following residues: ITGB8-ΔIC1: Asn712**, ITGB8-ΔIC2: Ile704**, ITGB8-ΔTM: Arg684**. All constructs were verified by Sanger sequencing.

GARP mutagenesis

The GARP-WT cDNA was amplified using primers designed to delete the intracellular (IC) tail and introduce a STOP codon after Cys648 (GARP-ΔIC). The amplified fragment was cloned back into the pDisplay vector using standard restriction (BglII-SalI)/ligation protocols. All constructs were verified by Sanger sequencing.

Lentivirus production and transduction

Lentiviruses were produced by transfecting 293T cells with pGenLenti vectors (GenScript) encoding ITGB8-WT or mutants (described hereabove), and packaging plasmids (VSVg and PAX2). Supernatants were collected 72 h post-transfection, filtered (0.45 µm), and concentrated 15-fold using Centricon Plus-70 columns (Merck Millipore, UFC703008). Viral particles were used concentrated 3-fold for infection. Jurkat cells were transduced by spin-infection (800 × g, 30 min, 30°C) in the presence of 8 µg/mL Polybrene (Sigma-Aldrich). Transduced cells were sorted by FACS for ITGB8+ populations.

TGF-β1 reporter assays (luciferase)

Activating mAbs directed against human and mouse latent TGF-β1

LMT7 and LHT22 antibodies, as well as LMT-7/LMT-7*, LMT-7/IgG1* and IgG1/IgG1* chimeric antibodies were obtained as previously described (*35*). Additional LMT7-28H6*, IgG1-28H6* were obtained by the same means (see Figure S3).

For plate-bound assays, mAbs were coated at 20 µg/mL in PBS for 2-3 h at room temperature (RT), followed by a single wash with PBS prior to cell plating.

Co-culture assays

293T *TGFB1*$^{-/-}$ cells were seeded in 6w plates (±1.10^6/w) and co-transfected using TransIT-LT1 (Mirus Bio) on the same day.

Source cells were co-transfected with 30% plasmid encoding human latent TGF-β1-WT or mutant, 70% plasmid encoding human GARP-WT or mutant, or empty vector controls, for a total of 2.5 µg DNA/well. **Reporter cells** were co-transfected with 7% plasmid encoding human ITGAV, 63% plasmid encoding human HA-ITGB8-WT or mutant, or empty vectors, 30% pCAGA-12-Fluc (Firefly luciferase under TGF-β-responsive promoter, Promega), 1% pRL-TK (Renilla luciferase under constitutive promoter, Promega), for a total of 2.5 µg DNA/well.

In figure 3B, source cells were transfected with 10% murine latent TGF-β1, 90% murine LRRC33, while reporter cells were transfected with 70% murine GARP, 30% pCAGA-12-Fluc, 1% pRL-TK for a total of 2,5µg/well.

24 h post-transfection, cells were harvested, counted, and mixed in 96-well plates (white optical Nuclon™ Delta surface, Thermo #136102) at a 1:1 ratio (2 × 10⁴ source cells + 2 × 10⁴ reporter cells/well) in a final volume of 100 µL. For dose-response experiments (Figure 1B), source cells were titrated (8 × 10⁴ to 0 cells) while keeping reporter cells constant (2 × 10⁴/well).

Co-cultures were treated directly with soluble or plate-bound mAbs (20 µg/mL), recombinant human TGF-β1 (rhTGF-β1, R&D Systems), latrunculin-A (0.5 µg/mL, Merck Life Science), anti-TGF-β1/2/3 (1D11, 20 µg/mL), and incubated for 16-24 h under standard conditions. Luciferase activity was measured using the Dual-Glo® Luciferase Assay System (Promega) and GloMax luminescence program (Promega). Firefly luciferase values were normalized to Renilla luciferase to control for transfection efficiency.

Monoculture assays

293T *TGFB1*$^{-/-}$ cells were seeded in 96-well plates at 1.8 × 10⁴ cells/well 24 h prior to transfection. Cells were co-transfected with 45% plasmid encoding mouse GARP, 10% plasmid encoding mouse latent TGF-β1, 45% pCAGA-12-Fluc, 1% pRL-TK, for a total of 0.1 µg DNA/well. 6 h post-transfection, cells were treated with mAbs (20 µg/mL), serial dilutions of rhTGF-β1 (R&D Systems), and incubated for 16-24 h before luciferase measurement.

Short-term stimulation of Jurkat cells and mAb-mediated activation assays

Jurkat cells (2.5×10^6 cells/mL) were plated in X-VIVO 10 serum-free medium (Lonza) with plate-bound anti-CD3 (orthoclone OKT3; 1 µg/mL; Janssen-Cilag) in TCR-stimulated condition. Cells were treated with mAbs (20 µg/mL), rhTGF-β1 (R&D Systems), latrunculin-A (0.5 µg/mL), 1D11 (20 µg/mL), and incubated for 24 h under standard conditions.

Molecular biology

Western blot analyses

Cells were counted, dry pelleted on dry ice for storage, then lysed in Laemmli buffer (Bio-Rad) supplemented with 5% 2-mercaptoethanol (Bio-Rad). Lysates were homogenized by passing through a 23G (293T) or 25G (Jurkat) needle, boiled (100°C, 5 min), and clarified by centrifugation (12,000 × g, 5 min, 4°C).

$5x10^4$ HEK 293T or 1.10^5 Jurkat cell equivalents were loaded on 4-12% Bis-Tris gels (Thermo Fisher Scientific) for proteins separation. Proteins were transferred to nitrocellulose membranes (iBlot2 system, Thermo Fisher Scientific). Membranes were blocked 1h in 5% non-fat milk in PBS-Tween 0.1% and incubated with primary antibodies: GARP (clone Plato-1, Enzo Life Sciences), HA (clone 16B12, BioLegend), mature TGF-β1 (clone A75-2, BD Pharmingen), pSMAD2 (clone 138D4, Cell Signaling Technology), β-actin (clone D6A8, Cell Signaling Technology). Secondary antibodies included: anti-mouse IgG2b-HRP (Jackson ImmunoResearch, #115-035-207), anti-mouse IgG light chain-HRP (Jackson ImmunoResearch, #115-035-174), anti-rat IgG-HRP (Cell Signaling Technology, #7077), anti-rabbit IgG-HRP (Cell Signaling Technology, #7074).

Signals were detected using SuperSignal West Pico or Femto substrates (Thermo Fisher Scientific) and imaged on a Fusion Solo 4S system (Vilber-Lourmat). Quantification was performed with Bio1D software (Vilber-Lourmat).

Flow cytometry

Single cell suspensions were counted on a Luna® cell counter with Acridine Orange/Propidium Iodide Stain (Logos Biosystem). Cells were resuspended in FACS buffer (2 mM EDTA, 1% FBS in PBS) and incubated with the following antibodies for 20 min at 4°C (1 or 2 layers staining): biotinylated anti-hGARP:TGF-β1 (clone MHG-8 (*28, 32*)), anti-αVβ8 integrin (clone ADWA-16, kind gift from Dean Sheppard (*43*), anti-mouse IgG1-PE (clone RMG1-1,

BioLegend), anti-GARP-PE (clone 7B11, BioLegend) and streptavidin-PE (BD Biosciences, #554061). Labeled cells were analyzed on an LSR Fortessa cytometer (BD Biosciences), and data were processed with FlowJo software (Tree Star).

BIBLIOGRAPHY

1. J. Massague, D. Sheppard, TGF-beta signaling in health and disease. *Cell* **186**, 4007–4037 (2023).
2. R. Derynck *et al.*, Human transforming growth factor-beta complementary DNA sequence and expression in normal and transformed cells. *Nature* **316**, 701–705 (1985).
3. C. M. Dubois *et al.*, Evidence that furin is an authentic transforming growth factor-beta1-converting enzyme. *Am J Pathol* **158**, 305–316 (2001).
4. L. E. Gentry, M. N. Lioubin, A. F. Purchio, H. Marquardt, Molecular events in the processing of recombinant type 1 pre-pro-transforming growth factor beta to the mature polypeptide. *Mol Cell Biol* **8**, 4162–4168 (1988).
5. A. Kelly, S. A. Houston, E. Sherwood, J. Casulli, M. A. Travis, Regulation of Innate and Adaptive Immunity by TGFbeta. *Adv Immunol* **134**, 137–233 (2017).
6. M. Shi *et al.*, Latent TGF-beta structure and activation. *Nature* **474**, 343–349 (2011).
7. W. Ma, Y. Qin, B. Chapuy, C. Lu, LRRC33 is a novel binding and potential regulating protein of TGF-beta1 function in human acute myeloid leukemia cells. *PLoS One* **14**, e0213482 (2019).
8. V. Ollendorff, T. Noguchi, O. deLapeyriere, D. Birnbaum, The GARP Gene Encodes a New Member of the Family of Lucin-rich Repeat-containing Proteins. *Cell growth & differentiation : the molecular biology journal of the American Association for Cancer Research* **5**, 213–219 (1994).
9. Y. Qin *et al.*, A Milieu Molecule for TGF-beta Required for Microglia Function in the Nervous System. *Cell* **174**, 156–171 e116 (2018).
10. D. B. Rifkin, W. J. Rifkin, L. Zilberberg, LTBPs in biology and medicine: LTBP diseases. *Matrix Biol* **71-72**, 90–99 (2018).
11. K. Wong *et al.*, Mice deficient in NRROS show abnormal microglial development and neurological disorders. *Nat Immunol* **18**, 633–641 (2017).
12. P. Aluwihare *et al.*, Mice that lack activity of alphavbeta6- and alphavbeta8-integrins reproduce the abnormalities of Tgfb1- and Tgfb3-null mice. *J Cell Sci* **122**, 227–232 (2009).
13. D. Mu *et al.*, The integrin alpha(v)beta8 mediates epithelial homeostasis through MT1-MMP-dependent activation of TGF-beta1. *J Cell Biol* **157**, 493–507 (2002).
14. J. Munger *et al.*, The Integrin avb6 Binds and Activates Latent TGFb1: A Mechanism for Regulating Pulmonary Inflammation and Fibrosis. *Cell* **96**, 319–328 (1999).
15. Z. Yang *et al.*, Absence of integrin-mediated TGFbeta1 activation in vivo recapitulates the phenotype of TGFbeta1-null mice. *J Cell Biol* **176**, 787–793 (2007).
16. J. P. Annes, Y. Chen, J. S. Munger, D. B. Rifkin, Integrin alphaVbeta6-mediated activation of latent TGF-beta requires the latent TGF-beta binding protein-1. *J Cell Biol* **165**, 723–734 (2004).
17. X. Dong *et al.*, Force interacts with macromolecular structure in activation of TGF-beta. *Nature* **542**, 55–59 (2017).
18. R. Wang *et al.*, GARP regulates the bioavailability and activation of TGFbeta. *Mol Biol Cell* **23**, 1129–1139 (2012).
19. M. Cheerathodi *et al.*, The Cytoskeletal Adapter Protein Spinophilin Regulates Invadopodia Dynamics and Tumor Cell Invasion in Glioblastoma. *Mol Cancer Res* **14**, 1277–1287 (2016).

20. J. H. McCarty, A. A. Cook, R. O. Hynes, An interaction between alphavbeta8 integrin and Band 4.1B via a highly conserved region of the Band 4.1 C-terminal domain. *Proc Natl Acad Sci U S A* **102**, 13479–13483 (2005).
21. A. Kelly *et al.*, Human monocytes and macrophages regulate immune tolerance via integrin alphavbeta8-mediated TGFbeta activation. *J Exp Med* **215**, 2725–2736 (2018).
22. A. De, J. E. Morales, Z. Chen, S. Sebastian, J. H. McCarty, The beta8 integrin cytoplasmic domain activates extracellular matrix adhesion to promote brain neurovascular development. *Development* **149**, (2022).
23. J. P. Edwards, A. M. Thornton, E. M. Shevach, Release of active TGF-beta1 from the latent TGF-beta1/GARP complex on T regulatory cells is mediated by integrin beta8. *J Immunol* **193**, 2843–2849 (2014).
24. J. Stockis *et al.*, Blocking immunosuppression by human Tregs in vivo with antibodies targeting integrin alphaVbeta8. *Proc Natl Acad Sci U S A* **114**, E10161–E10168 (2017).
25. M. G. Campbell *et al.*, Cryo-EM Reveals Integrin-Mediated TGF-beta Activation without Release from Latent TGF-beta. *Cell* **180**, 490–501 e416 (2020).
26. M. Jin *et al.*, Dynamic allostery drives autocrine and paracrine TGF-beta signaling. *Cell* **187**, 6200–6219 e6223 (2024).
27. M. Jin *et al.*, Latent-TGF-beta has a domain swapped architecture. *Nat Commun* **16**, 10469 (2025).
28. S. Lienart *et al.*, Structural basis of latent TGF-beta1 presentation and activation by GARP on human regulatory T cells. *Science* **362**, 952–956 (2018).
29. J. Stockis, D. Colau, P. G. Coulie, S. Lucas, Membrane protein GARP is a receptor for latent TGF-beta on the surface of activated human Treg. *Eur J Immunol* **39**, 3315–3322 (2009).
30. J. Stockis *et al.*, Comparison of stable human Treg and Th clones by transcriptional profiling. *Eur J Immunol* **39**, 869–882 (2009).
31. C. Bertrand *et al.*, Combined Blockade of GARP:TGF-beta1 and PD-1 Increases Infiltration of T Cells and Density of Pericyte-Covered GARP(+) Blood Vessels in Mouse MC38 Tumors. *Front Immunol* **12**, 704050 (2021).
32. J. Cuende *et al.*, Monoclonal antibodies against GARP/TGF-beta1 complexes inhibit the immunosuppressive activity of human regulatory T cells in vivo. *Sci Transl Med* **7**, 284ra256 (2015).
33. G. de Streel *et al.*, Selective inhibition of TGF-beta1 produced by GARP-expressing Tregs overcomes resistance to PD-1/PD-L1 blockade in cancer. *Nat Commun* **11**, 4545 (2020).
34. S. Lecomte *et al.*, Therapeutic activity of GARP:TGF-beta1 blockade in murine primary myelofibrosis. *Blood* **141**, 490–502 (2023).
35. F. Lambert *et al.*, Antibody-mediated TGF-beta1 activation for the treatment of diseases caused by deleterious T cell activity. *Cell Rep* **44**, 116061 (2025).
36. M. G. Zhao, G. B. Liang, H. F. Zhang, G. F. Zhao, Y. H. Luo, Soluble galectin 9 potently enhanced regulatory T-cell formation, a pathway impaired in patients with intracranial aneurysm. *Clin Exp Pharmacol Physiol* **45**, 1206–1212 (2018).
37. R. Wang, Q. Wan, L. Kozhaya, H. Fujii, D. Unutmaz, Identification of a regulatory T cell specific cell surface molecule that mediates suppressive signals and induces Foxp3 expression. *PLoS One* **3**, e2705 (2008).
38. D. A. Calderwood, I. D. Campbell, D. R. Critchley, Talins and kindlins: partners in integrin-mediated adhesion. *Nat Rev Mol Cell Biol* **14**, 503–517 (2013).
39. I. Spector, N. R. Shochet, Y. Kashman, A. Groweiss, Latrunculins: novel marine toxins that disrupt microfilament organization in cultured cells. *Science* **219**, 493–495 (1983).

40. A. Cormier *et al.*, Cryo-EM structure of the alphavbeta8 integrin reveals a mechanism for stabilizing integrin extension. *Nat Struct Mol Biol* **25**, 698–704 (2018).
41. J. Wang, Y. Su, R. E. Iacob, J. R. Engen, T. A. Springer, General structural features that regulate integrin affinity revealed by atypical alphaVbeta8. *Nat Commun* **10**, 5481 (2019).
42. V. T. Ruhoff, N. Leijnse, A. Doostmohammadi, P. M. Bendix, Filopodia: integrating cellular functions with theoretical models. *Trends Cell Biol* **35**, 129–140 (2025).
43. T. M. Fenton *et al.*, Inflammatory cues enhance TGFβ activation by distinct subsets of human intestinal dendritic cells via integrin αvβ8. *Mucosal Immunol* **10**, 624–634 (2017).

SUPPLEMENTARY FIGURES

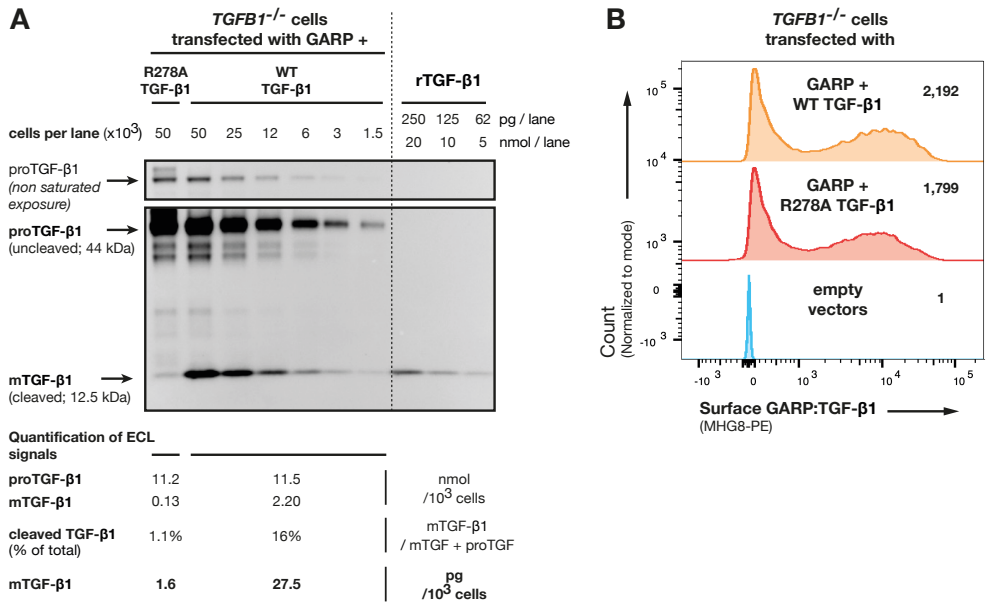

Figure S1: TGF-β1 R287A mutant is similarly expressed compared to WT but mature TGF-β1 cleavage is reduced

(**A**) SDS PAGE and Western blot analysis of serial dilutions of rTGF-β1 and lysates from the indicated transfected *TGFB1*$^{-/-}$ 293T cells, using an antibody (clone A75-2) against a C-ter TGF-β1 epitope present in pro- (uncleaved) and mature (cleaved) TGF-β1. ECL signals were quantified on non-saturated blots using the Bio1D software to estimate amounts of mTGF-β1, proTGF-β1. Proportion of cleaved TGF-β1 in cells transfected with GARP + WT or mutant R278A TGF-β1 were calculated based on these amounts. (**B**) Flow cytometry analysis of transfected *TGFB1*$^{-/-}$ 293T cells stained with antibody MHG-8, which binds GARP:TGF-β1 complexes but not GARP or latent TGF-β1 alone. Values indicated on the histograms represent mean surface levels of GARP:TGF-β1 (gMFI x % positive cells).

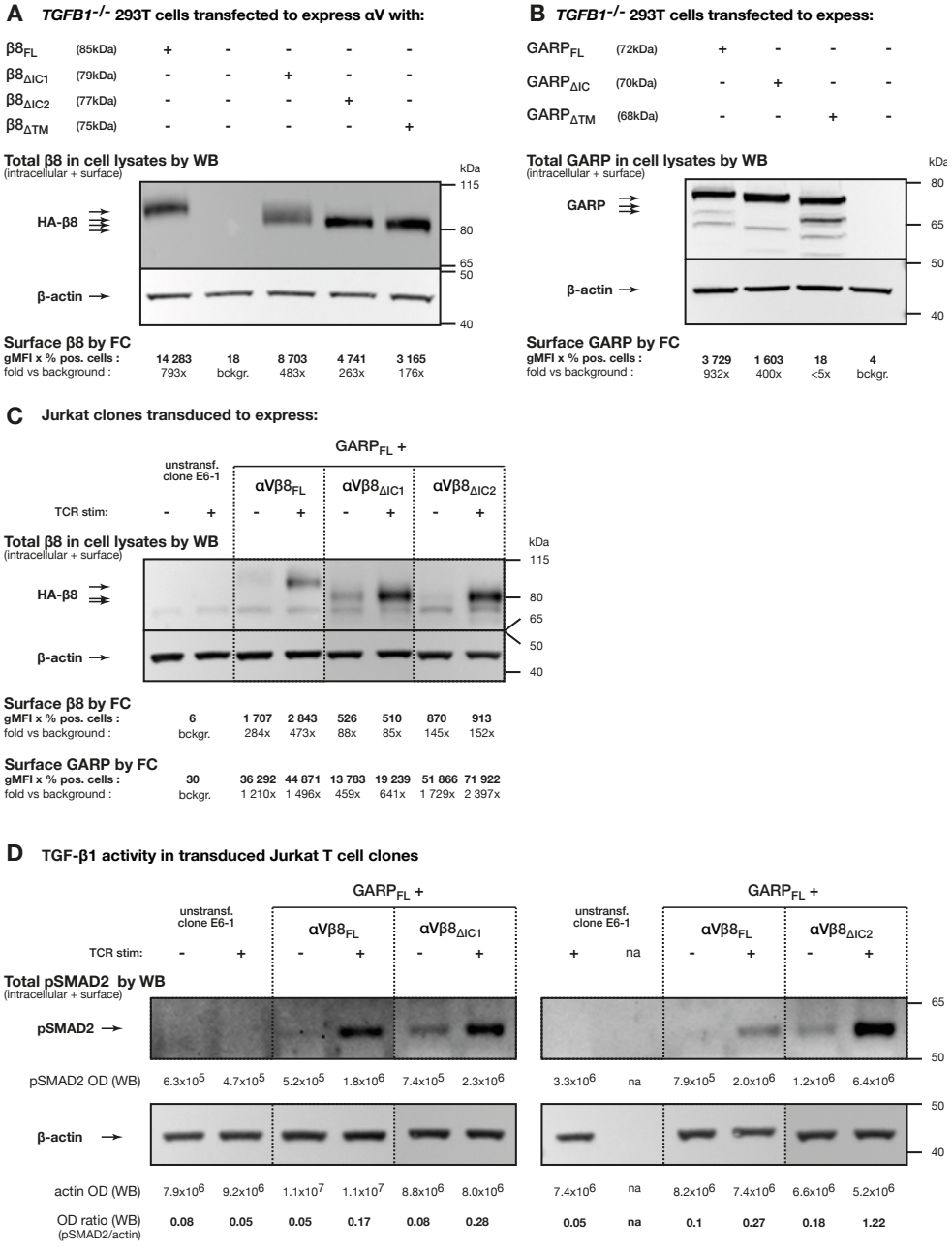
A TGFB1-/- 293T cells transfected to express αV with:
β8FL (85kDa) + - - - -
β8ΔIC1 (79kDa) - - + - -
β8ΔIC2 (77kDa) - - - + -
β8ΔTM (75kDa) - - - - +
Total β8 in cell lysates by WB
(intracellular + surface)
kDa
115
80
65
50
40
HA-β8
β-actin
Surface β8 by FC
gMFI x % pos. cells : 14 283 18 8 703 4 741 3 165
fold vs background : 793x bckgr. 483x 263x 176x
B TGFB1-/- 293T cells transfected to expess:
GARPFL (72kDa) + - - -
GARPΔIC (70kDa) - + - -
GARPΔTM (68kDa) - - + -
Total GARP in cell lysates by WB
(intracellular + surface)
GARP
β-actin
Surface GARP by FC
gMFI x % pos. cells : 3 729 1 603 18 4
fold vs background : 932x 400x <5x bckgr.
C Jurkat clones transduced to express:
GARPFL +
unstransf. clone E6-1
αVβ8FL
αVβ8ΔIC1
αVβ8ΔIC2
TCR stim: - + - + - + - +
Total β8 in cell lysates by WB
(intracellular + surface)
HA-β8
β-actin
Surface β8 by FC
gMFI x % pos. cells : 6 1 707 2 843 526 510 870 913
fold vs background : bckgr. 284x 473x 88x 85x 145x 152x
Surface GARP by FC
gMFI x % pos. cells : 30 36 292 44 871 13 783 19 239 51 866 71 922
fold vs background : bckgr. 1 210x 1 496x 459x 641x 1 729x 2 397x
D TGF-β1 activity in transduced Jurkat T cell clones
GARPFL +
unstransf. clone E6-1
αVβ8FL
αVβ8ΔIC1
αVβ8ΔIC2
TCR stim: - + - + - + + na - + - +
Total pSMAD2 by WB
(intracellular + surface)
pSMAD2
pSMAD2 OD (WB) 6.3x10^5 4.7x10^5 5.2x10^5 1.8x10^6 7.4x10^5 2.3x10^6 3.3x10^6 na 7.9x10^5 2.0x10^6 1.2x10^6 6.4x10^6
β-actin
actin OD (WB) 7.9x10^6 9.2x10^6 1.1x10^7 1.1x10^7 8.8x10^6 8.0x10^6 7.4x10^6 na 8.2x10^6 7.4x10^6 6.6x10^6 5.2x10^6
OD ratio (WB) (pSMAD2/actin) 0.08 0.05 0.05 0.17 0.08 0.28 0.05 na 0.1 0.27 0.18 1.22

Figure S2: Generation of GARP IC domain and ITGB8 IC and TM domains mutants
(**A**) Western blot analysis (anti-HA clone 16B12, β-actin clone D6A8) confirmed high expression of all ITGB8 constructs when transfected in *TGFB1*$^{-/-}$ 293T cells. FACS analysis using anti-αVβ8 antibody (ADWA-16) and anti-mIgG1-PE showed surface staining even in the Δ mutants (1.5-, 3- and 4.5-fold lower compared to FL). Fold increases are calculated by comparing staining values to background level. (**B**) Western blots (anti-GARP clone Plato-1, β-actin clone D6A8) showed high expression of all GARP constructs. FACS staining (anti-GARP-PE clone 7B11) revealed similar surface expression for $GARP_{\Delta IC}$ compared to $GARP_{FL}$ and no surface staining for the secreted ΔTM mutant. (**C**) $ITGB8_{FL}$ and mutants were force-expressed in Jurkat E6-1 stably expressing GARP. Western blots again confirmed total expression of all ITGB8 construct while flow cytometry analysis indicated good surface staining for the Δ mutants compared to FL. (**D**) A functional Western blot assay assessed TGF-β1 activation by Jurkat cells. Cells were incubated for 24h with or without plate bound anti-CD3. Cell lysates were analyzed by Western blot with anti-pSMAD2 and β-actin antibodies. pSMAD2 OD was normalized to β-actin.

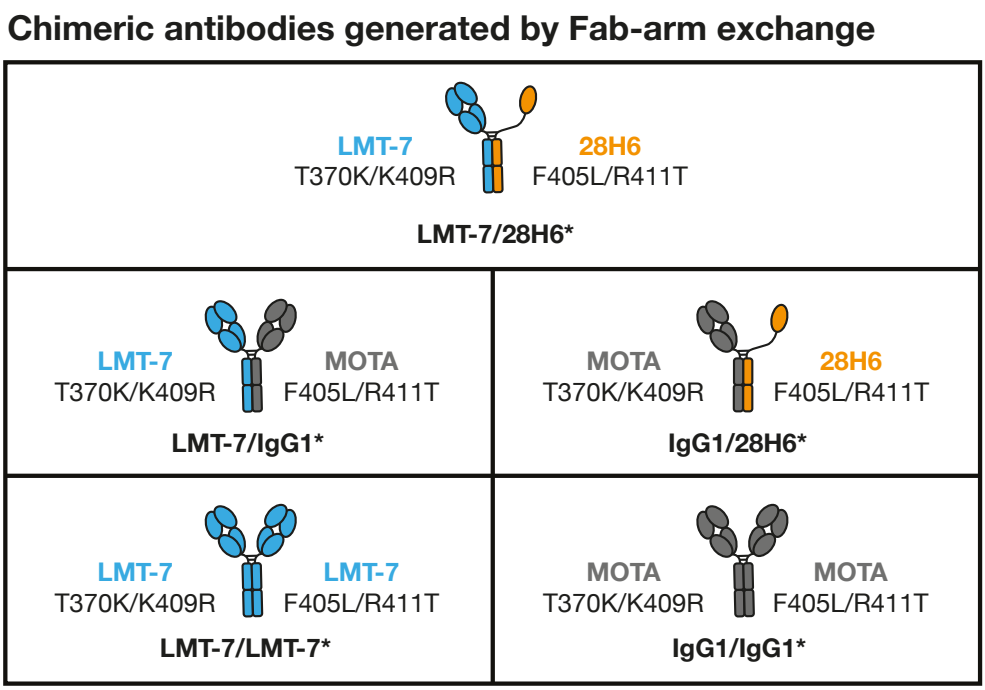

Figure S3: Bispecific mAbs description
Schematic representation of the bispecific antibody chimeras generated by Fab-arm exchange. LMT-7/28H6* (blue/orange): chimera with one arm from activating LMT-7 mAb and one arm from anti-GARP 28H6 Ab. LMT-7/IgG1* (blue/grey): chimera with one arm from LMT-7 and one arm from an irrelevant mouse IgG1. IgG1/28H6* (grey/orange): chimera with one arm from the IgG1 control and one arm from the 28H6 Ab. LMT-7/LMT-7* (blue): control chimera with two arms from LMT-7 mAb. IgG1/IgG1* (grey): control chimera with two arms from the irrelevant mouse IgG1.

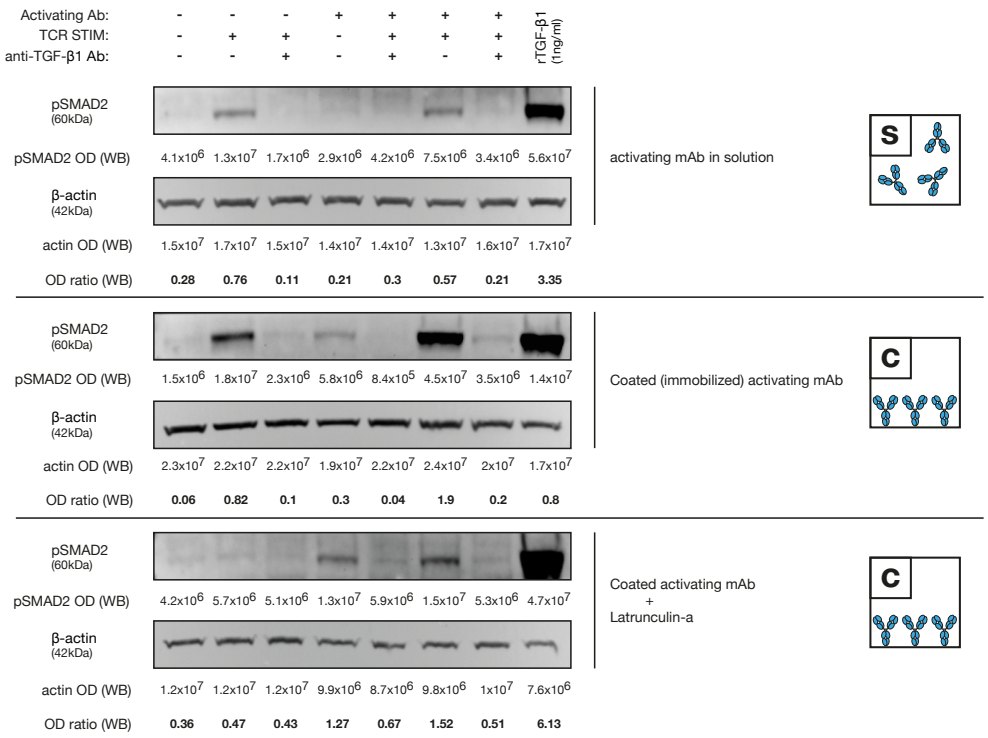

Figure S4: Cytoskeleton requirements on ITGB8- or mAb-dependent TGF-β1 activation in Jurkat cells

Jurkat T cells E6-1 cells stably transduced with *GARP* and *ITGB8*^{FL} were incubated for 24 h with coated anti-CD3 OKT3 mAb (Stim +) or left resting in FBS-free medium alone (Stim -). LHT22-activating mAb and IgG1 isotype were either used in solution (S) or immobilized on plastic (C). Cell lysates were analyzed by Western blot with antibodies against pSMAD2, and β-actin. ECL signals were quantified to establish pSMAD2/β-actin ratios.

SUPPLEMENTARY MATERIAL

Supplementary table 1: Primers

Name	Sequence	FW/RV	Function
OPC2800	ATTAACAAGGCCCAGCCGGCCGA AGACAATAGATGTGCATCTTCA	FW	ITGB8 amplification (no SP)
OPC2805	AACTGATTCCGCGGAATTATTAAC AATTCCAGTTTCCCA	RV	ITGB8 amplification
OPC4900	GAATAGTAATtagtgaAAGTCCTCATC AGATTACAGAG	FW	Site directed mutagenesis: truncated hITGB8_R705*Q706*
OPC4901	CATTGTAGTATCACCTGTC	RV	Site directed mutagenesis: truncated hITGB8_R705*Q706*
OPC4898	CCTGATCATTtagtgaGTGATACTACA ATGGAATAG	FW	Site directed mutagenesis: truncated hITGB8_K713*I714*
OPC4899	ACTTTAAGCAACCCAATC	RV	Site directed mutagenesis: truncated hITGB8_K713*I714*
OPC4912	CTACTTGAGAtagtgaTTCATCATTTT CATAGTTACATTCTTGATTGGGTTG	FW	Site directed mutagenesis: truncated hITGB8_I685*F686*
OPC4913	CTTGGGCTGGAGAAACATTC	RV	Site directed mutagenesis: truncated hITGB8_I685*F686*
OPC2277	GGTACTGCTGCTCTGGGTTCC	FW	pDisplay amplification
OPC4840	GTTAGTCGACCGGTTAGCAGGCGG CCAGC	RV	GARP amplification without IC (20-648*)

DISCUSSION

1 Starting point: the cDNA library and screening

Although the screen described in **Sections 1.3** and **1.4** of the **Results** did not identify clear new partners involved in TGF-β1 activation, it nevertheless helped orient our work toward a more mechanistic investigation. In this first section of the Discussion, we therefore briefly examine the cDNA library that constituted the starting material for this study, as well as the screening strategy that was implemented.

1.1 Limitations of the cDNA library

The cDNA library was generated in-house using mRNA extracted from two polyclonal $CD4^+CD25^+CD127^{low}$ Treg populations and one Treg clone. Library quality was assessed and found suitable for standard screening applications, with an estimated diversity of approximately 100,000 individual clones. The human genome contains roughly 20,000 genes, although the number of genes actively expressed decreases as cells become more differentiated. For example, a Treg cell is expected to express approximately 10,000 genes, suggesting that our library theoretically represents about ten times the expressed transcriptome of a single Treg cell.

Unexpectedly, *ITGB8* – the gene coding for the β chain of αVβ8 – was never identified as a positive candidate in the screening, despite being known to be required for TGF-β1 activation by Tregs and to be expressed in stimulated Tregs. Furthermore, *ITGB8* can be readily detected in the 293T-based screening assay used here, as confirmed by its use as a positive control. Therefore, if *ITGB8* transcripts were sufficiently represented in the library, they would be expected to emerge during the screening process.

RT-qPCR analysis revealed that although *ITGB8* expression is detectable and increases upon TCR stimulation of Tregs, its transcript levels remain very low, ranging from approximately 1

to 40 copies per 100,000 EF-1 transcripts. Despite these low transcript levels, *ITGB8* expression is sufficient to produce detectable protein and to support TGF-β1 activation (*121*).

When examining the cDNA derived from the Treg clones used to construct the library, *ITGB8* transcript levels were even lower, with only one to two copies per 100,000 EF-1 transcripts. At such low abundance, *ITGB8* transcripts would be expected to be poorly represented – or potentially absent – in a library containing 100,000 clones. Consequently, other genes expressed at similarly low levels and potentially involved in TGF-β1 activation may also have been underrepresented in the library and therefore remained undetected in the screening.

1.2 Is there any potential bias induced by the screening strategy?

A potential source of bias in our screening strategy lies in the initial selection of candidate genes, where we deliberately prioritized extracellular proteins. By intentionally excluding intracellular candidates, we may have overlooked factors that could influence TGF-β1 activation indirectly through intracellular signaling pathways or regulatory functions. However, the intracellular candidates identified during the initial screen either had no obvious connection to TGF-β1 biology or were associated with broad cellular processes, making them difficult to investigate in a targeted manner.

Another limitation of our system relates to the cell type used for the screening assay. HEK293T cells are widely used in basic research because they are easy to culture and highly transfectable. These properties make them particularly suitable for reporter assays, lentiviral production, and recombinant protein expression. Nevertheless, 293T cells differ substantially from Tregs. They are adherent cells derived from human embryonic kidney, although transcriptomic analyses suggest that they display characteristics closer to epithelial or neuronal lineage cells (*250, 251*). These cells are highly dynamic, forming cytoplasmic protrusions and displaying significant motility. As a result, observations made in 293T cells may not fully reflect the behavior of T cells, including Tregs or Jurkat cells. For instance, transfection of *ITGB8* leads to spontaneous activation of TGF-β1 in 293T cells, whereas no such activation is observed in Jurkat cells in the absence of TCR stimulation.

Developing a screening or reporter system based on Jurkat cells could therefore improve the physiological relevance of the assay. However, such approaches are technically more challenging because Jurkat cells are less amenable to transient transfection and currently lack a robust reporter system for monitoring TGF-β1 signaling.

Although debatable, the screening strategy we employed was likely the most appropriate at the time to address our research question, which aimed to identify novel partners involved in TGF-β1 activation in Tregs. In retrospect, however, Tregs likely do not require an additional partner for TGF-β1 activation, but rather depend on dynamic cellular processes induced by TCR stimulation. Consequently, no suitable “partner” could have been identified using this approach.

2 First candidate: the case of galectin-9

GAL-9 was the only candidate we investigated in detail, and most aspects related to this protein were already discussed in **Section 1.5** of the **Results**. However, the additional data and hypotheses emerging from the analysis of activating mAbs and integrins raise one final point that merits further discussion.

2.1 Could forces be implicated in TGF-β1 activation by GAL-9?

We previously discussed how bivalent binding by antibodies is required – at least in their soluble form – to transmit activating tensile forces between two cell-anchored complexes. GAL-9 is also a bivalent protein, containing two carbohydrate-recognition domains (CRDs) that bind glycosylated proteins. One possibility is that GAL-9 could interact with either GARP or LAP. However, no direct interaction between GAL-9 and these proteins has been demonstrated to date. If such interactions exist and occur with sufficient affinity, they could in principle allow GAL-9 to transmit tensile forces and thereby support force-dependent TGF-β1 activation, provided that the appropriate mechanical conditions are met. Nevertheless, this mechanism appears unlikely, as galectin-glycan interactions are generally low-affinity and highly dynamic, which would limit their ability to sustain the forces required for mechanical activation (*252*).

An alternative possibility is that GAL-9 could act through a mechanism similar to that described for thrombospondin-1 (TSP-1) (**Introduction, section 2.3.2.2**), whereby binding to the latent complex destabilizes its structure and promotes the release of mature TGF-β1 although we have no indication that such mechanism is implicated here.

3 Force-dependent activation mediated by αVβ8

During the second screening, only intracellular candidates were identified, which prompted us to re-evaluate our initial strategy that had focused primarily on extracellular candidates. From that point onward, we directed our work toward the potential role of the IC domains of both GARP and β8, while also seeking to refine the current understanding of the molecular requirements for force-dependent TGF-β1 activation, whether mediated by TGF-β1-activating mAbs (**see Section 4** of the **Discussion**) or by the integrin αVβ8. Our findings support a model in which αVβ8 mediates TGF-β1 activation through a force-dependent mechanism, which is difficult to reconcile with the recently proposed entropy-redistribution model developed by the group of Stephen Nishimura. In this section, we therefore examine the points of divergence and convergence between these two models, with the aim of clarifying the mechanisms underlying αVβ8-mediated TGF-β1 activation.

3.1 Reminder: αVβ8 *versus* other integrins

Integrin αVβ8 differs mechanistically from the other TGF-β-activating integrins (αVβ6 and αVβ1). Structural studies indicate that, unlike typical integrins that transit between bent-closed, extended-closed and extended-open conformations, αVβ8 predominantly adopts an extended-closed conformation. This conformational bias has been attributed to atypical features of the β8 lower leg, including the absence of conserved disulfide bonds in the I-EGF3/β-tail region, together with stabilizing contacts within the αV leg that favor extension (*134, 135*).

αVβ8 is also unusual at the level of its ligand-binding headpiece. In most integrins, maximal ligand affinity is associated with the extended-open state. By contrast, αVβ8 binds latent TGF-β1 with very high affinity while adopting the extended-closed conformation. Structural and mutational analyses have shown that this property arises from atypical features of the β8 βI domain, including loss of the canonical ADMIDAS metal-binding arrangement and a distinctive

β6-α7 loop configuration, which favor a high-affinity ligand-binding pocket without the large βI-to-hybrid domain rearrangements (headpiece opening) typical of other integrins (*135*).

Consistent with this, β8 lacks the canonical NPXY motifs used by most β integrins to recruit talin and kindlin, responsible for integrin activation and extension, suggesting that αVβ8 is less dependent on classical inside-out activation (*253*).

3.2 The entropy redistribution model is (in part) incompatible with our proposed model

Nishimura and colleagues recently proposed a model in which αVβ8-mediated TGF-β1 activation does not require mechanical force transmission (*49, 55, 136*). In this model, binding of αVβ8 to the LAP arm domain would induce an entropy redistribution within the latent complex, exposing residues of mature TGF-β1 near the cell membrane and thereby enabling signaling restricted to the producing cell.

Our observations do not readily support this model. In our co-culture system, αVβ8 clearly induces paracrine TGF-β signaling in neighboring cells. While we cannot formally exclude the possibility that autocrine signaling without cytokine release may also occur, the experimental system used by Jin et al. does not allow one to distinguish strictly autocrine signaling from paracrine responses, as neighboring cells remain capable of responding to TGF-β1. Addressing this question would likely require single-cell approaches capable of discriminating between cell-autonomous and intercellular signaling events. In addition, we note potential structural constraints that could limit receptor engagement in the absence of ligand release. Analysis of the published αVβ8:latent TGF-β1 cryo-EM structure (PDB: 8VSD) (*136*) performed by colleagues at the University of Ghent, indicates that in the αVβ8-bound latent complex, the helix forming the “thumb” of mature TGF-β1 adopts a position similar to that observed in the unbound latent state. In this configuration, the thumb remains separated from the β-sheet “fingers” of mature TGF-β1 due to the presence of the LAP α1 helix, a constraint that is normally relieved upon release of the mature cytokine (**Figure 3C of the Introduction**). Consequently, direct engagement of the thumb with the TβRI subunit appears sterically

unfavorable due to severe clashes, raising doubts about the feasibility of receptor binding without prior structural rearrangement or partial release of the mature cytokine.

Another of our experimental observations supports a force-dependent mechanism rather than the entropy redistribution model. We found that αVβ8-mediated TGF-β1 activation in 293T cells or stimulated Jurkat cells does not require the β8 IC domain but still depends on an intact actin cytoskeleton as cells treated with latrunculin lose their ability to activate TGF-β1. We therefore propose that αVβ8, owing to its constitutively ligand-competent ectodomain, binds latent TGF-β1 immediately upon expression at the cell surface, while the mechanical forces required for activation are generated indirectly by global cellular dynamics, such as membrane dynamics or cytoskeleton-associated cellular movements. In other words, αVβ8 does not need intracellular activation but still depends on cytoskeleton-originating cellular dynamics.

In addition, integrin-ligand binding can still occur in cells treated with latrunculin. Therefore, if TGF-β1 activation relied solely on entropy redistribution triggered by integrin binding, inhibition of actin dynamics should not block activation. The fact that latrunculin treatment prevents αVβ8-mediated TGF-β1 activation in our experimental system supports a mechanism in which cytoskeleton-dependent forces remain necessary for effective activation of the latent complex by the integrin.

These findings raise a broader question regarding integrin-mediated TGF-β1 activation. While it is generally assumed that activation by most integrins requires direct cytoskeletal coupling through the integrin IC tail, our results raise the possibility that the primary function of the IC domain may instead be to simply promote integrin activation and ligand binding. In this scenario, the mechanical forces required for TGF-β1 activation would not be transmitted directly through the integrin tail but would instead arise from more global cellular mechanical processes.

3.3 Do integrins need their IC tail for the transmission of activating forces?

Our data suggest that simple anchorage of the integrin αVβ8 at the plasma membrane, together with an active cytoskeleton is sufficient to transmit cell-generated forces to a cell-anchored GARP:latent-TGF-β1 complex and to activate it.

This interpretation is compatible with previous observations by Nishimura and colleagues, who showed that coating the αVβ8 ectodomain on plastic was sufficient to trigger TGF-β1 activation in adherent cells, whereas fully soluble forms were markedly less efficient (*49, 136*). Similarly, Jin et al. (2025) demonstrated that coated, truncated αVβ6 integrin can activate TGF-β1 presented by GARP on co-incubated reporter cells (*55*). Together, these findings suggest that activation can occur without direct cytoskeletal coupling of the β-subunit tail, even in the case of αVβ6, provided that the integrin is sufficiently immobilized, can bind with high affinity to its ligand, and that the latent cytokine remains anchored at the cell surface. A useful way to further test this hypothesis would be to treat cells plated with coated integrins with latrunculin.

Taken together, our findings and working hypothesis for αVβ8-mediated TGF-β1 activation do not support a model of entropy redistribution leading to autocrine-only signaling. Instead, we propose that, similar to αVβ6, αVβ8 relies on cytoskeleton-generated forces to mechanically disrupt the integrity of the latent TGF-β1 complex, ultimately resulting in the release of mature TGF-β1 and allowing paracrine signaling, which is more consistent with data from the literature.

We further raise the possibility that, contrary to the prevailing view in the field, integrins may not require their IC tails to directly transmit forces during TGF-β1 activation. Rather, the critical requirements may be strong ligand binding, stable anchorage of both the integrin and the latent complex, and sufficient cellular dynamics to generate the mechanical forces necessary to remodel LAP and release the cytokine.

4 Force-dependent activation mediated by mAbs

We recently developed TGF-β1-activating monoclonal antibodies (mAbs). Initial work by Lambert et al. defined a first set of requirements for mAb-mediated TGF-β1 activation: latent TGF-β1 must be presented and anchored at the cell surface via GARP or LRRC33; an active cytoskeleton is required; and bivalent binding is necessary. Importantly, this bivalent binding must crosslink two distinct latent complexes, as a single mAb cannot engage two epitopes within the same complex. In addition, binding of Fab fragments alone does not induce any detectable structural change in the latent complex, indicating that antigen binding itself is insufficient to trigger activation (*51*).

In the present study, we further refine the molecular requirements for mAb-mediated TGF-β1 activation and use these antibodies as tools to investigate force-dependent TGF-β1 activation that occurs without direct cytoskeletal coupling. In this context, mAbs provide a useful experimental system to further test the mechanistic hypothesis developed here for integrin-mediated activation.

4.1 Bivalent *versus* monovalent mAbs, soluble *versus* coated mAbs

In their soluble form and in the context of adherent cells, only bivalent antibodies were able to activate TGF-β1 (**Figure 3A**, *Jamez et al., unpublished*), confirming the results obtained by Lambert et al. Mechanistically, mAbs can crosslink two cell-anchored latent complexes, thereby enabling the transmission of deforming forces generated by cell adhesion and cellular movement to the LAP. By contrast, no soluble antibody – whether bivalent or monovalent – was able to induce TGF-β1 activation in non-adherent cells. This observation was not addressed in Lambert et al. We hypothesize that the absence of cell adhesion prevents the generation of opposing forces sufficient to trigger TGF-β1 activation. Indeed, in non-adherent cells the only anchoring point capable of providing retention is the membrane attachment of

the latent complex. Under these conditions, mono- or bivalent antibodies most likely crosslink two latent complexes on the same cell or on two non-adherent cells and therefore cannot transmit activating forces because the system lacks a stable counterforce.

In contrast, when the same antibodies were immobilized on a surface, TGF-β1 activation was observed even in non-adherent cells, whether the antibodies were monovalent or bivalent (**Figure 3C**, *Jamez et al., unpublished*). In this situation, two sources of retention are present: immobilization of the antibody on the solid surface and membrane anchoring of the latent complex on the cell. Passive cell movement while the cells remain suspended might therefore be sufficient to generate the mechanical forces required for activation.

All these observations suggest that mAb-mediated TGF-β1 activation occurs only when mAbs can provide mechanical resistance by linking two fixed points, allowing the tensile forces generated by cell movement or membrane dynamics to activate TGF-β1.

4.2 Bispecific mAbs

To better probe the requirement for crosslinking of two different complexes, we developed bispecific antibodies in collaboration with ArgenX that contain one TGF-β1-activating arm and a second arm recognizing GARP. When tested on cells expressing GARP:latent TGF-β1 complexes, the bispecific antibody failed to induce activation, most likely because it simultaneously recognized LAP and GARP within the same complex, thereby preventing crosslinking between two distinct complexes (**Figure 3A**, *Jamez et al., unpublished*).

To overcome this limitation, we co-transfected LRRC33 and TGF-β1 in one population of cells and co-cultured them with GARP-expressing cells. This experimental setup forces crosslinking between two different complexes: an empty GARP complex on one cell and an LRRC33:latent TGF-β1 complex on another cell. Under these conditions, TGF-β1 activation was observed (**Figure 3B**, *Jamez et al., unpublished*).

Conceptually, crosslinking two complexes located on the same cell membrane would be unlikely to generate sufficient activating forces, as both complexes are anchored within the same membrane and the two GARP molecules are unlikely to be pulled apart through their

short IC tails. A more plausible explanation is therefore that activation occurs through crosslinking of complexes located on two different cells. Although we cannot formally demonstrate this mechanism at this stage, the results obtained with the bispecific antibodies indicate that such *trans*-activation is possible and provide indirect support for this hypothesis. The potential contribution of *cis*- versus *trans*-activation will be discussed further in **Section 5** of the **Discussion**.

4.3 Can mAbs activate any latent TGF-β1 pool?

Lambert et al. developed these antibodies with the aim of treating allo- and autoimmune diseases. However, an important question is whether the activity of these TGF-β1-activating mAbs can be adequately controlled. In particular, could these antibodies activate any pool of latent TGF-β1 *in vivo*? Data obtained in a GvHD model suggest that the observed effects are largely Treg-dependent, with no evidence of excessive TGF-β1 activation, such as fibrosis (*51*). Séverine Wautier and I further investigated which cell types (here we discuss human cell types only), including primary immune and non-immune cells expressing GARP or LRRC33, could represent physiological sources of latent TGF-β1 that could be activated by these antibodies. Here, we present preliminary results obtained from four cell types that do express GARP:TGF-β1 complexes at baseline, or after stimulation: endothelial cells (HUVECs), primary fibroblasts (CROX), stimulated Tregs and B cells (**Figure 23**).

Human Tregs are difficult to study due to the limited numbers that can be obtained from healthy donors. To overcome this limitation, we used previously expanded Tregs that had been cryopreserved in our laboratory. As expected, stimulation of these cells through the TCR triggered activation of TGF-β1. Treatment with TGF-β1-activating mAbs further enhanced this activation. In contrast, Tregs that had not undergone TCR stimulation did not respond to activating mAbs, consistent with the absence of detectable GARP:TGF-β1 complexes at their surface (**Figure 23A**).

Previous work from our laboratory showed that B cells stimulated through the B-cell receptor (BCR) can activate TGF-β1 presented on GARP at their surface (*29*). Using freshly isolated $CD19^+$ B cells from patients with hemochromatosis, we confirmed that BCR stimulation induces TGF-β1 activation. This response was further amplified in the presence of TGF-β1-

activating mAbs (**Figure 23B**). Interestingly, treatment of unstimulated B cells with activating mAbs also resulted in a detectable, albeit modest, activation of TGF-β1, even though these cells do not express GARP. However, these resting B cells were found to express *LRRC33* mRNA (data not shown) at levels comparable to those observed in THP-1 monocytes, a cell line known to display LRRC33:TGF-β1 complexes at the cell surface. This observation raises the possibility that LRRC33 may provide an alternative membrane anchor for latent TGF-β1 in resting B cells, allowing antibody-mediated activation. Nevertheless, the presence of LRRC33 protein at the surface of resting human B cells, as well as its functional contribution, remains to be demonstrated.

We also observed GARP:TGF-β1 complexes on endothelial cells and some fibroblasts cell lines. Several attempts were made in our laboratory to determine whether these adherent cell types could activate TGF-β1 in the presence of activating mAbs. However, we were unable to detect clear antibody-mediated TGF-β1 activation in fibroblasts. In endothelial cells, the results were variable: although these cells exhibited relatively high basal levels of pSMAD2 signaling, the addition of activating mAbs did not produce a consistent increase (**Figure 23C-D**). Two possible explanations are either a lower surface density of the complexes or differences in the physical properties of these cells. Fibroblasts and endothelial cells are adherent and display limited motility compared to other cell types such as 293T cells. Because antibody-mediated TGF-β1 activation likely depends on cell-generated tensile forces, the restricted mobility of these cells may limit their ability to activate TGF-β1 under these conditions. Experimental strategies aimed at inducing cell movement, such as scratch-wound assays, could help determine whether cellular motility represents a limiting factor for TGF-β1 activation in these cell types.

Taken together, these observations suggest that immune cells, particularly Tregs and B lymphocytes, may represent major cellular sources of latent TGF-β1 that can be activated by these antibodies. Our data suggest that mAbs do not act on all cell types equally, and that their activity, similar to cellular TGF-β1 activation mechanisms, is cell- and context-dependent. To note, we did not examine here myeloid populations such as monocytes or macrophages, although these cells are known to express LRRC33:TGF-β1 complexes.

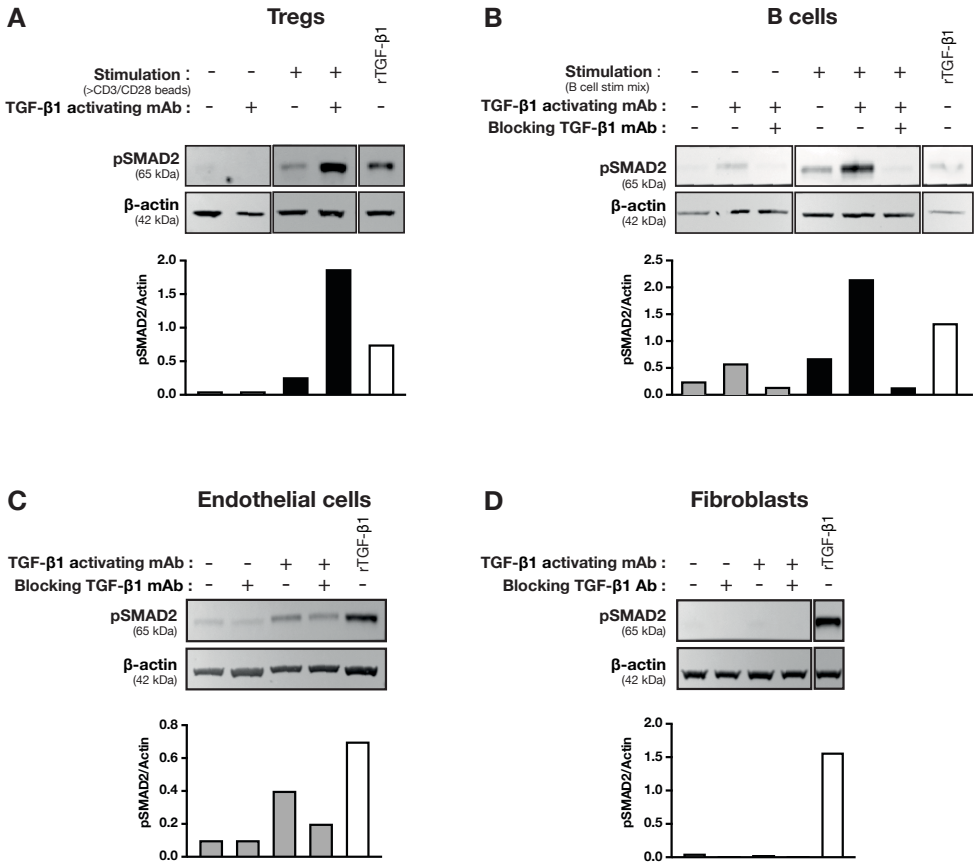

Figure 23: TGF-β1-activating mAbs enhance TGF-β1 signaling in stimulated B cells and Tregs. Cells were cultured for 20h with the indicated antibodies (20 μg/mL). (**A**) Tregs were stimulated with anti-CD3/CD28 beads, while B cells (**B**) were stimulated using a B-cell activation mixture composed of $F(ab')_2$ anti-human IgM, IL-21, IL-2 and CpG. B cells consisted of FACS-sorted $CD19^+$ cells (approximately 97% $CD3^-CD19^+$). (**C**) Endothelial cells were obtained from ATCC (HUVEC PCS-100-010) and cultured according to the recommended handling procedures. (**D**) Fibroblasts were isolated in-house from an abdominoplasty sample. (**A-D**) After incubation, cell lysates were analyzed by Western blot using antibodies against pSMAD2 and β-actin. Bar graphs represent the quantification of ECL (Enhanced Chemiluminescence) signals. Recombinant human TGF-β1 (1 ng/mL) was used as a positive control for pSMAD2 induction. Data shown are representative of at least two independent experiments.

5 *Cis*- or *trans*- activation?

Whether integrin-expressing cells can activate their own pool of latent TGF-β1 – for example, Tregs that express both GARP:TGF-β1 complexes and integrin αVβ8 – or whether activation requires *trans* interactions between distinct cells has been a long-standing question. Demonstrating *trans* activation can be relatively straightforward and has been shown in several *in vitro* settings and suggested *in vivo*. In **Section 3.2** of the **Introduction**, we discussed examples of *trans* activation between microglial cells and astrocytes, as well as situations where it has been proposed in epithelial cells and B cells. By contrast, *cis*-activation is more difficult to demonstrate experimentally and, to our knowledge, has not yet been firmly established. Demonstrating such a mechanism would likely require refined single cell approaches capable of resolving the geometry of the interacting partners.

From a molecular perspective, force-dependent activation is also easier to envision in *trans*, where two opposing cell surfaces can generate tensile forces, than in *cis*, where two molecules are crosslinked side-by-side within the same membrane. In the latter case, activation would require membrane deformation or cytoskeletal interactions capable of pulling the complexes apart. Such a mechanism appears unlikely in the case of mAb-mediated activation. Indeed, mAbs which crosslink two cell anchored latent complexes cannot directly couple to the cytoskeleton. Similarly, GARP or LRRC33 possess short IC tails that do not appear to mediate cytoskeletal interactions. Integrins, in contrast, are generally able to couple to the cytoskeleton through their IC domains and thereby transmit mechanical forces. However, our results indicate that integrin αVβ8 represents a notable exception, as its IC tail is not required for TGF-β1 activation and therefore cannot directly transmit cytoskeleton-derived forces. In this regard, and similarly to mAbs, a *trans*-activation mechanism appears more compatible with the available data.

More broadly, integrin biology also tends to support a *trans*-oriented model. Integrins behave as extracellular ligand sensors: upon activation, their extended headpiece scans the surrounding environment for ligands, a concept sometimes referred to as the “sunflower model” (*134*). Integrins are specialized in mediating cell-cell and cell-ECM adhesion, enabling force transmission and mechanotransduction. Although *cis* interactions between integrins and

other membrane proteins do occur, they appear to play primarily regulatory roles, modulating integrin activation, signaling, or the organization of membrane microdomains (*254, 255*).

In the following section, we discuss structural evidence together with preliminary immunofluorescence data that may help clarify whether TGF-β1 activation is more consistent with a "*trans*" activation model.

5.1 How can structural data guide us?

Integrins adopt a characteristic geometry during ligand binding. As discussed previously, active integrins exhibit an extended conformation (either extended-closed or extended-open), in which they display increased affinity for their ligands. In this configuration, ligand binding to a molecule located on the same cell surface would be geometrically unfavorable and would likely require substantial membrane curvature to bring the interacting partners into a compatible orientation (**Figure 24**).

Structural models of integrins bound to latent TGF-β1 – either alone or in complex with GARP – consistently show the two proteins oriented in opposite directions, with their apical surfaces facing each other. Such an arrangement naturally favors interactions occurring between opposing membranes, rather than within the same membrane plane. These structural considerations therefore support a *trans*-activation model over a *cis*-activation mechanism.

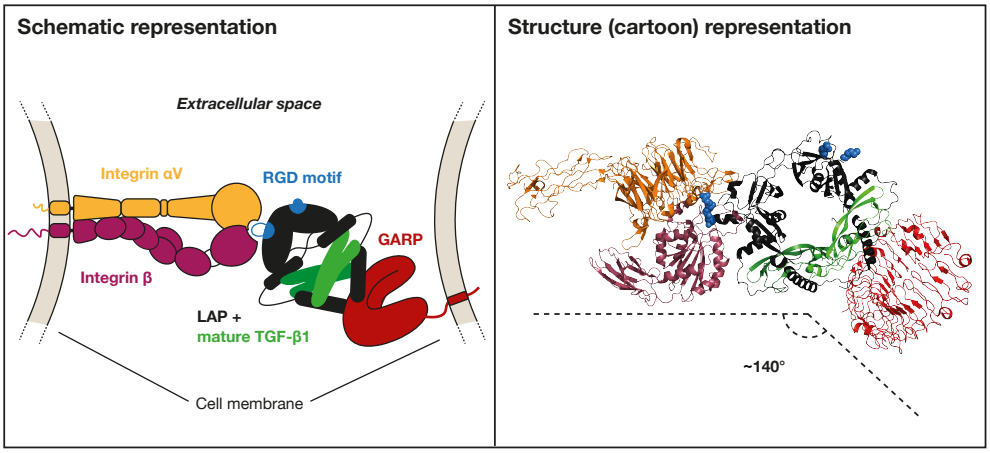

Figure 24: Integrins αVβ bind to the apical side of the LAP, opposite to its membrane anchorage. Left panel: schematic representation of an αVβ integrin binding a membrane-anchored latent complex (GARP:TGF-β1). Right panel: structural cartoon of the αVβ8:TGF-β1:GARP complex. The structure is derived from Jin et al. (2024), PDB: 8VSD. The angle formed between the two basal points of the complex is approximately 140°, without accounting for the flexibility of the GARP linker domain.

5.2 Preliminary results in immunofluorescence on adherent cells

During the final year of this project, we briefly explored immunofluorescence approaches to visualize integrin organization in the context of TGF-β1 activation. Although staining of Jurkat T cells did not yield interpretable results, transiently transfected HEK293T cells provided clearer signals and allowed visualization of both GARP and integrin αVβ8 at the surface of these adherent cells.

For these experiments, we used the anti-GARP antibody MHG6, a non-blocking antibody that recognizes both free GARP and GARP bound to latent TGF-β1, together with the blocking anti-αVβ8 antibody ADWA-16, kindly provided by Dean Sheppard.

Representative images obtained from these stainings are shown in **Figure 25**. Both GARP and αVβ8 appeared broadly distributed across the cell surface. Interestingly, however, the staining intensity for both molecules seemed enriched at regions where the plasma membranes of adjacent cells were in contact. Because these experiments were exploratory, only preliminary quantitative image analyses were performed and were not subjected to rigorous validation. Nevertheless, the signal observed at cell-cell interfaces appeared stronger than what would be expected from the simple superposition of two plasma membranes, suggesting a localized enrichment of the complexes at these contact zones.

Although these observations remain preliminary and require further validation and quantification, they are consistent with the idea that interactions between GARP:latent TGF-β1 complexes and αVβ8 may preferentially occur in *trans* at sites of cell-cell contact. Such enrichment at cellular interfaces could facilitate the mechanical coupling required for force-dependent TGF-β1 activation.

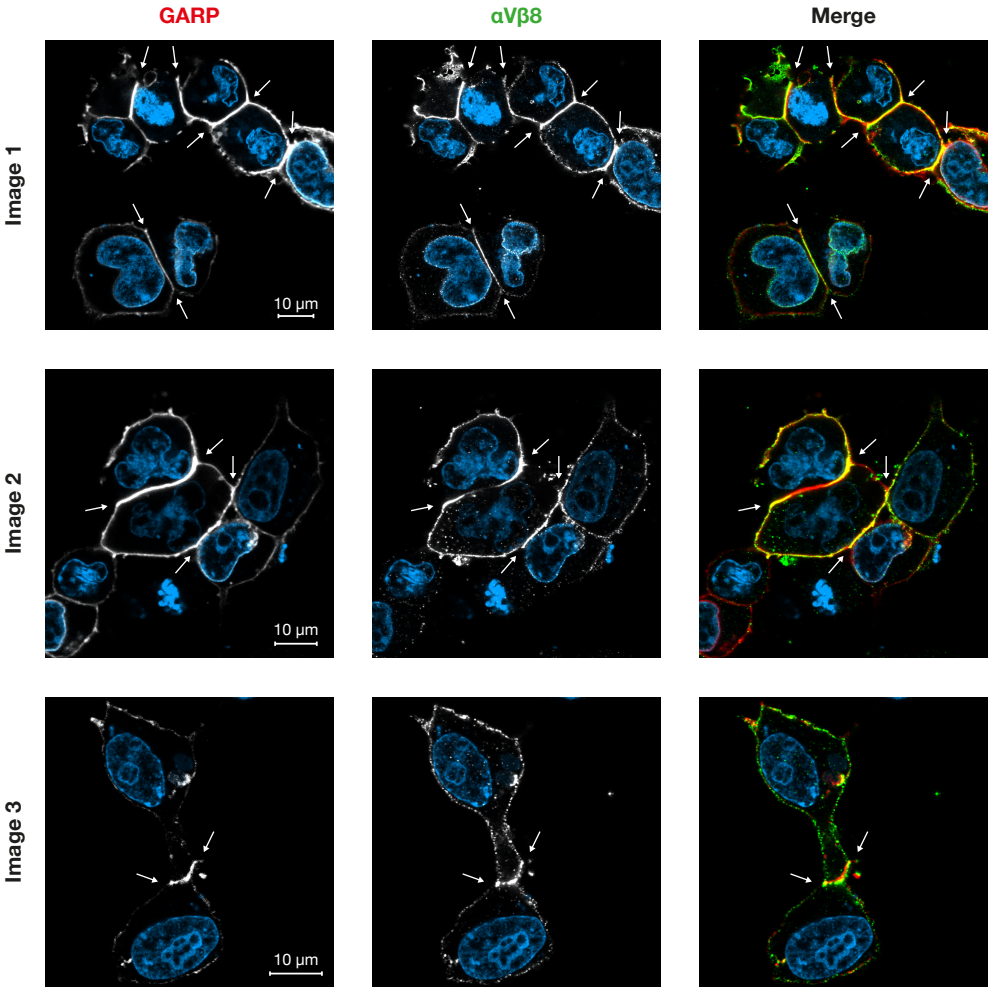

Figure 25: Immunofluorescence staining shows enrichment of GARP and αVβ8 at cell-cell interfaces.
The figure presents three images of fixed 293T cells transfected with GARP:TGF-β1 and αVβ8. Cells were stained with the following antibodies: anti-GARP (MHG6-AF647), blocking anti-αVβ8 (ADWA16) followed by anti-mouse IgG1-AF488, and Hoechst. Images are shown as single channels (including Hoechst) or merged. Arrows indicate cell–cell interfaces where signal enrichment is observed. In the merged images, GARP is shown in red, αVβ8 in green, and overlapping signals appear in yellow. Scale bars (10 μm) are indicated in the first column.

6 Conclusion and physiological relevance

Our findings support a model in which αVβ8-mediated TGF-β1 activation remains fundamentally force-dependent, despite the absence of direct engagement of the cytoskeleton through the β8 IC tail. Rather than relying on classical inside-out activation and direct cytoskeletal coupling through the integrin IC tail, αVβ8 appears able to exploit global cellular mechanics, such as membrane dynamics and cell motility, to generate the forces required to disrupt the latent TGF-β1 complex. This mechanism is consistent with the physiological environment of immune regulation, where Tregs and other immune cells constantly migrate and interact within mechanically dynamic tissues such as lymph nodes or inflamed sites. In such contexts, force generation at cell-cell interfaces may favor *trans*-activation of latent TGF-β1 complexes presented on neighboring cells. A force-dependent yet IC tail-independent mechanism could therefore provide a means to spatially restrict TGF-β1 activation, ensuring that cytokine release occurs only at sites of cellular interaction while preventing inappropriate systemic activation. Although our interest was initially motivated by mechanisms operating in Tregs, similar principles may apply to other αVβ8-expressing cells – such as astrocytes in the central nervous system or certain epithelial populations – where local mechanical cues may contribute to the regulation of TGF-β1 bioavailability. More broadly, these observations highlight the importance of mechanical forces and cellular dynamics as regulators of cytokine activation.

From a therapeutic perspective, it reinforces the idea that αVβ8 represents a privileged target for locally modulating TGF-β1 activity while potentially avoiding the systemic toxicity associated with pan-TGF-β inhibition. In cancer, inhibition of αVβ8-dependent TGF-β activation may reduce local immunosuppression mediated by Tregs or tumor cells and thereby improve antitumor immunity, promote immune infiltration, and synergize with immune checkpoint blockade or other immunomodulatory approaches (*121, 225*). More broadly, the force-dependent nature of αVβ8-mediated activation suggests that future therapeutic strategies could aim not only to block ligand binding, but also to interfere with the mechanical step that converts latent TGF-β1 into its active form. In other words, understanding how αVβ8 couples cellular mechanics to latent TGF-β1 activation may help guide the development of more selective therapies targeting the TGF-β pathway.

REFERENCES

REFERENCES

1. J. Massague, D. Sheppard, TGF-beta signaling in health and disease. *Cell* **186**, 4007–4037 (2023).
2. L. Z. Mi *et al.*, Structure of bone morphogenetic protein 9 procomplex. *Proc Natl Acad Sci U S A* **112**, 3710–3715 (2015).
3. G. Sengle, R. N. Ono, T. Sasaki, L. Y. Sakai, Prodomains of transforming growth factor beta (TGFbeta) superfamily members specify different functions: extracellular matrix interactions and growth factor bioavailability. *J Biol Chem* **286**, 5087–5099 (2011).
4. K. Nolan, T. B. Thompson, The DAN family: modulators of TGF-beta signaling and beyond. *Protein Sci* **23**, 999–1012 (2014).
5. C. J. David, J. Massague, Contextual determinants of TGFbeta action in development, immunity and cancer. *Nat Rev Mol Cell Biol* **19**, 419–435 (2018).
6. D. Danielpour, Advances and Challenges in Targeting TGF-β Isoforms for Therapeutic Intervention of Cancer: A Mechanism-Based Perspective. *Pharmaceuticals (Basel)* **17**, (2024).
7. A. P. Hinck, Structural studies of the TGF-βs and their receptors - insights into evolution of the TGF-β superfamily. *FEBS Lett* **586**, 1860–1870 (2012).
8. T. Sun *et al.*, TGFbeta2 and TGFbeta3 isoforms drive fibrotic disease pathogenesis. *Sci Transl Med* **13**, (2021).
9. K. C. Flanders *et al.*, Quantitation of TGF-β proteins in mouse tissues shows reciprocal changes in TGF-β1 and TGF-β3 in normal vs neoplastic mammary epithelium. *Oncotarget* **7**, 38164–38179 (2016).
10. A. B. Kulkarni, S. Karlsson, Transforming growth factor-beta 1 knockout mice. A mutation in one cytokine gene causes a dramatic inflammatory disease. *Am J Pathol* **143**, 3–9 (1993).
11. M. M. Shull *et al.*, Targeted disruption of the mouse transforming growth factor-beta 1 gene results in multifocal inflammatory disease. *Nature* **359**, 693–699 (1992).
12. J. Massague, TGF-beta signal transduction. *Annu Rev Biochem* **67**, 753–791 (1998).
13. Y. Shi, J. Massague, Mechanisms of TGF-beta signaling from cell membrane to the nucleus. *Cell* **113**, 685–700 (2003).
14. R. Derynck *et al.*, Human transforming growth factor-beta complementary DNA sequence and expression in normal and transformed cells. *Nature* **316**, 701–705 (1985).
15. C. M. Dubois *et al.*, Evidence that furin is an authentic transforming growth factor-beta1-converting enzyme. *Am J Pathol* **158**, 305–316 (2001).
16. L. E. Gentry, M. N. Lioubin, A. F. Purchio, H. Marquardt, Molecular events in the processing of recombinant type 1 pre-pro-transforming growth factor beta to the mature polypeptide. *Mol Cell Biol* **8**, 4162–4168 (1988).
17. A. Kelly, S. A. Houston, E. Sherwood, J. Casulli, M. A. Travis, Regulation of Innate and Adaptive Immunity by TGFbeta. *Adv Immunol* **134**, 137–233 (2017).
18. J. Munger *et al.*, The Integrin avb6 Binds and Activates Latent TGFb1: A Mechanism for Regulating Pulmonary Inflammation and Fibrosis. *Cell* **96**, 319–328 (1999).
19. M. Shi *et al.*, Latent TGF-beta structure and activation. *Nature* **474**, 343–349 (2011).
20. E. Gauthy *et al.*, GARP is regulated by miRNAs and controls latent TGF-beta1 production by human regulatory T cells. *PLoS One* **8**, e76186 (2013).
21. I. B. Robertson, D. B. Rifkin, Regulation of the Bioavailability of TGF-beta and TGF-beta-Related Proteins. *Cold Spring Harb Perspect Biol* **8**, (2016).
22. J. Stockis, O. Dedobbeleer, S. Lucas, Role of GARP in the activation of latent TGF-beta1. *Mol Biosyst* **13**, 1925–1935 (2017).
23. D. B. Rifkin, W. J. Rifkin, L. Zilberberg, LTBPs in biology and medicine: LTBP diseases. *Matrix Biol* **71-72**, 90–99 (2018).

24. V. Ollendorff, T. Noguchi, O. deLapeyriere, D. Birnbaum, The GARP Gene Encodes a New Member of the Family of Lucin-rich Repeat-containing Proteins. *Cell growth & differentiation : the molecular biology journal of the American Association for Cancer Research* **5**, 213–219 (1994).
25. R. Wang *et al.*, GARP regulates the bioavailability and activation of TGFbeta. *Mol Biol Cell* **23**, 1129–1139 (2012).
26. M. Probst-Kepper *et al.*, GARP: a key receptor controlling FOXP3 in human regulatory T cells. *J Cell Mol Med* **13**, 3343–3357 (2009).
27. J. Stockis, D. Colau, P. G. Coulie, S. Lucas, Membrane protein GARP is a receptor for latent TGF-beta on the surface of activated human Treg. *Eur J Immunol* **39**, 3315–3322 (2009).
28. R. Wang, Q. Wan, L. Kozhaya, H. Fujii, D. Unutmaz, Identification of a regulatory T cell specific cell surface molecule that mediates suppressive signals and induces Foxp3 expression. *PLoS One* **3**, e2705 (2008).
29. O. Dedobbeleer, J. Stockis, B. van der Woning, P. G. Coulie, S. Lucas, Cutting Edge: Active TGF-beta1 Released from GARP/TGF-beta1 Complexes on the Surface of Stimulated Human B Lymphocytes Increases Class-Switch Recombination and Production of IgA. *J Immunol* **199**, 391–396 (2017).
30. D. Q. Tran *et al.*, GARP (LRRC32) is essential for the surface expression of latent TGF-beta on platelets and activated FOXP3+ regulatory T cells. *Proc Natl Acad Sci U S A* **106**, 13445–13450 (2009).
31. E. Vermeersch *et al.*, The role of platelet and endothelial GARP in thrombosis and hemostasis. *PLoS One* **12**, e0173329 (2017).
32. G. de Streel *et al.*, Selective inhibition of TGF-beta1 produced by GARP-expressing Tregs overcomes resistance to PD-1/PD-L1 blockade in cancer. *Nat Commun* **11**, 4545 (2020).
33. R. Barbet, I. Peiffer, A. Hatzfeld, P. Charbord, J. A. Hatzfeld, Comparison of Gene Expression in Human Embryonic Stem Cells, hESC-Derived Mesenchymal Stem Cells and Human Mesenchymal Stem Cells. *Stem Cells Int* **2011**, 368192 (2011).
34. A. B. Carrillo-Galvez *et al.*, Mesenchymal stromal cells express GARP/LRRC32 on their surface: effects on their biology and immunomodulatory capacity. *Stem Cells* **33**, 183–195 (2015).
35. Y. Li *et al.*, Hepatic Stellate Cells Inhibit T Cells through Active TGF-beta1 from a Cell Surface-Bound Latent TGF-beta1/GARP Complex. *J Immunol* **195**, 2648–2656 (2015).
36. K. Slattery *et al.*, TGFbeta drives NK cell metabolic dysfunction in human metastatic breast cancer. *J Immunother Cancer* **9**, (2021).
37. W. Ma, Y. Qin, B. Chapuy, C. Lu, LRRC33 is a novel binding and potential regulating protein of TGF-beta1 function in human acute myeloid leukemia cells. *PLoS One* **14**, e0213482 (2019).
38. Y. Qin *et al.*, A Milieu Molecule for TGF-beta Required for Microglia Function in the Nervous System. *Cell* **174**, 156–171 e116 (2018).
39. K. Wong *et al.*, Mice deficient in NRROS show abnormal microglial development and neurological disorders. *Nat Immunol* **18**, 633–641 (2017).
40. Z. Duan *et al.*, Specificity of TGF-beta1 signal designated by LRRC33 and integrin alpha(V)beta(8). *Nat Commun* **13**, 4988 (2022).
41. A. Jiang, Y. Qin, T. A. Springer, Loss of LRRC33-Dependent TGFbeta1 Activation Enhances Antitumor Immunity and Checkpoint Blockade Therapy. *Cancer Immunol Res* **10**, 453–467 (2022).

42. T. Oida, H. L. Weiner, Overexpression of TGF-ß 1 gene induces cell surface localized glucose-regulated protein 78-associated latency-associated peptide/TGF-ß. *J Immunol* **185**, 3529–3535 (2010).
43. J. Trink *et al.*, Integrin beta1/Cell Surface GRP78 Complex Regulates TGFbeta1 and Its Profibrotic Effects in Response to High Glucose. *Biomedicines* **10**, (2022).
44. E. J. Goebel, K. N. Hart, J. C. McCoy, T. B. Thompson, Structural biology of the TGFbeta family. *Exp Biol Med (Maywood)* **244**, 1530–1546 (2019).
45. A. P. Hinck, T. D. Mueller, T. A. Springer, Structural Biology and Evolution of the TGF-beta Family. *Cold Spring Harb Perspect Biol* **8**, (2016).
46. U. A. Vitt, S. Y. Hsu, A. J. Hsueh, Evolution and classification of cystine knot-containing hormones and related extracellular signaling molecules. *Mol Endocrinol* **15**, 681–694 (2001).
47. S. Radaev *et al.*, Ternary complex of transforming growth factor-beta1 reveals isoform-specific ligand recognition and receptor recruitment in the superfamily. *J Biol Chem* **285**, 14806–14814 (2010).
48. F. Lambert, TGF-β1 activating antibodies for the immunotherapy of allo- and auto-immune diseases, PhD Thesis, Catholic University of Louvain, (2023).
49. M. G. Campbell *et al.*, Cryo-EM Reveals Integrin-Mediated TGF-beta Activation without Release from Latent TGF-beta. *Cell* **180**, 490–501 e416 (2020).
50. X. Dong *et al.*, Force interacts with macromolecular structure in activation of TGF-beta. *Nature* **542**, 55–59 (2017).
51. F. Lambert *et al.*, Antibody-mediated TGF-beta1 activation for the treatment of diseases caused by deleterious T cell activity. *Cell Rep* **44**, 116061 (2025).
52. S. Lienart *et al.*, Structural basis of latent TGF-beta1 presentation and activation by GARP on human regulatory T cells. *Science* **362**, 952–956 (2018).
53. K. Janssens *et al.*, Camurati-Engelmann disease: review of the clinical, radiological, and molecular data of 24 families and implications for diagnosis and treatment. *J Med Genet* **43**, 1–11 (2006).
54. S. Lienart, Blocking immunosuppression by human Tregs with antibodies against GArP/latent TGF-β1 complexes, PhD Thesis, Catholic University of Louvain, (2018).
55. M. Jin *et al.*, Latent-TGF-beta has a domain swapped architecture. *Nat Commun* **16**, 10469 (2025).
56. I. B. Robertson *et al.*, Latent TGF-beta-binding proteins. *Matrix Biol* **47**, 44–53 (2015).
57. J. Lack *et al.*, Solution structure of the third TB domain from LTBP1 provides insight into assembly of the large latent complex that sequesters latent TGF-beta. *J Mol Biol* **334**, 281–291 (2003).
58. D. Rifkin *et al.*, The role of LTBPs in TGF beta signaling. *Dev Dyn* **251**, 95–104 (2022).
59. M. Singh, M. Becker, A. R. F. Godwin, C. Baldock, Structural studies of elastic fibre and microfibrillar proteins. *Matrix Biol Plus* **12**, 100078 (2021).
60. J. P. Annes, Y. Chen, J. S. Munger, D. B. Rifkin, Integrin alphaVbeta6-mediated activation of latent TGF-beta requires the latent TGF-beta binding protein-1. *J Cell Biol* **165**, 723–734 (2004).
61. Q. Chen *et al.*, Potential role for heparan sulfate proteoglycans in regulation of transforming growth factor-beta (TGF-beta) by modulating assembly of latent TGF-beta-binding protein-1. *J Biol Chem* **282**, 26418–26430 (2007).
62. B. Kobe, A. V. Kajava, The leucine-rich repeat as a protein recognition motif. *Curr Opin Struct Biol* **11**, 725–732 (2001).

63. R. M. Lyons, L. E. Gentry, A. F. Purchio, H. L. Moses, Mechanism of activation of latent recombinant transforming growth factor beta 1 by plasmin. *J Cell Biol* **110**, 1361–1367 (1990).
64. F. J. Castellino, V. A. Ploplis, Structure and function of the plasminogen/plasmin system. *Thromb Haemost* **93**, 647–654 (2005).
65. J. J. Perona, C. S. Craik, Structural basis of substrate specificity in the serine proteases. *Protein Sci* **4**, 337–360 (1995).
66. T. H. Bugge, M. J. Flick, C. C. Daugherty, J. L. Degen, Plasminogen deficiency causes severe thrombosis but is compatible with development and reproduction. *Genes Dev* **9**, 794–807 (1995).
67. J. P. Annes, J. S. Munger, D. B. Rifkin, Making sense of latent TGFbeta activation. *J Cell Sci* **116**, 217–224 (2003).
68. A. Page-McCaw, A. J. Ewald, Z. Werb, Matrix metalloproteinases and the regulation of tissue remodelling. *Nat Rev Mol Cell Biol* **8**, 221–233 (2007).
69. Q. Yu, I. Stamenkovic, Cell surface-localized matrix metalloproteinase-9 proteolytically activates TGF-beta and promotes tumor invasion and angiogenesis. *Genes Dev* **14**, 163–176 (2000).
70. P. Garg *et al.*, Matrix metalloproteinase-9-mediated tissue injury overrides the protective effect of matrix metalloproteinase-2 during colitis. *Am J Physiol Gastrointest Liver Physiol* **296**, G175–184 (2009).
71. S. K. Kojima, Wakako; Domma, Nao, Antibody recognizing cut surface of TGF-β activation control region, WO2005023870A1, WO (World Intellectual Property Organization),
72. N. D. Rawlings, A. J. Barrett, A. Bateman, MEROPS: the database of proteolytic enzymes, their substrates and inhibitors. *Nucleic Acids Res* **40**, D343–350 (2012).
73. K. Holmbeck *et al.*, MT1-MMP-deficient mice develop dwarfism, osteopenia, arthritis, and connective tissue disease due to inadequate collagen turnover. *Cell* **99**, 81–92 (1999).
74. J. Oh *et al.*, Mutations in two matrix metalloproteinase genes, MMP-2 and MT1-MMP, are synthetic lethal in mice. *Oncogene* **23**, 5041–5048 (2004).
75. K. Miyazono, C. H. Heldin, Role for carbohydrate structures in TGF-beta 1 latency. *Nature* **338**, 158–160 (1989).
76. S. Schultz-Cherry, V. S. Hinshaw, Influenza virus neuraminidase activates latent transforming growth factor beta. *J Virol* **70**, 8624–8629 (1996).
77. T. R. Karhadkar, T. D. Meek, R. H. Gomer, Inhibiting Sialidase-Induced TGF-beta1 Activation Attenuates Pulmonary Fibrosis in Mice. *J Pharmacol Exp Ther* **376**, 106–117 (2021).
78. M. H. Barcellos-Hoff, T. A. Dix, Redox-mediated activation of latent transforming growth factor-beta 1. *Mol Endocrinol* **10**, 1077–1083 (1996).
79. M. H. Barcellos-Hoff, R. Derynck, M. L. Tsang, J. A. Weatherbee, Transforming growth factor-beta activation in irradiated murine mammary gland. *J Clin Invest* **93**, 892–899 (1994).
80. M. F. Jobling *et al.*, Isoform-specific activation of latent transforming growth factor beta (LTGF-beta) by reactive oxygen species. *Radiat Res* **166**, 839–848 (2006).
81. L. Hecker *et al.*, NADPH oxidase-4 mediates myofibroblast activation and fibrogenic responses to lung injury. *Nat Med* **15**, 1077–1081 (2009).
82. R. A. Louzada *et al.*, NADPH oxidase DUOX1 sustains TGF-beta1 signalling and promotes lung fibrosis. *Eur Respir J* **57**, 1901949 (2021).
83. S. Schultz-Cherry, J. E. Murphy-Ullrich, Thrombospondin causes activation of latent transforming growth factor-beta secreted by endothelial cells by a novel mechanism. *J Cell Biol* **122**, 923–932 (1993).

84. J. E. Murphy-Ullrich, M. Poczatek, Activation of latent TGF-beta by thrombospondin-1: mechanisms and physiology. *Cytokine Growth Factor Rev* **11**, 59–69 (2000).
85. S. M. Ribeiro, M. Poczatek, S. Schultz-Cherry, M. Villain, J. E. Murphy-Ullrich, The activation sequence of thrombospondin-1 interacts with the latency-associated peptide to regulate activation of latent transforming growth factor-beta. *J Biol Chem* **274**, 13586–13593 (1999).
86. S. Schultz-Cherry *et al.*, Regulation of transforming growth factor-beta activation by discrete sequences of thrombospondin 1. *J Biol Chem* **270**, 7304–7310 (1995).
87. S. Schultz-Cherry, J. Lawler, J. E. Murphy-Ullrich, The type 1 repeats of thrombospondin 1 activate latent transforming growth factor-beta. *J Biol Chem* **269**, 26783–26788 (1994).
88. G. D. Young, J. E. Murphy-Ullrich, The tryptophan-rich motifs of the thrombospondin type 1 repeats bind VLAL motifs in the latent transforming growth factor-beta complex. *J Biol Chem* **279**, 47633–47642 (2004).
89. S. E. Crawford *et al.*, Thrombospondin-1 is a major activator of TGF-beta1 in vivo. *Cell* **93**, 1159–1170 (1998).
90. W. A. Frazier, Thrombospondins. *Curr Opin Cell Biol* **3**, 792–799 (1991).
91. W. A. Border, E. Ruoslahti, Transforming growth factor-beta in disease: the dark side of tissue repair. *J Clin Invest* **90**, 1–7 (1992).
92. M. L. Iruela-Arispe, D. J. Liska, E. H. Sage, P. Bornstein, Differential expression of thrombospondin 1, 2, and 3 during murine development. *Dev Dyn* **197**, 40–56 (1993).
93. R. A. Majack, Beta-type transforming growth factor specifies organizational behavior in vascular smooth muscle cell cultures. *J Cell Biol* **105**, 465–471 (1987).
94. X. Dong, N. E. Hudson, C. Lu, T. A. Springer, Structural determinants of integrin beta-subunit specificity for latent TGF-beta. *Nat Struct Mol Biol* **21**, 1091–1096 (2014).
95. J. J. Worthington, J. E. Klementowicz, M. A. Travis, TGFβ: a sleeping giant awoken by integrins. *Trends Biochem Sci* **36**, 47–54 (2011).
96. I. D. Campbell, M. J. Humphries, Integrin structure, activation, and interactions. *Cold Spring Harb Perspect Biol* **3**, (2011).
97. T. A. Springer, M. L. Dustin, Integrin inside-out signaling and the immunological synapse. *Curr Opin Cell Biol* **24**, 107–115 (2012).
98. K. L. Wegener, I. D. Campbell, Transmembrane and cytoplasmic domains in integrin activation and protein-protein interactions (review). *Mol Membr Biol* **25**, 376–387 (2008).
99. M. Barczyk, S. Carracedo, D. Gullberg, Integrins. *Cell Tissue Res* **339**, 269–280 (2010).
100. R. O. Hynes, Integrins: bidirectional, allosteric signaling machines. *Cell* **110**, 673–687 (2002).
101. J. Takagi, B. M. Petre, T. Walz, T. A. Springer, Global conformational rearrangements in integrin extracellular domains in outside-in and inside-out signaling. *Cell* **110**, 599–511 (2002).
102. J. P. Xiong *et al.*, Crystal structure of the complete integrin alphaVbeta3 ectodomain plus an alpha/beta transmembrane fragment. *J Cell Biol* **186**, 589–600 (2009).
103. J. P. Xiong *et al.*, Crystal structure of the extracellular segment of integrin alpha Vbeta3. *Science* **294**, 339–345 (2001).
104. J. Zhu *et al.*, Structure of a complete integrin ectodomain in a physiologic resting state and activation and deactivation by applied forces. *Mol Cell* **32**, 849–861 (2008).
105. D. A. Calderwood, I. D. Campbell, D. R. Critchley, Talins and kindlins: partners in integrin-mediated adhesion. *Nat Rev Mol Cell Biol* **14**, 503–517 (2013).

106. S. Liu *et al.*, Binding of paxillin to alpha4 integrins modifies integrin-dependent biological responses. *Nature* **402**, 676–681 (1999).
107. B. A. Young *et al.*, The cytoplasmic domain of the integrin alpha9 subunit requires the adaptor protein paxillin to inhibit cell spreading but promotes cell migration in a paxillin-independent manner. *Mol Biol Cell* **12**, 3214–3225 (2001).
108. J. Zhu, J. Zhu, T. A. Springer, Complete integrin headpiece opening in eight steps. *J Cell Biol* **201**, 1053–1068 (2013).
109. N. J. Anthis *et al.*, The structure of an integrin/talin complex reveals the basis of inside-out signal transduction. *EMBO J* **28**, 3623–3632 (2009).
110. M. A. Travis, D. Sheppard, TGF-beta activation and function in immunity. *Annu Rev Immunol* **32**, 51–82 (2014).
111. Z. Yang *et al.*, Absence of integrin-mediated TGFbeta1 activation in vivo recapitulates the phenotype of TGFbeta1-null mice. *J Cell Biol* **176**, 787–793 (2007).
112. N. I. Reed *et al.*, The alphavbeta1 integrin plays a critical in vivo role in tissue fibrosis. *Sci Transl Med* **7**, 288ra279 (2015).
113. P. J. Wipff, D. B. Rifkin, J. J. Meister, B. Hinz, Myofibroblast contraction activates latent TGF-beta1 from the extracellular matrix. *J Cell Biol* **179**, 1311–1323 (2007).
114. X. Z. Huang *et al.*, Inactivation of the integrin beta 6 subunit gene reveals a role of epithelial integrins in regulating inflammation in the lung and skin. *J Cell Biol* **133**, 921–928 (1996).
115. J. Mohammed *et al.*, Stromal cells control the epithelial residence of DCs and memory T cells by regulated activation of TGF-beta. *Nat Immunol* **17**, 414–421 (2016).
116. D. Mu *et al.*, The integrin alpha(v)beta8 mediates epithelial homeostasis through MT1-MMP-dependent activation of TGF-beta1. *J Cell Biol* **157**, 493–507 (2002).
117. H. Kitamura *et al.*, Mouse and human lung fibroblasts regulate dendritic cell trafficking, airway inflammation, and fibrosis through integrin alphavbeta8-mediated activation of TGF-beta. *J Clin Invest* **121**, 2863–2875 (2011).
118. A. C. Melton *et al.*, Expression of alphavbeta8 integrin on dendritic cells regulates Th17 cell development and experimental autoimmune encephalomyelitis in mice. *J Clin Invest* **120**, 4436–4444 (2010).
119. J. J. Worthington, B. I. Czajkowska, A. C. Melton, M. A. Travis, Intestinal dendritic cells specialize to activate transforming growth factor-beta and induce Foxp3+ regulatory T cells via integrin alphavbeta8. *Gastroenterology* **141**, 1802–1812 (2011).
120. A. Kelly *et al.*, Human monocytes and macrophages regulate immune tolerance via integrin alphavbeta8-mediated TGFbeta activation. *J Exp Med* **215**, 2725–2736 (2018).
121. J. Stockis *et al.*, Blocking immunosuppression by human Tregs in vivo with antibodies targeting integrin alphaVbeta8. *Proc Natl Acad Sci U S A* **114**, E10161–E10168 (2017).
122. J. J. Worthington *et al.*, Integrin alphavbeta8-Mediated TGF-beta Activation by Effector Regulatory T Cells Is Essential for Suppression of T-Cell-Mediated Inflammation. *Immunity* **42**, 903–915 (2015).
123. J. Zhu *et al.*, beta8 integrins are required for vascular morphogenesis in mouse embryos. *Development* **129**, 2891–2903 (2002).
124. J. M. Proctor, K. Zang, D. Wang, R. Wang, L. F. Reichardt, Vascular development of the brain requires beta8 integrin expression in the neuroepithelium. *J Neurosci* **25**, 9940–9948 (2005).
125. S. Minagawa *et al.*, Selective targeting of TGF-β activation to treat fibroinflammatory airway disease. *Sci Transl Med* **6**, 241ra279 (2014).

126. M. A. Travis *et al.*, Loss of integrin alpha(v)beta8 on dendritic cells causes autoimmunity and colitis in mice. *Nature* **449**, 361–365 (2007).
127. J. J. Worthington *et al.*, Loss of the TGFbeta-activating integrin alphavbeta8 on dendritic cells protects mice from chronic intestinal parasitic infection via control of type 2 immunity. *PLoS Pathog* **9**, e1003675 (2013).
128. J. P. Edwards, A. M. Thornton, E. M. Shevach, Release of active TGF-beta1 from the latent TGF-beta1/GARP complex on T regulatory cells is mediated by integrin beta8. *J Immunol* **193**, 2843–2849 (2014).
129. A. L. Jannuzi, T. A. Bunch, R. F. West, D. L. Brower, Identification of integrin beta subunit mutations that alter heterodimer function in situ. *Mol Biol Cell* **15**, 3829–3840 (2004).
130. J. H. McCarty, A. A. Cook, R. O. Hynes, An interaction between alphavbeta8 integrin and Band 4.1B via a highly conserved region of the Band 4.1 C-terminal domain. *Proc Natl Acad Sci U S A* **102**, 13479–13483 (2005).
131. M. Moyle, M. A. Napier, J. W. McLean, Cloning and expression of a divergent integrin subunit beta 8. *J Biol Chem* **266**, 19650–19658 (1991).
132. M. Cheerathodi *et al.*, The Cytoskeletal Adapter Protein Spinophilin Regulates Invadopodia Dynamics and Tumor Cell Invasion in Glioblastoma. *Mol Cancer Res* **14**, 1277–1287 (2016).
133. J. Wang *et al.*, Atypical interactions of integrin alpha(V)beta(8) with pro-TGF-beta1. *Proc Natl Acad Sci U S A* **114**, E4168–E4174 (2017).
134. A. Cormier *et al.*, Cryo-EM structure of the alphavbeta8 integrin reveals a mechanism for stabilizing integrin extension. *Nat Struct Mol Biol* **25**, 698–704 (2018).
135. J. Wang, Y. Su, R. E. Iacob, J. R. Engen, T. A. Springer, General structural features that regulate integrin affinity revealed by atypical alphaVbeta8. *Nat Commun* **10**, 5481 (2019).
136. M. Jin *et al.*, Dynamic allostery drives autocrine and paracrine TGF-beta signaling. *Cell* **187**, 6200–6219 e6223 (2024).
137. R. G. Jenkins *et al.*, Ligation of protease-activated receptor 1 enhances alpha(v)beta6 integrin-dependent TGF-beta activation and promotes acute lung injury. *J Clin Invest* **116**, 1606–1614 (2006).
138. S. Sakaguchi, T. Yamaguchi, T. Nomura, M. Ono, Regulatory T cells and immune tolerance. *Cell* **133**, 775–787 (2008).
139. J. Cuende *et al.*, Monoclonal antibodies against GARP/TGF-beta1 complexes inhibit the immunosuppressive activity of human regulatory T cells in vivo. *Sci Transl Med* **7**, 284ra256 (2015).
140. G. de Streel, S. Lucas, Targeting immunosuppression by TGF-beta1 for cancer immunotherapy. *Biochem Pharmacol* **192**, 114697 (2021).
141. V. H. Villar *et al.*, Transforming Growth Factor-beta1 in Cancer Immunology: Opportunities for Immunotherapy. *Adv Exp Med Biol* **1408**, 309–328 (2023).
142. N. Csoma, Analysis of the expression pattern of the LRRC33 protein and its role in TGF-β1 activation, Master Thesis, Catholic University of Louvain, (2017).
143. A. Reboldi *et al.*, IgA production requires B cell interaction with subepithelial dendritic cells in Peyer's patches. *Science* **352**, aaf4822 (2016).
144. J. Niu, W. Yue, Z. Le-Le, L. Bin, X. Hu, Mesenchymal stem cells inhibit T cell activation by releasing TGF-beta1 from TGF-beta1/GARP complex. *Oncotarget* **8**, 99784–99800 (2017).
145. R. K. Assoian, A. Komoriya, C. A. Meyers, D. M. Miller, M. B. Sporn, Transforming growth factor-beta in human platelets. Identification of a major storage site, purification, and characterization. *J Biol Chem* **258**, 7155–7160 (1983).

146. K. Miyazono, U. Hellman, C. Wernstedt, C. H. Heldin, Latent high molecular weight complex of transforming growth factor beta 1. Purification from human platelets and structural characterization. *J Biol Chem* **263**, 6407–6415 (1988).
147. S. Lecomte *et al.*, Therapeutic activity of GARP:TGF-beta1 blockade in murine primary myelofibrosis. *Blood* **141**, 490–502 (2023).
148. S. Rachidi *et al.*, Platelets subvert T cell immunity against cancer via GARP-TGFbeta axis. *Sci Immunol* **2**, (2017).
149. J. E. Murphy-Ullrich, S. Schultz-Cherry, M. Hook, Transforming growth factor-beta complexes with thrombospondin. *Mol Biol Cell* **3**, 181–188 (1992).
150. M. Abdelouahed, A. Ludlow, G. Brunner, J. Lawler, Activation of platelet-transforming growth factor beta-1 in the absence of thrombospondin-1. *J Biol Chem* **275**, 17933–17936 (2000).
151. R. Blakytny *et al.*, Latent TGF-beta1 activation by platelets. *J Cell Physiol* **199**, 67–76 (2004).
152. A. Metelli *et al.*, Thrombin contributes to cancer immune evasion via proteolysis of platelet-bound GARP to activate LTGF-beta. *Sci Transl Med* **12**, (2020).
153. J. Ahamed *et al.*, In vitro and in vivo evidence for shear-induced activation of latent transforming growth factor-beta1. *Blood* **112**, 3650–3660 (2008).
154. X. Zhang *et al.*, GARP on hepatic stellate cells is essential for the development of liver fibrosis. *J Hepatol* **79**, 1214–1225 (2023).
155. F. Klingberg *et al.*, Prestress in the extracellular matrix sensitizes latent TGF-beta1 for activation. *J Cell Biol* **207**, 283–297 (2014).
156. J. C. Leemans *et al.*, The role of Toll-like receptor 2 in inflammation and fibrosis during progressive renal injury. *PLoS One* **4**, e5704 (2009).
157. J. Taipale, K. Miyazono, C. H. Heldin, J. Keski-Oja, Latent transforming growth factor-beta 1 associates to fibroblast extracellular matrix via latent TGF-beta binding protein. *J Cell Biol* **124**, 171–181 (1994).
158. L. Rouaud *et al.*, Spatial Distribution of Non-Immune Cells Expressing Glycoprotein A Repetitions Predominant in Human and Murine Metastatic Lymph Nodes. *Cancers (Basel)* **15**, 5621 (2023).
159. C. Dayer, I. Stamenkovic, Recruitment of Matrix Metalloproteinase-9 (MMP-9) to the Fibroblast Cell Surface by Lysyl Hydroxylase 3 (LH3) Triggers Transforming Growth Factor-beta (TGF-beta) Activation and Fibroblast Differentiation. *J Biol Chem* **290**, 13763–13778 (2015).
160. M. J. Goumans, F. Lebrin, G. Valdimarsdottir, Controlling the angiogenic switch: a balance between two distinct TGF-b receptor signaling pathways. *Trends Cardiovasc Med* **13**, 301–307 (2003).
161. A. Carambia *et al.*, TGF-beta-dependent induction of CD4(+)CD25(+)Foxp3(+) Tregs by liver sinusoidal endothelial cells. *J Hepatol* **61**, 594–599 (2014).
162. P. Carmeliet, R. K. Jain, Molecular mechanisms and clinical applications of angiogenesis. *Nature* **473**, 298–307 (2011).
163. A. Antonelli-Orlidge, K. B. Saunders, S. R. Smith, P. A. D'Amore, An activated form of transforming growth factor beta is produced by cocultures of endothelial cells and pericytes. *Proc Natl Acad Sci U S A* **86**, 4544–4548 (1989).
164. R. A. Scott, E. W. Fowler, X. Jia, K. L. Kiick, R. E. Akins, Regulation of neovasculogenesis in co-cultures of aortic adventitial fibroblasts and microvascular endothelial cells by cell-cell interactions and TGF-beta/ALK5 signaling. *PLoS One* **15**, e0244243 (2020).
165. M. Sweeney, G. Foldes, It Takes Two: Endothelial-Perivascular Cell Cross-Talk in Vascular Development and Disease. *Front Cardiovasc Med* **5**, 154 (2018).

166. P. C. Brooks, R. A. Clark, D. A. Cheresh, Requirement of vascular integrin alpha v beta 3 for angiogenesis. *Science* **264**, 569–571 (1994).
167. V. Sarrazy *et al.*, Integrins alphavbeta5 and alphavbeta3 promote latent TGF-beta1 activation by human cardiac fibroblast contraction. *Cardiovasc Res* **102**, 407–417 (2014).
168. T. H. Chun *et al.*, MT1-MMP-dependent neovessel formation within the confines of the three-dimensional extracellular matrix. *J Cell Biol* **167**, 757–767 (2004).
169. O. Tatti, P. Vehvilainen, K. Lehti, J. Keski-Oja, MT1-MMP releases latent TGF-beta1 from endothelial cell extracellular matrix via proteolytic processing of LTBP-1. *Exp Cell Res* **314**, 2501–2514 (2008).
170. J. C. Marie, D. Liggitt, A. Y. Rudensky, Cellular mechanisms of fatal early-onset autoimmunity in mice with the T cell-specific targeting of transforming growth factor-beta receptor. *Immunity* **25**, 441–454 (2006).
171. N. Romani, B. E. Clausen, P. Stoitzner, Langerhans cells and more: langerin-expressing dendritic cell subsets in the skin. *Immunol Rev* **234**, 120–141 (2010).
172. F. Tian *et al.*, Vaccination with transforming growth factor-beta insensitive dendritic cells suppresses pulmonary metastases of renal carcinoma in mice. *Cancer Lett* **271**, 333–341 (2008).
173. J. J. Kobie *et al.*, Transforming growth factor beta inhibits the antigen-presenting functions and antitumor activity of dendritic cell vaccines. *Cancer Res* **63**, 1860–1864 (2003).
174. M. Ito *et al.*, Tumor-derived TGFbeta-1 induces dendritic cell apoptosis in the sentinel lymph node. *J Immunol* **176**, 5637–5643 (2006).
175. G. E. Esebanmen, W. H. R. Langridge, The role of TGF-beta signaling in dendritic cell tolerance. *Immunol Res* **65**, 987–994 (2017).
176. S. Sanjabi, S. A. Oh, M. O. Li, Regulation of the Immune Response by TGF-beta: From Conception to Autoimmunity and Infection. *Cold Spring Harb Perspect Biol* **9**, a022236 (2017).
177. A. Bobr *et al.*, Autocrine/paracrine TGF-beta1 inhibits Langerhans cell migration. *Proc Natl Acad Sci U S A* **109**, 10492–10497 (2012).
178. L. E. Smythies *et al.*, Mucosal IL-8 and TGF-beta recruit blood monocytes: evidence for cross-talk between the lamina propria stroma and myeloid cells. *J Leukoc Biol* **80**, 492–499 (2006).
179. R. Rani, A. G. Smulian, D. R. Greaves, S. P. Hogan, D. R. Herbert, TGF-beta limits IL-33 production and promotes the resolution of colitis through regulation of macrophage function. *Eur J Immunol* **41**, 2000–2009 (2011).
180. J. P. Marcoe *et al.*, TGF-beta is responsible for NK cell immaturity during ontogeny and increased susceptibility to infection during mouse infancy. *Nat Immunol* **13**, 843–850 (2012).
181. R. A. Flavell, S. Sanjabi, S. H. Wrzesinski, P. Licona-Limon, The polarization of immune cells in the tumour environment by TGFbeta. *Nat Rev Immunol* **10**, 554–567 (2010).
182. L. K. Mackay *et al.*, T-box Transcription Factors Combine with the Cytokines TGF-beta and IL-15 to Control Tissue-Resident Memory T Cell Fate. *Immunity* **43**, 1101–1111 (2015).
183. T. L. Stephen *et al.*, Transforming growth factor beta-mediated suppression of antitumor T cells requires FoxP1 transcription factor expression. *Immunity* **41**, 427–439 (2014).
184. D. A. Thomas, J. Massague, TGF-beta directly targets cytotoxic T cell functions during tumor evasion of immune surveillance. *Cancer Cell* **8**, 369–380 (2005).

185. B. V. Park *et al.*, TGFbeta1-Mediated SMAD3 Enhances PD-1 Expression on Antigen-Specific T Cells in Cancer. *Cancer Discov* **6**, 1366–1381 (2016).
186. L. Gorelik, P. E. Fields, R. A. Flavell, Cutting edge: TGF-beta inhibits Th type 2 development through inhibition of GATA-3 expression. *J Immunol* **165**, 4773–4777 (2000).
187. S. Sad, T. R. Mosmann, Single IL-2-secreting precursor CD4 T cell can develop into either Th1 or Th2 cytokine secretion phenotype. *J Immunol* **153**, 3514–3522 (1994).
188. L. Gorelik, R. A. Flavell, Abrogation of TGFbeta signaling in T cells leads to spontaneous T cell differentiation and autoimmune disease. *Immunity* **12**, 171–181 (2000).
189. T. Brabletz *et al.*, Transforming growth factor beta and cyclosporin A inhibit the inducible activity of the interleukin-2 gene in T cells through a noncanonical octamer-binding site. *Mol Cell Biol* **13**, 1155–1162 (1993).
190. Y. Liu *et al.*, A critical function for TGF-beta signaling in the development of natural CD4+CD25+Foxp3+ regulatory T cells. *Nat Immunol* **9**, 632–640 (2008).
191. Y. Tone *et al.*, Smad3 and NFAT cooperate to induce Foxp3 expression through its enhancer. *Nat Immunol* **9**, 194–202 (2008).
192. B. B. Cazac, J. Roes, TGF-beta receptor controls B cell responsiveness and induction of IgA in vivo. *Immunity* **13**, 443–451 (2000).
193. M. Gaignage *et al.*, Blocking GARP-mediated activation of TGF-beta1 did not alter innate or adaptive immune responses to bacterial infection or protein immunization in mice. *Cancer Immunol Immunother* **71**, 1851–1862 (2022).
194. N. Frangogiannis, Transforming growth factor-beta in tissue fibrosis. *J Exp Med* **217**, e20190103 (2020).
195. S. M. Kutz, J. Hordines, P. J. McKeown-Longo, P. J. Higgins, TGF-beta1-induced PAI-1 gene expression requires MEK activity and cell-to-substrate adhesion. *J Cell Sci* **114**, 3905–3914 (2001).
196. S. K. Leivonen *et al.*, TGF-beta-elicited induction of tissue inhibitor of metalloproteinases (TIMP)-3 expression in fibroblasts involves complex interplay between Smad3, p38alpha, and ERK1/2. *PLoS One* **8**, e57474 (2013).
197. B. Chandra Jena, S. Sarkar, L. Rout, M. Mandal, The transformation of cancer-associated fibroblasts: Current perspectives on the role of TGF-beta in CAF mediated tumor progression and therapeutic resistance. *Cancer Lett* **520**, 222–232 (2021).
198. J. H. W. Distler *et al.*, Shared and distinct mechanisms of fibrosis. *Nat Rev Rheumatol* **15**, 705–730 (2019).
199. M. Lodyga *et al.*, Cadherin-11-mediated adhesion of macrophages to myofibroblasts establishes a profibrotic niche of active TGF-beta. *Sci Signal* **12**, (2019).
200. A. E. Postlethwaite, J. Keski-Oja, H. L. Moses, A. H. Kang, Stimulation of the chemotactic migration of human fibroblasts by transforming growth factor beta. *J Exp Med* **165**, 251–256 (1987).
201. M. B. Buechler, W. Fu, S. J. Turley, Fibroblast-macrophage reciprocal interactions in health, fibrosis, and cancer. *Immunity* **54**, 903–915 (2021).
202. E. Sahai *et al.*, A framework for advancing our understanding of cancer-associated fibroblasts. *Nat Rev Cancer* **20**, 174–186 (2020).
203. J. Su *et al.*, TGF-beta orchestrates fibrogenic and developmental EMTs via the RAS effector RREB1. *Nature* **577**, 566–571 (2020).
204. J. Larsson *et al.*, Abnormal angiogenesis but intact hematopoietic potential in TGF-beta type I receptor-deficient mice. *EMBO J* **20**, 1663–1673 (2001).

205. S. P. Oh *et al.*, Activin receptor-like kinase 1 modulates transforming growth factor-beta 1 signaling in the regulation of angiogenesis. *Proc Natl Acad Sci U S A* **97**, 2626–2631 (2000).
206. M. Oshima, H. Oshima, M. M. Taketo, TGF-beta receptor type II deficiency results in defects of yolk sac hematopoiesis and vasculogenesis. *Dev Biol* **179**, 297–302 (1996).
207. L. D. Urness, L. K. Sorensen, D. Y. Li, Arteriovenous malformations in mice lacking activin receptor-like kinase-1. *Nat Genet* **26**, 328–331 (2000).
208. J. Ma, G. Sanchez-Duffhues, M. J. Goumans, P. Ten Dijke, TGF-beta-Induced Endothelial to Mesenchymal Transition in Disease and Tissue Engineering. *Front Cell Dev Biol* **8**, 260 (2020).
209. R. Lugano, M. Ramachandran, A. Dimberg, Tumor angiogenesis: causes, consequences, challenges and opportunities. *Cell Mol Life Sci* **77**, 1745–1770 (2020).
210. M. J. Goumans *et al.*, Balancing the activation state of the endothelium via two distinct TGF-beta type I receptors. *EMBO J* **21**, 1743–1753 (2002).
211. C. Bertrand *et al.*, Combined Blockade of GARP:TGF-beta1 and PD-1 Increases Infiltration of T Cells and Density of Pericyte-Covered GARP(+) Blood Vessels in Mouse MC38 Tumors. *Front Immunol* **12**, 704050 (2021).
212. E. Batlle, J. Massague, Transforming Growth Factor-beta Signaling in Immunity and Cancer. *Immunity* **50**, 924–940 (2019).
213. S. Mariathasan *et al.*, TGFbeta attenuates tumour response to PD-L1 blockade by contributing to exclusion of T cells. *Nature* **554**, 544–548 (2018).
214. D. V. F. Tauriello *et al.*, TGFbeta drives immune evasion in genetically reconstituted colon cancer metastasis. *Nature* **554**, 538–543 (2018).
215. D. V. F. Tauriello, E. Sancho, E. Batlle, Overcoming TGFbeta-mediated immune evasion in cancer. *Nat Rev Cancer* **22**, 25–44 (2022).
216. B. Chen, C. Mu, Z. Zhang, X. He, X. Liu, The Love-Hate Relationship Between TGF-beta Signaling and the Immune System During Development and Tumorigenesis. *Front Immunol* **13**, 891268 (2022).
217. M. M. Rodari, N. Cerf-Bensussan, M. Parlato, Dysregulation of the immune response in TGF-beta signalopathies. *Front Immunol* **13**, 1066375 (2022).
218. R. Derynck, S. J. Turley, R. J. Akhurst, TGFbeta biology in cancer progression and immunotherapy. *Nat Rev Clin Oncol* **18**, 9–34 (2021).
219. C. H. Ong, C. L. Tham, H. H. Harith, N. Firdaus, D. A. Israf, TGF-beta-induced fibrosis: A review on the underlying mechanism and potential therapeutic strategies. *Eur J Pharmacol* **911**, 174510 (2021).
220. J. Wang, H. Xiang, Y. Lu, T. Wu, Role and clinical significance of TGF-beta1 and TGF-betaR1 in malignant tumors (Review). *Int J Mol Med* **47**, (2021).
221. K. Nakamura *et al.*, TGF-beta 1 plays an important role in the mechanism of CD4+CD25+ regulatory T cell activity in both humans and mice. *J Immunol* **172**, 834–842 (2004).
222. K. Nakamura, A. Kitani, W. Strober, Cell contact-dependent immunosuppression by CD4(+)CD25(+) regulatory T cells is mediated by cell surface-bound transforming growth factor beta. *J Exp Med* **194**, 629–644 (2001).
223. L. M. Wakefield *et al.*, Recombinant latent transforming growth factor beta 1 has a longer plasma half-life in rats than active transforming growth factor beta 1, and a different tissue distribution. *J Clin Invest* **86**, 1976–1984 (1990).
224. A. De, J. E. Morales, Z. Chen, S. Sebastian, J. H. McCarty, The beta8 integrin cytoplasmic domain activates extracellular matrix adhesion to promote brain neurovascular development. *Development* **149**, (2022).

225. E. Dodagatta-Marri *et al.*, Integrin alphavbeta8 on T cells suppresses anti-tumor immunity in multiple models and is a promising target for tumor immunotherapy. *Cell Rep* **36**, 109309 (2021).
226. A. Lainé *et al.*, Regulatory T cells promote cancer immune-escape through integrin αvβ8-mediated TGF-β activation. *Nat Commun* **12**, 6228 (2021).
227. N. Huyghe, Identification de protéines impliquées dans l'activation du TGF-β1 par les Tregs humains, Master Thesis, Catholic University of Louvain, (2017).
228. J. Stockis *et al.*, Comparison of stable human Treg and Th clones by transcriptional profiling. *Eur J Immunol* **39**, 869–882 (2009).
229. R. Heusschen, A. W. Griffioen, V. L. Thijssen, Galectin-9 in tumor biology: a jack of multiple trades. *Biochim Biophys Acta* **1836**, 177–185 (2013).
230. S. Chabot *et al.*, Regulation of galectin-9 expression and release in Jurkat T cell line cells. *Glycobiology* **12**, 111–118 (2002).
231. J. Hirabayashi *et al.*, Oligosaccharide specificity of galectins: a search by frontal affinity chromatography. *Biochim Biophys Acta* **1572**, 232–254 (2002).
232. M. Nagae *et al.*, Structural analysis of the human galectin-9 N-terminal carbohydrate recognition domain reveals unexpected properties that differ from the mouse orthologue. *J Mol Biol* **375**, 119–135 (2008).
233. M. Nagae *et al.*, Structural analysis of the recognition mechanism of poly-N-acetyllactosamine by the human galectin-9 N-terminal carbohydrate recognition domain. *Glycobiology* **19**, 112–117 (2009).
234. M. Sato *et al.*, Functional analysis of the carbohydrate recognition domains and a linker peptide of galectin-9 as to eosinophil chemoattractant activity. *Glycobiology* **12**, 191–197 (2002).
235. H. Yoshida *et al.*, X-ray structures of human galectin-9 C-terminal domain in complexes with a biantennary oligosaccharide and sialyllactose. *J Biol Chem* **285**, 36969–36976 (2010).
236. S. John, R. Mishra, Galectin-9: From cell biology to complex disease dynamics. *J Biosci* **41**, 507–534 (2016).
237. X. J. Ji *et al.*, HCV-infected hepatocytes drive CD4+ CD25+ Foxp3+ regulatory T-cell development through the Tim-3/Gal-9 pathway. *Eur J Immunol* **43**, 458–467 (2013).
238. K. Lv, Y. Zhang, M. Zhang, M. Zhong, Q. Suo, Galectin-9 promotes TGF-beta1-dependent induction of regulatory T cells via the TGF-beta/Smad signaling pathway. *Mol Med Rep* **7**, 205–210 (2013).
239. Y. A. Hsu *et al.*, Amelioration of bleomycin-induced pulmonary fibrosis via TGF-beta-induced Smad and non-Smad signaling pathways in galectin-9-deficient mice and fibroblast cells. *J Biomed Sci* **27**, 24 (2020).
240. A. T. H. Selno *et al.*, Transforming growth factor beta type 1 (TGF-beta) and hypoxia-inducible factor 1 (HIF-1) transcription complex as master regulators of the immunosuppressive protein galectin-9 expression in human cancer and embryonic cells. *Aging (Albany NY)* **12**, 23478–23496 (2020).
241. C. Wu *et al.*, Galectin-9-CD44 interaction enhances stability and function of adaptive regulatory T cells. *Immunity* **41**, 270–282 (2014).
242. R. D. Cummings, T cells are Smad'ly in love with galectin-9. *Immunity* **41**, 171–173 (2014).
243. R. M. Maizels, H. J. McSorley, H. H. Smits, P. Ten Dijke, A. P. Hinck, Cytokines from parasites: manipulating host responses by molecular mimicry. *Biochem J* **482**, 433–449 (2025).
244. R. M. Maizels, S. J. Newfeld, Convergent Evolution in a Murine Intestinal Parasite Rapidly Created the TGM Family of Molecular Mimics to Suppress the Host Immune Response. *Genome Biol Evol* **15**, (2023).

245. M. van Dinther *et al.*, CD44 acts as a coreceptor for cell-specific enhancement of signaling and regulatory T cell induction by TGM1, a parasite TGF-β mimic. *Proc Natl Acad Sci U S A* **120**, e2302370120 (2023).
246. S. P. Singh *et al.*, The TGF-β mimic TGM4 achieves cell specificity through combinatorial surface co-receptor binding. *EMBO Rep* **26**, 218–244 (2025).
247. T. R. Stachowski, M. E. Snell, E. H. Snell, Structural insights into conformational switching in latency-associated peptide between transforming growth factor β-1 bound and unbound states. *IUCrJ* **7**, 238–252 (2020).
248. Y. Zhang *et al.*, GP96 is a GARP chaperone and controls regulatory T cell functions. *J Clin Invest* **125**, 859–869 (2015).
249. T. M. Fenton *et al.*, Inflammatory cues enhance TGFβ activation by distinct subsets of human intestinal dendritic cells via integrin αvβ8. *Mucosal Immunol* **10**, 624–634 (2017).
250. G. Shaw, S. Morse, M. Ararat, F. L. Graham, Preferential transformation of human neuronal cells by human adenoviruses and the origin of HEK 293 cells. *Faseb j* **16**, 869–871 (2002).
251. A. A. Stepanenko, V. V. Dmitrenko, HEK293 in cell biology and cancer research: phenotype, karyotype, tumorigenicity, and stress-induced genome-phenotype evolution. *Gene* **569**, 182–190 (2015).
252. V. R. Wiersma, M. de Bruyn, W. Helfrich, E. Bremer, Therapeutic potential of Galectin-9 in human disease. *Med Res Rev* **33 Suppl 1**, E102–126 (2013).
253. J. H. McCarty, alphavbeta8 integrin adhesion and signaling pathways in development, physiology and disease. *J Cell Sci* **133**, (2020).
254. C. G. Gahmberg *et al.*, Regulation of cell adhesion: a collaborative effort of integrins, their ligands, cytoplasmic actors, and phosphorylation. *Q Rev Biophys* **52**, e10 (2019).
255. I. Tvaroska, S. Kozmon, J. Kona, Molecular Modeling Insights into the Structure and Behavior of Integrins: A Review. *Cells* **12**, (2023).

ANNEXES

Lambert et al. (2025): Antibody-mediated TGF-β1 activation for the treatment of diseases caused by deleterious T cell activity

Article

Cell Reports

Antibody-mediated TGF-β1 activation for the treatment of diseases caused by deleterious T cell activity

Graphical abstract

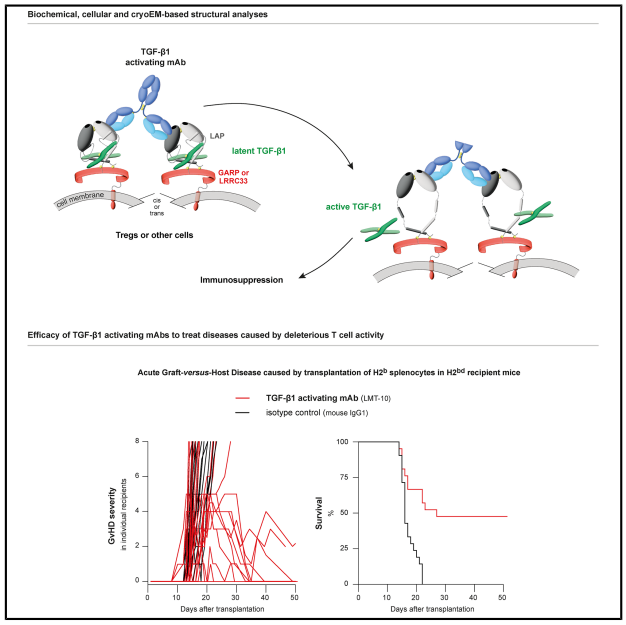

Highlights

- Latent TGF-β1 on the surface of cells can be activated by monoclonal antibodies
- TGF-β1 activation implies profound conformational changes and an active cytoskeleton
- Antibody-mediated TGF-β1 activation exerts therapeutic effects in graft versus host disease

Authors

Fanny Lambert, Jan Felix, Séverine Wautier, ..., Bas van der Woning, Savvas N. Savvides, Sophie Lucas

Correspondence

sophie.lucas@uclouvain.be

In brief

Lambert et al. describe an antibody-based approach targeting the pleiotropic TGF-β1 cytokine in a manner unexplored thus far. At variance with existing TGF-β1-targeting strategies aiming to block TGF-β1 immunosuppression in cancer or fibrosis, their antibodies augment TGF-β1 activity to treat severe diseases characterized by excessive immune responses.

Lambert et al., 2025, Cell Reports *44*, 116061
August 26, 2025 © 2025 The Authors. Published by Elsevier Inc.
https://doi.org/10.1016/j.celrep.2025.116061

CellPress

Cell Reports

CellPress
OPEN ACCESS

Article

Antibody-mediated TGF-β1 activation for the treatment of diseases caused by deleterious T cell activity

Fanny Lambert,[1,6] Jan Felix,[2,3,6] Séverine Wautier,[1,6] Emilie Dupré,[1] Mathieu Jamez,[1] Camille Michiels,[1] Mélanie Gaignage,[1] Lore Mariën,[4] Manon Lesage,[4] Bas van der Woning,[4] Savvas N. Savvides,[2,3,7] and Sophie Lucas[1,5,7,8,*]

[1]de Duve Institute, UCLouvain, 1200 Brussels, Belgium
[2]VIB Center for Inflammation Research, 9052 Ghent, Belgium
[3]Department of Biochemistry and Microbiology, Ghent University, 9052 Ghent, Belgium
[4]argenx BV, Industriepark Zwijnaarde 7, 9052 Ghent, Belgium
[5]WELBIO Department, WEL Research Institute, 1300 Wavre, Belgium
[6]These authors contributed equally
[7]Senior author
[8]Lead contact
*Correspondence: sophie.lucas@uclouvain.be
https://doi.org/10.1016/j.celrep.2025.116061

SUMMARY

Transforming growth factor β1 (TGF-β1) is an immunosuppressive cytokine produced as a latent homodimer, in which mature TGF-β1 is encapsulated and kept inactive by the latency-associated peptide (LAP). The transmembrane protein GARP presents latent TGF-β1 on the surface of regulatory T cells (Tregs) to enable activation and release of mature TGF-β1 by integrins. Here, we derived monoclonal antibodies (mAbs) that activate latent TGF-β1 anchored on cells by a transmembrane protein. Biochemical and structural studies by electron cryo-microscopy (cryo-EM) reveal that such mAb-mediated activation requires bivalent binding close to the LAP dimerization interface and crosslinking of two membrane-bound GARP:TGF-β1 complexes on the same cell or across different cells. Administration of mAbs to mice with graft versus host disease reduced disease severity and increased survival. The therapeutic effect required Tregs. Collectively, our findings demonstrate that activation of membrane-bound TGF-β1 *in vivo* is achievable with mAbs, introducing new immunotherapeutic options for allo- or autoimmune diseases characterized by deleterious T cell activity insufficiently controlled by Tregs.

INTRODUCTION

Due to the potent immunosuppression it exerts in mice and humans, production of transforming growth factor β1 (TGF-β1) is tightly regulated at a post-translation level, prior to its binding to a hetero-tetrameric receptor composed of TβRI and TβRII chains. Mice with a germline deletion of the *Tgfb1* gene or a T cell-specific deletion of *Tgfbr2* die 3–4 weeks after birth from a lymphoproliferative multisystemic autoimmune syndrome, indicating that TGF-β1 activity in T cells is required to maintain immune tolerance.[1–3] Due to the widespread expression of the TGF-β receptor, TGF-β1 also acts on most other if not all immune cell types, regulating their differentiation, proliferation, and activation.[4] Owing to these pleiotropic functions, production of active TGF-β1 is regulated at multiple levels.[5] Translation of *TGFB1* mRNA leads to a precursor comprising a signal peptide followed by a 43 kDa amino acid (aa) sequence called LAP (latency-associated peptide) and a 12.5 kDa sequence corresponding to the mature TGF-β1 cytokine. After signal peptide removal and interchain disulfide bond formation, the pro-TGF-β1 homodimer is cleaved by a furin convertase. The resulting LAP and mature TGF-β1 homodimers remain non-covalently associated, forming a complex called "latent TGF-β1" because LAP prevents binding of mature TGF-β1 to its receptor. Structural studies by X-ray crystallography revealed that the N-terminal α1 and α2 helixes and an intervening loop called the latency lasso act as a straitjacket embracing the extremities of the mature TGF-β1 dimer that are needed for interaction with the TGF-β receptor.[6] The C termini of the LAP monomers form rigid structures called the arms, overhung by a "bowtie" where the monomers are linked via interchain disulfide bonds.[6] Whereas most cell types and virtually all immune cells produce latent TGF-β1, only very few release mature TGF-β1 from the LAP straitjacket. This process is referred to as "TGF-β1 activation." It is required to induce autocrine or paracrine TGF-β1 signaling and occurs via highly regulated cell type-specific mechanisms.

We and others previously showed that immunosuppressive lymphocytes known as Tregs (regulatory T cells) activate latent

This is an open access article under the CC BY-NC-ND license (http://creativecommons.org/licenses/by-nc-nd/4.0/).

CellPress
OPEN ACCESS

Cell Reports
Article

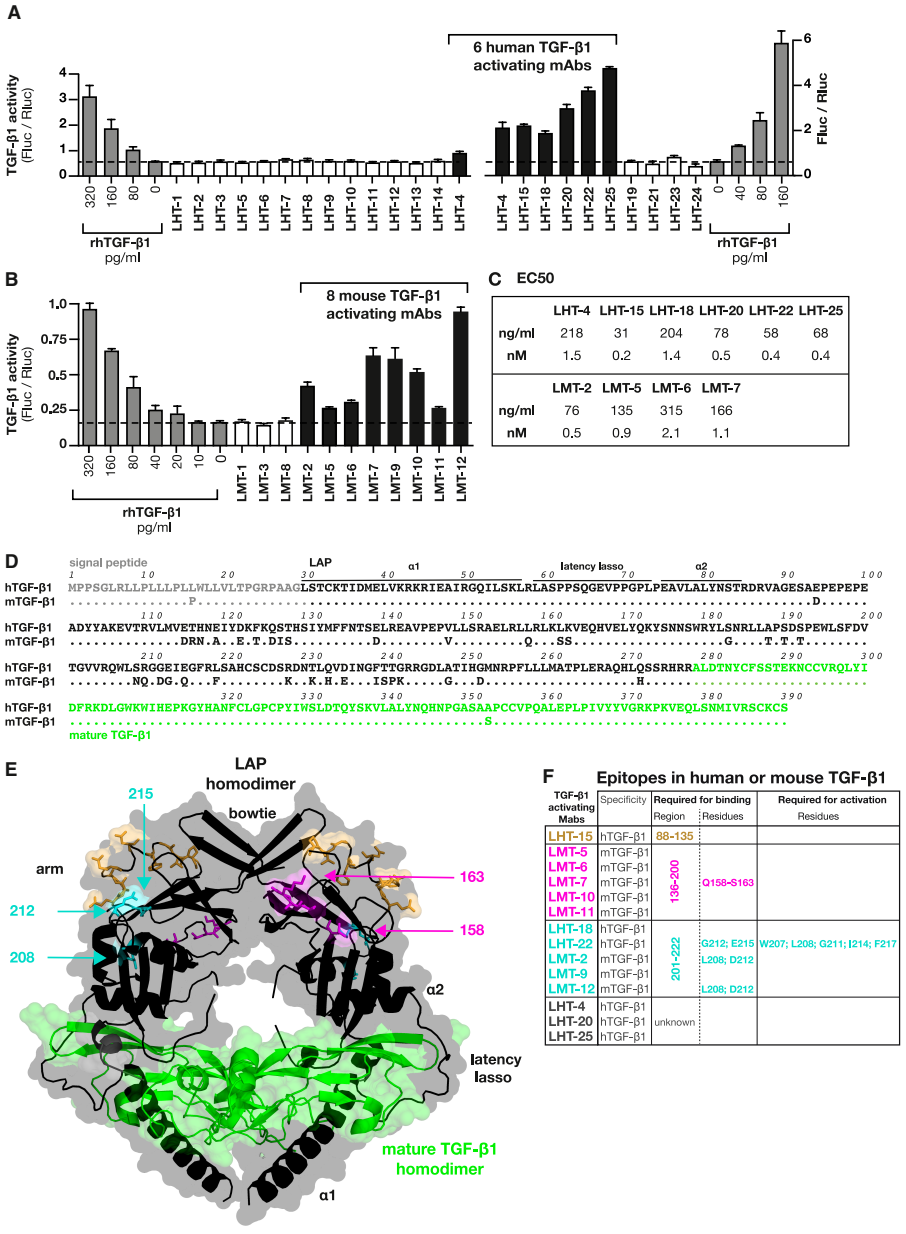

TGF-β1 activating Mabs	Specificity	Required for binding		Required for activation
		Region	Residues	Residues
LHT-15	hTGF-β1	88-135		
LMT-5	mTGF-β1	136-200		
LMT-6	mTGF-β1			
LMT-7	mTGF-β1		Q158-S163	
LMT-10	mTGF-β1			
LMT-11	mTGF-β1			
LHT-18	hTGF-β1	201-222		
LHT-22	hTGF-β1		G212; E215	W207; L208; G211; I214; F217
LMT-2	mTGF-β1		L208; D212	
LMT-9	mTGF-β1			
LMT-12	mTGF-β1		L208; D212	
LHT-4	hTGF-β1	unknown		
LHT-20	hTGF-β1			
LHT-25	hTGF-β1			

Figure 1. Human and mouse TGF-β1-activating mAbs bind close to the LAP dimerization interface

(A) HEK293T cells were co-transfected to express human GARP:TGF-β1 complexes, firefly luciferase (Fluc) under the control of a CAGA element as a reporter for TGF-β1 activity, and *Renilla* luciferase (Rluc) as a transfection control and then incubated with the indicated mAbs (20 μg/mL) or serial dilutions of active recombinant human TGF-β1 (rhTGF-β1). Bar graphs represent ratios of Fluc to Rluc activity (mean of triplicates + SD). Black bars highlight the 6 LHT activating

(legend continued on next page)

Cell Reports
Article

CellPress
OPEN ACCESS

TGF-β1 by a mechanism that requires the transmembrane proteins GARP and integrin $\alpha_V\beta_8$.[7–11] In the endoplasmic reticulum of Tregs, latent TGF-β1 is covalently linked to the extracellular leucin-rich repeat (LRR) domain of GARP via formation of disulfide bonds between one cysteine in each LAP monomer and two cysteines in the GARP monomer. This results in presentation on the Treg surface of membrane-bound latent TGF-β1, which can then bind integrin $\alpha_V\beta_8$ via an RGD motif in the arm region of LAP. T cell receptor (TCR) stimulation of Tregs induces surface expression of GARP:(latent)TGF-β1 complexes and $\alpha_V\beta_8$, leading to TGF-β1 activation and autocrine or paracrine signaling in Tregs and neighboring cells.[7,8,10,11] Another LRR-containing transmembrane protein called LRRC33 presents latent TGF-β1 on the surface of microglia (i.e., macrophages of the CNS) for activation by integrin $\alpha_V\beta_8$.[12]

The precise molecular mechanisms leading to activation of latent TGF-β1 presented by GARP or LRRC33 to $\alpha_V\beta_8$ are not completely resolved. Most studies suggest exertion of mechanical forces on latent TGF-β1 to release mature TGF-β1. A major mechanistic hypothesis is that application of pulling forces on latent TGF-β1 in opposing directions would unroll the LAP straitjacket and release mature TGF-β1 in the extracellular milieu.[13,14] Alternatively, it has been proposed that induction of modest conformational changes in the latency lasso could expose the extremities of mature TGF-β1 for binding to the cytokine receptor.[15]

We previously derived anti-GARP:TGF-β1 monoclonal antibodies (mAbs) that block TGF-β1 activation and immunosuppression by Tregs and showed that the mAbs enhanced anti-tumor T cell responses and exerted therapeutic anti-tumor activity in mice with solid tumors or myeloproliferative neoplasms.[11,14,16–18] Phase 1 and 2 trials are currently ongoing to test blocking anti-GARP:TGF-β1 mAbs in patients suffering from advanced or metastatic solid tumors as a novel form of cancer immunotherapy (ClinicalTrials.gov: NCT03821935, NCT05822752, and NCT06109272).

Here, we sought to develop mAbs that enhance rather than block TGF-β1 activation and Treg immunosuppression, with the objective to address diseases characterized by excessive T cell activity insufficiently controlled by Tregs. Integration of *in vitro* and *in vivo* experimental findings with structural insights obtained from complexes between GARP:TGF-β1 and antibody fragments (Fabs) reveals that TGF-β1 activation by a mAb requires crosslinking of at least two membrane-bound GARP:TGF-β1 complexes on cells and a profound conformational change in latent TGF-β1, shedding light on the molecular events that occur during TGF-β1 activation by integrins *in vivo*.

RESULTS

mAbs that activate human or mouse TGF-β1 recognize epitopes close to the LAP homodimerization interface

We screened 134 mAbs directed against human or mouse GARP, GARP:TGF-β1, or latent TGF-β1 for their ability to activate TGF-β1 in a reporter assay. HEK293T cells were co-transfected to express surface human or mouse GARP:TGF-β1 complexes, firefly luciferase under the control of a TGF-β1-responsive promoter, and *Renilla* luciferase to normalize for transfection efficacy. Luciferase activity was measured in transfected cells 18 h after incubation with mAbs. Fourteen mAbs activated TGF-β1 in the assay (Figures 1A and 1B): six are directed against human latent TGF-β1 (LHT-4, -15, -18, -20, -22, and -25) and eight against mouse latent TGF-β1 (LMT-2, -5, -6, -7, -9, -10, -11, and -12). None are directed against GARP or GARP:TGF-β1 complexes, and none are cross-reactive against human and mouse latent TGF-β1. Activation occurred at mAb concentrations in the nanomolar range (Figure 1C).

Because activating mAbs are not cross-reactive, we used human/mouse (h/m) latent TGF-β1 chimeras to map their epitopes. Most amino acid (aa) differences between human and mouse latent TGF-β1 are localized in LAP, downstream of a highly conserved region comprising helixes α1 and α2 and the latency lasso (Figures 1D and 1E). We constructed plasmids encoding hemagglutinin (HA)-tagged h/m latent TGF-β1 chimeras, in which aa from one segment of mouse LAP were replaced by the aa from the corresponding segment of human LAP. Constructs encoding HA-tagged human or mouse latent TGF-β1 in which a single residue was replaced by alanine allowed us to further refine binding requirements. HEK293T cells were co-transfected to express wild-type, chimeric, or single-Ala mutant latent TGF-β1 in complex with mouse GARP and analyzed for binding to mAbs by flow cytometry (Figures S1A–S1C). We also examined in the reporter assay whether some mAbs lost the ability to activate single-Ala mutants to which they could still bind (Figure S1D). Mapping analyses described in the supplemental information show that all activating mAbs bind loops close to the LAP dimerization interface, previously described as critical to maintain TGF-β1 latency by keeping the LAP monomers welded together[6] (Figure 1E). Amino acids 201–222 is the only region bound by anti-human and by anti-mouse latent TGF-β1 mAbs, including LHT-22 and LMT-12. To activate human TGF-β1, LHT-22 requires residues W207, L208, G211, G212, I214, E215, and F217; to activate mouse TGF-β1, LMT-12 requires residues L208 and D212 (Figures 1F and S1D). LHT-22 and LMT-12 epitopes in human and mouse latent TGF-β1, respectively, are very similar to each other and are not shared with non-activating mAbs.

mAbs (i.e., Fluc/Rluc in the presence of the mAb > Fluc/Rluc in the absence of rhTGF-β1 in ≥3 independent experiments). The dotted line shows the FLuc/Rluc ratio in the absence of rhTGF-β1 or mAb.
(B) Same as in (A), except that HEK293T cells were transfected with mouse GARP:TGF-β1. Black bars highlight the 8 LMT activating mAbs.
(C) Half-maximum effective concentration (EC_{50}) was measured by performing the reporter assay as in (A) or (B) with serial dilutions of the indicated mAbs.
(D) Annotated alignment of human (h) and mouse (m) latent TGF-β1 sequences.
(E) Tridimensional structure of porcine latent TGF-β1.[6] Black, LAP; green, mature TGF-β1; orange, magenta, and turquoise, important residues required for binding and activation by LMT or LHT mAbs.
(F) Summary of epitope mapping analyses shown in Figure S1, indicating the individual aa or aa stretches required for binding or activation by TGF-β1-activating mAbs. Residues indicated as required for activation by LHT-22 are not required for binding.

CellPress
OPEN ACCESS

Cell Reports
Article

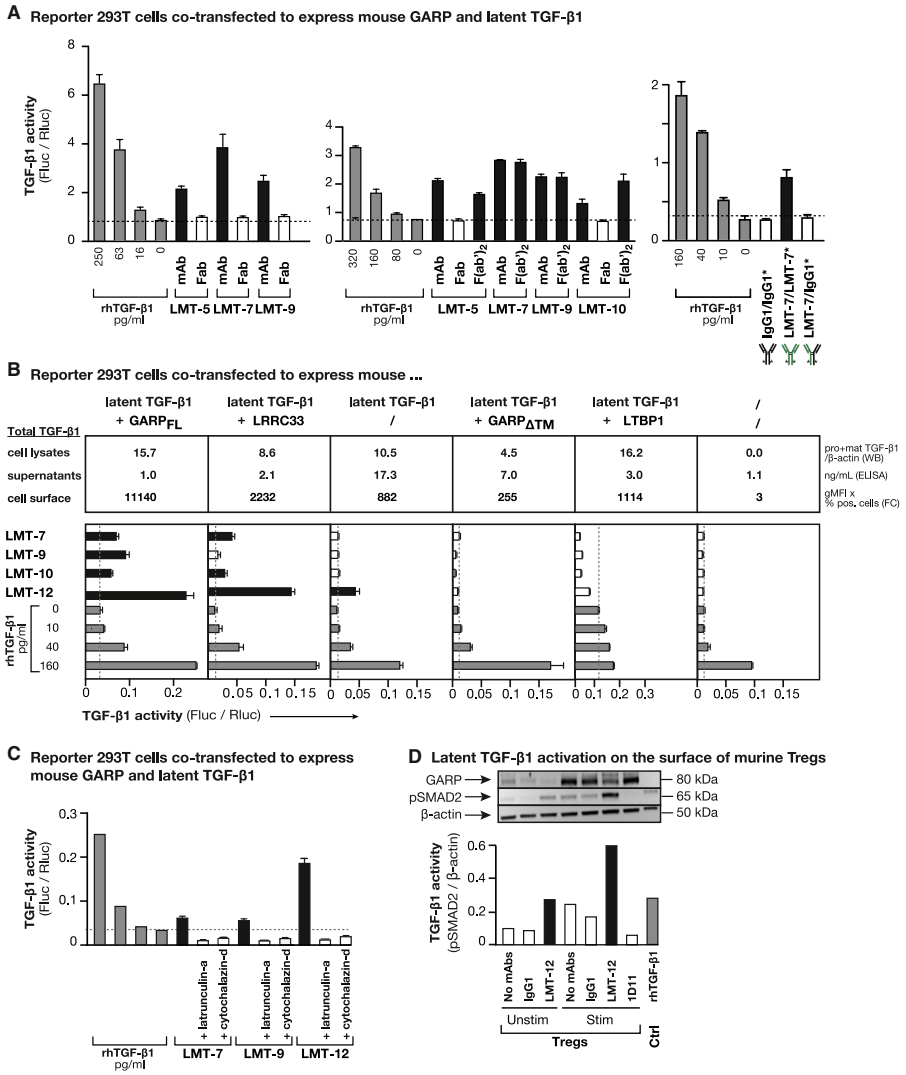

Figure 2. Bivalent binding, membrane anchorage, and actin polymerization are required for activation of latent TGF-β1 on the cell surface by mAbs

(A) Reporter assay as in Figure 1B, except that transfected cells were incubated with LMT antibodies under full (mAb), F(ab')$_2$, or Fab formats (left and middle) or with antibody chimeras generated by Fab-arm exchange (right). IgG1/IgG1* (black): control chimera with two arms from an irrelevant mouse IgG1. LMT-7/LMT-7* (green): control chimera with two arms from LMT-7. LMT-7/IgG1* (black/green): chimera with one arm from LMT-7 and one arm from the IgG1 control. Bar graphs represent ratios of Fluc to Rluc activity (mean of triplicate + SD). Black bars highlight antibody formats that activate TGF-β1. A dotted line shows FlLuc/Rluc in the absence of rhTGF-β1 or mAb.

(B) Reporter HEK293T *TGFB1* knockout (KO) cells transfected with CAGA-Fluc and Rluc were co-cultured at a 1:1 ratio with HEK293T *TGFB1* KO cells co-transfected to express latent TGF-β1 and the indicated presenting molecules in the presence or absence of LMT mAbs or rhTGF-β1. GARP$_{FL}$, full-length GARP; GARP$_{\Delta TM}$, GARP truncated from the C-terminal transmembrane and intracellular domains. Numbers above the bar graphs indicate levels of TGF-β1 protein expression as detected by western blot (WB) in cell lysates (top), by ELISA in supernatants (middle), and by flow cytometry (FC) on the cell surface (bottom). Bar graphs represent ratios of Fluc to Rluc activity (mean of triplicate + SD). Black bars highlight conditions in which the mAbs activate latent TGF-β1. A dotted line shows Fluc/Rluc in the absence of rhTGF-β1 or mAb.

(legend continued on next page)

Cell Reports
Article

CellPress
OPEN ACCESS

Bivalent binding, anchorage of latent TGF-β1 to the cell membrane, and actin polymerization are required for activation by mAbs

We tested 4 LMT antibodies as full length mAbs, F(ab')$_2$, or Fabs in the HEK293T reporter assay. All activated mouse TGF-β1 when they were used as mAbs or F(ab')$_2$ but not as Fabs (Figure 2A). We also constructed chimeric antibodies by Fab-arm exchange. The LMT-7/immunoglobulin 1* (IgG1*) chimera comprises H and L chains from LMT-7 on one hand and H and L chains from a control mouse IgG1 on the other. LMT-7/IgG1* thus binds latent TGF-β1 in a monovalent manner, with a half-maximum effective concentration (EC_{50}) similar to that of the bivalent LMT-7/LMT-7* control (Figure S2A). In contrast to LMT-7/LMT-7*, however, the LMT-7/IgG1* chimera does not activate latent TGF-β1 (Figure 2A). Thus, bivalent binding is required to activate TGF-β1 on the surface of cells *in vitro*.

Our screen to identify activating antibodies was performed in reporter cells transfected to express GARP, a transmembrane protein known to anchor and present latent TGF-β1 on the Treg surface. We examined whether membrane anchorage was required for mAb-mediated activation (Figure 2B). Reporter cells were transfected to express mouse latent TGF-β1 alone or in complex with full-length GARP ($GARP_{FL}$), GARP truncated from its transmembrane domain ($GARP_{\Delta TM}$), or LRRC33, another LRR-containing transmembrane protein that covalently binds and presents latent TGF-β1 on the surface of myeloid cells. We also tested latent TGF-β1 binding protein 1 (LTBP-1), a secreted protein lacking a transmembrane domain, known to bind and deposit latent TGF-β1 in the extracellular matrix. As expected, large amounts of TGF-β1 (proTGF-β1 + mature TGF-β1) were found in the lysates of all HEK293T cells transfected to express latent TGF-β1. Large amounts of latent TGF-β1 were secreted in the supernatants of cells transfected with TGF-β1 alone or with $GARP_{\Delta TM}$, whereas high levels were found on the surface of cells co-transfected with TGF-β1 and $GARP_{FL}$ or LRRC33. Surface TGF-β1 was also detected, albeit at lower levels, on cells transfected with TGF-β1 alone, or with $GARP_{\Delta TM}$ or LTBP-1, indicating that molecule(s) other than LRRC33 or $GARP_{FL}$ can retain some latent TGF-β1 on the HEK293T cell surface. The GRP78 chaperone, for example, has been reported to present latent TGF-β1 on cells.[19] All mAbs tested (LMT-7, -9, -10, and -12) bound surface TGF-β1 whether it was presented by GARP, LRRC33, or the unidentified molecule(s) expressed in HEK293T cells. All mAbs activated TGF-β1 presented by $GARP_{FL}$, as expected, and most (LMT-7, -9, and 12) activated TGF-β1 presented by LRRC33. In contrast, none activated TGF-β1 expressed alone, with $GARP_{\Delta TM}$, or with LTBP-1 (Figure 2B). These results show that mAbs activate latent TGF-β1 presented on the cell surface by a protein anchored in the membrane via a transmembrane domain.

We tested two inhibitors of actin polymerization in the reporter assay. Latrunculin-a and cytochalazin-d blocked TGF-β1 activation by LMT-7, LMT-9, and LMT-12 without reducing GARP:TGF-β1 levels on the cell surface (Figures 2C and S2B). This indicates that an active cytoskeleton is required for mAb-mediated activation of latent TGF-β1 on the surface of HEK293T cells.

mAbs can activate latent TGF-β1 presented on the surface of Tregs

We verified that the mAbs can also activate latent TGF-β1 presented on the surface of cells that naturally express surface GARP:TGF-β1. As expected, whereas resting (unstimulated) murine Tregs expressed low amounts of GARP and did not activate TGF-β1, TCR stimulation increased GARP levels and induced TGF-β1 activation[20,21] (Figure 2D). Incubation with LMT-12 was sufficient to induce TGF-β1 activation by resting Tregs and increased TGF-β1 activation by TCR-stimulated Tregs (Figure 2D).

Molecular and structural mechanism of TGF-β1 activation by mAbs

To obtain insights into the structural basis and mechanism of TGF-β1 activation by mAbs, we sought to determine the structure of human and mouse GARP:TGF-β1 in complex with Fabs derived from activating mAbs LHT-22 and LMT-12, respectively, by single-particle electron cryo-microscopy (cryo-EM). Initial attempts were hampered by extreme anisotropy observed in the obtained 3D reconstructions due to preferred particle orientations and the absence of top views. To overcome this, additional data were collected by applying 16° and 35° tilts for the human GARP:TGF-β1:LHT-22 complex and a 20° tilt for the mouse GARP:TGF-β1:LMT-12 complex. The acquisition of tilt data combined with balancing of sets of particles extracted from datasets obtained with and without tilting protocols resulted in isotropic maps for human and mouse GARP:TGF-β1:Fab complexes to a nominal resolution of 2.9 and 3.0 Å, respectively (Figures S3 and S4; Table 1). The cryo-EM maps and corresponding structural models reveal a 1:1:2 stoichiometry in the complexes, comprising one GARP, one latent TGF-β1 (i.e., one LAP_A/LAP_B and one mature TGF-$\beta1_A$/TGF-$\beta1_B$ dimer), and two LHT-22 or LMT-12 Fabs (Figures 3A and 3B). Each Fab copy binds one of the two LAP subunits to a region adjacent to the RGD motif, a structural and functional determinant for the binding of integrins to enable release of mature TGF-β1. A structural alignment of integrins $\alpha_V\beta_6$ (PDB: 5FFO)[13] and $\alpha_V\beta_8$ (PDB: 6UJA)[15] onto the human GARP:TGF-β1:LHT-22 complex demonstrates that integrin binding does not clash with LHT-22 and can occur when LHT-22 is bound to GARP:TGF-β1 (Figure S5). In both human and mouse GARP:TGF-β1:Fab complexes, the C termini of the two Fabs are too far apart to be accommodated in the context of a single, full-length mAb molecule (Figure S6).

Structural superposition of one of the two Fabs from a complete IgG molecule in either the T (PDB: 1IGT) or Y conformation (PDB: 1IGY) to one of the two individual LHT-22 Fabs binding to the human GARP:TGF-β1 complex reveals that >150 Å separate

(C) As in (B), except that co-cultures of transfected cells were also incubated with latrunculin-a (5 μg/mL) or cytochalazin-d (0.5 μM) where indicated.
(D) Mouse cells enriched in Tregs (MACS-sorted $CD25^+$ cells containing ~50% $CD4^+FOXP3^+$ cells) were incubated for 18 h with anti-CD3/CD28 beads (Stim) or left resting in medium alone (Unstim) in the presence of the indicated antibodies (20 μg/mL). 1D11, neutralizing anti-mature TGF-β1,2,3 mAb. Cell lysates were analyzed by western blot with antibodies against GARP, pSMAD2, and β-actin. Bar graphs show quantification of ECL signals. Splenocytes incubated with rhTGF-β1 (1 ng/mL) served as positive controls (Ctrl) for pSMAD2 signals. Results are representative of a total of 6 independent experiments.

CellPress
OPEN ACCESS

Cell Reports
Article

Table 1. Cryo-EM data collection, refinement, and validation statistics

	hGARP: TGF-β1:Fab LHT-22 complex EMDB: EMD-19110 (PDB: 8REW)	mGARP: TGF-β1:Fab LMT-12 complex EMDB: EMD-19111 (PDB: 8REX)
Data collection and processing		
Magnification	60,000	60,000
Voltage, kV	300	300
Electron exposure, $e^{-}/Å^2$	61.8	61.8
Defocus range, μm	0.8–2.0	0.8–2.0
Pixel size, Å	0.72	0.72
Symmetry imposed	C1	C1
Initial particle images, no.	4,585,815	4,293,248
Final particle images, no.	320,551	288,887
Map resolution, Å	2.89	3.00
FSC threshold	0.143	0.143
Map resolution range, Å	1.53–40.23	2.60–48.97
Refinement		
Initial model used, PDB code/Alphafold entry	6GFF	AF-G3XA59-F1 AF-P04202-F1
Model resolution, Å	3.20	3.50
FSC threshold	0.5	0.5
Model resolution range, Å	∞–3.20	∞–3.50
Map sharpening *B* factor, $Å^2$	−87.4	−84.0
Model composition		
Non-hydrogen atoms	12,426	12,355
Protein residues	1,609	1,588
Ligands	NAG: 11 BMA: 2 MAN: 2	NAG: 8
B factors, $Å^2$		
Protein	122	138
Ligand	93	99
RMSD		
Bond lengths, Å	0.004	0.004
Bond angles, °	0.792	0.821
Validation		
MolProbity score	1.68	1.87
Clashscore	7.81	8.42
Poor rotamers, %	0.15	0.07
CaBLAM outliers, %	1.23	3.02
CC (mask/volume)	0.80/0.79	0.73/0.73
EMRinger, sharpened/unsharpened	3.41/3.26	2.07/1.72
Ramachandran plot		
Favored (%)	96.25	93.83
Allowed (%)	3.75	6.17
Disallowed (%)	0.00	0.00
Ramachandran *Z* score		
Whole	−1.22	−1.71
Helix	−1.38	−1.54
Sheet	−0.70	−0.59
Loop	−0.72	−1.34

the second Fab of the IgG molecule from the other epitope in the same GARP:TGF-β1 complex (Figure S6A). Since the maximum distance between the ends of Fab domains in IgG1 mAbs is shorter than 110 Å, as shown by structural studies of mAbs in solution by small-angle X-ray and neutron scattering experiments,[22] or 120 Å as shown for IgG1 by electron tomography,[23] such a distance is not compatible with bivalent binding of one IgG1 molecule to a single GARP:TGF-β1. The same holds true for LMT-22 binding to mouse GARP:TGF-β1 (Figure S6B). To address possible bending of the Fab domains at the elbow angle and hinge region, we also performed a structural superposition of IgG Fabs with tilts around the elbow angle ranging from 127° to 220°[24] onto the hGARP:TGF-β1:LHT-22 complex. This analysis results in distances between the Fab C termini of over 135 Å, which is far more than twice the length of the linker between the IgG Fab and Fc domains at the hinge region (Figure S6C).

To confirm this experimentally, we performed size-exclusion chromatography-multi angle laser light scattering analyses after incubation of equimolar amounts of LHT-22 with GARP:TGF-β1 for either 1 h at 20°C or up to 18 h at 37°C (Figure S7). Under both conditions, megadalton complexes comprising GARP, LAP, mature TGF-β1, and L and H chains of LHT-22 were observed, likely corresponding to long filaments of GARP:TGF-β1:LHT-22 in which each bivalent LHT-22 binds 2 distinct GARP:TGF-β1, and each GARP:TGF-β1 is bound by 2 distinct LHT-22. Importantly, no peak corresponding to complexes comprising one GARP:TGF-β1 and one LHT-22 was observed at all.

Therefore, our combined structural and biophysical analyses indicate that a single GARP:TGF-β1 complex can only be bound by two distinct mAbs when both binding epitopes are occupied, while a single mAb can only bind to two distinct GARP:TGF-β1 complexes (Figure 4).

The elucidated structural epitopes agree closely with our epitope mapping data (Figures S1C and S1D) so that LHT-12 and LMT-22 address highly similar and overlapping epitopes on human and mouse LAP, respectively. The epicenter of the binding epitopes involves LAP residues 210–215 and helix α4 (136–142) and is situated ~20 Å away from the RGD motif that mediates recruitment of integrin $\alpha_V\beta_8$. Interestingly, the positions of the heavy (V_H) and light (V_L) chain variable domains are swapped in the two complexes; while human LAP G212 and E215 form hydrogen bonds with LHT-22 V_L (Y837) and V_H (Y125), respectively, mouse LAP D212 and Q215 interact with LMT-12 V_H (S123) and V_L (Y836), respectively (Figure 3; Table S1 and S2).

Cell Reports
Article

CellPress
OPEN ACCESS

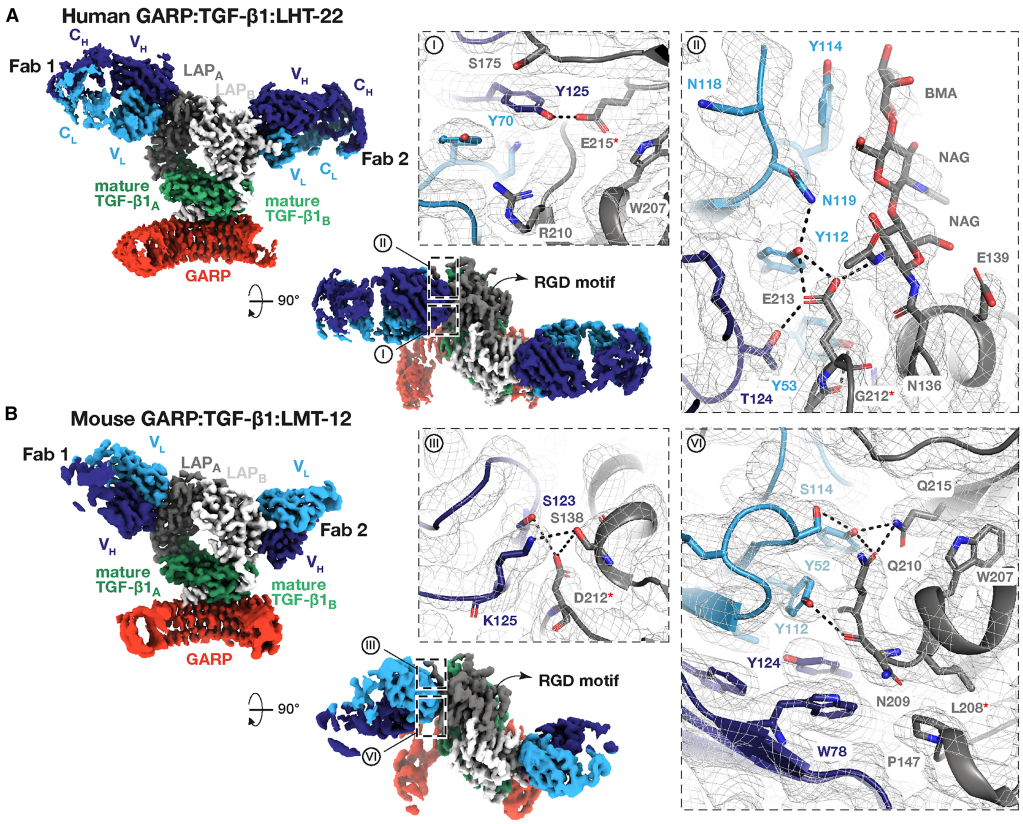

Figure 3. Cryo-EM structure of human and mouse GARP:TGF-β1 bound to Fabs from TGF-β1-activating mAbs

Shown are annotated side and top views of cryo-EM maps of GARP:TGF-β1:Fab complexes. Insets show magnifications of the Fab binding epitopes, with cryo-EM maps shown as a grey mesh. Structural models are shown as cartoons, with annotated residues shown as sticks, and hydrogen bonds are depicted as black dotted lines. Red asterisks indicate residues identified as binding hotspots using TGF-β1 single Ala mutants (Figure S1).

(A) Human GARP:TGF-β1:LHT-22 complex.

(B) Mouse GARP:TGF-β1:LMT-12 complex.

Structural superpositions of latent TGF-β1 in the GARP:TGF-β1:LHT-22 and GARP:TGF-β1:LMT-12 complexes with latent TGF-β1 in its complex with GARP and a Fab MHG-8 that reinforces latency (PDB: 6GFF)[14] revealed no major structural differences between latent TGF-β1 in the 3 complexes (root-mean-square deviation [RMSD] = 0.667 Å) (Figure S8). In particular, we note high structural similarity of helices α1 and the latency lassos of the LAP monomers, which mask residues in mature TGF-β1 and prevent its interaction with the TβRII receptor chain. Similarly, no structural differences were observed in helices α3 and 3_{10} (η1) helixes, or "thumbs," of the mature TGF-β1 monomers, which are fixed by the α1 helixes in LAP into positions incompatible with binding to the TβRI receptor chain. Thus, TGF-β1 presented by GARP and bound by two LHT-22 or two LMT-12 Fabs is latent and would be unable to interact with the TGF-β receptor to output signaling activity. Of note, the asymmetrical mode of binding of dimeric latent TGF-β1 inclining upon monomeric GARP in the context of the TGF-β1:MHG-8 complex[14] is also observed here in the GARP:TGF-β1:LHT-22 and GARP:TGF-β1:LMT-12 complexes (Figure 4A), indicating that this is the intrinsic interaction mode of GARP with latent TGF-β1.

Our structural data and analyses of antibody requirements for binding and activity lead us to conclude that TGF-β1 activation cannot be achieved when the LAP dimerization region close to the RGD motifs is bound by two individual Fab molecules. Activation requires binding of one bivalent mAb molecule to two latent TGF-β1 presented by GARP or another transmembrane protein on the cell surface. Whether the two GARP:TGF-β1 complexes need to be on the same cell (in *cis*; Figure 4A) or on

CellPress
OPEN ACCESS

Cell Reports
Article

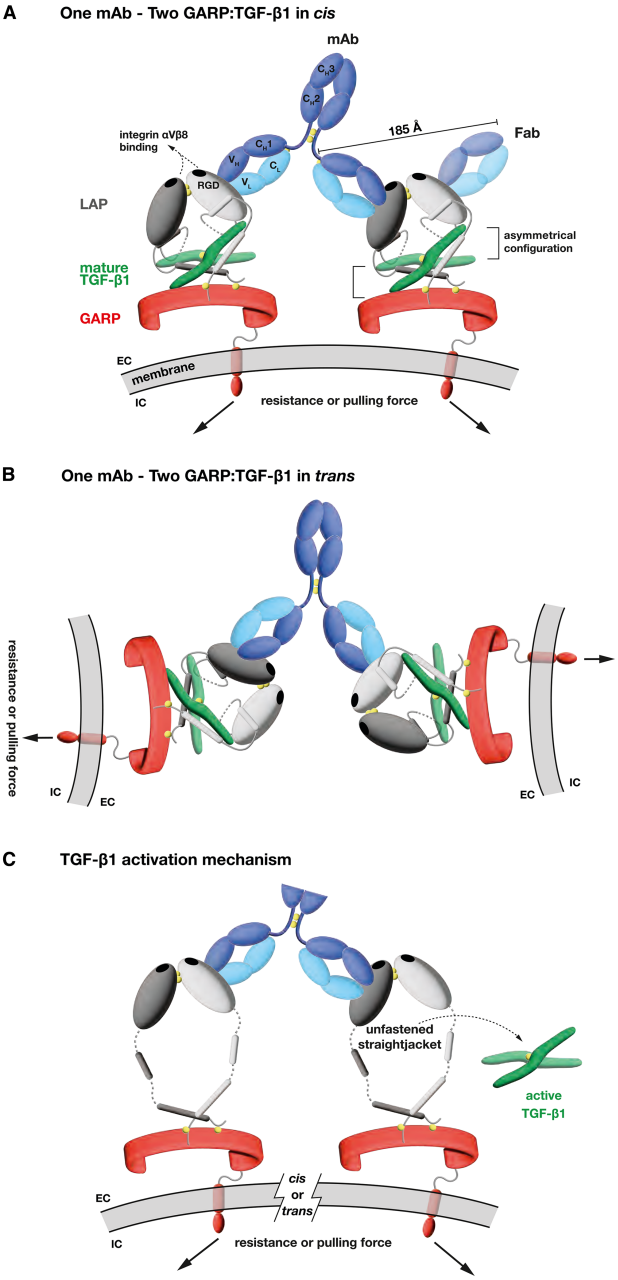

Figure 4. Molecular mechanism of TGF-β1 activation by mAbs

(A and B) Schematic of one activating mAb crosslinking two membrane-anchored GARP:TGF-β1 complexes located on the same cell (*cis*) or two adjacent cells (*trans*).

(C) Resistance or pulling force exerted on two membrane-bound GARP:TGF-β1 complexes crosslinked by one mAb results in unfastening of the LAP straitjacket and release of active TGF-β1.

Cell Reports
Article

CellPress
OPEN ACCESS

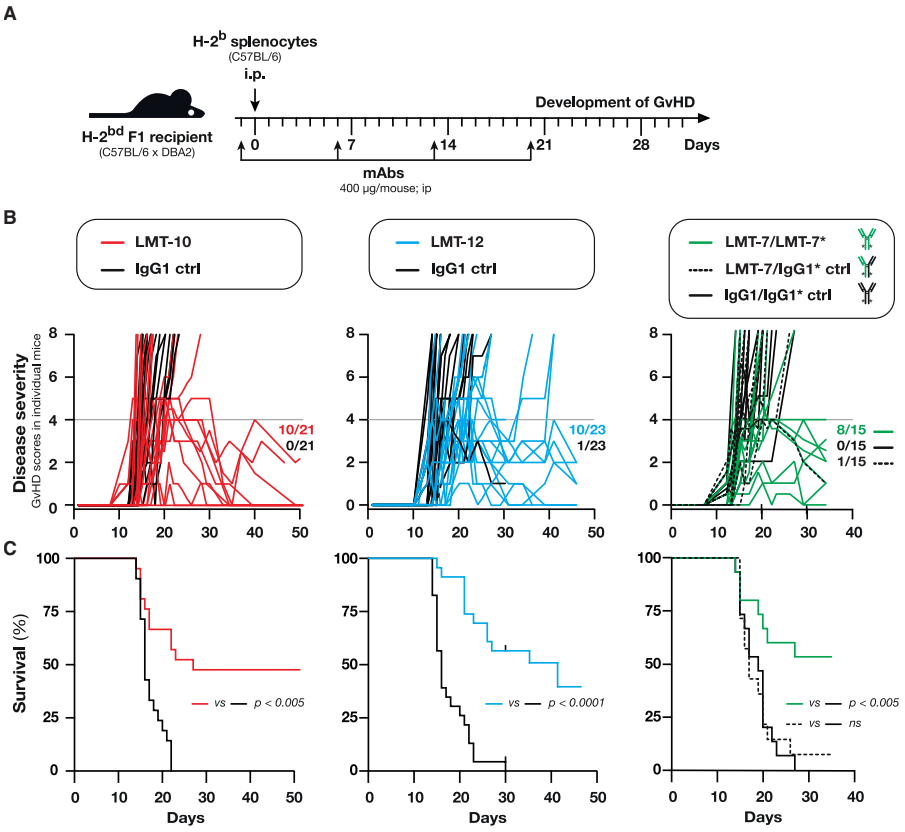

Figure 5. TGF-β1-activating antibodies reduce disease severity and increase survival in a mouse model of GvHD

(A) Schematic of the experimental design. H-2^{bd} F1 mice transplanted with H-2^{b} splenocytes (70–100 × 10^{6}) on day 0 were injected with TGF-β1 activating antibodies (mAbs or chimeras) or isotype controls once a week for 4 weeks, starting on day −1. Mice were scored for symptoms of GvHD, as indicated in the STAR Methods (maximum score, 8; mice were sacrificed when reaching a score of 6).

(B) Evolution of GvHD scores in individual mice. Each line represents one mouse. Ratios below the gray line indicate the proportion of mice in the corresponding group that were alive 30–50 days after transplantation.

(C) Kaplan-Meier plots representing the proportion of mice alive at the indicated days after transplantation. *p* values were calculated using a Gehan-Breslow Wilcoxon test. Data were pooled from 2–3 independent experiments for each of the LMT antibodies or chimeras and their respective controls. Vertical mark: censored data.

different cells (in *trans*; Figure 4B) is not known. Finally, steric constraints imposed by the LAP α1 helix are poised to prevent binding of mature TGF-β1 to the TβRI receptor chain unless a profound conformational change in LAP and mature TGF-β1 occurs to unwind the LAP straitjacket (Figure 4C). The plethora of structural data at hand support this mechanistic scenario.

mAb-mediated TGF-β1 activation *in vivo* reduces disease severity and increases survival in mice with graft versus host disease

Given that TCR-stimulated Tregs in humans and mice are known to express GARP:TGF-β1 complexes at their surface, we sought to determine whether the mAbs presented here could increase TGF-β1 activation and immunosuppression in a mouse model of a disease characterized by excessive T cell activity that is insufficiently controlled by Tregs. Graft versus host disease (GvHD) is a life-threatening side effect of allogeneic hematopoietic stem cell transplantation caused by donor T cells reacting against allogeneic antigens on recipient cells. We induced GvHD in mice by transplanting H-2^{b} (C57BL/6) splenocytes in H-2^{bd} F1 (C57BL/6 × DBA/2) recipients and treated the mice with TGF-β1-activating antibodies or controls (Figure 5A). Antibodies were administered once a week for 4 weeks, starting 1 day before cell transfer. H-2^{b} donor-derived T cells induced

CellPress
OPEN ACCESS

Cell Reports
Article

GvHD-like symptoms (GvHD score $\geq$1) within 10–20 days after transplantation in all recipient mice receiving control antibodies, leading to death of nearly all mice (72 of 74) by day 25 (Figure 5B). In contrast, approximately half of the mice treated with the activating LMT-10 or LMT-12 mAbs or the LMT-7/LMT-7* chimera experienced slower disease progression, reduced disease severity (GvHD score <4), or complete disease regression and long-term survival (Figure 5B). Notably, all mice treated with the activating antibodies developed GvHD-like symptoms early after cell transfer (days 9–20), indicating that donor alloreactive T cells had engrafted and that the therapeutic activity of the antibodies at later time points was not due to inhibition of donor T cell engraftment. Altogether, treatment with LMT-10, LMT-12, or LMT-7/LMT-7* significantly improved survival by comparison to IgG1, IgG1/IgG1*, and LMT-7/IgG1* controls (Figure 5C). Long-term survival induced by LMT-7/LMT-7* but not LMT-7/IgG1* indicates that, similar to TGF-β1 activation *in vitro* (Figure 2A), bivalent binding by mAbs is also required for their therapeutic activity *in vivo*.

Increased TGF-β1 activity and Treg numbers in spleens of mice treated with TGF-β1-activating mAbs

To search for signs of increased TGF-β1 activity *in vivo*, we repeated GvHD experiments that we interrupted on day 9 after transplantation to collect organs from recipient mice.

As a first readout, we measured levels of phosphorylated SMAD2 (pSMAD2) by western blot and expression of TGF-β1 target genes (*Smad7*, *Serpine1*, and *Col1a1*) by RT-qPCR. We observed significantly increased pSMAD2 and TGF-β1 target gene expression in the spleen after treatment with activating mAbs (Figure 6A). No such increase was observed in other organs (Figures S9A and S9B). No increase in active TGF-β1 levels was measured in the plasma of C57BL/6 mice 2, 6, or 24 h after administration of activating mAbs (Figure S9C). This suggests that mAb-mediated TGF-β1 activation occurs locally in the spleen but not in circulating blood.

As a second readout for increased TGF-β1 activity, we measured Treg numbers across various tissues. TGF-β1 signaling in secondary lymphoid organs such as the spleen is indeed known to drive the differentiation of activated naive CD4$^+$ T cells into peripheral Tregs (pTregs), which can then circulate to inflamed tissues. We observed a 1.5- to 2-fold increase in numbers of donor- and recipient-derived Tregs in the spleen of mice treated with activating mAbs, although the increase did not reach statistical significance for recipient-derived Tregs (Figure 6B). In a repeat experiment, similar trends for increased donor and recipient Tregs were observed in the spleen, mesenteric lymph nodes, and other organs, such as the liver (Figure S10). In line with increased Treg numbers in various organs, *Foxp3* mRNA levels were significantly increased in spleens and lungs after treatment with activating mAbs (Figure S11). In contrast to Tregs, numbers of CD4$^+$ or CD8$^+$ T cells and those of other immune cells were similar in all organs from mice receiving TGF-β1-activating or control mAbs (Figures 6B and S10).

GvHD is known to be associated with type 1 immune responses. As expected, expression of genes characteristic of Th1 and CTL activity (*Tbx21*, *Ifng*, *Gzmb*, or *Prf1*) was increased in most organs in mice with GvHD by comparison to C57BL/6 controls, whereas that of genes associated with Th2 and Th17 responses was not. In line with the observed reduction in GvHD severity, and although numbers of CD4$^+$ and CD8$^+$ T cells were not reduced, expression of Th1/CTL genes tended to decrease in mice receiving TGF-β1-activating mAbs (Figure S11).

Our observations suggest that, in mice with GvHD, activating mAbs can trigger TGF-β1 activation, at least in the spleen. This would favor local differentiation of naive CD4$^+$ T cells into pTregs, which would then circulate and accumulate in inflamed tissues to inhibit pathogenic Th1 and CTL activity without reducing the expansion of allo-reactive conventional T cells.

Pre-existing Tregs are required for TGF-β1-activating mAbs to exert therapeutic activity in mouse GvHD

Whereas on one hand increased TGF-β1 activity and consequent differentiation of CD4$^+$ T cells into Tregs may result in increased Treg numbers 9 days after treatment initiation, on the other hand, Tregs existing before transplantation in the graft or in recipients may serve as a source of latent TGF-β1 that can be activated by the mAbs.

To test whether pre-existing Tregs are required to mediate the therapeutic effects of TGF-β1-activating mAbs, we performed transplantation experiments using *H-2*$^{b/b}$ *Foxp3*$^{DTR/DTR}$ or *Foxp3*$^{WT/WT}$ females as splenocyte donors and *H-2*$^{b/d}$ *Foxp3*^{DTR} or *Foxp3*^{WT} males as recipients. We injected diphtheria toxin (DTx) at the time of transplantation to deplete pre-existing Tregs from donor, recipient, or both origins (Figures 7 and S12).[25] In all experiments, as expected, donor splenocytes induced GvHD, and LMT-12 increased survival when Tregs were not depleted (Figure 7, no DTx). In contrast, when both donor and recipient Tregs were depleted by DTx, the therapeutic activity of LMT-12 was lost, indicating that pre-existing Tregs are required to mediate this effect (Figure 7A). Loss of therapeutic activity was also observed when recipient Tregs, but not donor Tregs, were depleted by DTx (Figures 7B and 7C). This could indicate that pre-existing Tregs in recipients, but not donor Tregs present in the graft, are required for the therapeutic activity of the mAbs in mouse GvHD. Alternatively, it might reflect the fact that, at the time of transplantation, recipient Tregs vastly outnumber donor Tregs ($\sim$1.5 $\times$ 10^6 per graft) in recipient mice, which are not irradiated in this model. Pre-existing recipient Tregs thus represent a significantly larger reservoir of membrane-bound latent TGF-β1 than donor Tregs. Our results suggest that the latent TGF-β1 reservoir on the surface of pre-existing Tregs is required for activating mAbs to exert therapeutic activity in GvHD. TGF-β1 activity elicited by the mAbs *in vivo* may, in turn, drive differentiation of naive CD4$^+$ T cells into pTregs in secondary lymphoid organs, explaining the increased splenic Treg numbers observed 9 days after transplantation and treatment initiation (Figure 6B).

From the above, we conclude that TGF-β1 activation can be triggered by mAbs *in vivo* and could serve to treat diseases caused by excessive T cell activity. In mouse GvHD, the therapeutic effect requires the presence of Tregs.

DISCUSSION

The ubiquitous expression of TGF-β receptors across all cells and the pleiotropic nature of signaling mediated by TGF-β1

Cell Reports
Article

CellPress
OPEN ACCESS

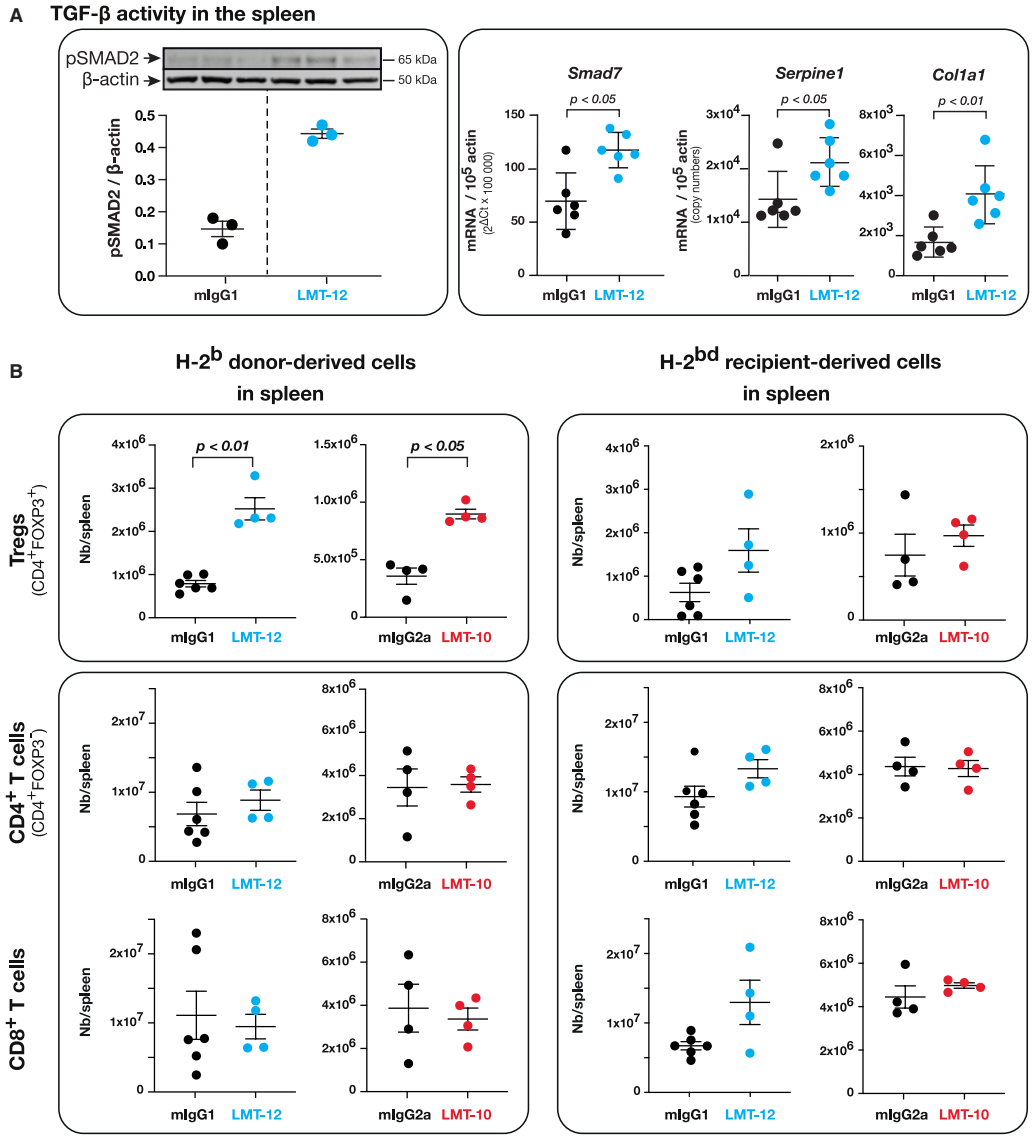

Figure 6. Increased TGF-β1 activity and Treg numbers in spleen of mice treated with TGF-β1-activating mAbs

GvHD was induced as indicated in Figure 5, except that recipient mice were euthanized 9 days after transplantation to collect spleens. Results from two independent experiments are shown in (A) and (B), respectively. Data points represent values measured in one individual mouse. Horizontal lines represent mean per group ± sem. Statistical analyses of *p* values were performed using an unpaired two-tailed Mann-Whitney test.

(A) Left: TGF-β1 signaling was analyzed by western blot with antibodies against pSMAD2 and β-actin. ECL signals were quantified to establish pSMAD2/β-actin ratios. Right: expression of TGF-β1 target genes was measured by RT-qPCR. Each lane in the western blot and data point in the graphs represent values measured in one individual mouse.

(B) Splenocytes were counted and analyzed by FC with antibodies against CD4, CD8, FOXP3, H-2D^d, and H-2K^b/H-2D^b to evaluate numbers of Tregs and CD8$^+$ and CD4$^+$ T cells of donor (H-2^b) and recipient (H-2^{bd}) origin.

CellPress
OPEN ACCESS

Cell Reports
Article

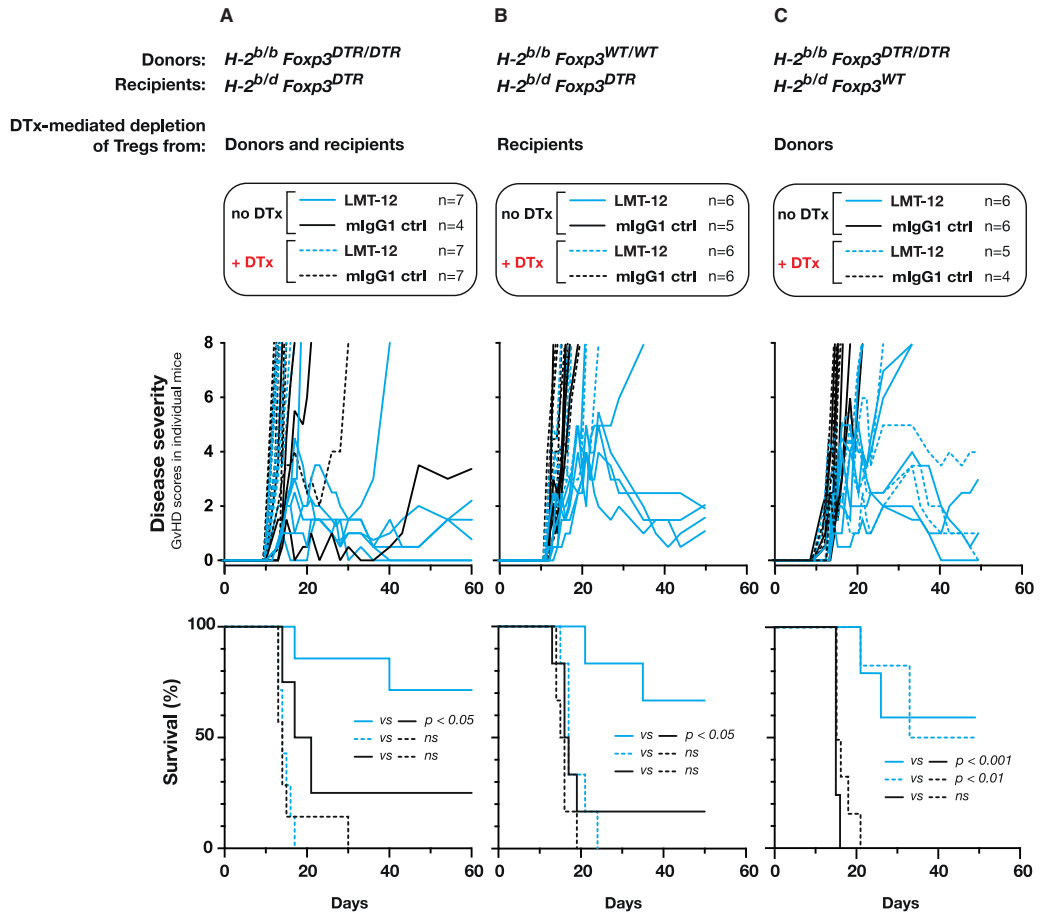

Figure 7. Tregs are required for the therapeutic effect of TGF-β1-activating mAbs

GvHD was induced in three independent experiments as described in Figure 5 by transplanting splenocytes from *H-2*$^{b/b}$ *Foxp3*$^{DTR/DTR}$ or *Foxp3*$^{WT/WT}$ female donors to *H-2*$^{b/d}$ *Foxp3*^{DTR} or *Foxp3*^{WT} male recipients on day 0.

DTx was injected into donors, recipients, or both between day −1 and +1 to deplete Tregs of donor, recipient, or both origins, as illustrated in Figure S12. Graphs at the top show evolution of GvHD scores in individual mice. Graphs at the bottom show Kaplan-Meier plots representing the proportion of mice alive on the indicated days after transplantation. *p* values were calculated using a Gehan-Breslow Wilcoxon test.

imposes tightly regulated maintenance of TGF-β1 latency under homeostatic conditions. To date, all mAbs developed to therapeutically target TGF-β1 aim at blocking its immunosuppressive, pro-tumoral, and pro-fibrotic activities in the context of cancer or fibrosis. The mAbs described here do the opposite: they activate latent TGF-β1 presented by a transmembrane protein on the cell surface, providing a targeted pharmacological approach to increase immunosuppression in the context of inflammatory or immune-related diseases.

Our biochemical and structural analyses of TGF-β1 binding and activation by mAbs, Fabs, and chimeric antibodies have not only shed light on the pathological context in which the mAbs could exert therapeutic activity but also on the physiological mechanism of TGF-β1 activation by integrins in mammals. Three important observations need to be considered: (1) in contrast to the bivalent activating mAbs and chimeras, the corresponding monovalent Fabs and chimeras cannot activate latent TGF-β1, (2) TGF-β1 activation by mAbs requires an active cytoskeleton and anchorage of latent TGF-β1 at the cell surface via a transmembrane protein such as GARP or LRRC33, and (3) the binding mode of two Fabs derived from an activating mAb to one GARP:TGF-β1 complex sterically excludes the possibility

Cell Reports
Article

CellPress
OPEN ACCESS

that the two Fabs can originate from the same mAb molecule *in vivo*. Therefore, a mAb can only activate TGF-β1 *in vivo* by crosslinking two distinct latent TGF-β1 molecules presented at the cell surface by transmembrane proteins such as GARP or LRRC33.

A major implication of these observations for translation into the clinic is that such activating mAbs are not expected to activate soluble latent TGF-β1 circulating in the blood or other biological fluids but will only activate TGF-β1 presented at a high density on the surface of single cells or in tissues abundantly infiltrated by spatially connected cells. This allows for specific targeting and activation of latent TGF-β1 presented by GARP or LRRC33 on the surface of immune cells such as TCR-stimulated Tregs or myeloid cells, respectively. Even though endothelial cells also express GARP:TGF-β1 on their surface and might serve as TGF-β1 reservoirs amenable to activation by therapeutic mAbs, activation of latent TGF-β1 by mAbs on the surface of endothelial cells was not sufficient to exert therapeutic activity in the absence of Tregs in mouse GvHD experiments. Furthermore, our *in vitro* experiments indicate that cell-free reservoirs of latent TGF-β1 deposited in the extracellular matrix via covalent binding to LTBPs would not be amenable to mAb-mediated activation. Altogether, the data presented here suggest that activating mAbs can exert potent immunosuppressive therapeutic activity *in vivo* in a Treg-dependent manner.

Another implication of our observations pertains to the molecular machinery of TGF-β1 activation: high-affinity binding to the two LAP monomers from a single latent TGF-β1 molecule is not sufficient to activate the cytokine, even when binding occurs close to the RGD motifs and dimerization interface. Activation requires profound conformational changes to allow access of the mature TGF-β1 dimer to the TβRI:TβRII heterotetrameric receptor. These changes include not only unmasking mature TGF-β1 residues from the LAP latency lasso to allow interaction with TβRII but also modification of the mature TGF-β1 helix α3 fixed by LAP α1 in a position precluding interaction with TβRI. Recently, elucidation of the cryo-EM structure of one $\alpha_V\beta_8$ ectodomain bound to a latent TGF-β1 dimer led to the suggestion that flexibility in TGF-β1 and integrin molecules in the complex is sufficient to expose mature TGF-β1 to a minimal TGF-β receptor comprising a single TβRI:TβRII heterodimer instead of the conventional TβRI:TβRII heterotetramer without complete dissociation of mature TGF-β1 from LAP. The authors suggested that this would result in a minimal TGF-β1 signaling cascade.[15] However, helix α3 of mature TGF-β1 in that structural analysis is in the same position as that observed here and in previously reported structures of latent TGF-β1, free or bound to GARP, LRRC33, or a Fab.[6,14,26] Therefore, this conformation is grossly incompatible with the proposed interaction between helix α3 in mature TGF-β1 and a TβRI receptor chain upon binding by a single $\alpha_V\beta_8$ due to severe steric clashes with helix α1 of LAP. Thus, we propose that TGF-β1 activation requires crosslinking of two membrane-bound latent TGF-β1 by one mAb or, alternatively, crosslinking of two membrane-bound integrins by one latent TGF-β1. This would allow the exertion of cellular forces in opposite directions, leading to unwinding of LAP and profoundly modify the conformation of TGF-β1, as suggested previously.[13] Our proposed model is compatible with recent work by Duan et al., who reported a more efficient activation of TGF-β1 presented by GARP or LRRC33 upon binding of two $\alpha_V\beta_8$ molecules rather than one.[26] Our mechanistic proposal also implies that latent TGF-β1 reservoirs deposited in cell-free extracellular matrix would not be activated by soluble activating mAbs, avoiding massive release of active TGF-β1 in tissues that are not inflamed or infiltrated by immune cells.

Our data from a murine model of GvHD indicate that TGF-β1-activating mAbs may serve to treat patients with severe alloreactive immune responses observed during allogeneic hematopoietic stem cell or solid organ transplantation. Several severe autoimmune or inflammatory diseases for which efficient treatments are still lacking, including systemic lupus erythematosus or inflammatory bowel disease, could also benefit from this novel therapeutic approach. Autoimmune diseases driven by Th17 cells, such as multiple sclerosis, would not qualify for these types of treatments *a priori* due to the role played by TGF-β1 in Th17 differentiation. Due attention will also need to be given to the development of fibrosis, which often accompanies chronic inflammatory diseases and could be favored by persistent TGF-β1 activity.

Collectively, our findings pave the way for clinical trials with TGF-β1-activating mAbs to investigate a targeted immunosuppressive therapy for diseases characterized by excessive immune activity insufficiently controlled by Tregs or TGF-β1.

Limitations of the study

We did not observe therapeutic activity with TGF-β1-activating mAbs in three murine models of autoimmunity. The activating mAbs did not improve autoimmune colitis induced by the transfer of Treg-depleted naive $CD4^+$ T cells in *Rag1*$^{-/-}$ mice. When Tregs were co-transferred with naive T cells at a 1 Treg to 10 naive T cell ratio, Tregs were still completely protective against colitis, leaving no room to observe an additive therapeutic effect of the activating mAbs. We also tested the mAbs in lupus-prone mice (*B6.Sle1.2.3*[27,28]), but long-term (>8 months) treatment did not delay or reduce development of glomerulonephritis or appearance of anti-dsDNA auto-antibodies. Activating mAbs also did not exert therapeutic activity in experimental autoimmune encephalitis (EAE). Interestingly however, the mAbs did not exacerbate inflammation or disease in any of these pro-inflammatory settings, including in EAE. It should also be noted that GvHD, in which we did observe therapeutic activity of the mAbs, shares significant features with autoimmune diseases. Nevertheless, we are pursuing our search for a model of autoimmune disease in which the TGF-β1-activating mAbs would exert therapeutic activity.

RESOURCE AVAILABILITY

Lead contact

Requests for further information, resources, and reagents should be directed to and will be fulfilled by the lead contact, Sophie Lucas (sophie.lucas@uclouvain.be).

Materials availability

Unique/stable reagents generated in this study are available from the lead contact upon signature of a material transfer agreement.

CellPress
OPEN ACCESS

Cell Reports
Article

Data and code availability

- All data associated with this study are available in the main text or the supplemental information. Cryo-EM maps of human and mouse GARP:TGF-β1:Fab complexes and corresponding structural models were deposited in the EMDB/PDB with accession codes EMDB: EMD-19110/PDB: 8REW and EMDB: EMD-19111/PDB: 8REX, respectively.
- No code was generated.
- Any additional information required to reanalyze the data reported in this paper is available from the lead contact upon request.

ACKNOWLEDGMENTS

This work was supported by grants from the Fondation contre le Cancer (2020-079), the Actions de Recherche Concertées (grant 19/24-098), the Fonds National de la Recherche Scientifique (PDR number 40003225), the F.N.R.S.-Télévie (PDR-TLV numbers 35005213 and 40007289), and the Flanders Institute for Biotechnology (VIB, grant nr. C0101 to S.N.S.). This work was also supported by grants from the WEL Research Institute (WELBIO department), Wavre, Belgium (CR-2019A-02 and CR-2019A-02R). F.L. was supported by a fellowship from the UCLouvain and by a fellowship from Salus Sanguinis, Belgium. S.W. is a research fellow with the F.N.R.S. M.J. is supported by a Télévie fellowship (F.R.S.-F.N.R.S.). E.D. and C.M. are postdoctoral researchers with the F.N.R.S. We thank the VIB-VUB facility for Bio Electron Cryogenic Microscopy (BECM) for infrastructural access and Marcus Fislage for technical support. We thank Wouter Van Putte (PUXANO, Belgium) for providing and screening graphene-coated EM grids.

AUTHOR CONTRIBUTIONS

S.W., F.L., and S.L. conceived and designed the overall project. L.M., M.L., and B.v.d.W. derived mAbs by phage display and designed constructs to express and purify recombinant protein complexes. F.L. developed the screening assay to identify activating mAbs and performed detailed epitope mapping analyses. F.L., S.W., C.M., and M.J. identified the requirements for mAb-mediated activation *in vitro*. F.L., S.W., C.M., M.G., and E.D. designed and performed the murine GvHD experiments *in vivo*. J.F. and S.N.S. performed cryo-EM (grid preparation, specimen screening, and data collection) and analyzed the data (image processing and model building and refinement). S.W., F.L., J.F., S.N.S., and S.L. wrote the manuscript with input from all authors.

DECLARATION OF INTERESTS

L.M., B.v.d.W., and M.L. are full-time employees of argenx. Patents pertaining to activating antibodies against TGF-β1 have been filed under the Patent Cooperation Treaty (international application number PCT/EP2023/056082) with S.L., F.L., L.M., and B.v.d.W. as inventors and UCLouvain as applicant.

STAR★METHODS

Detailed methods are provided in the online version of this paper and include the following:

- KEY RESOURCES TABLE
- EXPERIMENTAL MODEL AND STUDY PARTICIPANT DETAILS
  - 293T and 293T-TGFB1 KO cells
  - Murine Tregs
  - Mice
- METHOD DETAILS
  - mAbs directed against human and mouse latent TGF-β1
  - TGF-β1 reporter assays
  - Short-term TCR-stimulation of murine tregs *in vitro*
  - Western blot analyses
  - Epitope mapping
  - Recombinant protein expression and purification
  - Cryo-electron microscopy (cryo-EM)
  - Cryo-EM image processing
  - Cryo-EM model building and refinement
  - Cryo-EM Data availability
  - Induction and scoring of murine graft-versus-host disease
  - Flow cytometry
  - Real-time quantitative polymerase chain reaction
  - Enzyme-linked immunosorbant assay ELISA
- QUANTIFICATION AND STATISTICAL ANALYSIS

SUPPLEMENTAL INFORMATION

Supplemental information can be found online at https://doi.org/10.1016/j.celrep.2025.116061.

Received: December 20, 2024
Revised: February 27, 2025
Accepted: July 7, 2025
Published: July 29, 2025

REFERENCES

1. Kulkarni, A.B., Huh, C.G., Becker, D., Geiser, A., Lyght, M., Flanders, K.C., Roberts, A.B., Sporn, M.B., Ward, J.M., and Karlsson, S. (1993). Transforming growth factor beta 1 null mutation in mice causes excessive inflammatory response and early death. Proc. Natl. Acad. Sci. USA *90*, 770–774. https://doi.org/10.1073/pnas.90.2.770.
2. Shull, M.M., Ormsby, I., Kier, A.B., Pawlowski, S., Diebold, R.J., Yin, M., Allen, R., Sidman, C., Proetzel, G., Calvin, D., et al. (1992). Targeted disruption of the mouse transforming growth factor-beta 1 gene results in multifocal inflammatory disease. Nature *359*, 693–699. https://doi.org/10.1038/359693a0.
3. Marie, J.C., Liggitt, D., and Rudensky, A.Y. (2006). Cellular mechanisms of fatal early-onset autoimmunity in mice with the T cell-specific targeting of transforming growth factor-beta receptor. Immunity *25*, 441–454. https://doi.org/10.1016/j.immuni.2006.07.012.
4. Travis, M.A., and Sheppard, D. (2014). TGF-beta activation and function in immunity. Annu. Rev. Immunol. *32*, 51–82. https://doi.org/10.1146/annurev-immunol-032713-120257.
5. ten Dijke, P., and Arthur, H.M. (2007). Extracellular control of TGFbeta signalling in vascular development and disease. Nat. Rev. Mol. Cell Biol. *8*, 857–869.
6. Shi, M., Zhu, J., Wang, R., Chen, X., Mi, L., Walz, T., and Springer, T.A. (2011). Latent TGF-β structure and activation. Nature *474*, 343–349. https://doi.org/10.1038/nature10152.
7. Edwards, J.P., Thornton, A.M., and Shevach, E.M. (2014). Release of active TGF-β1 from the latent TGF-β1/GARP complex on T regulatory cells is mediated by integrin β8. J. Immunol. *193*, 2843–2849. https://doi.org/10.4049/jimmunol.1401102.
8. Stockis, J., Colau, D., Coulie, P.G., and Lucas, S. (2009). Membrane protein GARP is a receptor for latent TGF-β on the surface of activated human Treg. Eur. J. Immunol. *39*, 3315–3322.
9. Stockis, J., Fink, W., François, V., Connerotte, T., de Smet, C., Knoops, L., van der Bruggen, P., Boon, T., Coulie, P.G., and Lucas, S. (2009). Comparison of stable human Treg and Th clones by transcriptional profiling. Eur. J. Immunol. *39*, 869–882.
10. Stockis, J., Lienart, S., Colau, D., Collignon, A., Nishimura, S.L., Sheppard, D., Coulie, P.G., and Lucas, S. (2017). Blocking immunosuppression by human Tregs in vivo with antibodies targeting integrin alphaVbeta8. Proc. Natl. Acad. Sci. USA *114*, E10161–E10168. https://doi.org/10.1073/pnas.1710680114.
11. Cuende, J., Lienart, S., Dedobbeleer, O., van der Woning, B., De Boeck, G., Stockis, J., Huygens, C., Colau, D., Somja, J., Delvenne, P., et al. (2015). Monoclonal antibodies against GARP/TGF-beta1 complexes inhibit the

Cell Reports
Article

CellPress
OPEN ACCESS

immunosuppressive activity of human regulatory T cells in vivo. Sci. Transl. Med. *7*, 284ra256. https://doi.org/10.1126/scitranslmed.aaa1983.

12. Qin, Y., Garrison, B.S., Ma, W., Wang, R., Jiang, A., Li, J., Mistry, M., Bronson, R.T., Santoro, D., Franco, C., et al. (2018). A Milieu Molecule for TGF-beta Required for Microglia Function in the Nervous System. Cell *174*, 156–171. https://doi.org/10.1016/j.cell.2018.05.027.
13. Dong, X., Zhao, B., Iacob, R.E., Zhu, J., Koksal, A.C., Lu, C., Engen, J.R., and Springer, T.A. (2017). Force interacts with macromolecular structure in activation of TGF-beta. Nature *542*, 55–59. https://doi.org/10.1038/nature21035.
14. Liénart, S., Merceron, R., Vanderaa, C., Lambert, F., Colau, D., Stockis, J., van der Woning, B., De Haard, H., Saunders, M., Coulie, P.G., et al. (2018). Structural basis of latent TGF-beta1 presentation and activation by GARP on human regulatory T cells. Science *362*, 952–956. https://doi.org/10.1126/science.aau2909.
15. Campbell, M.G., Cormier, A., Ito, S., Seed, R.I., Bondesson, A.J., Lou, J., Marks, J.D., Baron, J.L., Cheng, Y., and Nishimura, S.L. (2020). Cryo-EM Reveals Integrin-Mediated TGF-beta Activation without Release from Latent TGF-beta. Cell *180*, 490–501. https://doi.org/10.1016/j.cell.2019.12.030.
16. de Streel, G., and Lucas, S. (2021). Targeting immunosuppression by TGF-beta1 for cancer immunotherapy. Biochem. Pharmacol. *192*, 114697. https://doi.org/10.1016/j.bcp.2021.114697.
17. Bertrand, C., Van Meerbeeck, P., de Streel, G., Vaherto-Bleeckx, N., Benhaddi, F., Rouaud, L., Noël, A., Coulie, P.G., van Baren, N., and Lucas, S. (2021). Combined Blockade of GARP:TGF-beta1 and PD-1 Increases Infiltration of T Cells and Density of Pericyte-Covered GARP(+) Blood Vessels in Mouse MC38 Tumors. Front. Immunol. *12*, 704050. https://doi.org/10.3389/fimmu.2021.704050.
18. Lecomte, S., Devreux, J., de Streel, G., van Baren, N., Havelange, V., Schröder, D., Vaherto, N., Vanhaver, C., Vanderaa, C., Dupuis, N., et al. (2023). Therapeutic activity of GARP:TGF-beta1 blockade in murine primary myelofibrosis. Blood *141*, 490–502. https://doi.org/10.1182/blood.2022017097.
19. Oida, T., and Weiner, H.L. (2010). Overexpression of TGF-ss 1 gene induces cell surface localized glucose-regulated protein 78-associated latency-associated peptide/TGF-ss. J. Immunol. *185*, 3529–3535. https://doi.org/10.4049/jimmunol.0904121.
20. de Streel, G., Bertrand, C., Chalon, N., Liénart, S., Bricard, O., Lecomte, S., Devreux, J., Gaignage, M., De Boeck, G., Mariën, L., et al. (2020). Selective inhibition of TGF-beta1 produced by GARP-expressing Tregs overcomes resistance to PD-1/PD-L1 blockade in cancer. Nat. Commun. *11*, 4545. https://doi.org/10.1038/s41467-020-17811-3.
21. Edwards, J.P., Fujii, H., Zhou, A.X., Creemers, J., Unutmaz, D., and Shevach, E.M. (2013). Regulation of the expression of GARP/latent TGF-beta1 complexes on mouse T cells and their role in regulatory T cell and Th17 differentiation. J. Immunol. *190*, 5506–5515. https://doi.org/10.4049/jimmunol.1300199.
22. Hui, G.K., Gardener, A.D., Begum, H., Eldrid, C., Thalassinos, K., Gor, J., and Perkins, S.J. (2019). The solution structure of the human IgG2 subclass is distinct from those for human IgG1 and IgG4 providing an explanation for their discrete functions. J. Biol. Chem. *294*, 10789–10806. https://doi.org/10.1074/jbc.RA118.007134.
23. Zhang, X., Zhang, L., Tong, H., Peng, B., Rames, M.J., Zhang, S., and Ren, G. (2015). 3D Structural Fluctuation of IgG1 Antibody Revealed by Individual Particle Electron Tomography. Sci. Rep. *5*, 9803. https://doi.org/10.1038/srep09803.
24. Stanfield, R.L., Zemla, A., Wilson, I.A., and Rupp, B. (2006). Antibody elbow angles are influenced by their light chain class. J. Mol. Biol. *357*, 1566–1574. https://doi.org/10.1016/j.jmb.2006.01.023.
25. Kim, J.M., Rasmussen, J.P., and Rudensky, A.Y. (2007). Regulatory T cells prevent catastrophic autoimmunity throughout the lifespan of mice. Nat. Immunol. *8*, 191–197.
26. Duan, Z., Lin, X., Wang, L., Zhen, Q., Jiang, Y., Chen, C., Yang, J., Lee, C. H., Qin, Y., Li, Y., et al. (2022). Specificity of TGF-beta1 signal designated by LRRC33 and integrin alpha(V)beta(8). Nat. Commun. *13*, 4988. https://doi.org/10.1038/s41467-022-32655-9.
27. Morel, L., Croker, B.P., Blenman, K.R., Mohan, C., Huang, G., Gilkeson, G., and Wakeland, E.K. (2000). Genetic reconstitution of systemic lupus erythematosus immunopathology with polycongenic murine strains. Proc. Natl. Acad. Sci. USA *97*, 6670–6675. https://doi.org/10.1073/pnas.97.12.6670.
28. Tilman, G., Dupre, E., Watteyne, L., Baert, C.A., Nolf, D., Benhaddi, F., Lambert, F., Daumerie, A., Bouzin, C., Lucas, S., and Limaye, N. (2023). p16(Ink4a), a marker of cellular senescence, is associated with renal disease in the B6.NZMSle1/Sle2/Sle3 mouse model of lupus. Lupus Sci. Med. *10*, e001010. https://doi.org/10.1136/lupus-2023-001010.
29. Ran, F.A., Hsu, P.D., Wright, J., Agarwala, V., Scott, D.A., and Zhang, F. (2013). Genome engineering using the CRISPR-Cas9 system. Nat. Protoc. *8*, 2281–2308. https://doi.org/10.1038/nprot.2013.143.
30. Bruhns, P. (2012). Properties of mouse and human IgG receptors and their contribution to disease models. Blood *119*, 5640–5649. https://doi.org/10.1182/blood-2012-01-380121.
31. Labrijn, A.F., Meesters, J.I., Bunce, M., Armstrong, A.A., Somani, S., Nesspor, T.C., Chiu, M.L., Altintaş, I., Verploegen, S., Schuurman, J., and Parren, P.W.H.I. (2017). Efficient Generation of Bispecific Murine Antibodies for Pre-Clinical Investigations in Syngeneic Rodent Models. Sci. Rep. *7*, 2476. https://doi.org/10.1038/s41598-017-02823-9.
32. Dennler, S., Itoh, S., Vivien, D., ten Dijke, P., Huet, S., and Gauthier, J.M. (1998). Direct binding of Smad3 and Smad4 to critical TGF beta-inducible elements in the promoter of human plasminogen activator inhibitor-type 1 gene. EMBO J. *17*, 3091–3100. https://doi.org/10.1093/emboj/17.11.3091.
33. Naydenova, K., and Russo, C.J. (2017). Measuring the effects of particle orientation to improve the efficiency of electron cryomicroscopy. Nat. Commun. *8*, 629. https://doi.org/10.1038/s41467-017-00782-3.
34. Punjani, A., Rubinstein, J.L., Fleet, D.J., and Brubaker, M.A. (2017). cryoSPARC: algorithms for rapid unsupervised cryo-EM structure determination. Nat. Methods *14*, 290–296. https://doi.org/10.1038/nmeth.4169.
35. Liebschner, D., Afonine, P.V., Baker, M.L., Bunkóczi, G., Chen, V.B., Croll, T.I., Hintze, B., Hung, L.W., Jain, S., McCoy, A.J., et al. (2019). Macromolecular structure determination using X-rays, neutrons and electrons: recent developments in Phenix. Acta Crystallogr. D Struct. Biol. *75*, 861–877. https://doi.org/10.1107/S2059798319011471.
36. Sanchez-Garcia, R., Gomez-Blanco, J., Cuervo, A., Carazo, J.M., Sorzano, C.O.S., and Vargas, J. (2021). DeepEMhancer: a deep learning solution for cryo-EM volume post-processing. Commun. Biol. *4*, 874. https://doi.org/10.1038/s42003-021-02399-1.
37. Emsley, P., Lohkamp, B., Scott, W.G., and Cowtan, K. (2010). Features and development of Coot. Acta Crystallogr. D Biol. Crystallogr. *66*, 486–501. https://doi.org/10.1107/S0907444910007493.
38. Pettersen, E.F., Goddard, T.D., Huang, C.C., Meng, E.C., Couch, G.S., Croll, T.I., Morris, J.H., and Ferrin, T.E. (2021). UCSF ChimeraX: Structure visualization for researchers, educators, and developers. Protein Sci. *30*, 70–82. https://doi.org/10.1002/pro.3943.
39. Lin, Z., Akin, H., Rao, R., Hie, B., Zhu, Z., Lu, W., Smetanin, N., Verkuil, R., Kabeli, O., Shmueli, Y., et al. (2023). Evolutionary-scale prediction of atomic-level protein structure with a language model. Science *379*, 1123–1130. https://doi.org/10.1126/science.ade2574.
40. Kidmose, R.T., Juhl, J., Nissen, P., Boesen, T., Karlsen, J.L., and Pedersen, B.P. (2019). Namdinator - automatic molecular dynamics flexible fitting of structural models into cryo-EM and crystallography experimental maps. IUCrJ *6*, 526–531. https://doi.org/10.1107/S2052252519007619.

CellPress
OPEN ACCESS

Cell Reports
Article

STAR★METHODS

KEY RESOURCES TABLE

REAGENT or RESOURCE	SOURCE	IDENTIFIER
Antibodies		
LHT-1 to 24: Llama anti-human latent TGF-β1	This paper	N/A
LMT-1 to 14: Llama anti-mouse latent TGF-β1	This paper	N/A
IgG1/IgG1*: chimeric antibody	This paper	N/A
LMT-7/IgG1*: chimeric antibody	This paper	N/A
LMT-7/LMT-7*: chimeric antibody	This paper	N/A
1D11: anti- TGF-β1,2,3	R&D System	Cat#MAB1835; RRID: AB_357931
mIgG1 isotype control (Motavizumab)	ImmunoPrecise Antibodies Ltd	N/A
AF700 rat anti-mouse CD45, clone 30-F11	Biolegend	Cat#103127; RRID: AB_493714
BV711 rat anti-mouse CD3, clone 17A2	Biolegend	Cat#100241; RRID: AB_2563945
BV510 rat anti-mouse CD4, clone RM4-5	Biolegend	Cat#100559; RRID: AB_2561388
PerCP rat anti-mouse CD8a, clone 53–6.7	BD Pharmigen	Cat#553036; RRID: AB_394573
APC rat anti-mouse Foxp3, clone FJK-16s	eBioscience	Cat#17-5773-82; RRID: AB_469457
APC rat IgG2a isotype control, clone eBR2a	ThermoFisher Scientific	Cat#17-4321-81; RRID: AB_470181
FITC mouse anti-mouse H-2Dd, clone 34-2-12	Biolegend	Cat#110606; RRID: AB_313487
PE mouse anti-mouse H-2Kb/H-2Db, clone 28-8-6	Biolegend	Cat#114607; RRID: AB_313598
PE/Cyanine 7 rat anti-mouse CD49b, clone DX5	Biolegend	Cat#108922; RRID: AB_2561459
BV785 hamster anti-mouse CD11c, clone N418	Biolegend	Cat#117335; RRID: AB_11219204
BV650 rat anti-mouse/human CD45R/B220, clone RA3-6B2	Biolegend	Cat#103241; RRID: AB_11204069
BV421 rat anti-mouse CD19, clone 6D5	Biolegend	Cat#115538; RRID: AB_10895761
Rat anti-mouse CD16/CD32 (TruStain FcX), clone 93	Biolegend	Cat#101320; RRID: AB_1574973
Rabbit anti-phospho-SMAD2, clone 138D4	Cell Signaling	Cat#3108; RRID: AB_10117720
Rabbit anti-βactin, clone D6A8	Cell Signaling	Cat#8457; RRID: AB_10950489
Sheep anti-mouse GARP, polyclonal	R&D System	Cat#AF6229
HRP donkey anti-sheep IgG, polyclonal	R&D System	Cat#HAF016; RRID: AB_562591
HRP goat anti-rabbit IgG, polyclonal	Cell Signaling	Cat#7074; RRID: AB_2099233
HRP goat anti-mouse IgG-light-chain, polyclonal	Jackson	Cat#115-035-174; RRID: AB_2338512
HRP goat anti-rat IgG, polyclonal	Cell Signaling	Cat#7077; RRID: AB_10694715
HRP goat anti-mouse IgG, polyclonal	R&D System	Cat#HAF007; RRID: AB_357234
Mouse anti-HA, clone 16B12	Eurogentec	Cat#MMS-101R; RRID: AB_2820200
Mouse anti-HA, clone GG8-1F3.3.1	Miltenyi	Cat#130-092-257; RRID: AB_871939
Rat anti-mouse/human mature TGF-β1, clone A75-2	BD Bioscience	Cat#555052; RRID: AB_395673
PE goat anti-mouse IgG, polyclonal	Biolegend	Cat#405307; RRID: AB_315010
APC anti-mouse LAP, clone TW7-16B4	Biolegend	Cat#141406; RRID: AB_10898159
PE anti-mouse GARP, clone YGIC86	eBioscience	Cat#12-9891-82; RRID: AB_1963598
Chemicals, peptides, and recombinant proteins		
Penicillin/Streptomycin	Sigma Aldrich	Cat#P4333
Diphtheria Toxin	Sigma Aldrich	Cat#D0654
Human recombinant TGF-β1	R&D System	Cat#240-B
DMEM	Gibco	Cat#10938
IMDM	Gibco	Cat#21980
X-vivo	Lonza	Cat#04-380Q
Fetal Bovine Serum	Cytiva	Cat#SV30160.03
Glutamax	Gibco	Cat#35050
Opti-MEM	Gibco	Cat#51985

(*Continued on next page*)

CellPress
OPEN ACCESS

Continued

REAGENT or RESOURCE	SOURCE	IDENTIFIER
Dual-Glo System	Promega	Cat#E2940
Acridine Orange/Propidium Iodide Stain	Logos Biosystem	Cat#F23001
Dynabeads™ mouse T-activator CD3/CD28	ThermoFisher Scientific	Cat#11452D
StrepTactin Sepharose High Performance beads	GE Healthcare	Cat#28-9355-99
Foxp3/Transcription factor/fixation/Permeabilization concentrate and diluate	eBioscience	Cat#00552100
CountBright Absolute Counting beads	Invitrogen	Cat#C36950
Latrunculin-a	Merck Life Science	Cat#428021
Cytochalazin-d	Merck Life Science	Cat#C2618
Fixable Viability Dye eFluor™	eBioscience	Cat#65-0865-14
TransIT-LT1	Mirus Bio	Cat#MIR2360
StrepTactin Sepharose High Performance beads	GE Healthcare	Cat#28-9355-99
Takyon™ Low ROX Probe 2x Master mix dTTP blue	Eurogentec	Cat#UF-LPMT-B0710
SuperSignal West Pico PLUS Chemiluminescent Substrate	Thermofisher Scientific	Cat#34578
SuperSignal West Femto Maximum Sensitivity Substrate	Thermofisher Scientific	Cat#34096
Bolt LDS sample buffer	Thermofisher Scientific	Cat#B0007
Bolt reducing Agent	Thermofisher Scientific	Cat#B0009
Red Blood Cell lysing Buffer (10X)	Invitrogen	Cat#00-4300-54
Krebs-Ringer buffer	Thermofisher Scientific	Cat#J67795-K2
Collagenase IV	Thermofisher Scientific	Cat#17104019
Dnase I	Roche	Cat#10104159001
HBBS (CaCl2 MgCl2)	Thermofisher Scientific	Cat#15266355
DTT	Sigma Aldrich	Cat#D0632
Percoll	GE Healthcare	Cat#GE17-0891-02
Laemmli buffer	Bio-Rad	Cat#161-0737
2-mercapto-ethanol	Bio-Rad	Cat#161-0710
Orthovanadate	Biolab	Cat#P0758
Halt protease inhibitor cocktail	Thermofisher Scientific	Cat#1861278
PMSF	Thermofisher Scientific	Cat#36978
Tween 20	Sigma Aldrich	Cat#P2287
Trypsin 0,25%-EDTA in HBSS	Biowest	Cat#L0931-100
UltraPure 0.5M EDTA	Life technologies	Cat#15575
RNA later	Invitrogen	Cat#AM7021
Critical commercial assays		
Q5 Site-Directed Mutagenesis kit	NEB	N/A
Human/Mouse TGF-β1 uncoated ELISA kit	Invitrogen	Cat#88-8350-88
NucleoSpin RNA, Mini kit for RNA purification	Macherey Nagel	Cat#740955
Maxima First Strand cDNA Synthesis Kit	Thermofisher Scientific	Cat#K1672
Miltenyi MACS CD25 MicroBeads kit	Miltenyi	Cat#130-091-072
Experimental models: Cell lines		
293T *TGFB1* KO cells	This paper	N/A
Experimental models: Organisms/strains		
Mouse: C57BL/6: C57BL/6J Ola Hsd	Harlan Laboratories	MGI ID: 4459305
Mouse: DBA/2: DBA/2 Ola Hsd	Harlan Laboratories	MGI ID: 3510418
Mouse: C57BL/6 *Foxp3*^{DTR}: B6.129(Cg)-*Foxp3*$^{tm3(Hbegf/GFP)Ayr}$/J strain	Jackson Laboratory	MGI ID: 3698131
Mouse: F1: C57BL/6 x DBA/2	This paper	N/A
Mouse: F1 *Foxp3*^{DTR}: C57BL/6 *Foxp3*$^{DTR/DTR}$ x DBA/2	This paper	N/A
Mouse: Foxp3$^{YFP-Cre}$ (B6.129(Cg)-*Foxp3*$^{tm4(YFP/icre)Ayr}$/J)	Jackson Laboratory	RRID: IMSR_JAX:016959

(*Continued on next page*)

CellPress
OPEN ACCESS

Cell Reports
Article

Continued

REAGENT or RESOURCE	SOURCE	IDENTIFIER
Recombinant DNA		
pCAGA-12-Fluc[11]	Kindly given by Aris Moustakas	N/A
pRL-TK	Promega	Cat#E2241
pDisplay	Kindly given by Laure Dumoutier	N/A
pcDNA3.1/V5-His-TOPO	Kindly given by Thomas Michiels	N/A
Latent TGF-β1: *pEF-BOS-puro-mTgfb1(cDNA)*	This paper	N/A
$GARP_{FL}$: *pDisplay-HA-mGarp(21–663)*	This paper	N/A
$GARP_{\Delta TM}$: *pcDNA3-Garp*$_{\Delta TM}$	This paper	N/A
LRRC33: *pDisplay-HA-mLrrc33(ORF)*	This paper	N/A
LTBP: *pcDNA3-mLtbp1(cDNA)*	VectorBuilder	N/A
Software and algorithms		
GraphPad Prism version 10	GraphPad Software	https://www.graphpad.com/
FlowJo v10	Tree Star	https://www.flowjo.com/
Adobe Illustrator 2022, 26.5	Adobe, inc	https://www.adobe.com
Design and analysis software for qPCR	ThermoFisher Scientific	https://apps.thermofisher.com/apps/da2/#/home/welcome
Bio1D software	Vilber-Lourmat	N/A
MacVector Software	MacVector, inc	N/A
Fusion Capt Advance Solo 4S	Vilber-Lourmat	N/A
BD FACSDiva™ Software	BD Biosciences	https://www.bdbiosciences.com/
Other		
LS column	Miltenyi	Cat#130-042-401
Superdex 200 HiLoad 16/600 column	GE Healthcare	Cat#GE28-9893-35
LUNA-FL™ Dual Fluorescence Cell Counter	Logos biosystems	Cat#L20001
NanoDrop 2000c	ThermoFisher Scientific	Cat#ND-2000C
Microson Ultrasonic cell disruptor	Misonix	N/A
Bolt 4–12% Bis-tris gels	ThermoFisher Scientific	Cat#NW04122BOX
iBlot™ 2 Transfer Stacks, nitrocellulose, regular size	ThermoFisher Scientific	Cat#IB23001X3
Fusion solo s	Vilber-Lourmat	N/A
gentleMACS™ C Tubes	Miltenyi Biotec	Cat#130-096-334
gentleMACS™ Dissociator	Miltenyi Biotec	Cat#130-093-235

EXPERIMENTAL MODEL AND STUDY PARTICIPANT DETAILS

293T and 293T-TGFB1 KO cells

The HEK 293T adherent cell line (referred to herein as 293T cells) was cultured at 37°C, 8% CO_2 in DMEM (Gibco) supplemented with 10% Fetal Bovine Serum (FBS, Cytiva), Glutamax 1% (Gibco) and antibiotics (Penicillin 100 U/ml and Streptomycin 0.1 mg/mL, Sigma Aldrich). When reaching 70–90% confluency, cells were detached with 0.05% Trypsin (Gibco), neutralized with culture medium and centrifuged to remove supernatant, then resuspended in fresh culture medium and passaged at a 1:20 dilution. A cell clone deleted for the *TGFB1* gene (293T-*TGFB1 KO*) was generated by CRISPR-Cas9, by transiently transfecting 293T cells with a *TGFB1*-targetting construct encoding GFP [Addgene plasmid # 48138; http://n2t.net/addgene:48138; RRID:Addgene_48138; corresponding to plasmid pSpCas9(BB)-2A-GFP (PX458), gift from Feng Zhang,.[29] GFP^+ cells were cloned by FACS, and deletion of *TGFB1* was validated by Western Blot. The 293T-*TGFB1 KO* clone was cultured like 293T cells.

Murine Tregs

$CD25^+$ splenocytes from $Foxp3^{YFP-Cre}$ mice were isolated using the Miltenyi MACS CD25 MicroBeads kit (Miltenyi) according to the manufacturer's protocol. Briefly, spleens were collected and mechanically dissociated using a sterile syringe plunger in IMDM medium +10% FCS. After red blood cells lysis (RBC lysis buffer 1X, Biolegend), cells were resuspended in degazed MACS buffer (PBS + EDTA 2mM + 1% FCS, filter-sterilized) and incubated with CD25 MicroBeads. Cells were then subjected to magnetic separation using an LS column (Miltenyi) and a MACS Separator (Miltenyi). The isolated $CD25^+$ fraction was assessed by flow cytometry to measure enrichment in $CD4^+YFP^+$ Tregs. Isolated cells were used immediately in *in vitro* assays.

Cell Reports
Article

CellPress
OPEN ACCESS

Mice

C57BL/6 (C57BL/6J Ola Hsd), DBA2 (DBA/2 Ola Hsd), *Foxp3*^{DTR} (B6.129(Cg)-*Foxp3*$^{tm3(Hbegf/GFP)Ayr}$/J strain), F1 (C57BL/6 x DBA/2), F1 *Foxp3*^{DTR} (C57BL/6 *Foxp3*$^{DTR/DTR}$ x DBA/2), and Foxp3$^{YFP-Cre}$ (B6.129(Cg)-*Foxp3*$^{tm4(YFP/icre)Ayr}$/J) mice were bred and maintained at the SPF animal facility of the UCLouvain (LAF facility with approval number LA2230397). As *Foxp3* is located on the X chromosome, F1 *H-2*^{b}*/day Foxp3*^{DTR} males were obtained by crossing C57BL/6 *Foxp3*$^{DTR/DTR}$ females to DBA/2 *Foxp3*^{WT} males. The facility is controlled to maintain the temperature between 20°C and 24°C; humidity rate between 40 and 65% and day–night cycles of 12 h–12 h. All animal studies were performed in accordance with national and institutional guidelines for animal care, under permit numbers 2017/UCL/MD/19, 2019/UCL/MD/032 and 2023/UCL/MD/37 at the UCLouvain. Female and male mice of 8–12 weeks of age were used as donors and/or recipients, respectively, to induce graft-versus-host disease. We only used females as donors and males as recipients to avoid graft rejection due to H-Y minor histocompatibility antigens.

METHOD DETAILS

mAbs directed against human and mouse latent TGF-β1

mAbs against GARP and GARP:TGF-β1 complexes were derived and described previously.[11,20] mAbs against latent TGF-β1 were obtained following immunization of llamas with plasmids encoding human or mouse TGF-β1, construction of V_H/V_k and V_H/V_λ Fab cDNA libraries and selection by phage display. Fab-coding regions were subcloned into plasmids encoding human (hIgG1) or mouse (mIgG1, or mIgG2a$_{DANA}$) IgGs. mIgG1 and mIgG2a mIgG2a$_{DANA}$ exert few or no FcγR-dependent activities.[30] Chimeric antibodies (LMT-7/LMT-7*, LMT-7/IgG1* and IgG1/IgG1*) were constructed by and purchased from ImmunoPrecise Antibodies Ltd by controlled Fab-arm Exchange.[31] Contamination of antibody preparations by active TGF-β1 was verified by Western Blot (Figure S13), by ELISA and in reporter assays. All mAb solutions used herein contained less than 0.8 pg of active TGF-β1 per μg of mAb.

TGF-β1 reporter assays

In Figures 1 and 2A and supplemental S1, 293T cells were plated one day before transfection in 96w plates (±2.10^4 cells/w). Cells were co-transfected using TransIT-LT1 (Mirus Bio) with plasmids encoding human or mouse GARP$_{FL}$ (50 ng/well), human or mouse latent TGF-β1 (10 ng/well), Firefly luciferase under the control of a TGF-β1-responsive promoter (*pCAGA-12-Fluc*,[32] 50 ng/well, Promega), and Renilla luciferase under a constitutive promoter (*pRL-TK*, 1 ng/well, Promega). Four to six hours after transfection, mAbs (20 μg/mL) or serial dilutions of active recombinant human TGF-β1 (rhTGF-β1, R&D System) were added to the culture medium. Firefly and Renilla luciferase activities were measured 24 h after transfection using the Dual-Glo System (Promega). EC50s were calculated with GraphPad Prism software based on results obtained with serial dilutions of the mAbs.

In Figures 2B and 2C and S2, 293T *TGFB1 KO* cells were plated in 6w plates (±1.10^6/w) and co-transfected on the same day with a plasmid encoding mouse latent TGF-β1 (0.5 μg/well) and a plasmid encoding mouse GARP$_{FL}$, GARP$_{\Delta TM}$, LRRC33, or LTBP-1 (2 μg/well). Another batch of 293T *TGFB1 KO* cells were co-transfected with plasmids encoding Firefly luciferase under the control of a TGF-β1-responsive promoter (*pCAGA-12-Fluc*,[32] 2 μg/well, Promega), and Renilla luciferase under a constitutive promoter (*pRL-TK*, 50 ng/well, Promega). One day after transfection, reporter cells (CAGA-Fluc) cells and cells expressing latent TGF-β1 alone or with a presenting molecule (GARP$_{FL}$, GARP$_{\Delta TM}$, LRRC33 or LTBP-1) were collected and counted, then mixed in co-cultures in 96w plates at a 1 reporter cell to 1 TGF-β1 expressing-cell ratio (2.10^4 + 2.10^4 cells/w). Co-cultures of transfected cells were incubated in the presence of mAbs (20 μg/mL), serial dilutions of active recombinant human TGF-β1 (rhTGF-β1, R&D System) or Latrunculin-a (0.5 μg/mL, Merck Life Science) or Cytochalazin-d (0.5 μM, Merck Life Science) during 24 h. Firefly and Renilla luciferase activities were measured using the Dual-Glo System (Promega).

Short-term TCR-stimulation of murine tregs *in vitro*

MACS-sorted CD25$^+$ splenocytes enriched in Tregs were seeded in 200 μL X-Vivo (Lonza) plus 1% Glutamax (Gibco) in the presence (Stim) or absence (Unstim) of murine CD3/CD28 Dynabeads (ThermoFisher Scientific) at a 2 beads: 1 cell ratio (10^6 cells/w in 48w plates). As indicated in Figure 2D, some wells were pre-coated with a control IgG1 or the LMT-12 mAb (20 μg/mL PBS) during 2 h at room temperature. Active rhTGF-β1 (1 ng/mL, R&D System) was added to unstimulated total splenocytes, as a positive control for TGF-b1 activity, and antibody 1D11 (anti-TGF-β1,2,3) was added to TCR-stimulated Tregs to verify the specificity of TGF-β signals. Cells were incubated during 16 h at 37°C in a humidified atmosphere containing 5% CO_2, then collected and analyzed by Western Blot with anti-posphorylated SMAD2 antibodies.

Western blot analyses

Dry pelleted HEK 293T cells or murine Tregs (enriched CD25$^+$ murine cells) were counted and lysed in Laemmli buffer (Bio-Rad) supplemented with 5% of 2-mercaptoethanol (Bio-Rad). Lysis of HEK 293T cells was facilitated using a 23G needle, and that of murine Tregs by sonication during 15 s using a Microson Ultrasonic cell disruptor (Misonix). Cell lysates were then denatured by boiling at 100°C for 5 min, and clarified by centrifugation at 12,000 rpm for 5 min at 4°C. Spleen or tissue fragments were snap-frozen, immersed in NP40 lysis buffer (1% NP40, 0.05M Tris-HCl Ph8, 0.15M NaCl, 1mM EDTA, 15% Glycerol, 100μM orthovanadate, 1X halt protease inhibitor and 100μM PMSF in H2O) and lysed using TissueLyser (Qiagen) for 4 min at 50Hz. Proteins were quantified using the Pierce BCA protein assay kit (ThermoFisher).

CellPress
OPEN ACCESS

Cell Reports
Article

For electrophoretic separation, equivalents of 2.5x10^4 HEK 293T or 2x10^5 murine Treg cells or 5 μg of proteins for tissues were diluted in Bolt LDS sample buffer and Bolt reducing Agent (ThermoFisher Scientific), then loaded on Bolt 4–12% Bis-tris gels (ThermoFisher Scientific). After migration, proteins were transferred to nitrocellulose membranes using the iBlot system (ThermoFisher Scientific). After blocking, membranes were incubated with primary antibodies directed against GARP (R&D), HA (Eurogentec), mature TGF-β1 (clone A75-2, BD Pharmigen), pSMAD2 (clone 138D4, Cell Signaling Technology), or β-actin (clone D6A8, Cell Signaling Technology), then with a relevant secondary HRP-coupled antibody [anti-sheep IgG-HRP (R&D), anti-rabbit IgG-HRP (Cell Signaling), anti-mouse-IgG-light-chain-HRP (Jackson), anti-rat-IgG-HRP (Cell Signaling) or anti-mouse IgG-HRP (R&D System)]. and revealed with using Pierce SuperSignal chemiluminescent substrates (SuperSignal WEST pico or femto; Thermo Fisher Scientific) on a Fusion Solo 4S system (Vilber-Lourmat). Quantifications were done with the Bio1D software (Vilber-Lourmat).

Epitope mapping

Alignment of mouse and human protein sequences was performed using MacVector software. DNA sequences encoding the h/m TGF-β1 chimeras and single Ala-mutants were obtained from IDT and cloned in vector *pDisplay* to add an N-ter HA-tag or in *pcDNA3* (for Ala-mutant). Other mutants were generated by site-directed mutagenesis with the Q5 Site-Directed Mutagenesis kit (NEB). HEK 293T cells (5.10^5) were transfected in 6 well plates with plasmids encoding mouse *GARP* (1250 ng/well) and h/m TGF-β1 chimeras or single-Ala TGF-β1 mutants (1250 ng/well). 24 h after transfection, cells were incubated with mAbs (5 μg/mL), washed, and incubated with secondary antibodies coupled to a fluorochrome or to streptavidin (+ biotin coupled to a fluorochrome), and analyzed by flow cytometry on a FACS Verse flow cytometer (BD Biosciences). The expression level of each mutant was measured by staining with an anti-HA antibody (Eurogentec) or an antibody against GARP:TGF-β1 complexes,[11,20] and used to normalize binding results. Flow cytometry data were computed using the FlowJo software (Tree Star). For each mAb, residual binding represents percentage of binding to a given chimera or single-Ala mutant by comparison to corresponding human or mouse wild type TGF-β1.

Recombinant protein expression and purification

To enable isolation and purification of soluble GARP:TGF-β1 complexes, coding regions of the GARP extracellular domain (hGARP$_{ECD}$ M1 to I628, mGARP$_{ECD}$ M1 -I629) were fused to sequences encoding a C-terminal TEV-cleavable Strep3x tag (EAAENLYFQG AAGG GSGGGS WSHPQFEKGA AWSHPQFEKG AAWSHPQFEK GAA) and cloned in pCDNA3.1. Sequences coding for h and m TGF-β1 were cloned in pCDNA3.1. One day prior to transfection, 293EBNA cells were seeded at an optimal density to transiently transfect the cells using 25 μg total DNA/50 mL of cell culture. Complexes were produced by co-transfecting TGF-β1 and GARP-ECD-TEV-Strep-encoding plasmids at a 2-to-1 ratio, to ensure that all GARP was in complex with TGF-β1. Six days after transfection, cells were centrifugated and supernatants were transferred to tubes containing StrepTactin Sepharose High Performance beads (GE Healthcare). After a minimal 2 h incubation period, allowing the beads to capture the complexes via the streptavidin tag on GARP, the beads were transferred to a column. Unbound material was washed away by PBS, and the complexes were competitively eluted with 2.5 nM desthiobiotin. The proteins were then buffer exchanged into PBS, followed by TEV digestion to remove the streptavidin tag. A second StrepTactin purification was done to remove free streptavidin tag, undigested complex and TEV-protease. Protein containing fractions of the StrepTactin purification flow-through were pooled, concentrated and further purified by gel filtration using a Superdex200 16/600 column (GE Healthcare) that had been equilibrated in 20 mM HEPES 150 mM NaCl pH 7.4. These protein containing fractions were analyzed by LabChip capillary electrophoresis. Recombinant human and mouse soluble GARP-TGF-β1 complexes were produced and purified at UProtein Express (UPE, Utrecht, The Netherlands).

Purified human and mouse GARP:TGF-β1 complexes were mixed with a 6x molar excess of purified Fab (derived from LHT-22 and LMT-12, respectively) prior to injecting the mixture onto a Superdex 200 HiLoad 16/600 column (GE Healthcare) equilibrated in HEPES-buffered saline buffer (HBS, 25 mM HEPES, pH 7.5, 150 mM NaCl). Peak fractions after size-exclusion chromatography (SEC) were collected and flash-cooled in liquid nitrogen for further use.

Cryo-electron microscopy (cryo-EM)

For both the human and mouse GARP:TGF-β1:Fab complexes, 4 μL of sample (at a conc. of 0.13 and 0.12 mg/mL respectively) was applied to glow-discharged Quantifoil R 0.6/1 300 mesh gold grids coated with graphene (PUXANO), blotted for 1 s at a blot force of 1 under 100% humidity at 22°C and plunged into liquid ethane using a FEI Vitrobot Mark IV device. Grid screening was performed on a JEOL 1400 Plus TEM (BECM, Brussels), and data was acquired on a JEOL cryoARM 300 microscope (BECM, Brussels) equipped with an Omega filter (JEOL) and a 6k × 4k K3 direct detector (Gatan) operated in correlated double-sampling (CDS) mode. For each sample, 60-frame movies were collected with a total exposure of 3.37 s, a total dose of 61.8 $e^-/Å^2$, an energy filter slit width of 20 eV and a pixel size of 0.72 Å/pixel at the specimen level. For the human GARP:TGF-β1:Fab complex, a total of 6678 untilted movies were collected with a defocus of 0.8–2 μm. Following untilted data collection, 4020 movies were collected at 16° tilt and 3200 movies were collected at 35° tilt, all using similar microscope settings. For the mouse GARP:TGF-β1:Fab complex, a total of 6605 untilted movies were collected followed by 3508 movies at 20° tilt. Optimal tilts for tilted data collection were acquired using cryoEF.[33]

Cryo-EM image processing

Processing of uncorrected movies was performed in CryoSPARC v4.2.1.[34] Recorded movies were motion corrected and dose weighted using Patch motion correction, and ensuing CTF estimation was performed using Patch CTF estimation. An initial particle

Cell Reports
Article

CellPress
OPEN ACCESS

stack was acquired using Blob picker with a minimum and maximum particle diameter of 100 and 200 Å respectively. Inspected particle picks were extracted using a box size of 480 pixels down-sampled to 240 pixels, corresponding to a pixel size of 1.44 Å/pixel. Extracted particle stacks were cleaned using several rounds of iterative 2D classification and subsequent 2D class selection to remove junk, and cleaned particle stacks were used for *Ab Initio* model generation with 3 classes as input. To obtain the best results in terms of map isotropy, different amounts of highest resolution 2D classes were mixed from untilted and tilted datasets to obtain following ratios: 0° tilt: 35%, 16° tilt: 45%, 35° tilt: 20% (human GARP:TGF-β1:Fab complex) and 0° tilt: 70%, 20° tilt: 30% (mouse GARP:TGF-β1:Fab complex). After *Ab Initio* model generation, a heterorefinement was performed using all 3 *Ab Initio* models as input for the human GARP:TGF-β1:Fab complex, and using 2 out of 3 *Ab Initio* models for the mouse GARP:TGF-β1:Fab complex. Particles corresponding to heterorefinement Class 1 and 2 of the human GARP:TGF-β1:Fab complex were grouped for subsequent homo- and Non-Uniform refinement jobs, while for the mouse GARP:TGF-β1:Fab complex only particles corresponding to heterorefinement Class 1 were used. For the human GARP:TGF-β1:Fab complex, the particle stack was used for a final round of 2D classification and class selection, resulting in a slightly trimmed final particle stack. For both complexes, a final Non-Uniform refinement run was performed using unbinned data (0.72 Å/pixel). Post-processing was performed using regular sharpening (using B-factors of −30 Å and −70 Å for human and mouse GARP:TGF-β1:Fab complex maps respectively) to obtain maps for subsequent model refinement in Phenix,[35] and using deepEMhancer[36] to obtain maps for model building in Coot[37] and visualization in ChimeraX[38] and Pymol. A schematic overview of cryo-EM image processing can be found in Figures S3 and S4.

Cryo-EM model building and refinement

For the human GARP:TGF-β1:Fab complex, the structure of human GARP:TGF-β1 was extracted from PDB 6gff[34] and rigid-body fitted in the deepEMhancer sharpened map using ChimeraX, together with extracted V_H and V_L chains of an hFAb LHT-22 model generated via ESMFold.[39] The resulting model was used as an input for automatic molecular dynamics flexible fitting using the NAMDINATOR webserver.[40] Next, the flexibly fitted model was used for several cycles of iterative manual model building in Coot guided by the deepEMhancer sharpened map, and real-space refinement in Phenix using the regularly sharpened map. Settings during refinement in Phenix were: enabled global minimization, local grid search, ADP refinement, secondary structure and Ramachandran restraints, and a non-bonded weight parameter of 100. A final refinement was performed using identical settings, but with a non-bonded weight parameter of 300. For the mouse GARP:TGF-β1:Fab complex the same strategy was used as described for the human complex, with the exception that the initial models for mouse GARP and mouse TGF-β1 were obtained from the AlphaFold Protein Structure database (AF-G3XA59-F1 and AF-P04202-F1), after trimming of regions with low per-residue confidence score (pLDDT<50). A summary of cryo-EM data collection, refinement and validation statistics can be found in Table 1.

Cryo-EM Data availability

Cryo-EM maps of human and mouse GARP:TGF-β1:Fab complexes and corresponding structural models are deposited in the EMDB/PDB with accession codes EMDB: EMD-19110/PDB: 8REW and EMDB: EMD-19111/PDB: 8REX, respectively.

Induction and scoring of murine graft-versus-host disease

Splenocytes (70-110.10^6) collected from C57BL/6 donor mice were injected i.p. in F1 (C57BL/6 x DBA/2) male recipients to induce GVHD. Starting one day before splenocyte transplantation, recipients received weekly i.p. injections of mAbs (LMT-10, LMT-12, LMT-7/LMT-7*, LMT-7/IgG1*, IgG1/IgG1* or mIgG1 isotype control; 400 μg/mouse). In experiments shown in Figures 7 and S12, diphtheria toxin (DTx, 0.5 μg/mouse, i.e., ±25μg/kg) was administrated to *FOXP3*$^{DTR/DTR}$ donor females and/or *FOXP3*^{DTR} recipient males to deplete pre-existing Tregs. Mice were evaluated for the development of GvHD symptoms twice a week starting on the day of transplantation until the development of a first symptom in one of the mice (usually around day 13), then daily thereafter (from days 13–20). GvHD scores were established based on weight loss (+1 or +2), posture (+1 or +2), reduced mobility (+1 or +2), and ruffled fur (+1 or +2). Mice were euthanized when they reached a score of 6, or at the end of the experiment (between day 30 and 50). Maximum score (death): 8. In some experiments, a pre-defined group of mice were euthanized on day 9 to collect organs for analyses.

Flow cytometry

Mouse organs were harvested immediately after euthanasia. Spleens and mLNs were mechanically dissociated, homogenates were clarified through 70 μm filters and red blood cells (RBC) were lysed using a standard RBC lysis buffer. Livers were washed in Krebs-Ringer buffer, transferred in C tubes (Miltenyi) containing prewarmed dissociation medium (Collagenase IV, Dnasel and HBSS supplemented with CaCl2 and MgCl2), and mechanical dissociation was performed using the gentleMax Tissue Dissociator following manufacturer instructions. Liver cell suspensions were filtered through 70 μm strainers, and immune cells were isolated using a 30% Percoll gradient (GE Healthcare) followed by RBC lysis. Ileums were cleaned of fat and Peyer's patches. Cell fractions from the epithelium and the lamina propria were separated, and immune cells from both fractions were isolated using a 30% Percoll gradient (GE Healthcare). All single cell suspensions were counted on a Luna cell counter with a live-dead cell marker (Acridine Orange/Propidium Iodide Stain, Logos Biosystem), centrifuged, resuspended in FACS Buffer (2 mM EDTA and 1% FCS in PBS, filter-sterilized) and clarified through 40μm filters prior to incubation with antibodies coupled to fluorochromes. 293T *TGFB1 KO* cells were resuspended in FACS Buffer prior to incubation with antibodies coupled to fluorochromes.

CellPress
OPEN ACCESS

Cell Reports
Article

All antibodies used in flow cytometry experiments are listed in the Key Ressources Table and indicated in the figure legends. Cells were sequentially incubated with primary and secondary antibodies coupled to fluorochromes during 20 min at 4°Cs. After staining for surface markers, splenocytes were washed, fixed and permeabilized with the Foxp3/Transcription Factor staining buffer set (eBioscience), then incubated with an anti-Foxp3 antibody (clone FJK-16s – eBioscience) in the presence of anti-CD16/32 to block Fcg receptors (Biolegend).

Cells were analyzed on a FACS LSR Fortessa flow cytometer (BD Biosciences) and data were computed using the FlowJo software (Tree Star).

Real-time quantitative polymerase chain reaction

Mouse spleens and tissues were collected, weighted and immersed in RNA later (Invitrogen) for 24 h before being stored at −80°C until processing. Tissue disruption was performed using the TissueLyser (Qiagen) for 5 min at 50Hz. Total RNA was extracted using NucleoSpin Mini Columns (Macherey Nagel) and RNA concentration was determined using the NanoDrop spectrophotometer (Thermo Scientific). Reverse transcription was carried out with the Maxima First Strand cDNA Synthesis Kit (Thermofisher). For real-time qPCR, a master mix was prepared containing Takyon Master Mix (0.025 U/µL, Eurogentec), primers (300nM of each), Takyon probe (100nM) and 1.25 µL of cDNA. Reactions were performed on a QuantStudio3 device (Thermofisher) under either standard conditions (95°C for 3 min; 45 cycles of 95°C for 10 s and 60°C for 60 s) or fast conditions (95°C for 3 min; 95°C for 10 s and 60°C for 30 s) depending on amplicon size. Primers and probes sequences are listed in Table S3. Data analysis was conducted using the Thermofisher Design and analysis software. Expression of genes of interest are expressed as a ratio of mRNA/10^5 β-actin (housekeeping gene), calculated either as $10^5 \times 2^{\Delta Ct}$ (where ΔCt = Ct for gene of interest – Ct for β-actin), or as a ratio of mRNA copy numbers evaluated using standard curves with recombinant DNA.

Enzyme-linked immunosorbant assay ELISA

Human/Mouse TGF-β1 uncoated ELISA kit (Invitrogen) was used following manufacturer's instructions to measure active and total (i.e., active + latent) TGF-β1 in untreated or acidified samples, respectively. For acidification, samples were treated with HCl 1N (1:5 v/v for 10 min) then neutralized with NaOH 1.2N/HEPES 0.5M (1:6 v/v).

QUANTIFICATION AND STATISTICAL ANALYSIS

Statistical analyses were performed using GraphPad Prism software (version 9).

Comparisons of measurements made on samples from mice receiving TGF-β1 activating mAbs or control antibodies were tested using an unpaired two-tailed Mann-Whitney test. For survival analyses, we used Kaplan Meier plots representing the proportion of mice alive at the indicated days after transfer of splenocytes, with *p* values calculated using a Gehan-Breslow Wilcoxon test. Numbers of experiments and numbers of mice (n) in the various experimental groups are indicated in the corresponding figure legend. Threshold for statistical significance: 0.05.

Cell Reports, Volume *44*

Supplemental information

Antibody-mediated TGF-β1 activation for the treatment of diseases caused by deleterious T cell activity

Fanny Lambert, Jan Felix, Séverine Wautier, Emilie Dupré, Mathieu Jamez, Camille Michiels, Mélanie Gaignage, Lore Mariën, Manon Lesage, Bas van der Woning, Savvas N. Savvides, and Sophie Lucas

SUPPLEMENTAL FIGURE TITLES AND LEGENDS

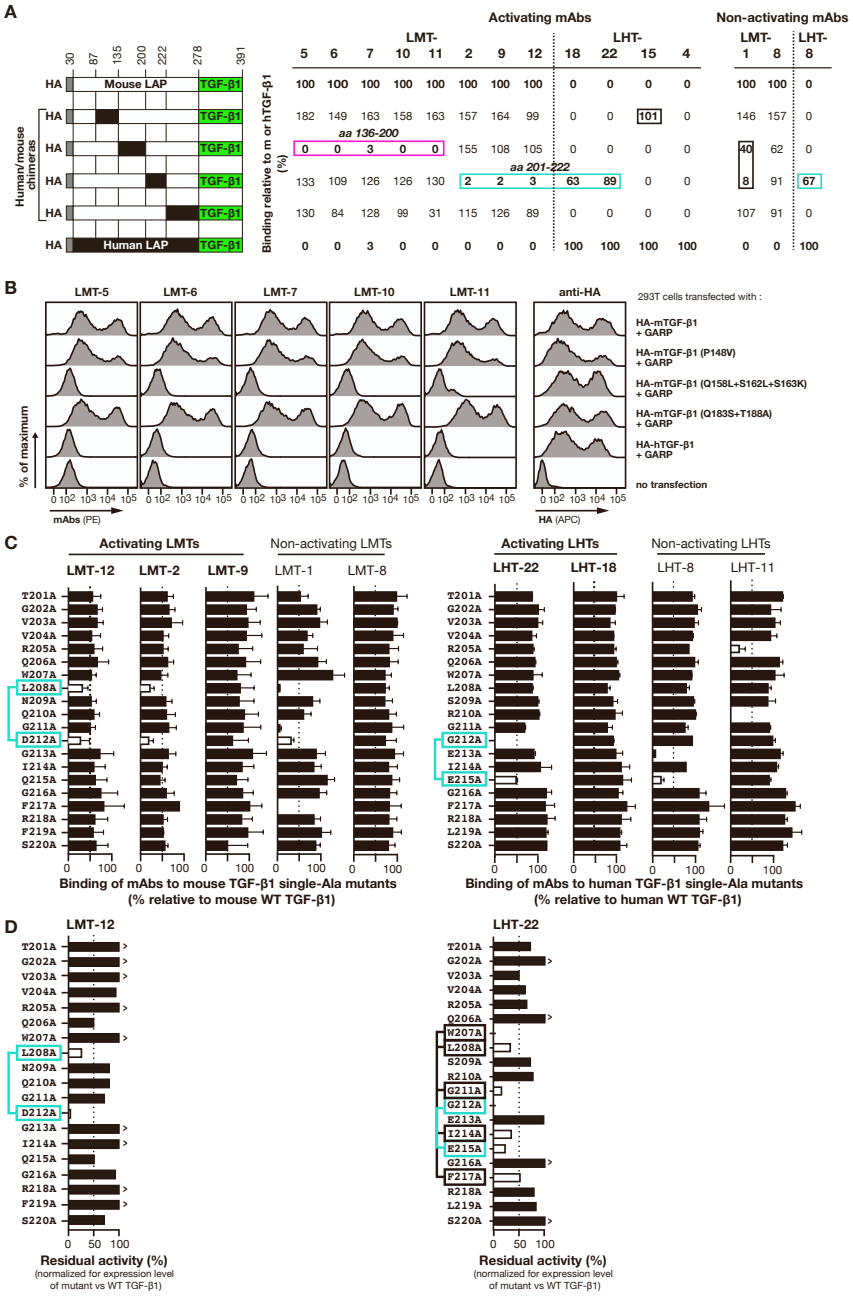

Figure S1. Mapping of epitopes recognized by TGF-β1 activating mAbs

(A) Left: Schematic representation of h/m latent TGF-β1 chimeras used to map regions required for binding by LMT and LHT mAbs. In each chimera, aa from one segment of mouse LAP were replaced by aa from the corresponding segment of human LAP. Right: 293T cells were co-transfected to express mouse GARP in complex with the HA-tagged wild type (WT) or h/m latent TGF-β1 chimera indicated on the left and analyzed for binding to mAbs by flow cytometry. Results are expressed as percent binding to the indicated h/m latent TGF-β1 chimera relative to mouse WT TGF-β1 for LMT mAbs, or human WT TGF-β1 for LHT mAbs. Magenta box: binding by 5 mouse TGF-β1 activating mAbs (LMT-5, 6, 7, 10 and 11) was lost when region 136-200 of mouse latent TGF-β1 was replaced by that of human latent TGF-β1. Turquoise box: binding by 3 other mouse TGF-β1 activating mAbs (LMT-2, 9 and 12) required aa from region 201-222. The same region was required for binding by 2 human TGF-β1 activating mAbs (LHT-18 and 22), as these were not able to bind h/m latent TGF-β1 chimeras unless region 201-222 was replaced by that of human latent TGF-β1. Black box: human TGF-β1 activating LHT-15 required region 87-135. No region required for binding could be identified for LHT-4, 20, 25.

(B) 293T cells were co-transfected to express mouse GARP in complex with the additional HA-tagged h/m chimeras indicated on the right and analyzed for binding to the indicated mAbs by flow cytometry. Histogram are gated on live cells. This allowed to refine the binding requirement of 5 mouse TGF-β1 activating mAbs (LMT-5, 6, 7, 10 and 11) to aa 158-163.

(C) 293T cells were co-transfected to express human or mouse GARP with the indicated HA-tagged human or mouse latent TGF-β1 single-Ala mutants, respectively, and analyzed for binding to mAbs by flow cytometry. Bar graphs indicate percent binding to each single-Ala mutant relative to WT TGF-β1 (mean of 2 to 4 experiments + SD). White bars: < 50% binding. Binding by LMT-2 and LMT-12 was lost only when mouse latent TGF-β1 L208 or D212 were mutated to A, and binding by LHT-22 was lost only when human latent TGF-β1 G212 or E215 were mutated to A (turquoise boxes). No other LMT or LHT required these residues but no other for binding.

(D) Reporter assay as in Figure 1A, with 293T cells co-transfected to express GARP in complex with the indicated HA-tagged latent TGF-β1 single-Ala mutants or WT controls. As expected, the mAbs lost the ability to activate mutants to which they do not bind (turquoise boxes). Interestingly, 5 residues that are not required for binding (W207, L208, G211, I214, and F217) are nevertheless required for LHT-22 to activate human TGF-β1 (black boxes). > : activity on the indicated latent TGF-β1 single-Ala mutant is superior to that on the corresponding WT TGF-β1.

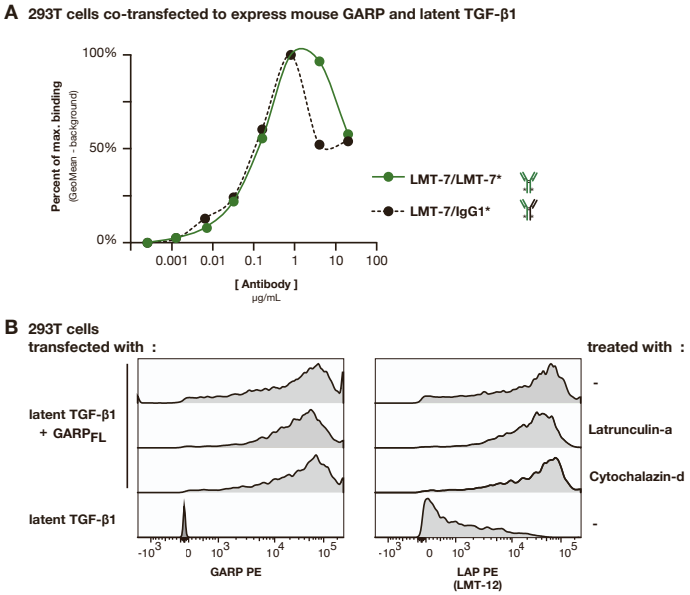

Figure S2. GARP:TGF-β1 on the cell surface is bound with similar affinities by LMT-7/LMT-7* and LMT-7/IgG1* chimeras, and is not decreased by treatment with inhibitors of actin polymerization

(A) 293T cells transfected as in Fig. 2A were incubated with LMT-7/IgG1*, LMT-7/LMT-7* or control IgG1/IgG1* at the indicated concentrations, then with a secondary goat anti-mouse IgG coupled to PE, and analyzed by flow cytometry. Background: geomMean fluorescence intensity in the presence of IgG1/IgG1* (no binding).

(B) 293T cells transfected as in Fig. 2A were incubated with Latrunculin-a, Cytochalazin-d or medium alone for 24h, then incubated with anti-GARP coupled to PE, or LMT-12 and a secondary anti-mouse IgG coupled to PE prior to analysis by flow cytometry.

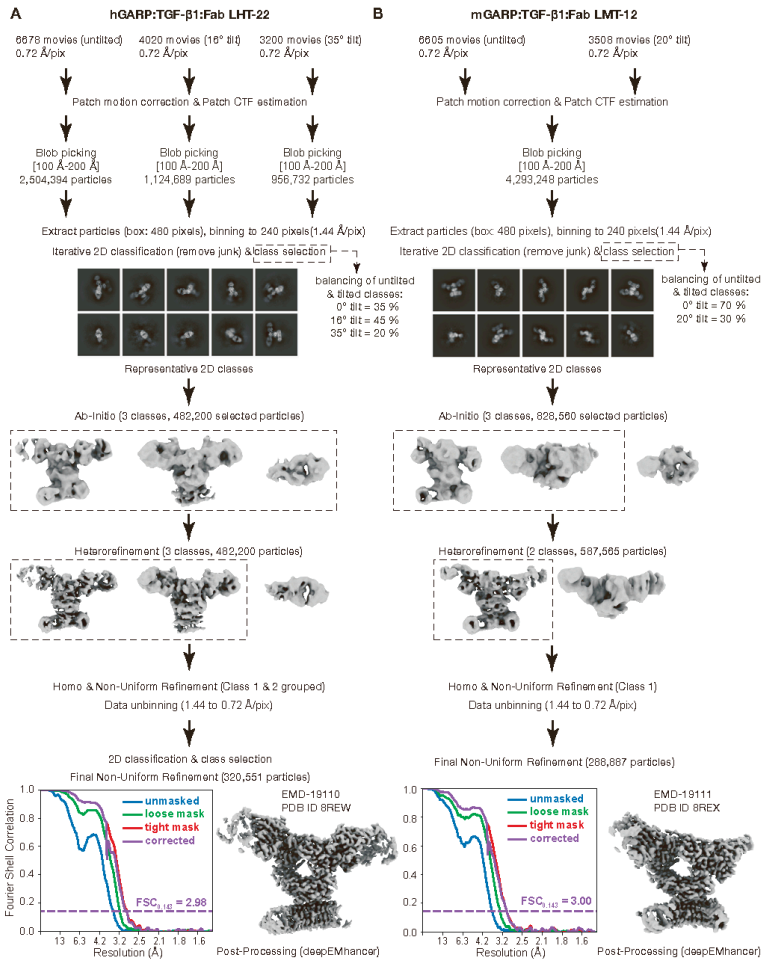

Figure S3. Cryo-EM data processing workflow of human (A) and mouse (B) GARP:TGF-β1:Fab complexes.

Data processing was performed using CryoSPARC v4.2.1 [S1]. Gold-standard Fourier Shell Correlation (FSC) curves are shown (A and B, bottom) after applying either no mask (blue curve), a loose mask (green curve), or a tight mask (red curve) to both half maps before calculating FSC curves. The purple curve depicts the corrected FSC calculated using an auto-tightened mask with correction by noise substitution [S2]. The estimated resolution at FSC = 0.143 (dotted purple lines) is shown for the corrected FSC (purple curve).

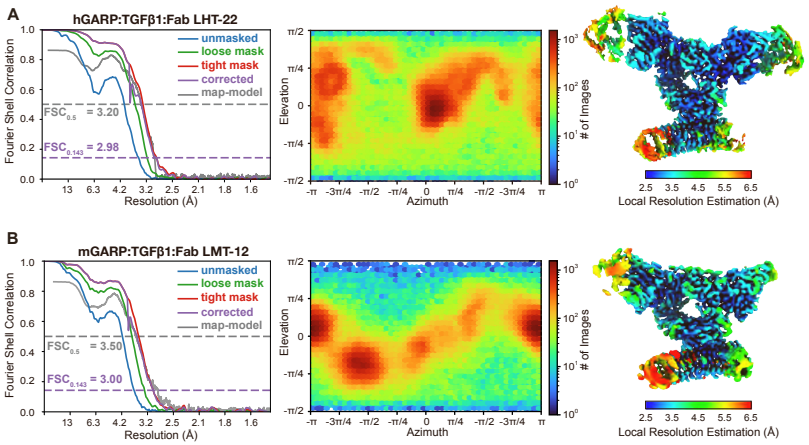

Figure S4. Gold-standard Fourier Shell Correlation (FSC) curves, particle orientation distribution plots and local resolution estimation of human (A) and mouse (B) GARP:TGF-β1:Fab complexes. FSC curves are calculated after applying either no mask (blue curve), a loose mask (green curve), or a tight mask (red curve) to both half maps. The purple curve depicts the corrected FSC calculated using an auto-tightened mask with correction by noise substitution [S2]. The estimated resolution at FSC = 0.143 (dotted purple lines) is shown for the corrected FSC (purple curve). Map-to-model FSC curves are shown as grey curves, and the estimated resolution at FSC = 0.5 is shown as a grey dotted line. To the right of each FSC curve, a particle orientation distribution plot is shown along with the corresponding map colored to local resolution.

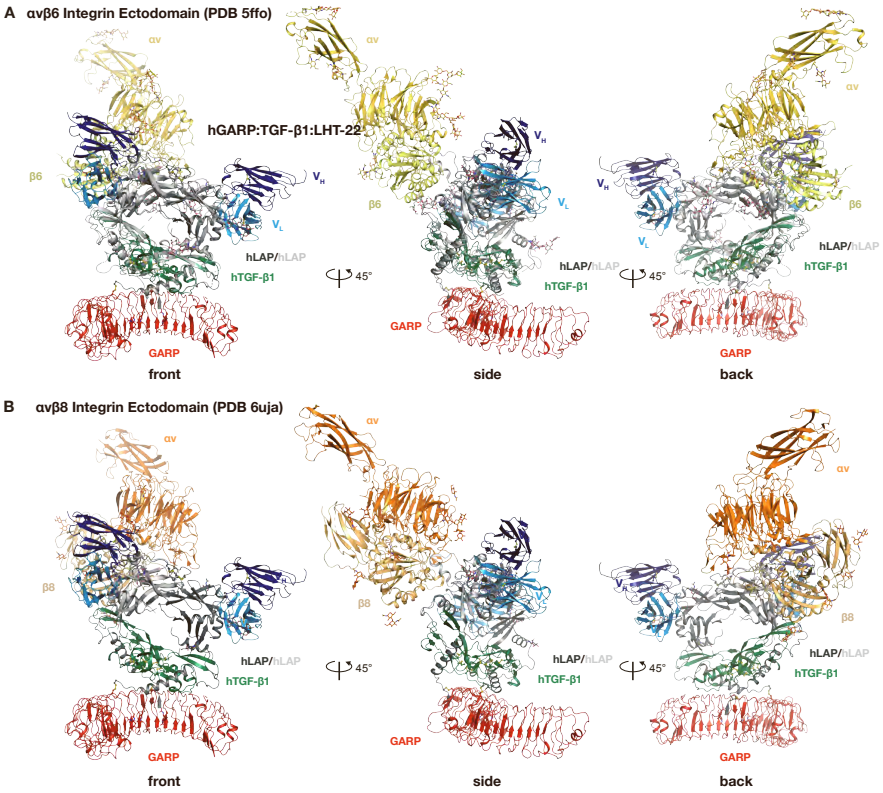

Figure S5. Structural alignment of αvβ6 and αvβ8 integrin complexes onto the human GARP:TGF-β1:LHT-22 complex.

(A) Front (left), side (middle) and back (right) views of the integrin αvβ6:TGF-β1 complex (PDB 5FFO [S3], colored yellow/gold for αv/β6 subunits and light grey for TGF-β1), aligned onto the human GARP:TGF-β1:LHT-22 Fab complex (hGARP: red, hTGF-β1: green, hLAP: grey, LHT-22 Fab V_L: light blue, LHT-22 Fab V_H: dark blue).

(B) Front (left), side (middle) and back (right) views of the Integrin αvβ8:lTGF-β1 complex (PDB 6UJA [S4], colored light orange/dark orange for αv/β6 subunits and light grey for lTGF-β1), aligned onto the human GARP:TGF-β1:LHT-22 Fab complex (hGARP: red, hTGF-β1: green, hLAP: grey, LHT-22 Fab V_L: light blue, LHT-22 Fab V_H: dark blue).

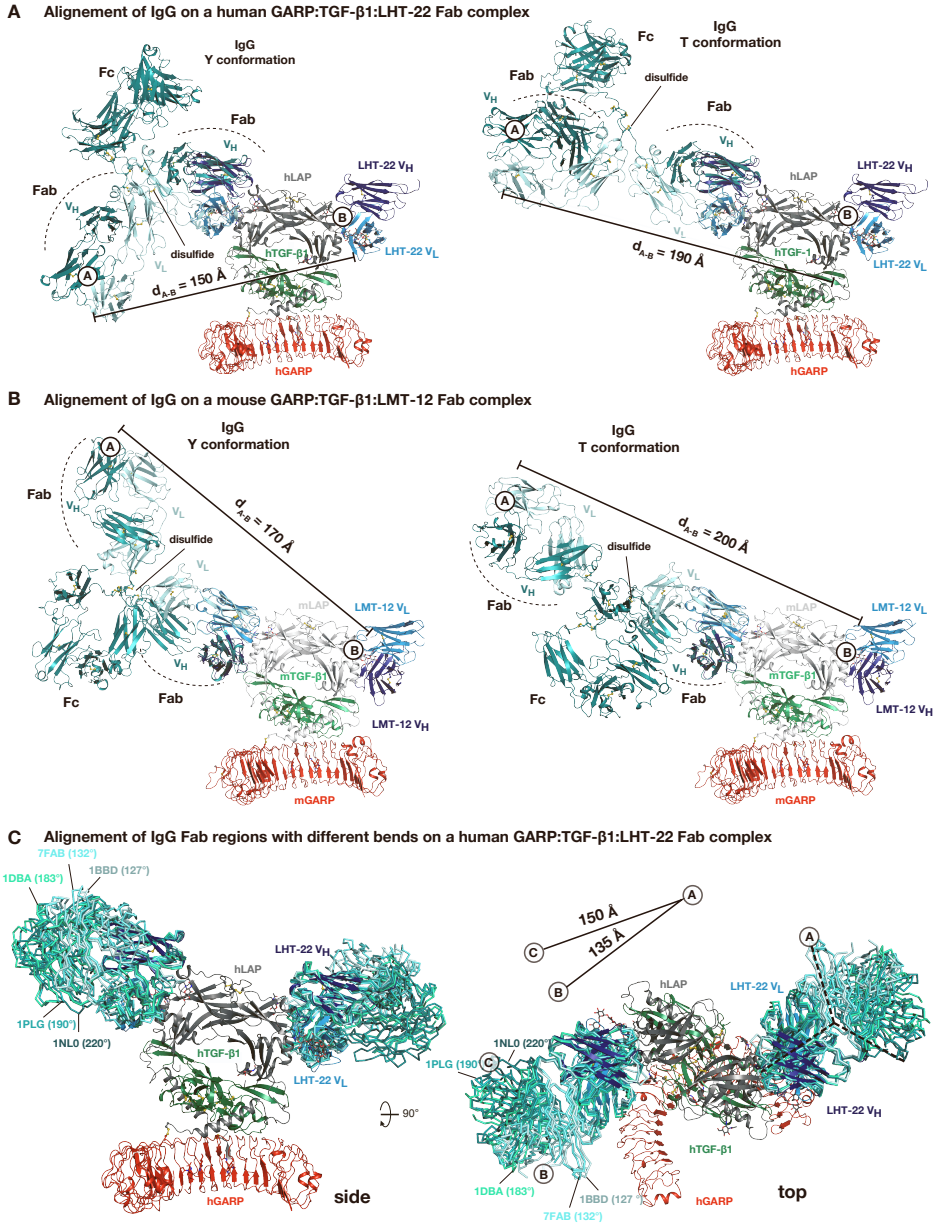

Figure S6.

(A-B) Structural alignment of IgG in Y and T conformations onto human GARP:TGF-β1:LHT-22 and mouse GARP:TGF-β1:LMT-12 complexes. Structural alignment of IgG (colored cyan) in the Y (left, PDB 1IGY [S5]) and T (right, PDB 1IGT [S5]) conformations onto LHT-22 or LMT-12 FAbs in the human (top) or mouse (bottom) GARP:TGF-β1:Fab complexes (human/mouse GARP: red,

human/mouse TGF-β1: dark/light green, human/mouse LAP: dark/light grey, LHT-22/LMT-12 Fab V_L: light blue, LHT-22/LMT-12 Fab V_H: dark blue). The distances d_{A-B} between the unoccupied epitopes on IgG (A) and the interfaces between human/mouse LAP and LHT-22/LMT-12 FAb (B) are annotated as black lines.

(C) Structural alignment of IgG1 Fab structures with different bends on the human GARP:TGF-β:LHT-22 Fab complex. Side (left) and top (right) views are shown of the human GARP:TGF-β1:LHT-22 Fab complex (hGARP: red, hTGF-β1: green, hLAP: grey, LHT-22 Fab V_L: light blue, LHT-22 Fab V_H: dark blue) with a set of Fab structures (colored light to dark cyan) aligned onto LHT-22 Fab. The aligned Fab structures display a wide range of tilts around the elbow angle, ranging from 127° to 220° [S6]: 1BBD: 127°, 7FAB: 132°, 1DBA: 183°, 1PLG: 190°, 1NL0: 220°. The distance between the extremities of the 127° (least) and 220° (most) bend Fabs is annotated as 135 Å (distance B-C) and 150 Å (distance A-C) respectively.

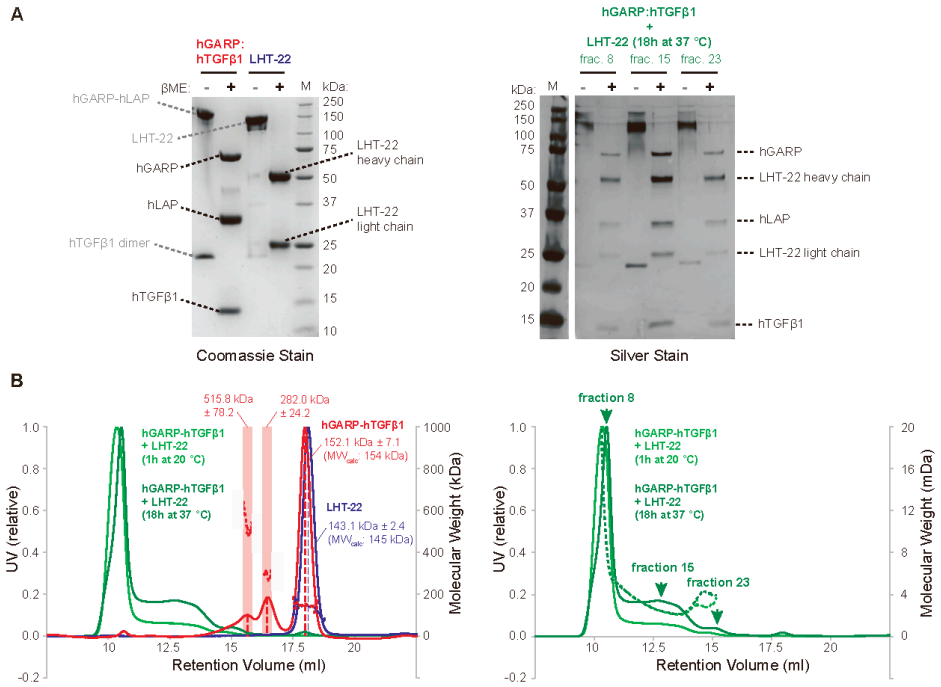

Figure S7. Size Exclusion Chromatography coupled to Multi-Angle Laser Light Scattering (SEC-MALLS) of human GARP:TGF-β1 mixed with LHT-22 mAb in equimolar amounts, after incubating for either 1 hour at 20 °C or 18 hours at 37 °C.

(A) SDS-PAGE gels of the main peak fractions of SEC-MALLS experiments annotated in B (top red peak: hGARP:ITGF-β1, top blue peak: LHT-22 mAb, green peak fractions 8, 15 and 23: hGARP: ITGF-β1 + LHT-22 mab (1:1 ratio, 18 hours incubation at 37° C). Annotated +/- βME corresponds to samples with or without added 2-Mercaptoethanol. Bands on the SDS-PAGE gel corresponding to disulfide linked hTGF-β1 dimer, hGARP-hLAP, or LHT-22 mAb in lanes without βME are annotated with grey dotted lines. Bands on the SDS-PAGE gel corresponding to hTGF-β1, hGARP, hLAP, LHT-22 mAb light chain and LHT-22 mAb heavy chain in lanes with added βME are annotated with black dotted lines.

(B) Molecular weight determination of hGARP:ITGF-β1 (red curve), LHT-22 mAb (blue curve), hGARP:ITGF-β1 + LHT-22 mab (1:1 ratio) after one hour incubation at 20° C (light green curves) and hGARP:ITGF-β1 + LHT-22 mab (1:1 ratio) after 18 hour incubation at 37° C (dark green curves) by SEC-MALLS. The determined molecular weight (right axis, dashed curves) is plotted along with the relative UV signal (light axis, full curves). The right plot (light and green curves) displays the same data as the left plot, but with added determined molecular weight (dashed curves) and annotated fractions used in SDS-PAGE gels for clarity.

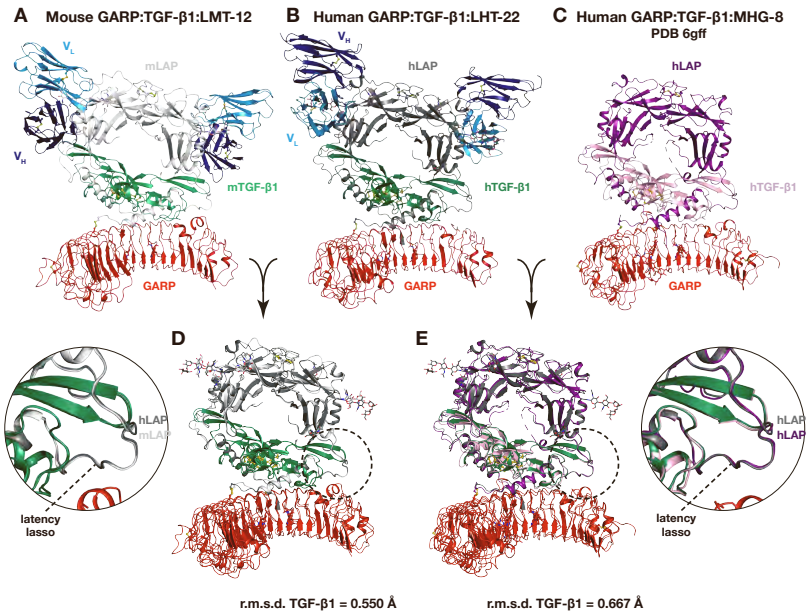

Figure S8. Structural alignment of GARP:TGF-β1:LHT-22, GARP:TGF-β1:LMT-12, and GARP:TGF-β1:MHG-8 complexes.

(A-C) Cartoon representation of the mouse GARP:TGF-β1:LMT-12 complex (A), the human GARP:TGF-β1:LHT-22 complex (B) and the human GARP:TGF-β1 extracted from PDB 6GFF (C).

(D) Structural alignment of TGF-β1 from mouse GARP:TGF-β1:LMT-12 and human GARP:TGF-β1:LHT-22 complexes.

(E) Structural alignment of TGF-β1 from human GARP:TGF-β1:LHT-22 and GARP:TGF-β1:MHG-8 complexes.

R.m.s.d. values depicted under each structural alignment were calculated in PyMOL. For the r.m.s.d. calculation between mouse GARP:TGF-β1:LMT-12 and human GARP:TGF-β1:LHT-22, 518 out of 615 Cα atoms were aligned, while for the r.m.s.d. calculation between human GARP:TGF-β1:LHT-22 and human GARP:TGF-β1:MHG-8, 536 out of 629 Cα atoms were aligned. Alignment of all 615 or 629 Cα atoms results in r.m.s.d. values of 1.594 Å and 1.224 Å respectively. Insets show a zoomed view of the latency lasso region of the 'straitjacket' domain of LAP.

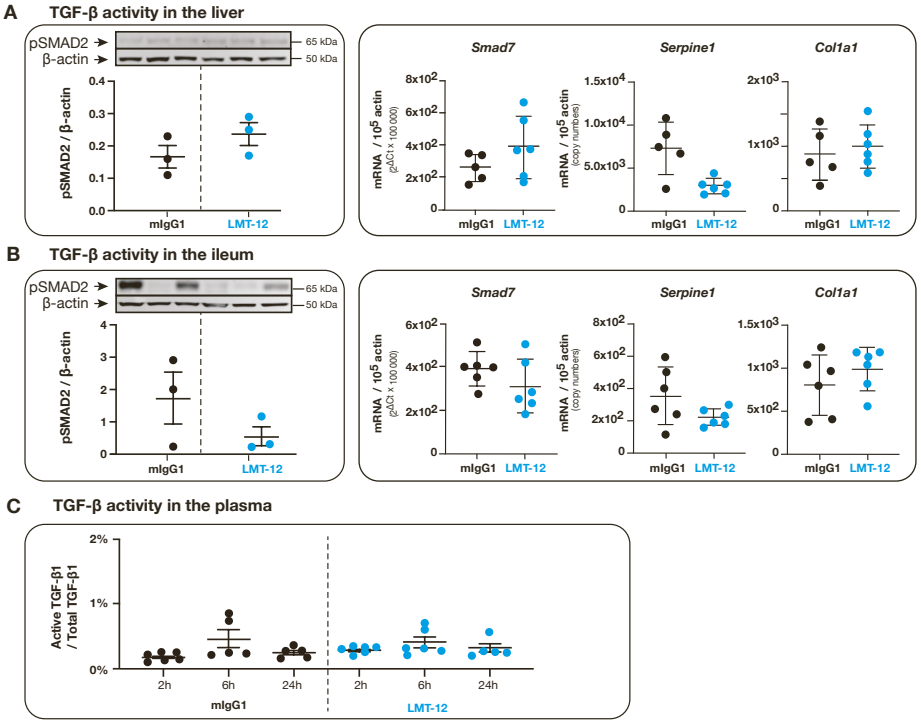

Figure S9. Treatment with LMT-12 does not increase TGF-β1 activity in liver and ileum in mice with GVHD and does not increase active TGF-β1 levels in the circulation of C57BL/6 mice.

(A-B) GvHD was induced as indicated in Figure 5, except that recipient mice were euthanized to collect various organs on day 9 after transplantation. Left panels: organs collected from recipient mice on day 9 after transplantation were lyzed and analyzed by Western Blot with antibodies against pSMAD2 and β-actin. Each lane in the Western blots and data point in the graphs show analysis of lysate from one individual mouse. ECL signals were quantified to establish pSMAD2/β-actin ratios. Right panels: expression of TGF-β1 target genes measured by RT-qPCR. Each data point represents value measured in one individual mouse. Organs were collected from the same mice shown in Figure 6A (spleens). **(C)** Plasma of healthy C57BL/B6 mice was collected at the indicated timepoints after i.p. injection of LMT-12 or a mouse IgG1 control mAb. Plasmatic concentrations of active and total (i.e. active + latent) TGF-β1 were measured by ELISA. Limit of detection: 16 pg/mL of active TGF-β1. TGF-β1 activity is represented as a proportion of active TGF-β1 in total TGF-β1.

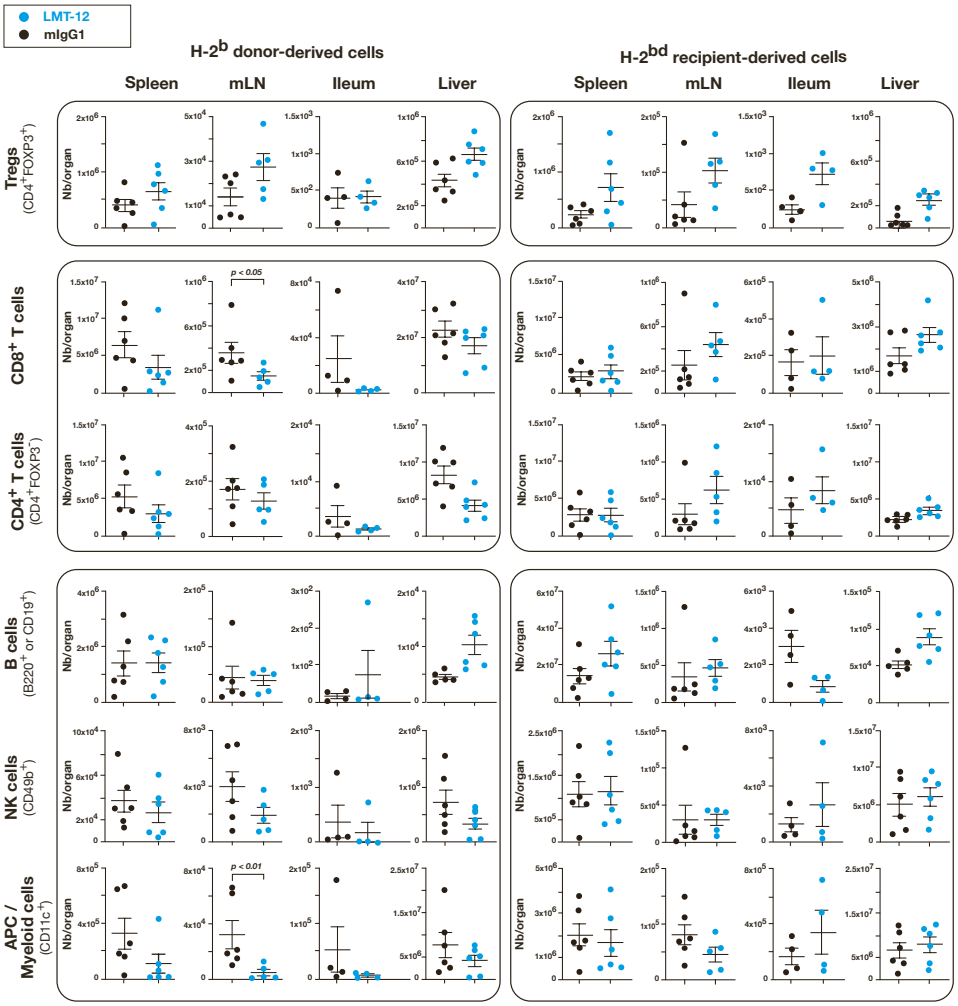

Figure S10. Treatment with LMT-12 does not modify most immune cell populations in spleen, mLN, ileum and liver.

Spleen, mesenteric lymph nodes (mLN), ileum and liver were collected 9 days after transplantation from the same recipient mice shown in Figure S9A-B. Single cell suspensions were prepared on Percoll density gradients for liver and ileum epithelia. Cells were counted and analyzed by flow cytometry with antibodies against CD4, CD8, B220, CD19, CD49b, CD11b, FOXP3, H-2D^{d} and H-2K^{b}/H-2D^{b} to evaluate numbers of cells from donor (H-2^{b}) and recipient (H-2^{bd}) origin. Statistical analysis was performed using an unpaired two-tailed Mann-Whitney test.

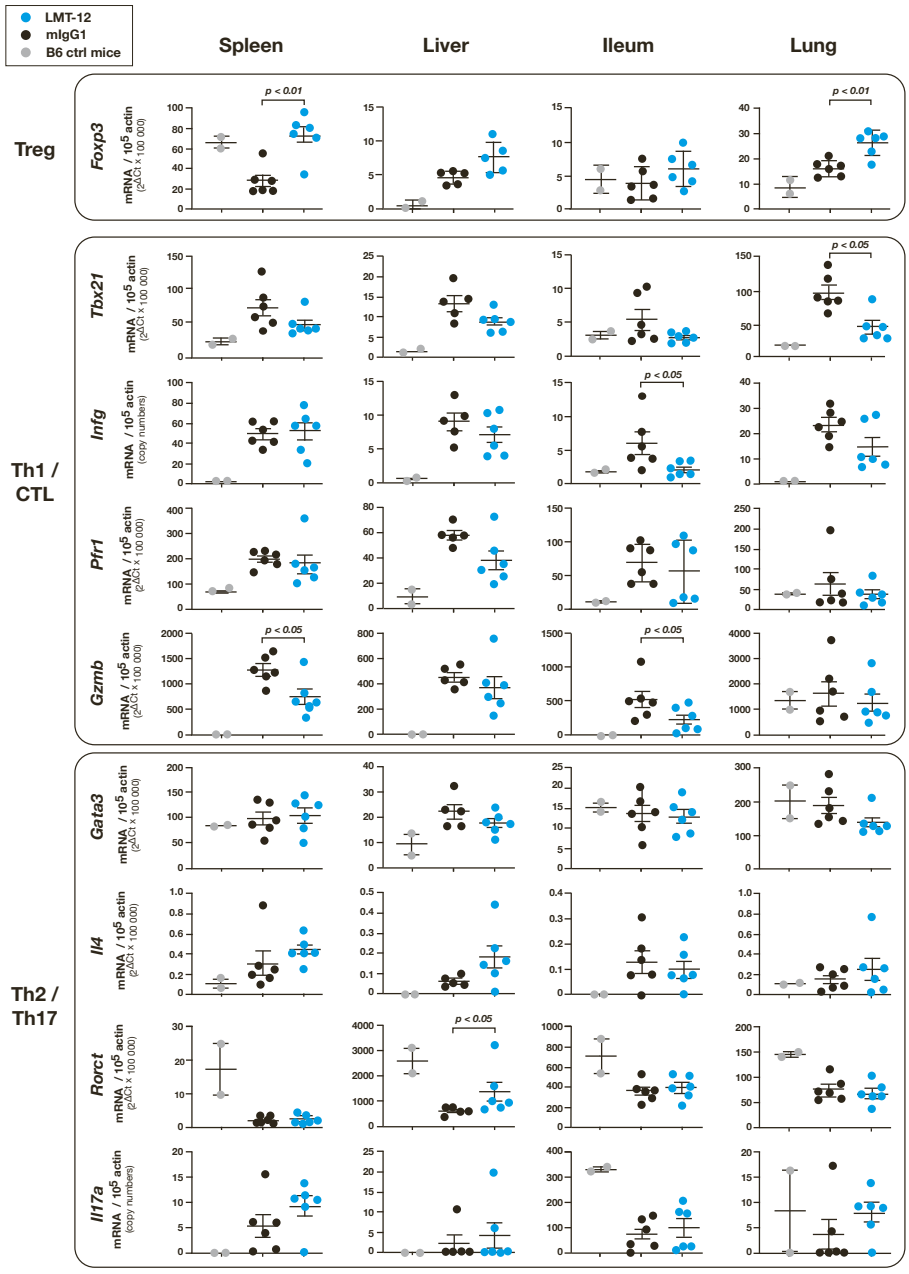

Figure S11. Expression of Th1/CTL genes tend to decrease in mice treated with TGF-β1 activating mAbs.

RT-qPCR analyses on organs collected 9 days after transplantation from the same recipient mice shown in Figure S9A-B and S10, or from healthy B6D2 F1 mice as controls. Each data point represents expression level in one individual mouse. Statistical analysis was performed using an unpaired two-tailed Mann-Whitney test.

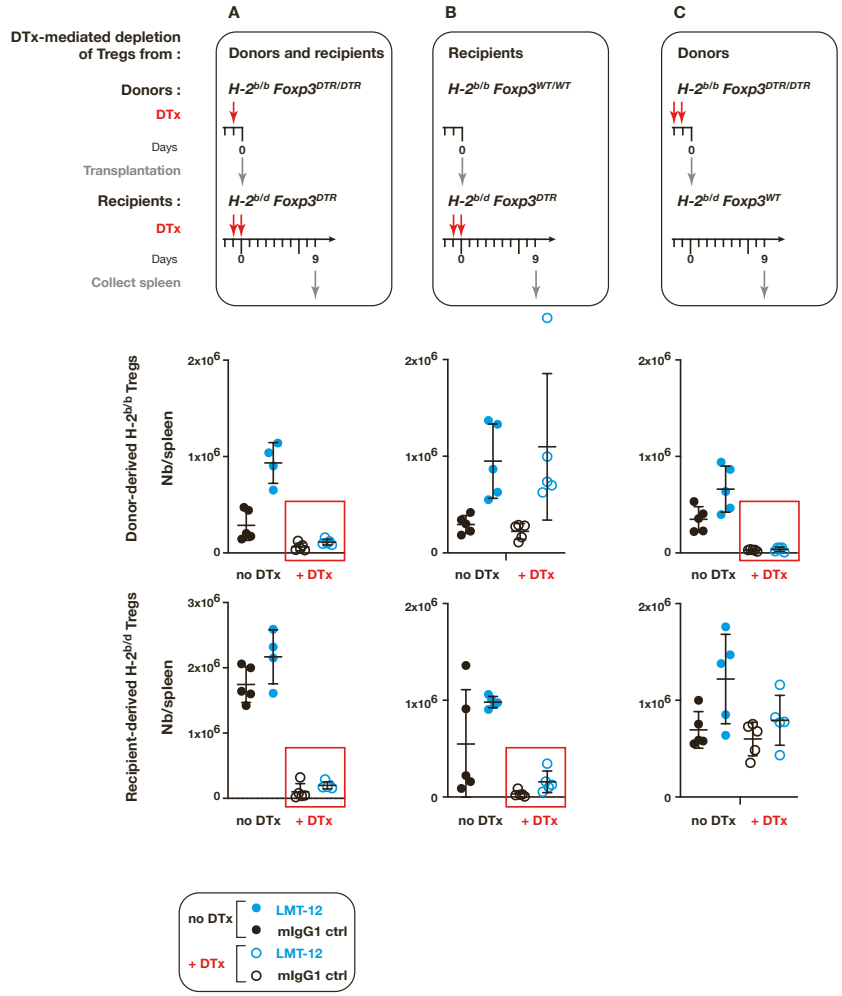

Figure S12. Depletion of Tregs from donor, recipient or both origins by injection of diphteria toxin

Splenocytes from recipient mice of experiments illustrated in Figure 7 were collected on day 9 after transplantation and analyzed by flow cytometry with antibodies against CD4, FOXP3, H-2D^{d} and H-2K^{b}/H-2D^{b}. Depending on the genotypes of donors and recipients, DTx injections induced depletion of Tregs (CD4^{+}FOXP3^{+} cells) from donor (H-2^{b}), from recipient (H-2^{bd}) or from both donor and recipient origin.

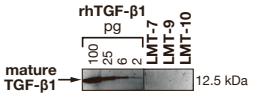

Figure S13. Absence of contaminating active TGF-β1 in antibody preparations

Western Blot analysis of mature TGF-β1 content in 25 µg of the indicated mAb preparations. The indicated amounts of rhTGF-β1 were used as references.

SUPPLEMENTAL TABLE 1

Interaction between human latent TGF-β1 and a Fab derived from LHT-22
Analysis performed with PISA server (https://www.ebi.ac.uk/pdbe/pisa/**)**

LAP - LHT-22 V_L interaction
Hydrogen bonds (pairwise interactions, chain A: LAP, chain F: LHT-22 V_L)

	Chain F (LHT-22 V_L)	Dist.(Å)	Chain A (LAP)
1	F:ARG 50[NH1]	2.57	A:SER 209[O]
2	F:ASN 51[ND2]	3.30	A:SER 138[O]
3	F:ASN 51[ND2]	2.99	A:GLU 142[OE2]
4	F:TYR 53[OH]	2.95	A:GLY 212[O]
5	F:TYR 53[OH]	3.27	A:SER 138[OG]
6	F:TYR 53[OH]	2.72	A:ARG 141[NH1]
7	F:ASN 71[ND2]	2.98	A:ARG 210[O]
8	F:TYR 112[OH]	3.08	A:GLU 213[OE1]
9	F:TYR 112[OH]	3.05	A:GLU 213[OE2]

Full list of interfacing residues (not pairwise, chain A: LAP, chain F: LHT-22 V_L)

	Chain F (LHT-22 V_L)		Chain A (LAP)	
1	F:ARG 50	(H*)	1 A:SER 138	(H)
2	F:ASN 51	(H)	2 A:ARG 141	(H)
3	F:TYR 53	(H)	3 A:GLU 142	
4	F:TYR 70		4 A:PRO 145	
5	F:ASN 71	(H)	5 A:GLU 146	
6	F:VAL 73		6 A:PRO 147	
7	F:ALA 74		7 A:LEU 208	
8	F:ARG 75		8 A:SER 209	(H)
9	F:TYR 112	(H)	9 A:ARG 210	(H)
10	F:ASN 119		10 A:GLY 211	
			11 A:GLY 212	(H)
			12 A:GLU 213	(H)
			13 A:GLU 215	

*H: Hydrogen Bond

LAP - LHT-22 V_H interaction
Hydrogen bonds (pairwise interactions, chain A: LAP, chain G: LHT-22 V_H)

	Chain G (LHT-22 V_H)	Dist.(Å)	Chain A (LAP)
1	G:THR 124[OG1]	3.29	A:GLU 213[OE1]
2	G:TYR 125[OH]	2.30	A:GLU 215[OE2]
3	G:ASP 50[OD1]	2.89	A:LYS 123[NZ]
4	G:ASP 49[O]	2.51	A:LYS 123[NZ]
5	G:ASP 122[OD2]	3.57	A:ILE 214[N]

Salt bridges (pairwise interactions, chain A: LAP, chain G: LHT-22 V_H)

	Chain G (LHT-22 V_H)	Dist.(Å)	Chain A (LAP)

```
 1   G:ASP  50[ OD1]   2.89    A:LYS 123[NZ]
```

Full list of interfacing residues (not pairwise, chain A: LAP, chain G: LHT-22 V_H)

	Chain G (LHT-22 V_H)		**Chain A (LAP)**
1	G:ASP 49	1	A:GLU 119
2	G:ASP 50 (H*/S**)	2	A:ILE 120
3	G:TYR 51	3	A:ASP 122
4	G:ARG 71	4	A:LYS 123 (H/S)
5	G:TRP 72	5	A:PHE 124
6	G:ASN 73	6	A:PHE 134
7	G:VAL 75	7	A:LYS 173
8	G:THR 76	8	A:TYR 174
9	G:GLY 119	9	A:SER 175
10	G:SER 120	10	A:ASN 176
11	G:ILE 121	11	A:ASN 177
12	G:ASP 122 (H)	12	A:ARG 210
13	G:LEU 123	13	A:GLY 211
14	G:THR 124 (H)	14	A:GLY 212
15	G:TYR 125 (H)	15	A:GLU 213 (H)
		16	A:ILE 214 (H)
		17	A:GLU 215 (H)

*H: Hydrogen Bond
**S: Salt Bridge

SUPPLEMENTAL TABLE 2

Interaction between mouse latent TGF-β1 (LAP) and a Fab derived from LMT-12
Analysis performed with PISA server (https://www.ebi.ac.uk/pdbe/pisa/**)**

LAP – LMT-12 V_L interaction
Hydrogen bonds (pairwise interactions, chain A: LAP, chain I: LMT-12 V_L)

	Chain I (LMT-12 V_L)	Dist.(Å)	Chain A (LAP)
1	I:TYR 52[OH]	3.11	A:GLN 210[OE1]
2	I:TYR 53[N]	3.40	A:ASP 212[O]
3	I:TYR 112[OH]	3.31	A:ASN 209[O]

Full list of interfacing residues (not pairwise, chain A: LAP, chain I: LMT-12 V_L)

	Chain I (LMT-12 V_L)		Chain A (LAP)
1	I:SER 55	1	A:SER 138
2	I:SER 46	2	A:TYR 174
3	I:GLY 50	3	A:SER 175
4	I:GLY 51	4	A:ASN 176
5	I:TYR 52 (H*)	5	A:ASN 209 (H)
6	I:TYR 53 (H)	6	A:GLN 210 (H)
7	I:TYR 112 (H)	7	A:GLY 211
8	I:SER 113	8	A:ASP 212 (H)
9	I:SER 117	9	A:GLY 213
		10	A:ILE 214
		11	A:GLN 215

*H: Hydrogen Bond

LAP – LMT-12 V_H interaction
Hydrogen bonds (pairwise interactions, chain A: LAP, chain H: LMT-12 V_H)

	Chain H (LMT-12 V_H)	Dist.(Å)	Chain A (LAP)
1	H:LYS 125[NZ]	3.46	A:SER 138[OG]
2	H:TYR 52[OH]	2.27	A:PRO 145[O]
3	H:SER 71[OG]	2.84	A:GLU 146[OE1]
4	H:GLY 75[N]	3.36	A:GLU 146[OE1]
5	H:TYR 52[OH]	3.26	A:ARG 141[NH1]
6	H:ARG 122[O]	3.86	A:GLU 142[N]
7	H:TYR 124[O]	2.68	A:ASP 212[N]

Full list of interfacing residues (not pairwise, chain A: LAP, chain H: LMT-12 V_H)

	Chain H (LMT-12 V_H)		Chain A (LAP)
1	H:SER 49	1	A:SER 138 (H)
2	H:TYR 52 (H)	2	A:ARG 141 (H)
3	H:SER 71 (H)	3	A:GLU 142 (H)
4	H:ILE 72	4	A:PRO 145 (H)
5	H:GLY 73	5	A:GLU 146 (H)
6	H:GLY 75 (H)	6	A:PRO 147
7	H:SER 76	7	A:PRO 148
8	H:TRP 78	8	A:LEU 149

9	H:ASN 120	9	A:LEU 208
10	H:SER 121	10	A:ASN 209
11	H:ARG 122 (H)	11	A:GLN 210
12	H:SER 123	12	A:GLY 211
13	H:TYR 124 (H)	13	A:ASP 212 (H)
14	H:LYS 125 (H)	14	A:LEU 265
		15	A:GLU 266

*H: Hydrogen Bond

SUPPLEMENTAL TABLE 3

List of primers used for RT-qPCR

Primer Sequence (5' - 3')	Definition
TCAAGTGGCATAGATGTGGAAGAA	Forward primer in *mIfng* mRNA
TGGCTCTGCAGGATTTTCATG	Reverse primer in *mIfng* mRNA
TCACCATCCTTTTGCCAGTTCCTCCAG	Taqman probe in *mIfng* mRNA
AAGAGAGCAAGGACAACACTC	Forward primer in *mGzmb* mRNA
CATGTCCCCCGATGATCTC	Reverse primer in *mGzmb* mRNA
ACAAGGTCAGCAGTAGCAGGAGGA	Taqman probe in *mGzmb* mRNA
CAGTAGAGTGTCGCATGTACAG	Forward primer in *mPrf1* mRNA
GATGAGCCTGTGGTAAGCAT	Reverse primer *in mPrf1* mRNA
TCGCCTGGTACAAAAACCTCCACTC	Taqman probe in *mPrf1* mRNA
CATCTTCTCAAAATTCGAGTGACAA	Forward primer in *mTnfa* mRNA
GGGTTGTACCTTGTCTACTCCCA	Reverse primer in *mTnfa* mRNA
CACGTCGTAGCAAACCACCAAGTGGA	Taqman probe in *mTnfa* mRNA
CAAGACCACATCCACAAACATC	Forward primer in *mTbx21* mRNA
TTCAACCAGCACCAGACAG	Reverse primer in *mTbx21* mRNA
TCACTAAGCAAGGACGGCGAATGT	Taqman probe in *mTbx21* mRNA
CCTTATCAAGCCCAAGCGAA	Forward primer in *mGata3* mRNA
GTCCCCATTAGCGTTCCTC	Reverse primer in *mGata3* mRNA
TGTCCCTGCTCTCCTTGCTGC	Taqman probe in *mGata3* mRNA
GCTCCAGAAGGCCCTCAG	Forward primer in *mIl17a* mRNA
CTTTCCCTCCGCATTGACA	Reverse primer in *mIl17a* mRNA
ACCTCAACCGTTCCACGTCACCCTG	Taqman probe in *mIl17a* mRNA
TCTGCAAGACTCATCGACAAG	Forward primer in *mRorc* mRNA
GAGGTGCTGGAAGATCTGC	Reverse primer in *mRorc* mRNA
CTAGCCAAGCTGCCACCCAAAG	Taqman probe in *mRorc* mRNA
CCCCGCCACCTGGAAGAAT	Forward primer in *mFoxp3* mRNA
CTCCCTTCTCGCTCTCCAC	Reverse primer in *mFoxp3* mRNA
CCATCCGCCACAACCTGAGCC	Taqman probe in *mFoxp3* mRNA
CTGTGTTGCTGTGAATCTTACG	Forward primer in *mSmad7* mRNA
CATTGGGTATCTGGAGTAAGGAG	Reverse primer in *mSmad7* mRNA
AGATCAACCCCGAGCTGGTGTG	Taqman probe in *mSmad7* mRNA
CGCAAAGAGTCTACATGTCTAGG	Forward primer in *mCol1a1* mRNA

CATTGTGTATGCAGCTGACTTC	Reverse primer in *mCol1a1* mRNA
CCGGAGGTCCACAAAGCTGAACA	Taqman probe in *mCol1a1* mRNA
AGTAACTTCGTGCCTAGCAAC	Forward primer in *mCol1a2* mRNA
CATCAACACCATCTCTGCCT	Reverse primer in *mCol1a2* mRNA
CCCTTTCGTACTGATCCCGATTGCA	Taqman probe in *mCol1a2* mRNA
GAGCTATCCATTTCACCTTCAGA	Forward primer in *mFn1* mRNA
TTGTTCGTAGACACTGGAGAC	Reverse primer in *mFn1* mRNA
CAGGAGATTTGTTAGGACCACGGCA	Taqman probe in *mFn1* mRNA
GAGCTACGAACTGCCTGAC	Forward primer in *mActa2* mRNA
CTGTTATAGGTGGTTTCGTGGA	Reverse primer in *mActa2* mRNA
CCGCTGACTCCATCCCAATGAAAGA	Taqman probe in *mActa2* mRNA
AAGAACCAGGAGCATGTAGAA G	Forward primer in *mFap* mRNA
TTGTAACCATCCTTGTCGCTA	Reverse primer in *mFap* mRNA
ACA AAG AAT CCA CCA GCC CAT CCT	Taqman probe in *mFap* mRNA
CTATGGTGAAACAGGTGGACT	Forward primer in *mSerpine1* mRNA
CGTGTCAGCTCGTCTACAG	Reverse primer in *mSerpine1* mRNA
ACCTTTGGTATGCCTTTCCACCCA	Taqman probe in *mSerpine1* mRNA

SUPPLEMENTAL REFERENCES

1. Punjani, A., Rubinstein, J.L., Fleet, D.J., and Brubaker, M.A. (2017). cryoSPARC: algorithms for rapid unsupervised cryo-EM structure determination. Nat. Methods *14*, 290-296. 10.1038/nmeth.4169.
2. Chen, D.S., and Mellman, I. (2013). Oncology meets immunology: the cancer-immunity cycle. Immunity *39*, 1-10. 10.1016/j.immuni.2013.07.012.
3. Dong, X., Zhao, B., Iacob, R.E., Zhu, J., Koksal, A.C., Lu, C., Engen, J.R., and Springer, T.A. (2017). Force interacts with macromolecular structure in activation of TGF-beta. Nature *542*, 55-59. 10.1038/nature21035.
4. Campbell, M.G., Cormier, A., Ito, S., Seed, R.I., Bondesson, A.J., Lou, J., Marks, J.D., Baron, J.L., Cheng, Y., and Nishimura, S.L. (2020). Cryo-EM Reveals Integrin-Mediated TGF-beta Activation without Release from Latent TGF-beta. Cell *180*, 490-501 e416. 10.1016/j.cell.2019.12.030.
5. Harris, L.J., Larson, S.B., Hasel, K.W., and McPherson, A. (1997). Refined structure of an intact IgG2a monoclonal antibody. Biochemistry *36*, 1581-1597. 10.1021/bi962514+.
6. Stanfield, R.L., Zemla, A., Wilson, I.A., and Rupp, B. (2006). Antibody elbow angles are influenced by their light chain class. J. Mol. Biol. *357*, 1566-1574. 10.1016/j.jmb.2006.01.023.